Schweizerische Eidgenossenschaft
Confédération suisse
Confederazione Svizzera
Confederaziun svizra

Bundesamt für Energie BFE
Swiss Federal Office of Energy SFOE

Implementierung einer Nuclear Education, Skills and Technology (NEST)-Ausbildungskomponente in das HYMERES-2 Projekt der OECD/NEA zusammen mit dem Paul-Scherrer Institut (*Projektakronym: "NEST-HYMERES"*)

- ZWISCHENBERICHT Dezember 2021-

BFE-Projektnummer: SI/501656

Start-/Enddatum: 01.10.2017-31.12.2021

Author: Andreas Pautz, Paul Scherrer Institut (PSI)

Abstract / Kurzbeschreibung

The NEST (**N**uclear **E**ducation, **S**kills, and **T**echnology) framework is an initiative of the OECD Nuclear Energy Agency (NEA), which addresses the important issue of maintaining nuclear know-how for the use of nuclear technology worldwide, by fostering nuclear skills capability building, knowledge transfer and technical innovation within an international context. In Switzerland, the necessity of preserving nuclear competences for the safe long-term operation of nuclear power plants, their decommissioning and the disposal of nuclear waste in deep geological repositories has been widely recognized. NEST is a project-based scheme, which employs large-scale joint international research endeavors, such as those governed by the OECD/NEA, as platforms to implement dedicated nuclear education and training activities. In this particular case, the OECD/NEA joint project HYMERES-2 (**HY**drogen **M**itigation **E**xperiments for **Re**actor **S**afety, Phase 2) serves as a vehicle to attract young talent into the area of nuclear containment phenomena and safety assessment. NEST-HYMERES aims to advance the understanding around the release, distribution and mitigation of hydrogen in Light Water Reactor containment structures, with the goal to enhance modeling capabilities in support of safety assessments for existing and new nuclear power plants. Within NEST-HYMERES, it was originally foreseen to host up to eighteen so-called NEST Fellows (typically graduate students, Postdocs, or young industry professionals) within four years at the PANDA facility of the Paul Scherrer Institut. While this goal could not be reached due to the enduring Covid-19 situation, causing significant lack of mobility of the fellows, substantial modeling and experimental results for HYMERES-2 have nevertheless been produced as part of the fellows' work, which are being outlined in this report.

*Das NEST-Rahmenprogram (**N**uclear **E**ducation, **S**kills, and **T**echnology) ist eine Initiative der OECD Nuclear Energy Agency, die sich mit der wichtigen Frage des Erhalts des nuklearen Know-hows für die weltweite Nutzung der Nukleartechnologie befasst, indem sie den Aufbau nuklearer Kompetenzen, den Wissenstransfer und die technische Innovation im internationalen Kontext fördert. In der Schweiz ist die Notwendigkeit des nuklearen Kompetenzerhalts für den sicheren Langzeitbetrieb von Kernkraftwerken, deren Stilllegung und die Entsorgung nuklearer Abfälle in geologischen Tiefenlagern weithin anerkannt. NEST ist ein projektbasiertes System, das multilaterale internationale Forschungsprojekte, wie sie von der OECD/NEA geleitet werden, als Plattformen für die Durchführung spezifischer Aus- und Weiterbildungsmaßnahmen im Nuklearbereich nutzt. Im vorliegenden Fall dient das OECD/NEA-Gemeinschaftsprojekt HYMERES-2 (**HY**drogen **M**itigation **E**xperiments for **Re**actor **S**afety, Phase 2) als Vehikel, um junge Talente für das Gebiet der Phänomene des nuklearen Sicherheitsbehälters und der Sicherheitsbewertung zu gewinnen. NEST-HYMERES zielt darauf ab, das Verständnis für die Freisetzung, Verteilung und Vermeidung von Wasserstoff in Containment-Strukturen von Leichtwasserreaktoren zu verbessern mit dem Ziel, die Modellierungsmöglichkeiten zur Unterstützung von Sicherheitsbewertungen für bestehende und neue Kernkraftwerke zu verbessern. Im Rahmen von NEST-HYMERES war ursprünglich vorgesehen, innerhalb von vier Jahren bis zu 18 sogenannte NEST-Fellows (in der Regel Doktoranden, Postdocs oder junge Fachleute aus der Industrie) in der PANDA-Anlage des Paul Scherrer Instituts mit Forschungsaufgaben zu betrauen. Während dieses Ziel bedingt durch Covid-19 wegen der mangelnden Mobilität der Fellows nicht erreicht werden konnte, wurden nichtsdestotrotz im Rahmen der Arbeit der Fellows wesentliche Modellierungs- und experimentelle Ergebnisse für HYMERES-2 erzielt, die in diesem Bericht dargestellt werden.*

Table of Contents

1 Introduction: Background of the OECD/NEA NEST Initiative

The member countries of the OECD's Nuclear Energy Agency (NEA) need scientists, engineers and technology experts to ensure the safe, secure and sustainable use of nuclear energy, in order to meet global energy demands and cope with environmental challenges, regardless of which role nuclear energy is to play in their future energy mix. The NEA is addressing the concerns of its member countries about the potential loss of nuclear expertise and knowledge by creating new approaches to retain, nurture and expand this knowledge base, as well as building new capabilities needed for innovative nuclear technologies in plant construction/operation, decommissioning, and waste disposal. The NEST (**N**uclear **E**ducation, **S**kills, and **T**echnology) Framework is one of the principal responses of NEA to this need. It is a joint international initiative bringing together public and private organisations such as academia, research centres and industries.

Several NEA countries are constructing or planning to construct Generation III+ and Generation IV nuclear power plants, while others need to deal with their nuclear legacies. Most NEA countries are looking at long-term options to deal with high-level radioactive waste and spent nuclear fuel, lifetime extension for an ageing fleet of nuclear power plants, as well as better ways to decommission old facilities. There are also challenging issues in other fields, ranging from medicine to the environment. Switzerland, as one of the member countries of the OECD/NEA, has strongly vested stakes in this NEA initiative, due to its extended nuclear phase-out time horizon, and the corresponding threat of losing important competences in the nuclear safety and geological waste disposal area in the long-term.

The goal of the NEST Framework is to encourage postgraduate students, postdoctoral researchers and young professionals to pursue careers in the nuclear field by exposing them to challenging projects and real-world problems. The NEST Framework aims to transfer the knowledge accumulated by the current generation of nuclear experts to the future workforce. Its overall objectives are to:

- assist NEA member countries to maintain and strengthen academic nuclear-related education programmes and to build both technical and non-technical skills in the field of nuclear science, the safe use of nuclear technology, and its applications;
- facilitate the skills development of students and young professionals in the nuclear sector through the transmission of practical knowledge and hands-on training;
- establish sustainable international exchanges and cooperation among the participating organisations and countries.

The benefits of the NEST framework are therefore manifold: it provides fast-track processes to build up the next generation of nuclear experts and professionals through hands-on exposure to real-world problems and by working on challenging and innovative projects. Moreover, it grants access to a critical mass of capacities (e.g. experimental facilities and infrastructures, construction or decommissioning projects, innovative activities…) in close co-operation with universities, available within the NEST membership to the so-called NEST Fellows (typically master of PhD students, Postdocs, or young professionals) via international co-operation. Finally, it supports the development of a network of promising young professionals, nuclear experts and leaders in the field.

NEST is implemented through dedicated projects and activities in the participating countries. The NEST projects are multi-disciplinary in nature, and must involve organisations (universities, research centres, industries, technical support organisations [TSOs], regulators) from at least three NEST

member countries. Master, PhD, Postdocs and young professionals, i.e. the NEST fellows, will develop skills and acquire competences and knowledge in new areas of nuclear science and technology through hands-on activities developed as part of these NEST projects. Each project addresses a specific real-world issue or challenge (nuclear safety, decommissioning, nuclear new builds, radioactive waste management…). Each NEST fellow is assigned a NEST mentor, to help them acquire knowledge and critical thinking skills that come from working in close contact with experts and leaders in the field. In a second phase, fellows continue working on exploratory research projects related to the challenges and issues faced. This will eventually lead to development of new technologies and greater innovation. Finally, through networking among themselves as well as with a wide range of experts from different countries and disciplines, NEST fellows broaden their knowledge of the nuclear field, which could lead to new opportunities crucial for their career development.

The NEST framework was formally established on February 15, 2019 with the signing of the "FRAMEWORK AGREEMENT ON THE OECD NUCLEAR ENERGY AGENCY (NEA) JOINT UNDERTAKING ON NUCLEAR EDUCATION SKILLS AND TECHNOLOGY (NEST)" (see Appendix A to this document, and appendices therein). Fifteen technical-scientific organisations from 10 NEST member countries (Belgium, Canada, France, Germany, Italy, Japan, Korea, Russia, Switzerland and United States) are currently participating in the NEST Framework. These countries and organisations have all expressed their wish to cooperate through international exchanges and activities to strengthen nuclear-related education programmes, build technical and non-technical skills in the field of nuclear science, and foster the safe use of nuclear technology and its applications.

Fig. 1: The fifteen organizations currently participating in NEST

As the main decision body of the NEST Framework, the NEST Management Board has been incepted, which includes one member plus one alternate from each NEST Country. The NEST Management Board has been meeting twice per year since 2019 and assumes several important roles and responsibilities, including the following:

- Adoption of the NEST program of work and the NEST budget;
- Selection of the NEST projects;
- Steering of the NEST Framework.

Prof. Dr Andreas Pautz from PSI, the author of the report at hand, has been Chair of the Management Board since 2019; his two-year mandate was renewed in 2021 by unanimous decision of the Management board. The work of the Management board is supported by the NEST bureau, a four-person subset of the management board, that advises the chairman and the NEA/NEST secretariat in the preparation of the board meetings. Corresponding information regarding the governance of NEST is available on https://www.oecd-nea.org/jcms/pl_24302/nest-management-board. The major working body of NEST is located at the OECD/NEA in form of the abovementioned NEA/NEST secretariat. The NEST Secretariat's tasks comprise the monitoring of the progress of the different NEST projects, the support of the Management Board in the monitoring and evaluation process and providing the interface between the NEST Projects and the Management Board. More information regarding the NEST secretariat can be found on the following webpage: https://www.oecd-nea.org/jcms/pl_24319/nest-secretariat.

At the heart of the NEST Framework are the so-called NEST multinational and multidisciplinary projects. These NEST projects are being developed to meet specific education and skills development needs of several NEST member countries. To meet real world contexts and challenging problems of industry/regulatory bodies, and to benefit from experienced practitioners, a NEST project can be defined and implemented as a part of a broader existing project that can meet agreed NEST criteria, such as national projects open to international co-operation, ongoing NEA joint projects, etc.

Currently, six NEST projects are in progress, with a seventh one in preparation; information on each project is readily available on the NEST project webpage https://www.oecd-nea.org/jcms/pl_24310/nest-projects#toc_1. The six ongoing projects are namely:

- Hydrogen containment experiments for reactor safety (NEST-HYMERES)
- Small modular reactors (NEST-SMR)
- Advanced remote technology and robotics for decommissioning (ARTERD)
- Radioactive waste management of i-graphite
- Medical applications, nuclear technologies, radioprotection and safety (MANTRAS)
- Building competence, Expert knowledge, Applied techniques, Safe decommissioning, Train fellows (BEAST)

The project NEST-HYMERES has been one of the first NEST projects being established and has since served as a "prototype" of a successful NEST implementation. It is led by the Paul Scherrer Institut with the author of the report at hand being the project leader. Since the support of the Swiss Federal Office of Energy is geared specifically towards this project, the remainder of the report will focus on NEST-HYMERES.

2 The NEST-HYMERES Project within the NEST Framework

In the early phases of the conception of the NEST framework, it was discussed favorably amongst NEA member countries to establish NEST projects as augmenting education and training components to existing large joint international research endeavors, such as those hosted by the OECD/NEA Committee for the Safety of Nuclear Installations (CSNI). The CSNI is the host of numerous of these large-scale projects, which by their construction represent an excellent basis for NEST. At the time of the inception of NEST, i.e. around 2017, the Switzerland-based OECD/NEA/CSNI project HYMERES was completed and due for renewal; it therefore seemed timely to integrate NEST as an integral component into the succeeding project, HYMERES-2.

The Paul Scherrer Institut (PSI) therefore proposed in 2017 to build a NEST project, **NEST-HYMERES**, as the education/training component of the newly launched OECD/NEA/CSNI joint project HYMERES-2 (**HY**drogen **M**itigation **E**xperiments for **Re**actor **S**afety, Phase 2). In HYMERES-2, PSI acts as the so-called operating agent, through making accessible its large-scale thermal-hydraulic test facility PANDA to the international research community. HYMERES-2 is the third project in an extremely successful series of OECD/NEA/CSNI joint research projects at PSI focusing on Severe Accident phenomenology and mitigation. The PANDA facility, which is the main tool of the HYMERES-2 project, is located in the Laboratory for Reactor Physics and Thermal Hydraulics of PSI, and represents an essential infrastructure of PSI's Nuclear Energy and Safety division. In chapter 3, a short overview of the goals of the HYMERES-2 project is provided.

In the NEST context, the Paul Scherrer Institut acts, according to the NEST nomenclature, as the **Managing Research Institution** (MRI), which will closely cooperate with the **NEST Performing Institutions** (NPI) in countries participating in HYMERES-2 and/or NEST-HYMERES. The following partners from ten institutions in eight countries are the founding members of NEST-HYMERES:

- University of Stuttgart, Germany;
- Oregon State University, USA;
- Texas A&M University, USA;
- Royal Institute of Technology (KTH), Sweden;
- Universidad Politécnica de Madrid, Spain;
- Université d'Orléans, France;
- Seoul National University, Korea;
- Swiss Federal Institute of Technology Zurich (ETH), Switzerland;
- University of Tokio, Japan.

In this project context, PSI provides the necessary professional guidance and infrastructure to conduct world-class experimental research work supported by the PANDA team, while the NPI join forces in scientific cooperation in the HYMERES-2 context and beyond. This is supposed to be achieved primarily by delegating NEST fellows to PSI (or other NPI) for short-, medium- or long-term stays, through organizing educational and training events together with other NEST project partners, or through participation in analytical benchmark activities within the HYMERES-2 collaboration. The aim is to create a deep understanding of severe accident phenomena and mitigation measures, as well as provide profound training in working with advanced instrumentation and high-fidelity fluid dynamics codes to the next generation of nuclear engineers.

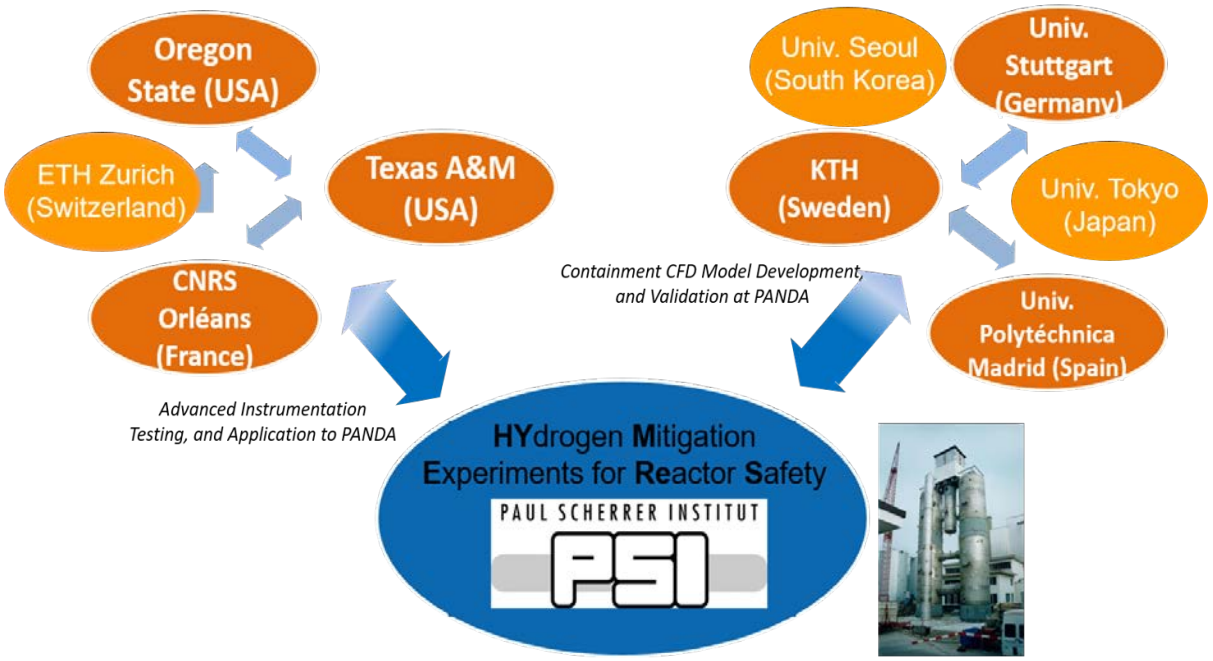

Fig. 2: The NEST concept supports the spawning of new research networks

NEST-HYMERES promotes the idea of not only using the outstanding experimental facilities of the cooperation partners, but features a much further academic outreach: on a long-term perspective the initiative will spawn strong and sustainable university networks that provide education at the highest international level. Figure 2 sketches the long-term vision of the partners involved in NEST-HYMERES, one that would go far beyond the time horizon of the HYMERES-2 project alone. Through NEST-HYMERES, the formation of new networks of excellence around the areas of "Advanced Instrumentation Techniques" and "Containment CFD Development" is promoted, thereby establishing strong links not only to PSI, but also in between all other partners involved.

3 Brief overview of the OECD/NEA/CSNI HYMERES-2 project

The containment in a nuclear power plant is the last physical barrier to prevent the release of radiological material to the environment. Therefore, plant safety systems must ensure containment integrity for all possible postulated accidents. Hydrogen generated during a postulated severe accident with core degradation is a major safety issue, since explosive mixtures may form in the containment. The generation and particularly the distribution of hydrogen is therefore a key aspect in the safety assessment of Light Water Reactors.

The analysis of hydrogen distribution is very complex due to the effects of hydrogen transport, hydrogen mixing or stratification with steam, air or nitrogen, and the condensation or re-evaporation of steam. Moreover, various reactor types (BWRs, PWRs, Heavy Water Reactors, etc.) have a number of design-specific differences, which need to be properly accounted for in any analysis.

Advanced Lumped Parameters (LP) and Computational Fluid Dynamics (CFD) codes are valuable tools for analyzing LWR behavior during postulated design and beyond-design-basis accidents. At present,

the extent of code validation is one limiting factor in their application for reactor safety analyses. One of the obstacles in the process of assessment and validation of computational tools is the lack of adequate experimental data at the required spatial and time resolution.

The OECD/NEA/CSNI HYMERES-2 project has been carried out in the period 1st July 2017 – 30th June 2021 with experimental investigations at PSI's PANDA facility to continue improving the understanding of the containment phenomena during postulated severe accident scenarios and to further extend the experimental database to phenomena not investigated previously. The HYMERES-2 investigations addressed the following four main topics:

1. ***Extend the database on flows impacting obstructions and containment internal structures.*** The experimental database has been extended with respect to jet flow impacting flow obstructions by considering flow geometries resembling those of nuclear containment internal structures. The primary target of the program was to provide data for testing the codes against a variety of flow obstruction geometries up to scaled-down real containment internal structures.

2. ***Evaluation of the importance of radiative heat transfer.*** Tests have been performed to evaluate the importance of radiative heat transfer on the phenomena affecting the evolution of gas species distribution (i.e. hydrogen transport, mixing, etc.) during a postulated Beyond Design Basic Accident (BDBA).

3. ***Solve important issues regarding suppression pressure pool and BWR systems.*** The effect of the following parameters has been investigated in the experimental campaigns: Height of the pool and depth of the sparger; sparger design including blowdown pipe; BWR containment system tests, which involve the interplay of e.g. Drywell, Wetwell, Reactor Pressure Vessel and components e.g. venting pipes, vacuum breaker, spray, etc.

4. ***Extend the database on the performance of safety component operation.*** Two types of safety components, namely spray and cooler were investigated in detail:

   I. Specific spray tests were performed by considering a number of nozzles embedded in a ring installed near the PANDA vessel wall such that the phenomena would be more representative of real plant containment conditions. In this series, the tests were defined by considering cases with or without sump drainage, to address the importance of condensate liquid re-evaporation, and for scenarios addressing both Design Basic Accident (DBA) and BDBA scenarios;

   II. Further tests were performed with more than one cooler and varying the distance between the activated coolers. Coolers were installed at the same elevation, circumferentially in the vessel dome of PANDA. The activation of individual coolers allowed to gain insights into the cooler modelling needs under DBA and BDBA scenarios, in particular how coolers could be better modelled, e.g., using a detailed 3D representation or by a porous media approach.

The above four topics describe the overall investigation plan for the HYMERES-2 project. It needs to be pointed out that at the time of writing of the original NEST-HYMERES proposal (March 2019), several PANDA tests and analytical activities for the topics 1,2, and 3 mentioned above had already been presented to the HYMERES-2 Program Review Group (PRG) and Management Board (MB) meetings, held so far within HYMERES phase 2. The HYMERES-2 Management Board had endorsed the

possibility to embed a NEST component (i.e. the activities described in the present document) within HYMERES-2 from 2019 onwards, and strongly welcomed the NEST initiative as a timely investment.

4 Progress made so far in NEST-HYMERES

With the HYMERES-2 project having had started in 2017 already, it was originally anticipated that the first NEST fellows could arrive at PSI as soon as in spring 2018. The Swiss Federal Office of Energy therefore granted financial support for the NEST-HYMERES initiative starting in October 2017 (hence the start date of the SFOE project at hand, i.e. the "Implementierung einer Nuclear Education, Skills and Technology (NEST)-Ausbildungskomponente in das HYMERES-2 Projekt der OECD/NEA zusammen mit dem Paul-Scherrer Institut" was chosen to be 1st of October 2017).

However, the formation of a new international nuclear education and training scheme like NEST turned out to be a rather formidable task, and it took ultimately until 15th of February of 2019 (!) that the NEST framework could be formally established amongst the initial 10 NEST member countries. The formal reception of NEST fellows at PSI within NEST-HYMERES could thus not take place earlier than 2019. In fact, the formal completion of a NEST-HYMERES project agreement between all partners involved in NEST-HYMERES took until June 2021 (!). The complete project agreement with all signatures and appendices can be found in Appendix A.

The implementation of NEST activities within the HYMERES-2 project has been planned through the four following means:

1. **NEST internships** embedded in master projects, or as part of PhD or post-doctoral program, where the NEST fellow receives a mobility grant and per diem to allow for an extended stay at another research institution;
2. Active presence and **participation of NEST fellows during the HYMERES-2 experimental test** campaigns and in the accompanying project meetings;
3. **HYMERES-2 Workshops** and dedicated **NEST educational events**;
4. **Participation of NEST fellows in conferences, international workshops, etc.** that are generally relevant to the overarching field of severe accidents and containment behavior.

While writing the NEST-HYMERES proposal together with the partners in 2019, it was estimated that up to 18 NEST Fellows could potentially be hosted at PSI, with some more fellows across the research network (as it is depicted in Figure 2). The original work plan is attached to this this report in Appendix A, and gives a good insight into the wealth of proposals for research work suitable for NEST fellows.

In 2019, the following four NEST fellows were hosted at the Paul Scherrer Institut (for a brief overview of these fellows and their achievements, consult the NEA webpage: https://www.oecd-nea.org/jcms/pl_25328/2019-nest-fellows):

- Carlos Vászquez-Rodríguez (Universidad Politécnica de Madrid, Spain), for analytical activities (H2P4 test series) using the CFD containment code GOTHIC, **for three months;**
- Stephen King (Texas A&M, USA), for analytical activities (H2P1 series) using the CFD code FLUENT, **for four months;**

- Lea Zimmermann (ETH Zürich, Switzerland), for the experimental Characterization of Flow Velocity Development Downstream of Tube Bends, **for six months;**
- Kevin Manoha (McMaster University, Canada), for testing/exploring new measurement techniques e.g. a fast gas concentration sensor, **for 12 months;**
- Dmitry Grishchenko (KTH, Sweden), for the experimental thermal-hydraulics, modelling and simulations, safety and risk analysis for GEN-III and IV nuclear reactors and SMRs; **for three months.**

In February 2020, three students/NEST fellows from Texas A&M University joined PSI for a NEST fellowship. For each of them, a duration of stay between 3 and 6 months was foreseen:

- Michael Gorman,Texas A&M, USA
- Denise Chavez, Texas A&M, USA
- Brent Hollrah, Texas A&M, USA

However, due to the emerging Covid-19 pandemic, all of these students needed to be sent home again only two weeks after their arrival, such that their originally intended research goals could not be achieved.

Due to the pandemic situation from March 2020 until the time of writing of this report (December 2021), the hosting of NEST fellows was basically not practical, therefore the NEST-HYMERES activities came to a sudden and practically complete halt. Until today the project is far away from the originally targeted eighteen fellows by 2021. For that reason, a cost-free extension of the NEST-HYMERES support contract until December 2023 has been requested from the SFOE and recently been granted. It is expected that another two years of project duration should be sufficient to reach the originally targeted number of fellows, provided the pandemic crisis will come to an end in 2022.

5 Technical Achievements in NEST-HYMERES

The project HYMERES-2 was officially concluded on June 30, 2021; the final report of HYMERES-2, prepared by the PANDA team at PSI, has been submitted in a timely manner to the OECD/NEA and the HYMERES-2 participants and is currently (status of December 2021) under review by the partners. With the explicit permission of the HYMERES-2 project partners, we include in this intermediate NEST-HYMERES report the one specific section of the HYMERES-2 final report, which is dedicated to the work of the NEST fellows, in particular those five students that were hosted at PSI in 2019 (see section 4 above).

The students performed their activities primarily at PSI and the duration of the internship at PSI was between 3 months to 1 year. In some cases, the students continued to be involved in the HYMERES-2 project also after the completion of their NEST activity in Switzerland.

Below are some outcomes from the NEST activities in HYMERES-2.

5.1 Separate effect experiments in IDEFIX small scale facility

This NEST activity related to the HYMERES-2 project was carried out by Ms. Lea Zimmermann (ETH Zurich), supervised at PSI by Dr. Ralf Kapulla and has contributed to her thesis for a Master of Science degree in nuclear engineering at ETH Zurich (see Appendix B).

The activity consisted in performing separate effect experiments in a small- scale facility providing experimental data suitable also for the interpretation and analyses of PANDA experiments. In fact, within the H2P1 series (subseries H2P1p-sh and H2P1g-sh), several PANDA experiments were carried out using the injection pipe shown in PANDA vessel 1, Figure 5.1.

Figure 5.1: Rendering of PANDA Vessel 1 and the injection line.

The injection pipe has several bends and the length of the pipe after the last bend is 10 times the exit diameter of the injection pipe. Therefore, it is to be expected that the flow is not fully developed and that the bends have an effect on the exit flow velocity profiles. Characterization of 2D velocities near the exit of the injection pipe were performed in PANDA. However in PANDA it is challenging (due to the location of optical accesses and overall vessel dimensions) to perform detailed 3D characterization

of flow exit velocities which could provide more insight on the effect of bend to the exit flow velocity. The characterization of tube exit velocities is a very important initial and boundary condition for the CFD analyses. The NEST activity consisted in designing scaled tubes (shown in Figure 5.2) in separate set-ups (IDEFIX facility at PSI/NES/LRT) where 2D and 3D PIV can be more easily used to characterize tube exit velocities.

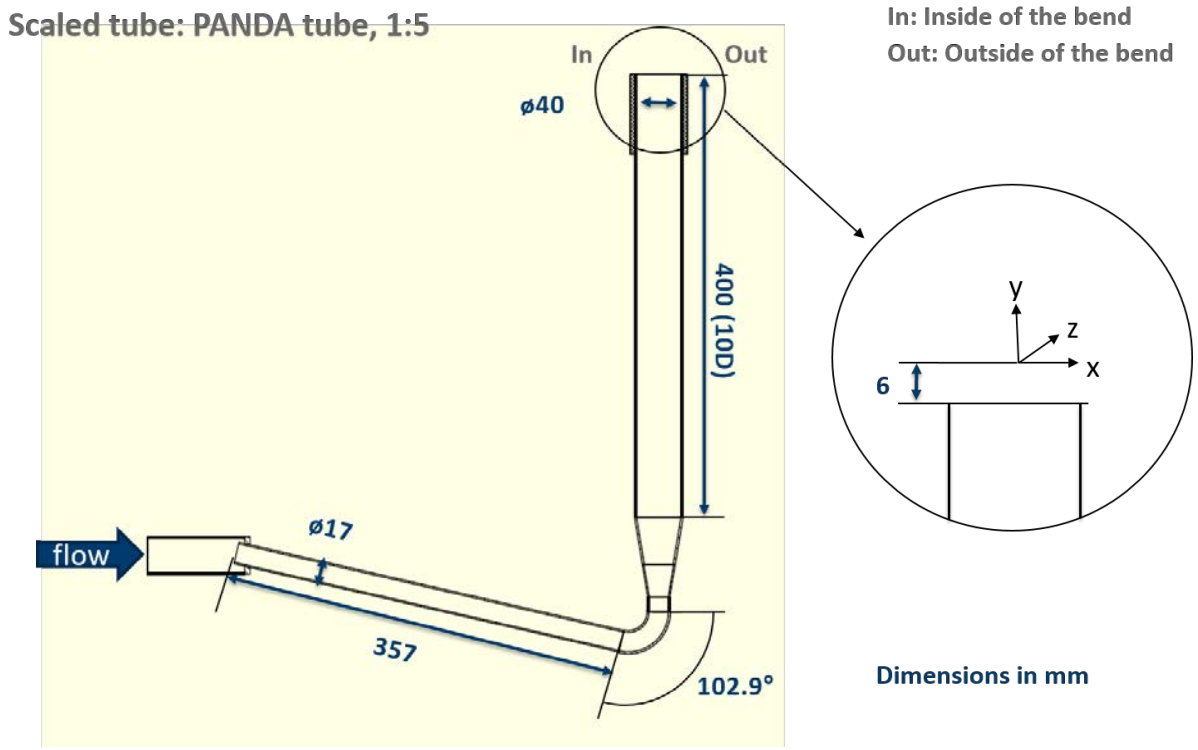

Figure 5.2: schematic of the scaled (1:5) injection pipe.

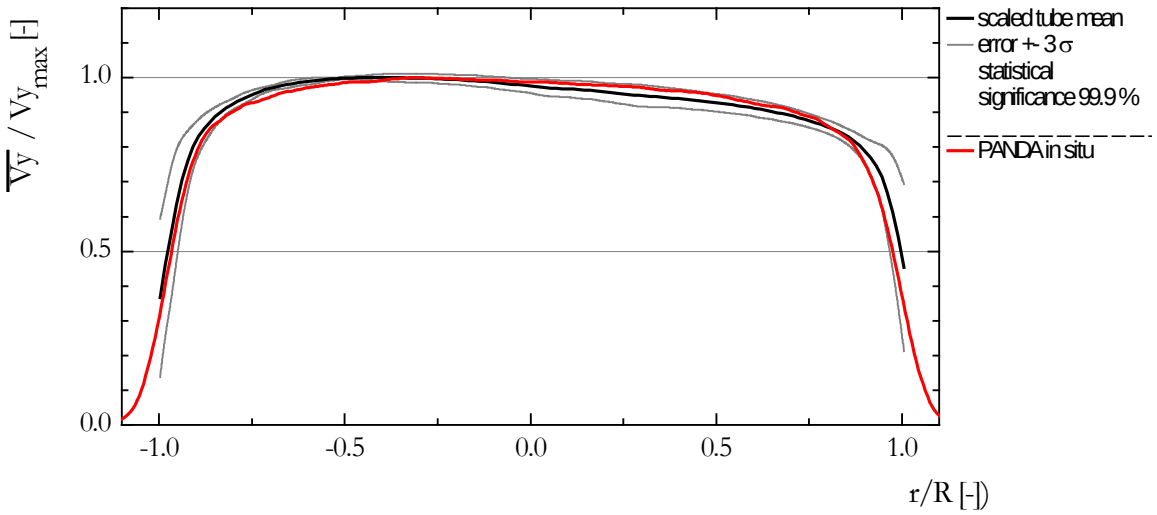

Figure 5.3: Horizontal velocity profiles of the axial velocity measured in PANDA are compared to the scaled tube results for the mid-plane of the tube (also named as Pos_C).

Figure 5.3 shows the horizontal velocity profiles of the axial velocity measured in PANDA compared to the scaled tube results for the mid-plane of the tube (Pos C). The velocities are normalized with their respective maximum axial velocity. The dotted lines correspond to the upper and lower margins of

the 99% confidence interval for the scaled tube results. The agreement between the measurements is fairly good and especially position C reveals that the velocity profile in PANDA is slightly flatter compared with the scaled tube velocities. The Master thesis of Ms. Lea Zimmermann included characterization of tube velocities of different injection tubes, which go beyond the scope of the present report and the H2P1 series.

5.2 Procedures to compute the CFD porous medium properties

This NEST activity related to the HYMERES-2 project was carried out by Mr. Stephen King (Texas A&M, USA), supervised at PSI by Dr. Abdel Dehbi as a NEST mentor.

Within the H2P1 series, the subseries H2P1g-sh was performed using as a flow obstruction a grating platform. In Figure 5.4 is shown a rendering of the test configuration with focus on the injection pipe and the inclined grating platform at some distance above the exit of the pipe.

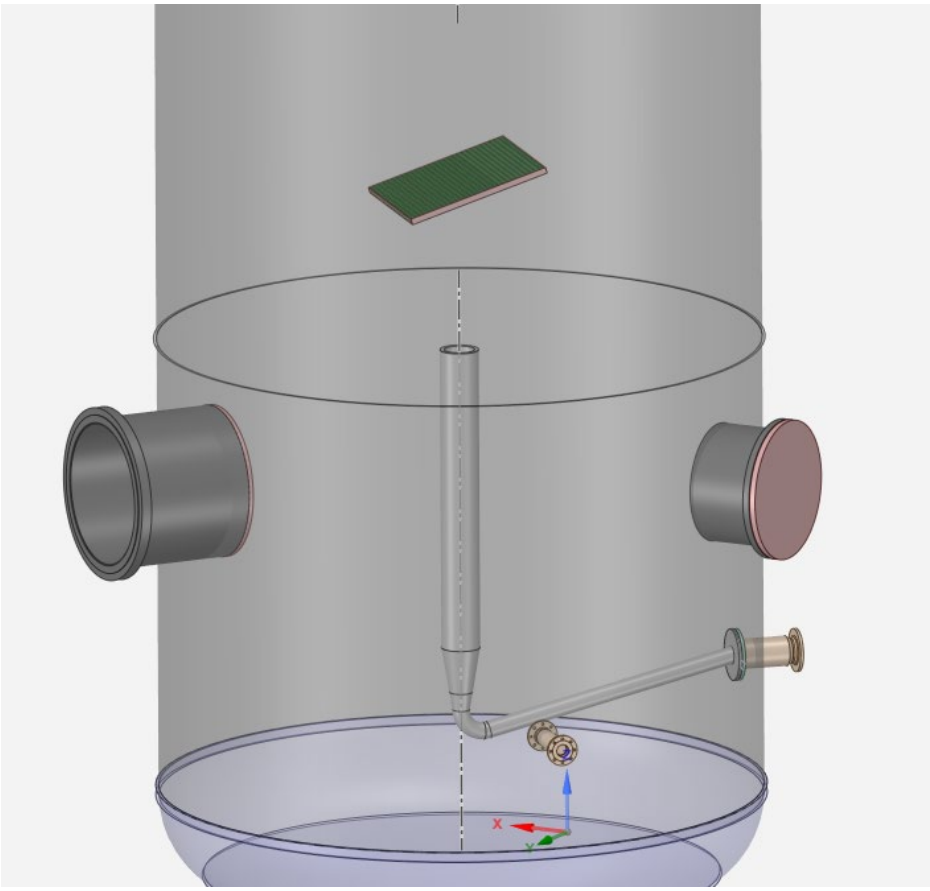

Figure 5.4. The PANDA vessel in the HYMERES-2 configuration.

A porous media volume or block was evaluated in a study to replace the inclined grid in the PANDA facility (as shown in Figure 5.4). This porous media modeling allows a drastic reduction of the number of computational cells needed to model the grating platform in comparison with a detailed model and this in turn will reduce the overall computational time by a considerable amount.

To implement the porous model, the friction factors have to be chosen and applied in each of the X, Y, Z directions to match the pressure loss of the open medium (Thin Grid).

This implementation of the porous media was done in two steps. First, a simple 2D model was created, one with the grid geometry and one with the porous block, to find the X and Y friction factors. Then a simple 3D model was constructed, one with the grid and one with the porous block, in order to find the Z vector porous coefficient. The results of the simple 2D model are shown in Fig. 5.5. The coefficients for the loss terms were tuned and transferred between the 2D and 3D cases, and the resulting tuning of the 3rd coefficient is shown in Figure 5.6.

There are important differences that could be addressed to further enhance the porous media model in the CFD code ANSYS Fluent. One major discrepancy between the physical and porous media block becomes apparent when comparing the turbulent kinetic energies (TKE), as the porous media, by default, only transfers the turbulent kinetic energy through the porous region and does not change its value. This is in contrast to the physical grid with multiple walls, which produces a higher turbulent kinetic energy downstream of the jet impingement region. To address this, a user defined function (UDF) could be designed to provide a source term in the TKE equation in order to generate the correct amount of TKE downstream of the jet impingement.

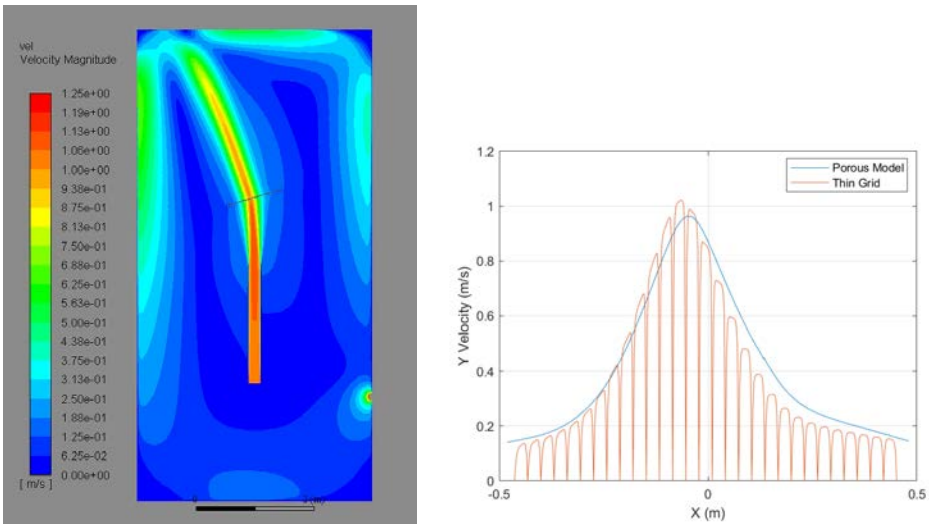

Figure 5.5. The simple 2D case (Left) and resulting vertical velocity distribution at the outlet of the grid along the horizontal axis (Right) are shown.

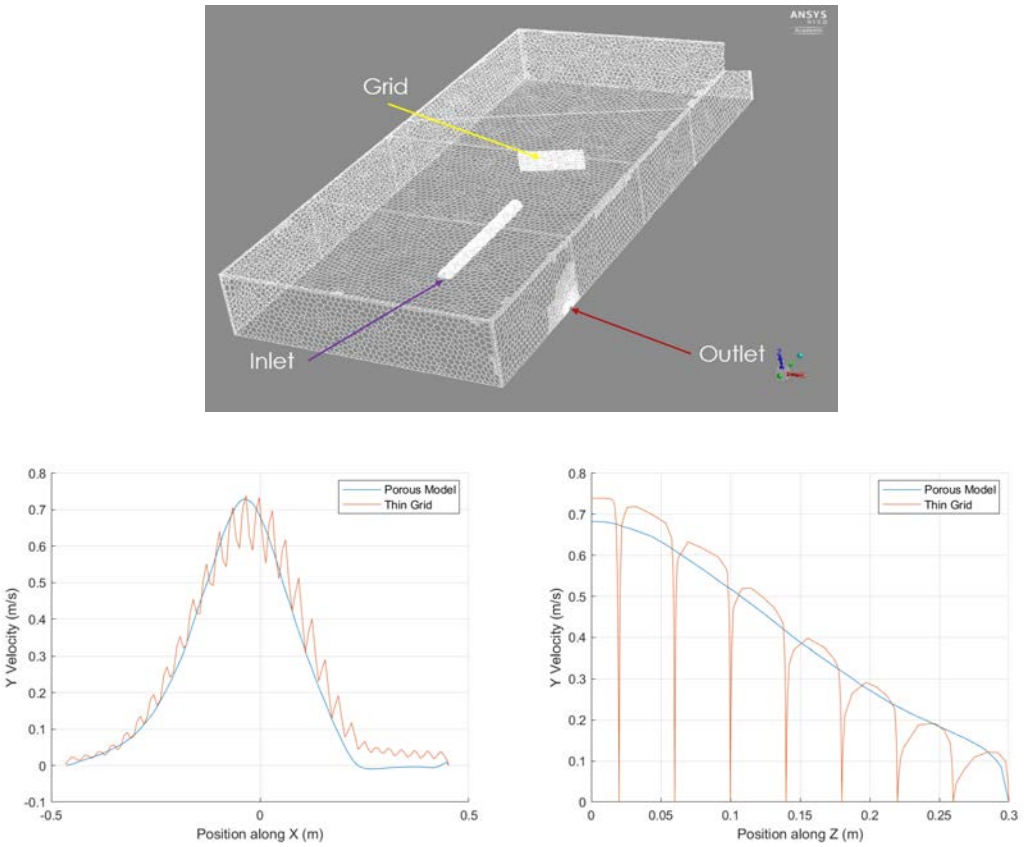

Figure 5.6. The simple 3D case (Top) and resulting vertical velocity at outlet of the grid along the horizontal axis (Bottom Left) and vertical axis (Bottom Right).

5.3 Scoping analyses to define the H2P4 PANDA experiments

This NEST activity was performed by Mr. Carlos Vázquez-Rodríguez, PhD student from Universidad Politécnica de Madrid (Spain), supervised at PSI by Dr. Michele Andreani.

The H2P4 series focused on assessing the BWR containment system response. One main concern associated with the performance of Pressure Suppression Pools (SPS) is the decrease of its heat sink capacity in case of a possible thermal stratification induced by the direct steam condensation phenomenon. If the PSP is stratified, the higher surface temperature of the pool will induce undesired faster pressurization of the containment. Thus, the scoping calculations were aimed to design experiments helping to understand the pressurization of the containment induced by the stratification of the pool.

The scoping calculations were performed with GOTHIC 8.3QA. The balance between the level of detail and the computational cost of the simulations, as well as the extensive use of the code for the pre-tests of PANDA experiments for several years, make GOTHIC an appropriate tool for designing the tests. However, the calculation of the thermal stratification of the pool is not straightforward for the code, as extensively discussed in previous works. Thus, the first task of the NEST activity was to propose a modelling approach to capture the pool stratification with GOTHIC. After several iterations,

the developed models were validated using the pool stratification experiments of the HP5 series of HYMERES. Figure 5.7 shows an example of how the proposed models were able to capture the evolution of the pool temperature above the sparger in the HP5 series. These results are a part of more extensive research, which lead to conclude that the proposed approach should be accurate enough to perform the scoping calculation on the facility pressurization.

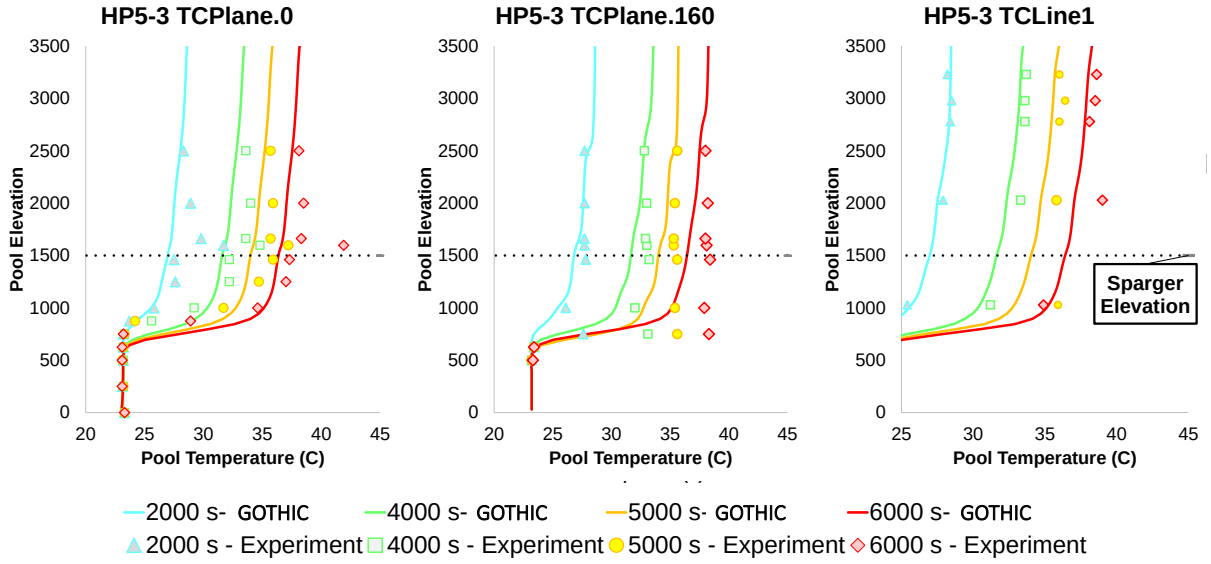

Figure 5.7. Validation of the GOTHIC models with the results of the stratification phase of the HYMERES experiment HP5-3.

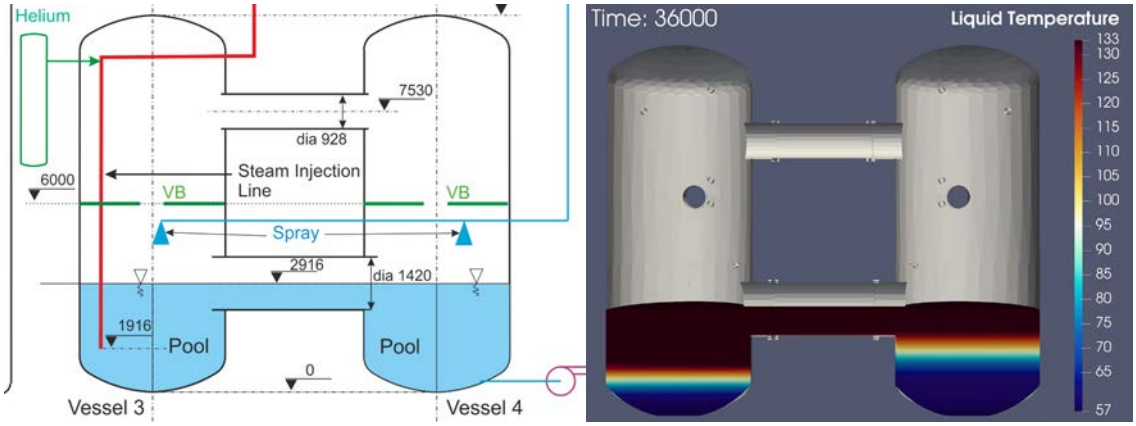

Figure 5.8. On the left, PANDA configuration for the Fukushima-like experiments; On the right, pool temperature at the end of the stratification phase.

Although the experiments performed in PANDA for the H2P4 series were eventually simplified, the initial stage of scoping calculations aimed to design an experiment based on the containment behaviour recorded during the accident of the Unit 3 of Fukushima Daichii 1. Figure 5.8 includes a sketch of the configuration of the facility intended to represent the different phases of the accident (pool stratification, spray actuation, and hydrogen release). The GOTHIC model validated with the HP5 series was used to determine the initial and boundary conditions inducing an evolution of the thermal-hydraulics of PANDA, representing the main phenomena of a plausible explanation of the accident evolution. For example, Figure 5.8 below shows the pool temperature after 10 hours injecting steam, which was the duration of the stratification phase required to reach the pressure recorded at

Fukushima injecting the same mass flow rate of steam as in the HP5 series at 1 m depth. Also as an example of characteristic analyses for the scoping calculations, Figure 5.9 shows an evaluation of the initial temperature required to reach the target pressure (>3.5 bar) in acceptable times (<10 hours).

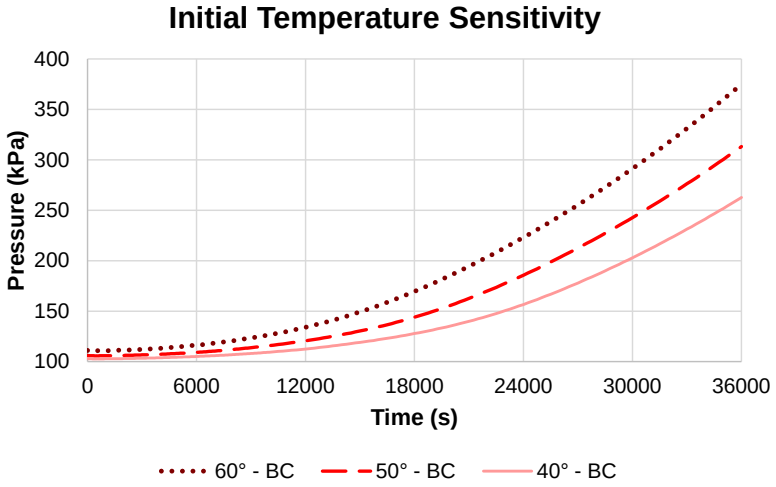

Figure 5.9. Sensitivity of the pressure evolution to the initial temperature of the pool.

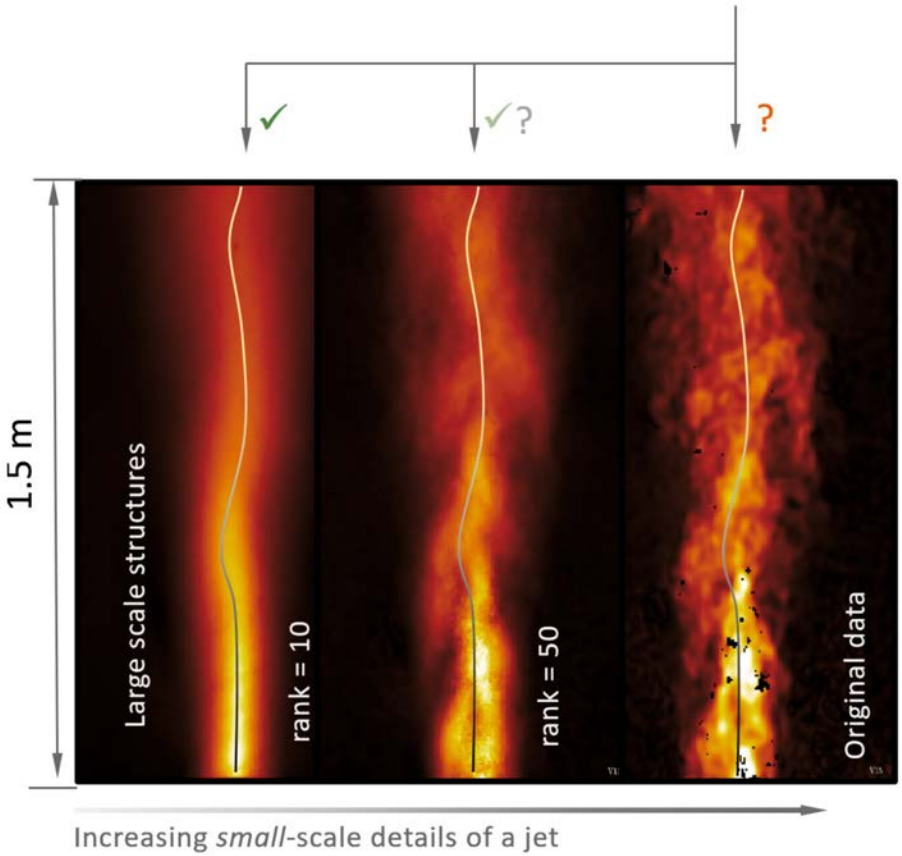

Figure 5.10: Visibility of the meandering of a jet as a function of the POD approximation.

5.4 POD Analysis of a Large-Scale Turbulent Round Jet

This NEST activity related to the HYMERES-2 project was carried out by Mr. Kevin Manohar (Calgary University), supervised at PSI by Dr. Ralf Kapulla.

The entire study is an experimental investigation into the self-similarity behavior of first and second order statistical quantities derived from a large-scale jet flow taken from one of the experiments in the PANDA facility using the Proper Orthogonal Decomposition (POD). A more general discussion of the underlying dimensional analysis in terms of self-similarity for physical processes can be found in in the context of the π-theorem [1]. What is presented, are the merits, the potential and the characteristics of the corresponding underlying POD analysis. Proper Orthogonal Decomposition (POD) is a mathematical framework to extract large-scale structures which are otherwise masked by the complexity of the fully turbulent flow; example: the meandering of a jet which is not so obvious for the original data as shown in Figure 5.10.

Background

Even though experimental results or numerical simulations typically have a high dimensionality (degrees of freedom), they can often be well-characterized by (low-dimensional) dominating coherent structures. In this context, it is worth mentioning, that in contrast to the increasing availability of highly resolved data obtained from experiments and numerical simulations, there is a correspondingly significant need to describe high-dimensional fluid systems in a more elementary fashion. This is because low-dimensional data could highlight certain flow features that are otherwise masked (and are therefore not accessible) because of the complexity of the fully turbulent flow. These reduced order models (ROMs) effectively filter out the small-scale turbulent structures, which do not contribute much to the convergence towards a valid representation of the essential flow physics according to Hamilton [2]. Proper Orthogonal Decomposition (POD) is a mathematical framework to extract and characterize these large-scale structures, as initially outlined and suggested by Lumley [3].

As a gentle introduction to the POD method, it is stated, that for a Fourier decomposition of a time dependent signal *f(t)* according:

$$f(t) = a_0 + \sum_{n=1}^{\infty} \left\{ a_n cos\frac{n\pi t}{L} + b_n \sin\frac{n\pi t}{L} \right\}$$

the basis functions for the approximations of the signal *f(t)* – *sine* and *cosine* – are known and the problem posed is to derive the coefficients a_0, a_n and b_n to represent the function *f(t)* with an appropriate – and hopefully sufficient – truncation. The respective truncation depicts a maximum value of *n* for which the summation is finally stopped to sufficiently represent the underlying signal for the present purpose – much below the required infinite limit of ∞ as outlined by the theory to fully represent the signal.

A POD analysis can be understood and treated as an extension and generalization of the Fourier decomposition of a signal in space and time [4], with the corresponding problem on where and by what criteria to truncate the corresponding approximation. It was outlined above, that for a Fourier decomposition; the basic functions – sine and cosine – are well known. This is now fundamentally different for a POD analysis!

If we consider the approximation of an instantaneous 2D velocity field u(**x**,t) based on an ensemble of N instantaneous velocity fields through a POD analysis, this results in this framework in the following POD approximation:

$$\mathbf{U}(\mathbf{x},t) = \sum_{n=1}^{N} \mathbf{\Phi}_{\mathrm{n}}(\mathbf{x})\mathbf{T}_{\mathrm{n}}(\mathrm{t})$$

The POD algorithm separates the spatio-temporal ensemble of velocities **U** into space-dependent orthonormal POD modes **Φ** (spatial modes, also referred to as the basis functions) and time-dependent orthogonal modes **T** (referred to as temporal modes), respectively. For the algorithm on how to calculate the POD decomposition for a given ensemble of velocity fields or other data see Sirovich [5]. It is worth mentioning at this point, that the basis functions $\Phi_n(x)$ as well as the coefficients $T_n(t)$ are a priori unknown and have to be derived from the data itself. In that, the POD method is data driven.

Results

As for a Fourier decomposition, the POD approximation of the velocity field is usually truncated after a few modes. The predominant method in the literature to select the relevant basis functions for the final approximation is based on the energy of the flow the spatial modes represent. An example of the energy distribution among the spatial modes for the jet under consideration is presented in Fig. 5.11.

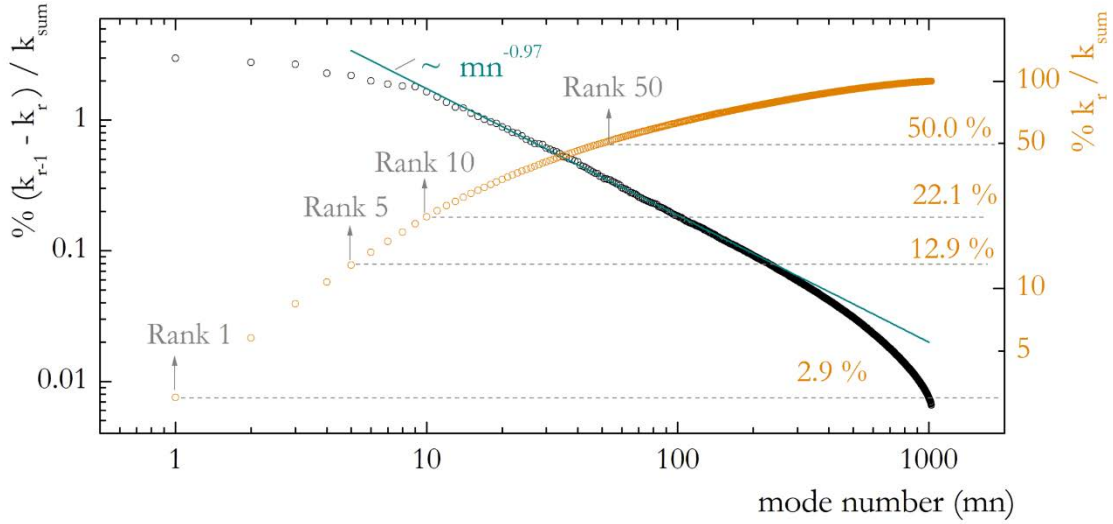

Figure 5.11: Discrete energy distribution of the single spatial modes Φ (left-scale) and the cumulative energy as represented by a potential corresponding rank approximation based on a pure energy criterion (right-scale).

In total, the energies distribute across nearly three orders of magnitude from mode 1 to mode 1024; the latter depicting the maximum number of snapshots recorded. For the mode energies, we observe a distinct slope change around mode ≈ 10, i.e. we find modal energies within the same order of magnitude for mn < 10 whereas the energies past mn > 15 decay more rapidly. The former region is

usually attributed to the importance these modes have for the reconstruction of the flow field. In contrast to this, it was possible to show, that spatial modes which are usually not caught by a pure energy-based criterion also play an important role in the reconstruction of the flow field. A refinement of this energy criterion for the relevant modes to be considered for the truncation can be found in [6].

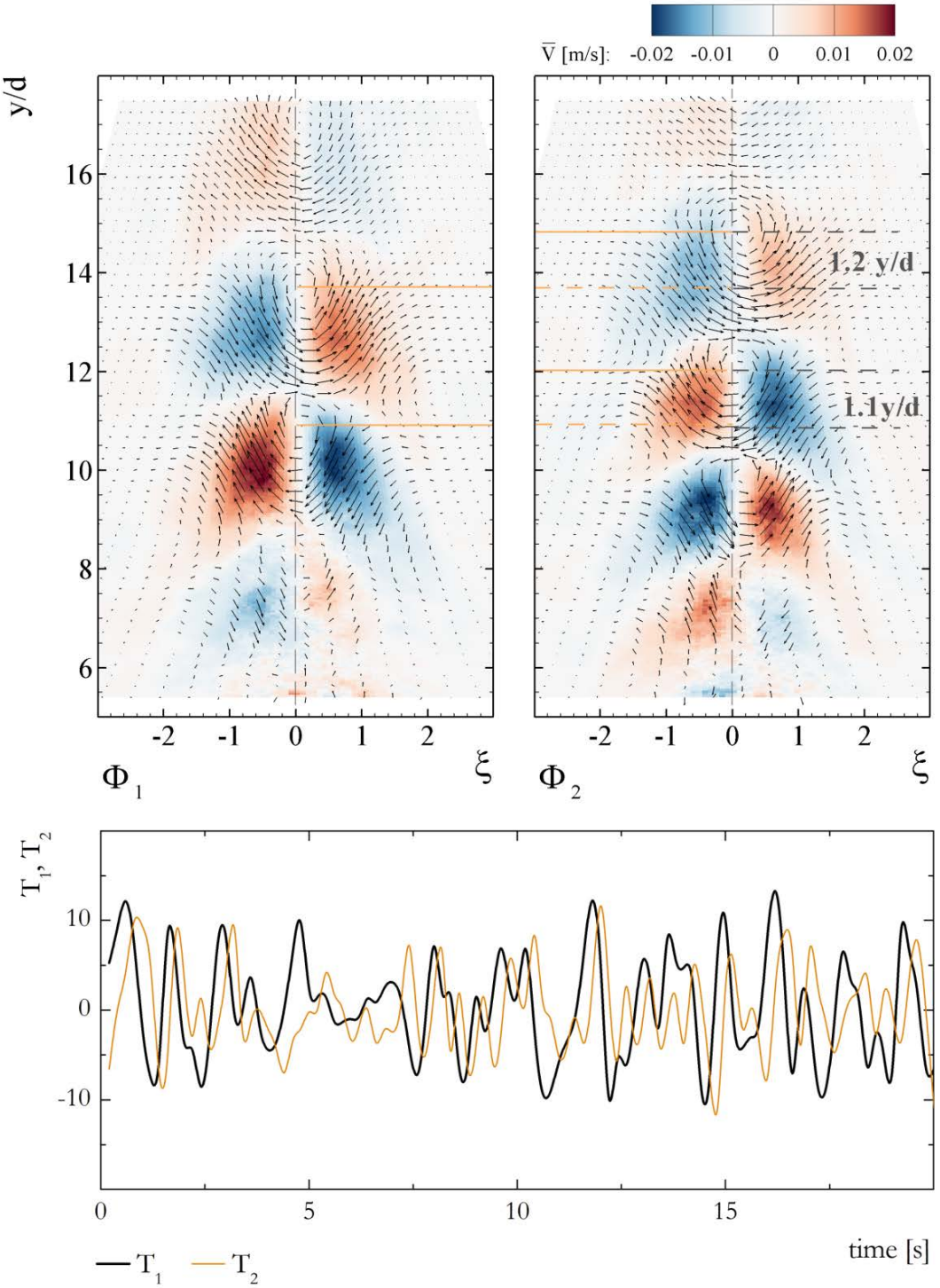

Figure 5.12: First two spatial modes Φ_1 and Φ_2 and the corresponding temporal modes T_1 and T_2 from a POD analysis of the round jet H2P1_17 recorded in the PANDA facility.

Examples of the resulting spatial and temporal modes are presented in Fig. 5.12. The spatial structures of the first two spatial modes Φ_1 and Φ_2 are almost identical showing the presence of 3 successive large-scale vortical structures downstream of y/d ≈ 8 which are centered around ξ ≈ 0, except that they experience a spatial phase shift with y/d ≈ 1.15 – or multiples of it. This opens the door for a refined analysis of these structures and their importance towards the route to and their importance for self-similarity of the entire flow field. A classical subject of fluid dynamics.

Conclusions

- It was shown that experiments conducted in the PANDA facility might be subject to a refined analysis provided through the Proper Orthogonal Decomposition (POD).
- It was possible to show, that spatial modes which are usually not caught by a pure energy-based criterion for the POD also play an important role in the reconstruction of the flow field.
- The more elaborate results and conclusions can be found in the corresponding publication [6].

References to chapter 5.4

[1] L. Yarin, The PI-Theorem - Applications to Fluid Mechanics and Heat and Mass Transfer, Springer, 2012.

[2] N. Ali, N. Hamilton, D. DeLucia, R. Bayoán Cal, Assessing spacing impact on coherent features in a wind turbine array boundary layer, Wind Energy Science 3 (2018) 43?56.

[3] J. L. Lumley, The structure of inhomogeneous turbulent flow, in: Atmospheric Turbulence.

[4] S. L. Brunton, J. N. Kutz, Data-driven science and engineering – Maschine learning, dynamical systems and control, Cambridge University Press, 2019.

[5] L. Sirovich, Turbulence and the dynamics of coherent structures. Part I, Quarterly of Applied Mathematics (1987).

[6] R. Kapulla, K. H. Manohar, S. Paranjape and D. Paladino, Self-similarity for statistical properties in low-order representations of a large-scale turbulent round jet based on the proper orthogonal decomposition, Experimental Thermal and Fluid Science, Volume 123, 2021, 110320.

6 Conclusion on the current Status of NEST-HYMERES

Despite the setback of the NEST-HYMERES project due to the Covid-19 pandemic in particular, and of the entire NEST program in general, the concept of NEST has been unanimously described as success by the NEST participating NEA countries, and the institutions working on NEST projects. More information on NEST, dissemination of results, feedback reports by NEST fellows (amongst which are also those of two NEST-HYMERES fellows, Lea Zimmermann: https://www.oecd-nea.org/jcms/pl_60923/insights-into-the-nest-framework-a-chat-with-lea-zimmermann, and Stephen King: https://www.oecd-nea.org/jcms/pl_60358/insights-into-the-nest-framework-a-chat-

with-stephen-king), NEST leaflets etc. can be found on www.oecd-nea.org/nest. The last project meeting of NEST-HYMERES took part in early December 2021. All NEST-HYMERES participating partners confirmed their continued interest in the NEST activity, and several institutions have committed to sending NEST fellows to PSI (and other partners within the network), as soon as the pandemic situation would allow them to do. The PSI NEST-HYMERES team (including the author of this report) are therefore confident, that NEST-HYMERES can be brought to successful conclusion until 2023, albeit with very significant delays.

Appendix A: NEST-HYMERES-2 PROJECT AGREEMENT

NEST-HYMERES-2 PROJECT AGREEMENT

This Agreement is made the 26th day of the 02nd month of the 2021 year

BETWEEN:

Paul Scherrer Institut (PSI), whose registered office is at Villigen PSI, Switzerland,

AND Forschungszentrum Jülich GmbH, represented by its Board of Directors, for: Nuclear Waste Management and Reactor Safety - IEK-6, established at Wilhelm-Johnen-Straße, 52428 Jülich, Germany, hereafter "JUELICH",

AND Oregon State University, whose registered office is at Corvallis, USA,

AND Texas A&M Engineering Experiment Station, whose registered office is at College Station, USA,

AND Royal Institute of Technology (KTH), whose registered office is at Stockholm, Sweden,

AND Universidad Politécnica de Madrid (UPM), whose registered office is at Madrid, Spain,

AND Seoul National University R&DB Foundation, whose registered office is Seoul, South Korea,

AND École Polytechnique Fédérale de Lausanne (EPFL), whose registered office is at Lausanne, Switzerland,

AND The University of Tokyo, Japan, whose registered office is at Tokio, Japan,

AND The Governors of the Calgary University, Canada, whose registered office is at Calgary, Canada,

AND Institut de Radioprotection et de Sûreté Nucléaire (Institute for radiological protection and nuclear safety - IRSN), a French public body with industrial and commercial activities regulated by articles L592-45 to L592-49 and R592-39 to R592-61 of the French Environmental Code, registered at the RCS (Companies Register of Nanterre-France) under number 440 546 018, having its registered office at 31 avenue de la Division Leclerc,

92260, Fontenay-aux-Roses, France, and represented by Mr Jean Christophe NIEL, Director General,

AND The Centre National de la Recherche Scientifique, a public scientific and technological establishment, having its registered office at 3 rue Michel-Ange 75794 Paris cedex 16, represented by its CEO, Mr Antoine PETIT who has delegated signing authority for this agreement to the Regional Representative of the Délégation Centre Limousin Poitou Charentes, Mr Ludovic Hamon at 3E, avenue de la recherche scientifique - 45071 Orléans Cedex 2 – France, Hereinafter referred to as the "CNRS", the CNRS acting on its own name and on behalf of the Institut de combustion, aérothermique,réactivité et environnement (ICARE), Research Unit n° 3021, directed by Mr Philippe DAGAUT. Hereinafter referred to as "ICARE".

(hereinafter individually referred to as a "Participating Organisation" and collectively as "the Participating Organisations"; Paul Scherrer Institut may also be referred to as the "Leading Organization").

Preamble

Considering that the NEST-HYMERES-2 Project ("Project") aims to advance the understanding around the release, distribution and mitigation of hydrogen in Light Water Reactor containment structures, and to study suppression pool systems issues, with the goal to enhance modeling capabilities in support of safety assessments for current and new nuclear power plants, which is a key aspect in the safety assessment of Light Water Reactors;

Considering that the scope of work proposed in this Agreement is of interest to the Participating Organisations and they want to collaborate in providing resources and expertise;

Considering that the Paul Scherrer Institut (PSI) has the necessary expertise and facilities to lead the proposed Programme of Work;

The Participating Organisations agree to take part in the NEST-HYMERES-2 Project on the terms and conditions described in this Project Agreement ("Agreement").

Details of the Project are described in the "Proposal for the Implementation of a NEST Component in the OECD/NEA/CSNI Project HYMERES-2" (Appendix A), which was accepted by OECD/NEA on July 24th, 2019 (see Appendix C, Acceptance letter of the OECD/NEA for NEST-HYMERES-2).

IT IS HEREBY AGREED AS FOLLOWS:

Art. 1. Purpose

The purpose of this NEST-HYMERES-2 Project Agreement is to implement the Project within the overall NEST Framework Agreement (Appendix B). This Agreement sets out the relationship between the Participating Organisations and the organisation of their work.

Art 2. Leading Organisation and Participating Organisations

The Paul Scherrer Institut will act as the Leading Organisation among the Participating Organisations listed above.

The Leading Organisation provides the necessary professional guidance to coordinate and structure research collaborations around a number of evolving case studies (proposed by each Participating Organisation) dedicated to understanding release, distribution and mitigation of hydrogen in Light Water Reactor containment structures, and as well pressure suppression pool phenomena and issues.

Participating Organisations will provide educational training to NEST Fellows, will coordinate placement of NEST Fellows for short-term cross-institution training opportunities, and facilitate placement in international summer schools or other internship opportunities.

Art 3. Management Structure

The Project will be led by Prof. Andreas Pautz at Paul Scherrer Institut, who will act as Project Coordinator. He will be assisted by Dr. Domenico Paladino at the Paul Scherrer Institut who will act as Assistant Project Coordinator. The persons assigned as Project Coordinator and Assistant Project Coordinator can be replaced by their country's NEST Management Board member from time to time without a need to amend this Agreement.

The Project will have a Project management board ("Project Board"). This board will consist of a lead investigator from each Participating Organisation. Project decisions will be made by consensus of the Project Board. If consensus cannot be reached, decisions will be made by the Project and Assistant Project Coordinators, consistent with the Articles of this Project Agreement. If the Project and Assistant Project Coordinators cannot agree, the decision will be made by the NEST Management Board in accordance with Article 3(d) of the NEST Framework Agreement. No rights or powers may be vested in the Project Board unless the Participating Organizations expressly so agree in writing.

Art 4. Duration of the NEST-HYMERES-2 Project

The NEST-HYMERES-2 Project will be carried out for a three-year term, which has started on July 24th, 2019 and is set to end on July 23rd, 2022, with funds being available from the OECD/NEA/NEST program.

Art 5. Programme of Work

The NEST-HYMERES-2 project's Programme of Work covered by this Agreement includes:

1. NEST fellowships embedded into master thesis projects, or being part of PhD or post-doctoral programs, or for young professionals;
2. Active presence and participation of NEST fellows during the HYMERES-2 experimental test campaigns and in the accompanying project meetings;
3. Workshops, seminars and dedicated NEST educational events; and
4. Developing dedicated exploratory research tasks (e.g. based on experimental and/or analytical activities in LWR containment safety) that engage the professors at the Participating Organizations in order to ensure continuity. These tasks may also be carried out in timeframes and for research areas beyond the HYMERES-2 project.

The basis for the Project's Programme of Work, in particular the anticipated fellowships and exploratory research tasks, are described in Appendix A. Appendix A may be frequently updated by consensus of the Project Board, depending on the availability of NEST fellows and research tasks. For the avoidance of doubt, a revision of Appendix A shall not affect the terms of this Project Agreement, which shall continue to take precedence.

Art 6. Budget, allocation, expenditure and claims

Budget

The budget of the Project originates from different sources of funding e.g.:

- Direct NEST contributions, from funding available at the OECD/NEA through the NEST initiative ;
- National funds;
- Funds for other projects closely related to NEST, e.g. HYMERES-2, or others projects.

The present Project Agreement provides the indications for the management of the direct NEST contribution. The other sources of funding are managed through separate project contracts/agreement with the specific project sponsors or consortia. While Participating Organizations of NEST-HYMERES-2 from non-NEST member countries (the NEST member countries are currently: Belgium, Canada, France, Germany, Italy, Japan, Korea, Russia, Switzerland, United States of America) cannot financially benefit from the direct OECD/NEA NEST contribution, they may be financially supported through separately managed funding sources upon separate agreement with other Participating Organizations.

The direct NEST contribution originates from the OECD/NEA, collected through the NEST membership fees of the NEST participating countries. This contribution will be transferred from the OECD/NEA to the Leading Organisation, being Paul Scherrer Institut, which takes over responsibility to manage the project funds with due diligence.

The Participating Organisations shall share the qualitative awareness of the different resources mobilized to guarantee the implementation of the Project.

The Participating Organisations, provided they are beneficiaries of the direct NEST contribution, shall report quantitatively to the Project Board on the expenditure arising from the these contributions in the frame of the NEST/HYMERES-2 Project.

The Participant Organisations shall not have the obligation to report on the non-NEST contributions but are encouraged to include non-NEST contributions as a way of demonstrating the value of the overall NEST framework.

Expenditure and Claims

The Participating Organizations may invoice Paul Scherrer Institut for the mobility grant and per diem, as described in Article 7 of this Agreement, for accepted NEST Fellows affiliated to their institution. Invoices to Paul Scherrer Institut must be accompanied by official NEST-HYMERES-2 Project Board approval as described in Article 7 of this Agreement. Official Project Board approval will indicate the amount of the mobility grant and per diem (guiding figure: 6'000 € per fellow). These funds are intended for NEST Fellows from NEST member countries only. Institutional overhead is not supported. Invoices will not be paid unless an Approval Notice (hereinafter defined) has been submitted along with the invoice. Invoices shall be for no more than the amount indicated on the official Project Board approval. Invoices will be settled on a first come first serve basis and have to be submitted in Euros. Invoices will not be paid if the NEST account at Paul Scherrer Institut contains insufficient funds, as determined at Paul Scherrer Institut's sole discretion. Payment of invoices is conditional on Paul Scherrer Institut's receipt of funding from OECD.

Invoices shall be submitted to:

Paul Scherrer Institut
Prof. Andreas Pautz
Head of Nuclear Energy and Safety Division
Forschungsstrasse 111
CH-5232 Villigen PSI
Tel: +41 56 310 3497
Andreas.Pautz@psi.ch

Reporting

As a condition of receiving funding,under the Approval Notice, and as a necessary condition for receiving NEST fellowship certificates for the Participating Organization's fellows, the Participating Organizations are required to report to the Leading Organization on the progress of their contribution to the NEST-HYMERES-2 project no later than September 1 of every year for the preceding twelve (12) months period during which funding has been received. This report should be submitted to Prof. Andreas Pautz (Andreas.Pautz@psi.ch) and Dr. Domenico Paladino (Domenico.Paladino@psi.ch) unless otherwise requested. The reports should include the following information:

Main Information:

1.1. Name of NEST project, Acronym
1.2. Years from-to:
1.3. Duration:
1.4. Year of reporting:

2. NEST Fellows

Please complete for each fellow (add a section for each additional fellow)

2.1. Fellow name
2.2. Home Organization, Country
2.3. Host Organization, Country
2.4. Date from/to:
2.5. Experience/Education level: MSc/PhD/PostDoc/Young Professional
2.6. Expectations on the competences to be acquired
2.7. Summary of competences acquired (copy and paste from the self-assessment done by the Fellow in his/her reporting):

- Technical
- Behavioural and social
- Innovative capacity

3. NEST Project contribution

3.1. Description of the contributions to the project and activities planned
3.2. Short description of the objectives planned
3.3. Objectives met vs criteria for the project

Highlight how the objectives were met in relation to the NEST criteria for projects, which are:

- ***Multinational*** *- include at least 3 NEST countries*
- *Address concrete and* ***multidisciplinary*** *challenges in the field of nuclear science, technology and applications*
- *Offer* ***hands-on*** *training opportunities in the field of nuclear science, technology and applications to NEST fellows. The Parties are also encouraged to offer skills development and education programmes*

3.4. E&T activities, any workshops and summer schools

Describe the E&T activities, workshop and summer schools that took place and any other conferences where the Fellow participated

3.5. Skills and Competences acquired by Fellows

Describe how the project and activities carried out during the Project allowed the Fellows to acquire the required competences (what theoretical and practical experiments, case studies were conducted, training on instrumentation etc…)

3.6. Competences and Knowledge transfer

Describe how the transfer of competences and knowledge was reached in the Participating Organization

3.7. Exploratory research projects

Describe how the Fellows applied the knowledge and competences to address real-world issues and challenges and developing technologies.

4. **Follow-up activities**

   Describe what other follow-up activities are taking place in the Participating Organization to develop further these competences which were not initially planned

5. **Outcomes and impacts**
   - *Describe the outcomes and impacts reached by the Participating Organization's contribution to the NEST project*
   - *Describe any discrepancy with the outcomes and impacts of each Activity within the Project as anticipated in the Programme of Work.*

6. **Future recommendations on the NEST Projects and the NEST Framework to the Management Board**

Mention anything it seems relevant to develop further the NEST Projects and the NEST Framework

Art 7. NEST Fellows

The process and criteria for selection of NEST-HYMERES-2 Project fellows ("NEST Fellows") under this Agreement are decided by the NEST-HYMERES-2 Project Board as described in Article 4(c)(1)v of the NEST Framework Agreement attached as Appendix B.

Participating Organisations will agree on fellowship candidates based on the criteria listed below, and any other considerations selected by the hosting Participating Organisation, and then propose the candidates to the Project Board for approval. In general, fellows from both NEST member countries and non-NEST member countries are welcome to participate in NEST-HYMERES-2. The Project Board approves candidates for a NEST Fellowship by unanimous decision, based on the established criteria. Upon Project Board approval, a notice of approval, indicating the amount of support ("Approval Notice") will be issued which will include the approved amount of support in Euros. Approved NEST Fellows and their fellowship activities will be reported to the NEST Board in accordance with Article 9 of this Agreement.

To be eligible to participate as a NEST Fellow in the Project, the following criteria must be met:

- The Fellow must be either a currently enrolled student, a postdoctoral associate, or a young Professional at an institution supporting an active study as part of the NEST-HYMERES-2 Project.
- The Fellow must be in good academic standing at their home institution.
- The Fellow must be supporting the research program that is the basis for the case study.
- The Fellow must be capable of meeting the requirements for visitors for any NEST-HYMERES-2 participating organization that is hosting an exchange.

Placement and activities of NEST Fellows must be consistent with the hosting country's applicable laws, regulations and policies, including on such matters as technology transfer, export control, and immigration rules.

The selected NEST Fellows will receive a mobility grant and per diem from the NEST Budget (provided the academic institution they are affiliated to is located in a NEST member country, see Article 6) to allow for an extended stay at another research institution, as outlined in the Approval Notice.

Art 8. Collaboration Plan between NEST Participating Organisations

The NEST-HYMERES-2 Participating Organizations shall co-operate in participating in analytical activities and experimental campaigns related to the Project by using the facilities of the Participating Organizations and in organizing educational and training events together as described in Appendix A.

Art 9. Responsibilities of the Leading Organisation to the Management Board

The Leading Organisation, under the direction of Prof. Andreas Pautz and Dr. Domenico Paladino shall report to the NEST Management Board and request the decisions of the Project Board and in particular on:

a. The NEST/HYMERES-2 Project's programme of work
b. Expenditure of the NEST-HYMERES-2 Project
c. Final selection of NEST Fellows
d. Participation of an entity from a non-NEST country, in particular to its added-value to the NEST-HYMERES-2 Project and on the sources of its funding.

Art 10. Confidential Information, Publication, and Intellectual Property Rights

Confidential Information

Information exchanged between Participating Organizations must follow the provisions of the NEST Framework Agreement Article 8a, Confidential Information. For the avoidance of doubt, the Participating Organizations acknowledge and agree that information exchange between the NEST Participating Organizations and the HYMERES-2 Consortium (OECD/NEA/CSNI) will be allowed in order to enhance the knowledge base within the Project.

Publications

All Participating Organizations understand that publications are an important aspect of each Participating Institution's academic mission. All Participating Organizations shall be free to publish with the consent of

all authors and co-authors on a given publication. Authorship and co-authorship will be determined according to standard academic practice.

Publications supported under this Project Agreement shall include the following acknowledgement: "The work presented in the [paper/conference/etc.] was carried out under the auspices of the NEA NEST Framework. The authors would like to acknowledge the Nuclear Energy Agency for its support in the collaborations that supported this publication."

The experimental data which are generated within the OECD/NEA/CSNI HYMERES-2 project cannot be used for publications by the NEST Fellows, unless there is a written approval of the publication by the OECD/NEA HYMERES-2 Management Board.

Intellectual Property

If it appears that cooperative activities under this Project Agreement may result in the creation of intellectual property, the Participating Organizations concerned should enter into a written agreement therefore or restructure the cooperative activities to avoid the creation of joint intellectual property.

Participating Organisations hosting NEST Fellows may sign directly an agreement with the NEST Fellows to ensure the respect of the policies of the hosting organisation regarding the disclosure, protection and ownership of information and intellectual property rights provided to and/or arising from the Project as well as the dissemination of research information.

Intellectual property conceived, developed, or created by a Participating Organization outside the scope of the Agreement (“Background IP”) shall remain the property of such Participating Organization. Nothing herein should be construed as transferring any ownership rights to such Background IP which the original owner thereof will continue to own. Each Participating Organization commits to reference and cite the contributions of other Participating Organizations in accordance with accepted scholarly standards.

Art 11. Formalities for the Participation of the NEST Fellows

Each Participating Organisation shall ensure completion of formalities required for the execution of the Fellowships, assume responsibilities for the NEST Fellows present on its premises, and share this information with the other relevant Participating Organisations as appropriate.

When hosting a NEST Fellow, the policies of the host institution, including any formal hosting agreement, will be followed in order to allow for the administration of NEST Fellows in accordance with the host institution's established practices.

If need be, the Participating Organisation hosting the NEST Fellows may require the signature of a separate written agreement with the other Participating Organisation concerned by the hosting and/or the NEST Fellows concerned.

Art 12. Adhesion and Withdrawal of Participating Organisations

Additional Participating Organisations wishing to join this NEST project should submit a written application to the Project Board. The Project Board shall either reject or unanimously approve the application, subject to any additional conditions that it might determine and following consultation with and approval from the NEST Management Board.

A Participating Organisation may withdraw from this Project Agreement upon six-months written notice to the other Participating Organisations, unless otherwise unanimously approved by the Project Board.

Art. 13. Amendments

This Project Agreement may be amended by mutual written decision of all Participating Organizations, following consultation with the NEST-HYMERES-2 Project Board. The amendment shall be signed by the legal representatives of each Participating Organization.

Art 14. Liability

Each Participating Organization hereby releases and discharges every other Participating Organization, its faculty, staff, students, agents or employees of and from all manner of actions, causes of action, suits, claims, liabilities, losses, covenants, demands, or accounts whatsoever against any Participating Organization, its faculty, staff, students, agents or employees which Participant Organization ever had, now have or may hereafter have, arising out of this Agreement, the Project, or any component or part thereof. This liability clause shall not apply to the extent that the claim arises as a result any Participating Organization's gross negligence or the deliberate breach of this Agreement.

For the avoidance of doubt, in no event shall a Participating Organization be liable to any other Participating Organization for loss of business or profit or for any special, indirect, punitive or consequential loss or damage, regardless of whether such loss or damage arises under contract, tort, or based upon strict liability or other theory of law or equity, where such loss or damage arose in connection with this Agreement, or the Project, even if advised of the possibility of such damages or if such damages are foreseeable.

Art 15. Relationship of the Participating Organizations

This Project Agreement is not intended to create a partnership or joint venture between any of the Participating Organizations. No Participating Organization may bind or otherwise act in any way as the representative of one or more of the other Participating Organizations, unless specifically authorized, in advance and in writing by the Participating Organization, to do so, and then only for the limited purpose stated in such authorization.

The Participating Organisations have caused this Project Agreement to be duly signed by the undersigned authorised representatives in one (1) original, in separate signature pages the day and year first above written, which shall be considered as valid proof. The Leading Organisation shall send one fully signed scanned copy of the Project Agreement with the mention "Certified copy of the original" to all the Participating Organisations. The Leading Organisations shall keep the sole original copy in its files for an unlimited duration and shall give at first request of any Participating Organisation a duplicate.

SIGNATURES FOR PARTICIPATING ORGANISATIONS

The Leading Organisation

Paul Scherrer Institut (PSI)

By: _____ Date: 19.04.2021

Name: Prof. Dr. Andreas Pautz

Title: Head of Nuclear Energy and Safety Division

By: _____ Date: 19.04.2021

Name: Dr. Didier Gavillet

Title: Deputy Head of Nuclear Energy and Safety Division

Forschungszentrum Jülich GmbH

Jülich, 19.3.2021

Prof. Dr.-Ing. Wolfgang Marquardt

Chairman of the Board of Directors

i.V. Prof. Dr. Hans-Josef Allelein

Director of the Institute of Research for the safe management of nuclear waste and reactor safety

Oregon State University

By: DocuSigned by: Zach Gill 22F9CBD4E4464AE... Date: 3/4/2021 | 07:46:23 PST

Name: Zach Gill

Title: Director of Sponsored Programs, Award Contracting

Texas A&M Engineering Experiment Station

By: Marcie Avery Digitally signed by Marcie Avery Date: 2021.04.29 11:05:01 -05'00' Date:_____

Name: Marcie Avery

Title: Assistant Director, Contracting
TEES Contracting Officer

Royal Institute of Technology (KTH)

Date:_____

By:_____

Name: Sandra Di' Rocco.

Title: Head of school

Universidad Politécnica de Madrid (UPM)

Name: Prof. Asunción Gómez-Perez

Title: Vice-Rector for Research, Innovation and Doctoral studies

By:_____ Date: 15 MAR. 2021

Seoul National University R&DB Foundation

By: Haecheon Choi Date: 08 March, 2021

Name: Haecheon Choi

Title: Head of Seoul National University

R&DB Foundation

École Polytechnique Fédérale de Lausanne (EPFL)

By:_____ Date: **18.03.2021**

Name: **Prof. Dr. Andreas Pautz**

Title: **Professeur ordinaire, Directeur du Laboratoire de physique des réacteurs et de comportement des systèmes (LRS)**

University of Tokyo

By: General Manager Date: Mar. 18. 2021

Name: Takashi Mitomo

Title:

University of Calgary

By: _____ Date: APR 1 2 2021

Name:

Title:

Robert I. Thompson P.Phys., Ph.D
Associate Vice-President (Research)
Director of Research Services
University of Calgary

Institut de Radioprotection et de Sûreté Nucléaire (IRSN)

By:_____ Date:_____

Name: Jean-Christophe NIEL

Title: Director General

Signature numérique de Jean-Christophe NIEL
Date : 2021.04.19 16:31:13 +02'00'

Centre National de la Recherche Scientifique (CNRS/ICARE)

By:_____ Date: 23 MARS 2021

Name:

Title:

Pour le Délégué Régional,
l'Adjointe au Délégué Régional
Marion BLIN

Délégation Centre Limousin Poitou-Charentes
3E avenue de la Recherche Scientifique
45071 ORLEANS Cedex 2

APPENDIX A

Proposal for the Implementation of a NEST (NEA Education Skills and Technology) Component in the OECD/NEA/CSNI Project HYMERES-2

Prepared to the attention of the NEST Management Board, and to be presented during the 1st NEST Management Board Meeting on 28th of March, 2019

Authors:
Ahmed Bentaïb, IRSN, France
Nabiha Chaumeix, CNRS-ICARE / Université d'Orléans, France
Nedjet Erkan, University of Tokio, Japan
Hyoung Kyu Cho, Seoul National University, South Korea
Yassin Hassan, Texas A&M University, USA
Gonzalo Jiménez, Universidad Politécnica de Madrid (UPM), Spain
Pavel Kudinov, Royal Institute of Technology (KTH), Sweden
Eckart Laurien, University of Stuttgart, Germany
Guillaume Mignot, Oregon State University, USA
Koji Okamoto, University of Tokyo, Japan
Domenico Paladino, Paul Scherrer Institut (PSI), Switzerland
Andreas Pautz, Paul Scherrer Institut (PSI), Switzerland
Lee Peddicord, Texas A&M University, USA
Rodolfo Vaghetto, Texas A&M University, USA
Karen Vierow-Kirkland, Texas A&M University, USA

Table of Contents

1. Introduction: Background of NEST project

The OECD Nuclear Energy Agency (NEA) is developing the concept of the NEA Education Skills and Technology framework (NEST), which addresses the important issue of maintaining nuclear know-how for the increasing use of nuclear technology worldwide, by fostering nuclear skills capability building, knowledge transfer and technical innovation within an international context.

Many NEA countries are constructing or planning to construct Generation III+ and Generation IV nuclear power plants, while others need to deal with their nuclear legacies. Most NEA countries are looking at long-term options to deal with high-level radioactive waste and spent nuclear fuel, life-time extension for an ageing fleet of nuclear power plants, as well as better ways to decommission old facilities. There are also challenging issues in other fields, ranging from medicine to the environment.

The NEST Framework is intended to boost the development of shared activities by institutions in participating countries that are responsible for the education and training of young engineers and scientists in collaboration with organizations that are highly experienced in nuclear research and development. In order to fulfil the NEST objectives, the NEA wishes to launch **NEST projects** that shall benefit from having the following key characteristics (the **NEST criteria**):

- they shall be matched with state-of-the-art science and technology in a real-world context, that is connected to challenging problems faced by industry, regulatory bodies or within national programs;
- they offer hands-on training opportunities, working alongside experienced practitioners, complemented by training sessions to develop broad awareness of nuclear culture;
- they are multidisciplinary and multinational in character;
- they serve to strengthen university nuclear related programs by establishing or developing long-term relationships between them and with experienced research organizations.

In the document at hand, we propose to build a NEST project as the education/training component of the OECD/NEA/CSNI joint project HYMERES-2 (**HY**drogen **M**itigation **E**xperiments for **Re**actor **S**afety, Phase 2), in which the Paul Scherrer Institut (PSI) acts as the so-called operating agent, through making accessible its large-scale thermal-hydraulic test facility PANDA to the international research community. HYMERES-2 is the third project in an extremely successful series of OECD/NEA joint research projects at PSI focusing on Severe Accident phenomenology and mitigation.

In the NEST context, the Paul Scherrer Institut will act, according to the NEST nomenclature, as the **Managing Research Institution** (MRI), which will closely cooperate with the **NEST Performing Institutions** (NPI) in countries participating in HYMERES-2 and/or NEST. Currently, partners from the following nine universities and institutes from eight countries are fully committed to join the NEST/HYMERES-2 activities as NPI, and are also co-authors of this proposal:

- Forschungszentrum Jülich GmbH
- Oregon State University, USA;
- Texas A&M University, USA;
- Royal Institute of Technology (KTH), Sweden;

- Universidad Politécnica de Madrid, Spain;
- Université d'Orléans, France;
- Seoul National University, Korea;
- Swiss Federal Institute of Technology Zurich (ETH), Switzerland;
- University of Tokio, Japan
- Institut de radioprotection et de sûreté nucléaire (IRSN), France.

We expect that additional university partners from other HYMERES-2 member countries will join this NEST project endeavor as NPI.

PSI will provide the necessary professional guidance and infrastructure to conduct world-class experimental research work supported by the PANDA team, while the NPI will join forces in scientific cooperation in the HYMERES-2 context and beyond. This can be achieved e.g. by delegating NEST fellows to PSI or other NPI for short-, medium- or long-term stays, through organizing educational and training events together with other NEST project partners, or through participation in analytical benchmark activities within the HYMERES-2 collaboration. The aim is to create a deep understanding of severe accident phenomena and mitigation measures, as well as provide profound training in working with advanced instrumentation and high-fidelity fluid dynamics codes to the next generation of nuclear engineers.

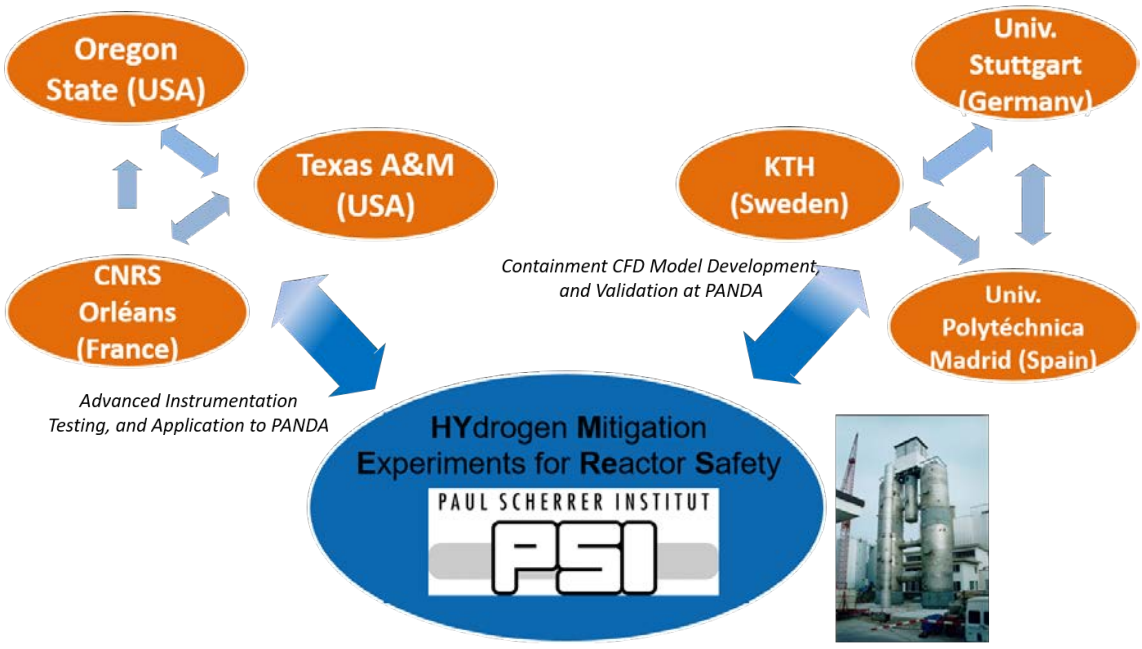

Fig. 1: The NEST concept supports the spawning of new research networks

NEST/HYMERES-2 promotes the idea of not only using the outstanding experimental facilities of the cooperation partners, but features a much further academic outreach: we are convinced that on a long-term perspective this initiative will spawn strong and sustainable university networks that provide education at the highest international level. Figure 1 sketches the long-term vision of the involved

partners, one that would go far beyond the time horizon of the HYMERES-2 project alone: through NEST/HYMERES-2, the formation of new “networks of excellence” around the areas of “Advanced Instrumentation Techniques” and “Containment CFD Development” is promoted, thereby establishing strong links not only to PSI, but also between the university partners themselves.

2. Overview of PSI and the Nuclear Energy and Safety Division

PSI with its approximately 2000 employees is Switzerland’s largest Federal research institute for natural and engineering sciences, and is highly renowned worldwide for its large-scale research facilities, like e.g. the Swiss Synchroton Light Source (SLS), the Swiss Neutron Spallation Source (SINQ) and, most recently, the Swiss Free Electron Laser (SwissFEL). At the same time, it features an extensive nuclear infrastructure, consisting of the Hot Laboratory (one of the few places in Europe where full-length spent-fuel rods can be handled), several waste management facilities and a set of thermal-hydraulics test rigs, amongst which is also PANDA.

These nuclear infrastructures are operated and managed by the Nuclear Energy and Safety (NES) division of PSI, which has currently around 220 employees (approx. 120 permanent scientific and technical staff, around 45 PhD students, 25 Postdocs, and 30 junior scientists). The NES division is structured into seven research laboratories, which cover a wide spectrum of nuclear expertise, necessary for the safe and economic operation of Swiss nuclear power plants. Figure 2 below shows the current organization of PSI, with the NES research division highlighted in blue.

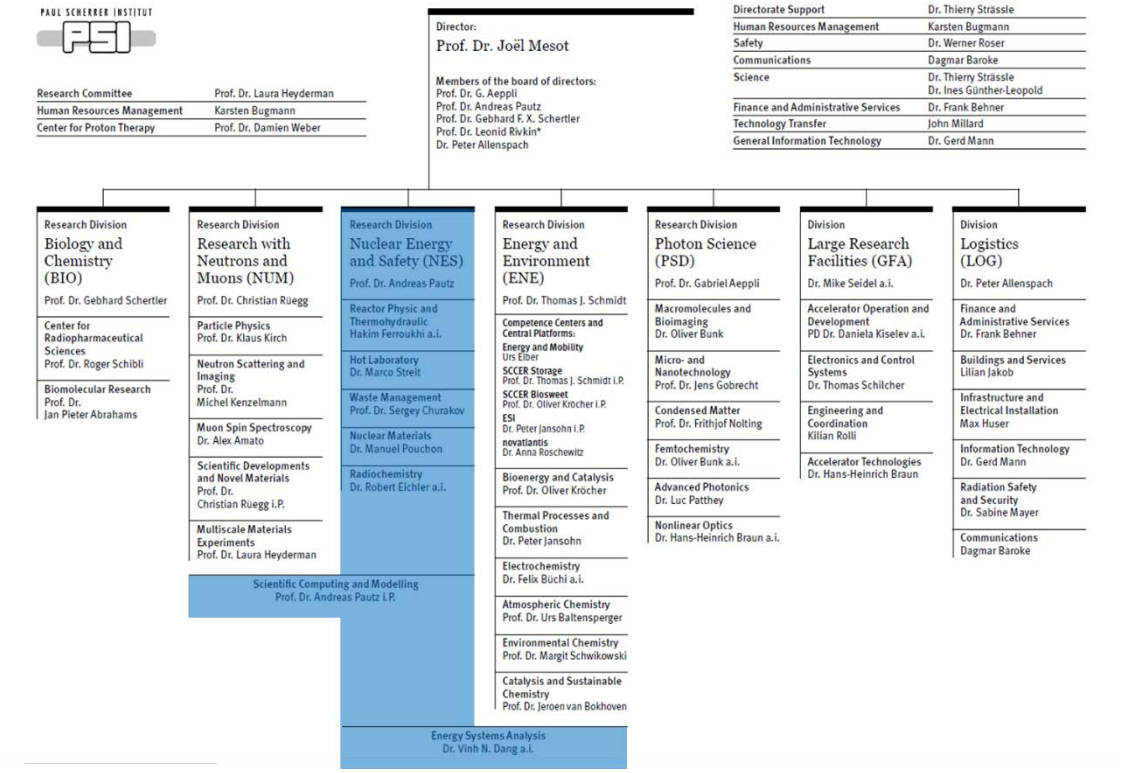

Fig. 2: Organization chart of the Paul Scherrer Institut, with the NES division highlighted in blue

The Nuclear Energy and Safety division fulfils several important mandates in Switzerland, and it is commonly referred to as the **Swiss Nuclear Center of Excellence**. It acts, on the one hand, as the Technical Safety Organization (TSO) of the Swiss Nuclear Regulator, ENSI, providing scientific support to questions arising from licensing and oversight of Swiss nuclear power plants. On the other hand, NES cooperates closely with industry, especially in the areas of materials performance, fuel integrity, as well as severe accident management and phenomenology. Moreover, the laboratory for waste management addresses the scientific issues of geochemistry and transport processes in deep geological repositories for nuclear waste. With the establishment of the new Laboratory for Scientific Computing and Modelling, NES has also replied to the increasing needs of the scientific community for consolidated large-scale simulation and high-performance computing support, through dedicated partnerships with the Swiss Supercomputing Center (CSCS), and the Swiss Data Science Center (SDSCS).

The PANDA facility, which is the main tool of the HYMERES-2 project, is located in the Laboratory for Reactor Physics and Thermal Hydraulics, and represents an essential infrastructure of the division's Severe Accident research group. In the following paragraphs, we will provide a short overview of the HYMERES-2 project, before we enter into the description of a possible NEST implementation.

3. Brief overview of the OECD/NEA HYMERES-2 project

The containment in a nuclear power plant is the last physical barrier to prevent the release of radiological material to the environment. Therefore, plant safety systems must ensure containment integrity for all possible postulated accidents. Hydrogen generated during a postulated severe accident with core degradation is a major safety issue, since explosive mixtures may form in the containment. The generation and particularly the distribution of hydrogen is therefore a key aspect in the safety assessment of Light Water Reactors.

The analysis of hydrogen distribution is very complex due to the effects of hydrogen transport, hydrogen mixing or stratification with steam, air or nitrogen, and the condensation or re-evaporation of steam. Moreover, various reactor types (BWRs, PWRs, Heavy Water Reactors, etc.) have a number of design-specific differences, which need to be properly accounted for in any analysis.

Advanced Lumped Parameters (LP) and Computational Fluid Dynamics (CFD) codes are valuable tools for analyzing LWR behavior during postulated design and beyond-design-basis accidents. At present, the extent of code validation is one limiting factor in their application for reactor safety analyses. One of the obstacles in the process of assessment and validation of computational tools is the lack of adequate experimental data at the required spatial and time resolution.

The OECD/NEA HYMERES-2 project is being carried out in the period 1st July 2017 – 30th June 2021 with experimental investigations in the PANDA facility to continue improving the understanding of the containment phenomena during postulated severe accident scenarios and to further extend the experimental database to phenomena not investigated previously. All experiments are carried out at PSI in the PANDA facility.

The HYMERES-2 investigations address the following four main topics:

1. ***Extend the database on flows impacting obstructions and containment internal structures.*** The experimental database is extended with respect to jet flow impacting flow obstructions by considering flow geometries resembling those of nuclear containment internal structures. The primary target of the new program will provide data for testing the codes against a variety of flow obstruction geometries up to scaled-down real containment internal structures.

2. ***Evaluation of the importance of radiative heat transfer****.* Tests are performed to evaluate the importance of radiative heat transfer on the phenomena affecting the evolution of gas species distribution (i.e. hydrogen transport, mixing, etc.) during a postulated Beyond Design Basic Accident (BDBA).

3. ***Solve important issues regarding suppression pressure pool and BWR systems.*** The effect of the following parameters is investigated in the experimental campaigns: Height of the pool and depth of the sparger; sparger design including blowdown pipe; BWR containment system tests, which involve the interplay of e.g. Drywell, Wetwell, Reactor Pressure Vessel and components e.g. venting pipes, vacuum breaker, spray, etc.

4. ***Extend the database on the performance of safety component operation****.* Two types of safety components, namely spray and cooler are investigated in detail:

   I. Specific spray tests are performed by considering a number of nozzles embedded in a ring installed near the PANDA vessel wall such that the phenomena would be more representative of real plant containment conditions. In this series, the tests are defined by considering cases with or without sump drainage, to address the importance of condensate liquid re-evaporation, and for scenarios addressing both Design Basic Accident (DBA) and BDBA scenarios;

   II. Further tests are performed with more than one cooler and varying the distance between the activated coolers. Coolers are being installed at the same elevation, circumferentially in the vessel dome of PANDA. The activation of individual coolers would allow to gain insights into the cooler modelling needs under DBA and BDBA scenarios, in particular how coolers could be better modelled, e.g., using a detailed 3D representation or by a porous media approach.

The above four topics lay out the overall investigation plan for the HYMERES-2 project. It needs to be pointed out that at the time of writing of the NEST/HYMERES-2 proposal (March 2019), several PANDA tests and analytical activities for the topics 1,2, and 3 mentioned above have already been presented at the HYMERES-2 Program Review Group (PRG) and Management Board (MB) meetings, held so far within HYMERES phase 2. The HYMERES-2 MB has endorsed the possibility to embed a NEST component (i.e. the activities described in the present document) within HYMERES-2.

4. NEST criteria and how they match HYMERES-2

We have juxtaposed the NEST criteria (see the introductory chapter 0) with the targets of the HYMERES-2 project, and describe below how they comply with each other.

NEST Criterion 1: State-of-the-art science and technology and real-world context. HYMERES-2 is being conducted at PANDA, one of the world's most advanced containment test facilities with continuously improving state-of-the-art instrumentation (Particle Image Velocimetry 2D and 3D, Mass Spectrometer, etc.). By addressing jet flow impacting onto obstructions and structures resembling those of nuclear containment internal structures (topic 1), detailed experiments to highlight key features on suppression pressure pool behavior (topic 3), as well as testing the performance of safety component operation (topic 4), together with benchmarking code calculations against these experiments, the technology and real-world aspects of the experiments are well covered. With the evaluation of the importance of radiative heat transfer onto the mixing phenomena and the corresponding time scales through dedicated experiments (topic 2), we intend to shed light onto one important field with a controversial discussion in the scientific community.

NEST Criterion 2: Offer hands-on training opportunities. PANDA is operated by a team of 3 experienced scientists and 3 technicians, and has hosted multiple graduate and postgraduate students in the past. This successful approach will be continued for the ongoing experiments in the context of the HYMERES-2 project. Additionally, all the experiments are accompanied by strong pre- and post-analytical activities (system codes, CFD, etc.) at PSI and the HYMERES-2 international partner institutions, where people with different experiences and expertise (from 'beginners' just entering the field to senior scientists) exchange their knowledge through presenting and discussing their results within dedicated workshops accompanying the regular project meetings (twice a year).

NEST Criterion 3: Multidisciplinary and multinational in character. HYMERES-2 and its predecessors have attracted the worldwide interest of many international partners, typically from national research centers, universities and nuclear regulatory bodies. The participating organizations/countries of the HYMERES-2 project are currently:

- the Paul Scherrer Institut (PSI), Switzerland
- the UJV Rez, a.s., Czech Republic
- the Teknologian tutkimuskeskus (VTT), Finland
- the Gesellschaft für Anlagen- und Reaktorsicherheit (GRS), Germany
- the Nuclear Regulatory Authority (NRA), Japan
- the Korea Atomic Energy Research Institute (KAERI), Korea
- the Russian Academy of Sciences Nuclear Safety Institute (IBRAE) together with the State Atomic Energy Corporation "Rosatom" (ROSATOM), Russian Federation
- the Consejo de Seguridad Nuclear (CSN), Spain
- the Swedish Radiation Safety Authority (SSM), Sweden
- the State Power Investment Corporation Research Institute (SPICRI) together with the China Nuclear Power Technology Research Institute Co. Ltd. (CNPRI), China

- the United States Nuclear Regulatory Commission (NRC), USA

Discussions between the HYMERES-2 partners and organizations in further countries for joining the HYMERES-2 project are currently ongoing. The HYMERES-2 Management Board is also helping to identify additional university partners in their respective countries in order to encourage them to engage also into NEST/HYMERES-2 activities.

NEST Criterion 4: Serve to strengthen university nuclear related programs. HYMERES-2 is first and foremost a regulatory research project under the auspices of CSNI, and is primarily conducted by non-university organizations (see the list of participants above). Nevertheless, education has always been an integral part of CSNI projects, and HYMERES-2 is no exception. PSI as the operating agent in HYMERES-2 has significant experience in cooperation with universities, both on a national and international scale. Implementing a NEST component into HYMERES-2 is therefore a unique opportunity to strengthen the link between the HYMERES-2 partners and academia. Together with the university partners participating in NEST/HYMERES-2, the project will become an enormous asset and excellent platform for educational activities. It is also important to note that Professors at PSI and at the NEST Performing Institutions can act as academic supervisors and award degrees through their university affiliation.

5. Proposal for the Implementation of NEST into HYMERES-2

We intend to implement NEST activities within the HYMERES-2 project through the four following means:

5. **NEST internships** embedded in master projects, or as part of PhD or post-doctoral program, where the NEST fellow receives a mobility grant and per diem to allow for an extended stay at another research institution;
6. Active presence and **participation of NEST fellows during the HYMERES-2 experimental test** campaigns and in the accompanying project meetings;
7. **HYMERES-2 Workshops** and dedicated **NEST educational events**;
8. **Participation of NEST fellows in conferences, international workshops, etc.** that are generally relevant to the overarching field of severe accidents and containment behavior;

5.1 Internships embedded in Master, PhD or post-doctoral programs

These types of activities are expected to be carried out for a duration between 3 and 6 months. Therefore, they would be typically designed on the time scale of a Master project (supervised by one of the NEST Performing Institutions) and hosted at one of the NEST/HYMERES-2 institutions. These internships can, however, also be suitable for PhD or postdoctoral students, who want to spend part of their educational program elsewhere, e.g. at PSI being integrated into the PANDA team. These young researchers would benefit from a NEST fellowship through financial and organizational support. While such candidates would join NEST typically as part of their higher academic education, in principle one could also envisage welcoming young professionals from industry or regulatory bodies at a more advanced stage in their career. However, in this proposal we have not pursued this idea any further.

PSI and each NEST/HYMERES-2 university partner have prepared a tentative list of proposals with research topics adequately matching the HYMERES-2 scope that would lend themselves favorably for internships involving extended stays abroad. These proposals can be found in Appendix A of this document. It is strongly anticipated that other activities will be defined during the HYMERES-2 project meetings, as a result of the identified research needs. Therefore, the list of topical proposals in Appendix A is neither complete nor exclusive, but gives a good first overview of the wealth of research activities that can be offered in the NEST/HYMERES-2 context.

5.2 Participation in the HYMERES-2 test campaign and in the project meetings

NEST Fellows from the NEST Performing Institutions could also be delegated to PSI as the Managing Research Institution for shorter durations, in order to participate in the final preparation and performance of the PANDA tests and to the project meetings, i.e. Workshops and Program Review Group meetings of HYMERES-2, which are being held on a regular basis. This opportunity is particularly well suited for those NEST Fellows who perform computational activities for the HYMERES-2 tests at their home Institutions. We believe that it is of particular importance for those scientists who work mainly analytically to understand the setup, the boundary conditions, as well as possible shortcomings of experimental campaigns, to build a solid simulation case for code validation and qualification.

PSI will plan the performance of selected HYMERES-2 PANDA tests back-to-back to the project meetings, allowing for the NEST Fellows to gain insight and some experience in performing tests in a large scale thermal-hydraulics facility. The PANDA tests to be performed in these instances should be a repetition of previously performed HYMERES-2 test and would therefore allow to assess the “test-repeatability” and reproducibility of results, which is one of the most important requirements to a successful test program.

5.3 Workshops and educational events

Within this category we propose to implement three types of activities:

- Participation in the HYMERES-2 project workshops;
- Dedicated educational events focusing on what is at stake through contributions from leading staff from TSOs, regulators or industry. Such events are meant to look far beyond the current HYMERES-2 activities, and shall give NEST fellow a broader perspective on the field of severe accidents.
- Periodic workshops on the NEST projects supported by the NEA. It is foreseen that up to three NEST research projects could be carried out in parallel and the workshops would offer a tool for exchange on experience between the different NEST projects, as the concept matures.

5.3.1 Project workshops

One of the common objectives of the OECD/NEA/CSNI projects is the creation of an experimental database on physical phenomena, which have high relevance for nuclear safety, and to use this database for the assessment and validation of the advanced computational tools used for safety analyses. This is the goal of the HYMERES-2 analytical workshops that take place once per year during the HYMERES-2 project duration.

We propose to organize the HYMERES-2 analytical workshops with the participation of those NEST fellows that contribute to NEST/HYMERES-2 with computational research tasks. These research tasks will be defined and structured taking into account the type of computational tools used by the NPIs and the type of needs arising from the HYMERES-2 project, and therefore will be beneficial to both the MRI and the NPIs.

The research tasks will be challenging and innovative, but will be realistic in the sense that they will take into account the specific features of the computational tools and the time which will be allocated to the NEST Fellow for the research task; however it is not excluded that more complex tasks can be extended to more than one NEST Fellow period in subsequent timeframes. The definition and coordination of research tasks carried out by the NPIs in different Countries will favor international and multidisciplinary cooperation and exchange between NPIs.

5.3.2 Educational Events

We proposed to organize an intensive summer course of about one week on subjects within and beyond the research areas covered by the HYMERES-2 project. The lecturer and the lectures will be proposed by the organizing institution that will be hosting the summer course. Several of the NEST/HYMERES-2 partners have already volunteered to host such an event, which will likely take place in the summer of 2020 or 2021. To enhance the multidisciplinary character of NEST, the course will also cover areas related to investigations carried out in some other OECD/NEA CSNI projects that address related topics of equally high importance in nuclear safety research.

The areas which will be addressed in the course will include, but will not be limited to:

- Severe Accident Phenomena and Severe Accident Management;
- Passive Safety systems of Advanced LWR;
- Computational Fluid Dynamics for Containment Applications;
- Design of Large-Scale Nuclear and Thermal-Hydraulics facilities, experimental technology etc. and methodologies.

Moreover, an effort will be made to design the course such that redundancy with the content of other well established courses at the OECD/NEA is avoided. Furthermore, we strive at inviting industry and regulatory bodies to these workshops, in order to establish contacts between NEST fellows and the nuclear stakeholders at an early stage. The participants of the course should be primarily NEST fellows, however, it could also be opened to other students and engineers who may have not been involved directly in the HYMERES-2 project.

5.3.3 Intermediate and concluding workshop on the NEST project

An intermediate-term and a concluding workshop on the NEST project will be organized during the first half of the project (2019-2020), and shortly after the conclusion of the HYMERES-2 project (2021) respectively, and should (if possible and compatible with the fellows' schedule) involve all NEST fellows that have participated in the four-year project duration of HYMERES-2. The workshop will include:

- Presentations by each NEST Fellow on her/his experimental and/or analytical activities carried out during their enrolment in NEST at HYMERES-2;
- the main outcomes and scientific highlights of the NEST Fellow work and the HYMERES-2 project;
- the lessons learnt in the NEST project and recommendations for future work, also involving NEST.

We propose that awards are being granted to particularly successful NEST projects.

5.3.4 Participation in International Conferences, Workshops, and Summer Schools

Besides the dedicated NEST and HYMERES-2 events, NEST fellows shall be able to visit the relevant international conferences in the field of severe accident research, passive safety systems, hydrogen mitigation etc. For that purpose, we propose the following (non-exhaustive) list of events that are recommended for NEST fellows to attend:

- 18th International Topical Meeting on Nuclear Reactor Thermal Hydraulics (NURETH-18) in Portland, Oregon, USA, August 18-23, 2019
- 2019 International Congress on Advances in Nuclear Power Plants (ICAPP '19). Juan les Pins - French Riviera May 12-15, 2019.
- 27th International Conference on Nuclear Engineering (ICONE27). Tsukuba International Congress Center, Tsukuba, Ibaraki, Japan. May 19-24, 2019.
- Advances in Thermal Hydraulics (ATH '20). Palaiseau, France March 31-April 3, 2020.
- International Congress on Advances in Nuclear Power Plants (ICAPP2020). Abu Dhabi, UAE April 12-16, 2020.
- 13th International Topical Meeting on Nuclear Reactor Thermal Hydraulics, Operation and Safety (NUTHOS-13). Vancouver, British Columbia, Canada August 23-27, 2020.
- 28th International Conference on Nuclear Engineering (ICONE28). Date and location yet to be determined.
- 10th European Review Meeting on Severe Accident Research Severe Accident Research (ERMSAR 2021), date and location yet to be determined.

The NEST/HYMERES-2 Project Management Board will frequently update this list and provide it to the NEST fellows, respectively their host institutions. Vice versa, NEST fellows can request from the PMB the approval of events that are not listed yet. Such requests must, however, be submitted to the PMB at least 30 days in advance.

6. NEST/HYMERES-2 Governance and Budget

NEST/HYMERES-2 is a cooperative project of the Paul Scherrer Institut as the Managing Research Institution (MRI), and currently eight university partners, the so-called NEST Performing Institutions (NPI). The following paragraphs lay out some organisational guidelines and governance aspects for the conduction of such a project. The overall NEST initiative is still in its infancy, therefore the following paragraphs are to be understood as only one possible approach to setting up a NEST project; adaptions or amendments can be made wherever they seem suitable.

6.1 NEST/HYMERES-2 Project Management Board

At the official kick-off meeting of NEST/HYMERES-2, foreseen in spring 2019, a **Project Management Board** (PMB) is to be established. Each participating research organisation will be represented therein by a single member, typically a professor or teaching staff at the NPI, or a research group leader with comparable responsibilities. The PMB will elect during its constituting meeting a chairperson and deputy chairperson.

The authors of this proposal explicitly welcome the participation of additional research institutions joining as NPI, who will then also be invited to delegate a representative into the PMB. The PMB shall meet once per year (i.e. in 2019, 2020, and 2021), preferably at the OECD/NEA premises in Boulogne-Bilancourt.

6.2 Nomination of NEST Fellows

Each institution participating in NEST/HYMERES-2 can propose candidates for a NEST Fellowship. The nomination process requires the submittal of a CV, an academic transcript, and the proposed research plan of the candidate to the NEST/HYMERES-2 Project Management Board. The PMB nominates candidates for a NEST Fellowship by unanimous decision only, based on the following preconditions and criteria:

- the candidate is affiliated to one of the NPI or the MRI, and is a master student, a PhD student, or holds a postdoctoral position;
- the topic of the research plan is either directly linked to the HYMERES-2 research program, or delivers scientifically relevant contributions to closely related topics, like advanced instrumentation techniques, Computational Fluid Dynamics for containment flows, or hydrogen mitigation measures;
- the work program outlined in the research plan corresponds to at least 6 months full-time research work (corresponding to 30 ECTS in the Europe Credit Transfer System or approx. 900 work hours);
- the research plan clearly states whether the NEST fellow is supposed to conduct research work at his/her home institution/NPI only, or whether an extended internship at PSI or a HYMERES-2 partner organization is envisaged.

After nomination by the PMB, the candidates have to await formal approval of their NEST fellow status by the OECD/NEA NEST secretariat. If extended internships are foreseen in the research plan, additional approval by the Management Board of the OECD/NEA/CSNI project HYMERES-2 is required.

6.3 Conduction of NEST Fellowships

Each NPI is free to decide where their NEST fellows will perform their fellowships. An NPI can decide that the fellow conducts research entirely at his/her home institution, with only occasional visits to the MRI, and the attendance to relevant conferences. Alternatively, the fellow can enroll in an internship elsewhere, either at PSI or a HYMERES-2 partner organization. In addition to the demonstration of a

successfully completed research task, the NEST fellow has to attend and actively participate in at least two events out of the following list:

- The NEST/HYMERES-2 summer course, taking place in 2020 or 2021 (see section 5.3.1);
- One of the HYMERES-2 analytical workshops (see section 5.3.2);
- Either the intermediate or the concluding NEST workshop (see section 5.3.3);
- One or several of the relevant international conferences in the field.

Upon successful completion of the research work, and participation in the abovementioned NEST events, the NEST/HYMERES-2 PMB will recommend the candidate to the OECD/NEA for being awarded the NEST certificate.

6.4 NEST/HYMERES-2 Budget

The budget allocated to NEST/HYMERES-2 will come from different sources of funding, i.e.:

- **The direct contribution from the OECD/NEA** through the NEST membership fees of the participating countries. Based on the number of NEST countries and initial projects, it is reasonable to assume for the moment a **net amount of 100'000 €** (i.e. after the deduction of the cost incurred by the OECD/NEA NEST secretariat) for the entire runtime of NEST/HYMERES-2;
- **HYMERES-2 contribution:** the HYMERES-2 management welcomes the NEST initiative, and has integrated in the financial planning of the HYMERES-2 project **an uncommitted amount of 2.5% of the overall project budget, i.e. 120'000 €**, which could in principle entirely be used for the support of NEST fellows, provided there is a direct link of their work to HYMERES-2. **Making use of this contribution will, however, inevitably require approval by the HYMERES-2 management board**;
- **Swiss government contribution:** finally, the Swiss government through its Federal Office of Energy is in strong support of the NEA's NEST initiative, and has thus **granted an additional 110'000 € to NEST/HYMERES-2**, which shall be used in its entirety for the support of NEST fellows and the organization of NEST events.

In total, we therefore estimate that an **amount of 330'000 €** is available for the support of NEST Fellows in NEST/HYMERES-2. As for the infrastructure being used by the NEST fellows at PSI or the NPI, e.g. office space, IT and experimental equipment/consumables, and administration: these are considered in-kind contributions of the NPI/MRI, hence any costs incurred will be borne by the hosting institution.

6.5 Budget Allocation and Financial Redemption to NEST/HYMERES-2 Partners

A NEST/HYMERES-2 fellowship derives its strength from providing efficient and unbureaucratic financial support for mobility, networking events, and fast access to experiments and data. It also benefits from the strong coordination between the project partners, thus promoting the intended network character of NEST. In order to accommodate for this, the NEST/HYMERES-2 institutions have agreed that:

- all NPI welcome the exchange of NEST fellows, i.e. fellows are encouraged to spend part of their research activities at an institution other than their home institution. No formal permission for such an exchange is required once a NEST fellow has been accepted in NEST/HYMERES-2. However, NPI and fellows are advised to take into account possible processing delays, e.g. due to visa restrictions, and ensure medical insurance;

- the budget for travels, accommodation, conference fees shall be available "on the spot", i.e. no complex or lengthy approval process shall be necessary. This becomes indispensable e.g. if fellows want to participate in experimental campaigns, which are often scheduled on rather short-notice;

- each NEST fellow is obliged to participate in the dedicated network events around NEST/HYMERES-2. We believe this in an integral and indispensable component of building and strengthening a sustainable network of experts.

These considerations lead to the following distribution of funding to the different NEST components:

- **The direct contribution from the OECD/NEA** (i.e. approx. 100'000 €) shall be used primarily for participation to international conferences, HYMERES-2 workshops, and other short-term travels (experimental campaigns at PANDA or elsewhere, and visits to other NPI). **Each NPI shall be enabled to manage these financial means independently and under its own financial responsibility**.

- The financial rules of OECD/NEA/CSNI-organized joint projects require that the **HYMERES-2 contribution** of 120'000 € has to be strictly used for research tasks intimately related to the conduction of the experimental campaigns at PANDA, or accompanying analytical activities in HYMERES-2. We therefore propose to use this amount partially or entirely to support long-term stays (3-6 months) of NEST fellows at PSI, an NPI, or other HYMERES-2 institutions (see the list of HYMERES-2 partners in section 0). **The management of this fund will be under the responsibility of PSI**;

- The contribution from the Swiss government of 110'000 € will be partially transferred to the OECD/NEA NEST secretariat (approx. 50'000 €) and shall be used for the organization and corresponding costs of the dedicated NEST/HYMERES-2 events. Once the PMB has decided where these events take place, the money is being transferred to the hosting NPI.

- The remaining 60'000 € of the Swiss government contribution shall be used to augment the HYMERES-2 contribution for enabling short or extended stays at PSI (or in well-justified cases also at another institution), **and will thus also remain under the auspices of PSI**.

6.6 Estimated Expenses for NEST Fellows

We estimate that a student visiting PSI could afford a stay at monthly living costs of approx. 2'000 €. This amount includes the monthly rent for a room at the PSI guesthouse or other subsidized accommodation in the vicinity of PSI, as well as a reasonable per-diem on which the student could "survive". A fixed contingent of rooms at the PSI guest house dedicated to accommodating NEST fellows, or even

permanently renting a separate furnished apartment for the duration of HYMERES-2 for NEST fellows could be envisaged to further reduce costs. With the assumption of 2'000 €/month for a fellow visiting PSI, and an additional one-time travel allowance of 1'500 €, **a six-months internship would thus amount to 13'500 €**.

For shorter stays, conference trips, and visits to other NPI, the following estimate seems reasonable:

- 1'500 € for international airfare, or 500 € for domestic/European flights;
- Per-diem of 100 €, therein included accommodation and all other expenses.

A visit to the NEST summer school (international travel) in 2020/21 would thus amount to 1'500 € + 5 days x 100 € = 2'000 €, a 1-month stay for an experimental campaign at PSI to 1'500 € + 30 days x 100 € = 4'500 €.

Given the fact that a NEST/HYMERES-2 fellow is supposed to participate in at least two NEST/HYMERES-2-related events or conferences during his/her fellowship duration, it is reasonable **to allocate an initial amount of 6'000 € per NEST fellow. We propose that once a NEST fellowship is approved by the NEST/HYMERES-2 PMB, this amount is directly transferred by the OECD/NEA NEST secretariat to the NPI hosting the fellow.** This will grant flexibility and independence of the NPI to use this amount to the best benefit of the fellow. The NPI is responsible to practice due diligence, and will provide a financial report to the OECD/NEA secretariat at the end of the financial year, as well as an account of settlement at the end of the NEST/HYMERES-2 project.

Under the assumption that the direct NEST contribution from the OECD/NEA amounts to 100'000 €, the proposed budget allocation would suffice to host up **to 16 NEST fellows, i.e. on average two fellows per (currently) participating NPI**.

The HYMERES-2 contribution of 120'000 € for extended internships at PSI or other HYMERES-2 partner institutions is managed by PSI. If the internship had already been part of the approved research plan of the NEST fellow, no further approval is necessary. Otherwise, approval by the NEST/HYMERES-2 PMB and the HYMERES-2 management board needs to be obtained beforehand (ideally through an e-mail circulation procedure). The reimbursement or advanced payment of travel costs, as well as the financial redemption of the NEST fellow (i.e. 2'000€/month, see above) will be handled according to PSI procedures. PSI will also support the fellows in obtaining the necessary visa information and medical insurance.

Under the assumption that the 120'000 € HYMERES-2 contribution to NEST can be fully exploited, this amount would be sufficient **to sponsor up to 9 six-months internships at PSI** (or at another NPI or HYMERES-2 partner).

Finally, the Swiss government contribution dedicated to short-term stays covers the equivalent of approximately 13 one-month stays at PSI (at estimated costs of 4'500 € per stay). This mobility support can be granted on short notice, since no approval from the HYMERES-2 management board is necessary. PSI commits to establish a swift procedure for handling such requests.

In summary, the available budget of the NEST/HYMERES-2 initiative should be sufficient to:

- Provide travel costs for an estimated number of **16 NEST fellows** of up to 6'000 € each. Given the current number of partner organizations this would amount to approximately two fellows per participating NPI, which seems very reasonable given the limited time frame until 2021;

- Enable approximately **9 NEST fellows** (i.e. around one fellow per participating NPI) to perform an extended 6-months internship at PSI or another HYMERES-2 partner. This number of fellows could be reasonably handled by the PANDA team, if all fellows were to stay at PSI.

- Invest around 50'000 € into the organization of dedicated NEST events, and

- Provide a sufficient financial reserve for *ad-hoc* short-term stays at PSI (or elsewhere), that can be granted on very-short notice.

The combination of these different components into the NEST/HYMERES-2 framework, and the number of fellows that could be supported with travel grants and internship support can make for a meaningful contribution to HYMERES-2 and the severe accident research field in general.

7. Conclusion

We believe that the implementation of a NEST component in the HYMERES-2 project bears the potential to make an important contribution to the education and training of the next generation of nuclear engineers, in an area that will remain of high relevance in nuclear safety research. PSI and the participating NPI offer an attractive working and research environment, with an excellent experimental infrastructure and highly skilled senior scientist experienced in the supervision of research projects. The HYMERES-2 project itself is multidisciplinary in nature, since it combines analytical activities (CFD and system code calculations, uncertainty and sensitivity analysis, etc.) with a broad range of experimental work. As an additional benefit, the foreseen project funding will be partially covered by the Swiss government, as well as through the HYMERES-2 partner institutions.

Appendix A: Summary of research topics for NEST fellowships

During a meeting at the OECD/NEA in Paris on July 16-17, 2018, the authors of this proposal agreed to discuss the path for progressing the NEST initiative with HYMERES-2. During this meeting, it was decided to include possible research contributions from each NEST/HYMERES-2 participating organization, i.e. MRI and NPI. The topics collected so far are listed below. It is expected that other topics will be identified once the NEST-HYMERES project will be officially launched.

A1: Work topics proposed by PSI for Extended Internships

In order to give a tentative overview of NEST fellowship topics to be performed within HYMERES-2, a first list of attractive research tasks (listed in the table below) has been drafted by the PSI team operating the PANDA facility. This list will be discussed and finalized in collaboration with the NPI and the prospective NEST fellow, and then be submitted along with the fellow's research plan to the NEST/HYMERES-2 Project Management Board (PMB) for approval. Nomination of the NEST fellow is a matter of the PMB, but needs to be reconciled with the HYMERES-2 project management board.

Table 1: Overview of potential research topics for NEST Fellowships with extended internship at PSI

#	Type of experimental investigation	Type/For/duration
1	*Design and implementation of an automated PIV camera positioning system for velocity measurements in PANDA* A prototype (hardware & software) is already available, but the system requires some fine-tuning and testing.	Experimental/ Master student/ 3 months
2	*Wind tunnel setup* We have a skeleton of a small wind tunnel with some missing components. Goal is: order the missing components, integrate them, write a small control unit with a user interface (LabView) and make some test runs and measure the outlet velocity profile (LDA, Pitot Tubes). It is foreseen to use this wind tunnel for the calibration of the velocity sensors (time-of-flight) capable of measuring very low velocities in PANDA.	Experimental/ Master student/ 4 months
3	*Testing specific measurements techniques and setups in HOMER/GAMILO, before to apply them in PANDA for the HYMERES-2 tests.* Since this activity includes all kinds of optical measurement techniques (PIV & LIF), the complexity of this task would rather require a Ph.D. student or a Postdoc with some previous experience in such measurement techniques.	Experimental/ Ph.D. student or a Post doc/ 3-6 months
4	*Testing/exploring new measurement techniques e.g. a fast gas concentration sensor* This work could be made in conjunction with a PhD program	Experimental/ Ph.D. student/ 2-3 months

5	*Test optical fibers for temperature measurements, possible directly in PANDA (one fiber is already installed there) or in LINX (fibers need to be installed)* New (and advanced) measurement technique which would improve our portfolio on what to offer to our partners.	Experimental/ Master student Ph.D. student or a Post doc/ 2-4 months
6	*Use color LIF for temperature measurements* New (and advanced) measurement technique which would improve our portfolio on what to offer to our partners. The base concept is available, but it was never tested. Necessary: proof of concept either in PANDA x or in a smaller facility (e.g. the LINX at the Laboratory for Thermal Hydraulics at PSI).	Experimental/ Ph.D. student or post doc. 4 to 6 months
7	*Developing and testing different measurement techniques for the tests addressing thermal radiation effect on gas species distribution* The instrumentation will be tested in mock-up facilities or in LINX before to be implemented in PANDA	Experimental/ Master student 4 to 6 months
8	*Scoping calculations, Pre- and post-test analyses of the experiments at PSI with GOTHIC and FLUENT for selected cases of the six series.* Maximum 2 students in parallel one working with GOTHIC and one with FLUENT	Analytical/ Master student Ph.D. student or a Post doc/ 4-6 months
9	*Error quantification for simulations* This work addresses the increasingly important topic of uncertainty and sensitivity analysis, and aims at quantifying the experimental error, which could then serve as input for e.g. a Bayesian calibration model.	Analytical/ Master student Ph.D. student or a Post doc/ 4-6 months
10	*Developing modeling strategies for thermal radiation representation.* This includes a thorough check of the steam properties implemented in the different codes	Analytical/ Master student Ph.D. student or a Post doc/ 4-6 months
11	*Developing modeling strategies for the representation of cooler array* This includes analyses weather coolers must be modelled with a porous media approach or as single objects.	Analytical/ Master student Ph.D. student or a Post doc/ 4-6 months
12	*Develop an experimental mock-up to study the induced convection in a humid environment by a radiation source* The mock-up is intended to be designed and tested in the LINX facility and it should allow to complement with separate effect studies the study of thermal radiation effects	Experimental/ Master student Ph.D. student or a Post doc/ 4-6 months

A2: Contribution provided by Royal Institute of Technology (KTH), Stockholm, Sweden

Steam condensation in a large pool can induce thermal stratification or mixing. These phenomena are of safety importance for the existing fleet of boiling water reactors and advanced light water reactors, which employ passive safety systems. In the framework of the HYMERES2 project, KTH provides analytical support for the development of PANDA experiments addressing pressure suppression pool phenomena. Scaling and pre-test simulations with CFD helped to define experimental design and test matrix for the fifth series of PANDA tests in HYMERES-2. Post-test code validation was very helpful in collaboration with PSI helped on interpretation of the obtained experimental data, which has already resulted in a number of archival publications [1-5]. The CFD modelling of the PPOOLEX and PANDA experiments with sparger has shown that the prediction of the pool behavior requires the knowledge of four independent parameters: (i) Effective momentum magnitude; (ii) injection angle: at the injection holes, due to significant steam velocity components inside the sparger pipe; (iii) momentum profile in the azimuthal direction: determined by interaction between neighboring jets; (iv) turbulence generated by the steam condensation: which affects the turbulent and momentum transport towards the cold layer (i.e. the erosion velocity). Relatively large uncertainties remain in estimation of those parameters from the previous PANDA tests.

KTH is going to participate in continuation of HYMERES-2 project in order to provide analytical support for the development and interpretation of the new series of tests that should help to reduce the uncertainty and improve accuracy in prediction of the large pool behavior using the models developed at KTH. In this framework, a postdoctoral researcher shall be supported through the NEST/HYMERES-2 initiative. It is envisaged that the following support shall be needed:

(i) Visits to the PANDA facility and participation in the tests (Number of visits: 2 , Duration of each visit: 1 month). Total requested support for travel and accommodation: 2 x (flight 500 EUR + 30 days x 100 EUR) = 7000 EUR.

(ii) Participation in the HYMERES-2 meetings (Number of meetings: 3 years x 2 per year = 6)- Total requested support for travel and accommodation: 6 meetings x (flight 500 EUR + 3 days x 100 EUR) = 6x800 = 4800 EUR.

References

1. I. Gallego-Marcos, W. Villanueva, P. Kudinov, 2018. Modelling of pool stratification and mixing induced by steam injection through blowdown pipes. Annals of Nuclear Energy, 112, 624-639.

2. I. Gallego-Marcos, P. Kudinov, W. Villanueva, R. Kapulla, S. Paranjape, D. Paladino, J. Laine, M. Puustinen, A. Räsänen, L. Pyyd, E. Kotro, 2018. Pool stratification and mixing during a steam injection through spargers: analysis of the PPOOLEX and PANDA experiments. Nuclear Engineering and Design, 337, 300-316

3. I. Gallego-Marcos, P. Kudinov, W. Villanueva, R. Kapulla, S. Paranjape, D. Paladino, J. Laine, M. Puustinen, A. Räsänen, L. Pyyd, E. Kotro. Pool stratification and mixing during a steam injection through spargers: CFD modelling of the PPOOLEX and PANDA experiments. Under review in Nuclear Engineering and Design, NED_2018_344.

4. I. Gallego-Marcos, P. Kudinov, W. Villanueva, M. Puustinen, A. Räsänen, K. Tielinen, E. Kotroet. Effective momentum induced by steam condensation in the oscillatory bubble regime. Under review in the International Journal of Heat and Mass Transfer, HTM_2018_ 3843.

5. I. Gallego-Marcos, P. Kudinov, W. Villanueva. Thermal stratification and mixing in a Nordic BWR pressure suppression pool. To be submitted to the Annals of Nuclear Energy.

A3: Contribution provided by University of Stuttgart, Germany

Uncertainty Analysis of a CFD Simulation Method and Comparison with PANDA Experiments. As a step to define Best Practice Guidelines for CFD simulations in nuclear containment applications, a three-dimensional natural convection flow simulation of flow and heat transfer in the PANDA facility shall be performed using the CFD package Ansys CFX. The purpose of this investigation is to test and demonstrate the quantification of the numerical errors using the method of "Grid Convergence Index (GCI)", which was previously developed in [1]. Three variants of the method exist and shall be compared (i) the Standard method REM, (ii) the Blend Factor Method BFM and the (iii) Least Squares Method LSQ. Using these methods, the spatial discretization errors can be quantified using results obtained on various grids with different refinement levels. As error inidicators various volume integrated quantities such as vorticity, temperature, mass flows and pressure can be used. The insight and results of the GCI, wall treatment and scalability studies serve as guideline, on which the numerical erros of future CFD containment simulations can be estimated. Finally, the comparison of the simulation results with the experimental data of the PANDA facility will be carried out.

The activity will be conducted by a master student in the study program of Energy Technology or Thermo-Fluid Dynamics. This NEST fellow should spend 2 month at PSI and the remaining 4 month at Stuttgart.

[1] A. Mansour and E. Laurien: Numerical error analysis for three-dimensional CFD simulations in the tworoom model containment THAI+: Grid convergence index, wall treatment error and scalability tests, Nuclear Engineering and Design 326 (2018) 220–233.

A4: Contributions provided by Oregon State University, USA

Proposal 1: Ex-situ helium concentration measurement. Gas concentration measurements in large experimental facility rely mainly on ex-situ mass spectrometry measurements. Alternative in-situ measurements, such as mini-katharometers, have also been used but with the constraint of a dry atmosphere. Mass spectrometry (MS) using residual gas analyzer necessitates sampling gas from the inside of the facility to the mass spectrometer inlet maintaining the sampling lines at temperature high enough to avoid undesired condensation. Two sampling approaches have been followed:

- A continuous sampling of all the channels (up to 80 per MS in PANDA) with the measurement of one sample at a time, which leads to the loss of information for the 79 remaining lines through the exhaust.
- The sampling and storing of all the channels at a discrete time (MISTRA). Each sample is analyzed afterwards to create a “simultaneous “concentration measurement map.

In both cases, the sampling rate for the concentration measurement is low, which either limits the used of the system for slow process or the number of channel that can be used. Our proposal is thus two-fold:

- Investigation and development of new measurement methods that can be used ex-situ to measured specific gas concentration (for example helium), in particular (but not limited to) optical method. In our research group at Oregon State University, we are currently working on developing optical techniques to measure the helium molar density in a pressurized chamber. The measurement principle is based on light absorption at specific wavelength. We are currently building a measurement system and conducting tests as a proof of concept. Based on the results, this technique could be the first candidate to be tested under PANDA test conditions. Conductivity measurement techniques could be considered as well.
- Design of an intermediate test section that can be installed between the facility and the mass spectrometer. We propose to design a test section that allows for simultaneous measurement in each single sampling line. Using the speed of optical method, this would allow for continuous measurement.

The proposed scope of work could be initially conducted at Oregon State University as a Master program level with the option upon success to implement the technique in the PANDA facility during an extended internship at PSI.

Proposal 2: Implementation and testing of optical fiber for temperature measurement. The thermal hydraulic research group at Oregon State University is using extensively the optical fiber measurement technique developed by LUNA (currently 2 systems in our laboratory). Optical fibers are currently used to measure strain on surrogate fuel plates in new compact fuel assemblies designed for domestic research reactor under high flow condition. It is also used to measure flow-induced vibration on individual fuel rod and rod assembly for liquid metal fast reactor design. Few members of our group have had experience with the LUNA system for many years and have deep understanding of the system, its intricacy as well as

the post processing associated with it. We are interested in developing and testing procedure for temperature measurement that could be directly applied to the PANDA facility. A non-exhaustive list of tasks to be conducted could be the development of feed through system, testing of fiber under flow conditions to optimize the installation (bare fiber or capillary sleeve, pre strained), calibration procedure development.

Many of these tasks could be tackled in our laboratory using existing facilities and in/house equipment allowing for quick turn-around satisfying the priority list given by PSI. This activity would involve under-graduate and graduate students under the supervision of a Post-doc (NEST Fellow) whose PhD thesis topic was directly related to the use of optical fiber for flow-induced vibration.

References:

[1] Nixon, C.A., Marcum, W.R., Weiss, A.W., Steer, K.M., Jackson, R.B, Martin, M.G., "On the Fluid Structure Interactions of a Wire-Wrapped Pin Bundle", Advances in Thermal Hydraulics, 2018 American Nuclear Society Winter Meeting, Orlando, Florida, United States, November 11-15, 2018.
[2] Nixon, C.A., Marcum, W.R., Steer, K.M., Jackson, R.B., "A New Method for Experimentally Quantifying Dynamic Deflection of a Cylindrical Structure", Experimental Mechanics, 2018, 1-19.
[3] Nixon, C.A., Marcum, W.R., Steer, K.M., Jackson, R.B., Weiss, A.W., "The Dynamic Response of a Wire-Wrapped Pin in Axial Flow via Fiber Optic Distributed Strain Sensing", 17th International Topical Meeting on Nuclear Reactor Thermal Hydraulics, Xi'an, China, September 3-8, 2017.
[4] C.A. Nixon, "On the Flow-Induced Vibration of Solitary Wire-Wrapped Cylinders in Axial Flow", Oregon State university, PhD Thesis, 2018
[5] S.S Goodrich, "Natural Convection Heat Transfer and Boundary Layer Transition for Vertical Heated Cylinders", Oregon State university, PhD Thesis, 2017

Proposal 3: Developing modelling strategies for the representation of cooler array. Simulating coolant flows and heat transfer in complicated geometries is a complex and challenging task. To understand the underlying phenomena and optimize the design of the application, sufficiently accurate numerical simulations of the considered system are necessary. While the availability of high resolution Computational Fluid Dynamics (CFD) and affordable computing power have advanced considerably in recent year's calculations accuracy is still a trade of between available computing resources and time. It is imperative for the representation of the cooler array to develop modeling strategies that will not conform results validity. For the analysis of the cooler array, porous domain approximation can be potentially applied. The porous model allows for the macroscopic representation of the flow in the considered structure, without modeling the microscopic flow details. This is achieved through a momentum sink term where pressure drop is dependent on the superficial velocity, inertial and viscous resistance coefficients.

The performed study should consider comparative analysis between direct cooler array CFD model and porous domain approach. CFD modeling strategies shall also include mesh refinement study (using Grid Convergence Index) and turbulence model selection assessment. Results should be validated against experimental data, if available. Solution verification should be performed according to the procedure outlined in the ASME V&V 20-2009. [1]

The OSU Collage of Engineering hardware, that can be used to perform CFD analyses includes the HPC Cluster that is currently operating with 1,554 processor nodes. The HPC Cluster is used by several of OSU's Engineering schools including the School of Nuclear Science and Engineering, for various research and graduate projects in parallel computing. OSU School of Nuclear Science and Engineering has licenses for CFD software such as Star-CCM+ and other code with 3-D capabilities such as GOTHIC
The proposed scope of work would be conducted at Oregon State University as a Master program level. Participation to analytical workshop of HYMERES project would be of interest to share results and expertise.

[1] American Society of Mechanical Engineers, “Standard for Verification and Validation in Computational Fluid Dynamics and Heat Transfer”, ASME, V&V 20-2009.

For all these proposal it is envisaged that the following support shall be needed:

(i) Participation in the HYMERES-2 meetings and/or Analytical workshop (Number of meetings: 3 years x 2 per year = 6)- Total requested support for travel and accommodation: 6 meetings x (flight 1500 EUR + 3 days x 100 EUR) = 6x1800 = 10800 EUR.

(ii) Visits to the PANDA facility, implementation and testing of instrumentation for proposal 1 and 2 (Number of visits: 2 , Duration of each visit: 2 month). Total requested support for travel and accommodation: 2 x (flight 1500 EUR + 2x2000 EUR) = 11000 EUR.

A5: Contributions provided by Texas A&M University, USA

Proposal 1: Contribution of the Thermal-Hydraulic Research Laboratory of Texas A&M University to the NEST-HYMERES-2 Project. Representatives of the Thermal-Hydraulic Research Laboratory have participated to the first co-ordination meeting "Progressing the NEST Initiative with HYMERES-2" of the OECD/NEA HYMERES-2/NEST Project. During the meeting Prof. Hassan, Dr. Rodolfo Vaghetto, and Dr. Thien Nguyen, principal investigators and researchers of the Thermal-hydraulic Research Laboratory have confirmed their interest and intension to participate to the activity.

The Thermal-Hydraulic Research Laboratory of the Nuclear Engineering Department at Texas A&M University has developed state-of-the-art experimental and computational techniques that are currently applied to conduct research on Light Water Reactors (LWR), and Advanced Reactors technologies.

The thermal-hydraulic research laboratory proposes to collaborate to the HYMERES-2 project, and helping applying these advanced flow and temperature measurement techniques to the experimental activity of the project. These techniques include:

1. Advanced high-resolution measurements of the temperature: these techniques can be potentially applied to walls temperature measurements, and fluid temperature measurements. The technique is based on of Distributed Temperature Sensors (DTS)
2. High resolution velocity measurements. These state-of-the-art laser based techniques have been largely used in the laboratory and applied to a wide variety of flows conditions, and geometries.

The development and application of these advanced techniques to the HYMERES-2 project will be conducted in two separate phases:

Phase 1. Benchtop Experiments.
We suggest to use these advanced methodologies on simple benchtop tests, in order to verify the applicability of these techniques, and refine installation and measurements procedures.

Phase 2. Final application to HYMERES-2 Experimental Facilities.
Once techniques are refined, they will be directly applied to the experiment facilities that are included in the HYMERES-2 project.

The participation of the thermal-hydraulic research laboratory will take place through:

- Graduate student exchange supported by the HYMERES-2 project. Selected graduate students that have gained experience on the use of advanced measurement techniques developed in the laboratory can be involved in the collaborative project at locations to be defined.
- Workshops and other programmed meetings and presentations at locations to be defined

Proposal 2: Contribution provided by the Nuclear Heat Transfer Systems Laboratory, Texas A&M University, College Station, Texas, USA. The Nuclear Heat Transfer Systems Laboratory (NHTSL) at Texas A&M University under the leadership of Professor Karen Vierow Kirkland performs state-of-the-art research on key reactor safety issues including investigation of condensation heat transfer mechanisms, experimentally and analytically evaluating reactor designs and safety systems, and advancing the state-

of-the-art in reactor safety analysis. Funding from the U.S. Department of Energy and Japanese nuclear utilities support Master's and Ph.D. students to perform experimental investigations of heat removal systems in light-water reactors and to quantify uncertainties in the modeling of reactor designs. In addition, projects from the U.S. Nuclear Regulatory Commission and Sandia National Laboratories have led to the construction of advanced thermal hydraulic facilities for testing current and advance safety system concepts, deriving theoretical formulations for condensation heat removal in the presence of a non-condensable gas and contributing to severe accident analysis methodologies. The Lab is equipped with a 150-kW steam supply, a high-speed camera system, unique thermal hydraulic instrumentation and a state-of-the-art data acquisition system. Activities in the Lab contribute to improving best estimate analyses with probabilistic risk analysis methodologies.

The NHTSL at Texas A&M proposes to be part of the HYMERES-2 project (**HY**drogen **M**itigation **E**xperiments for **Re**actor **S**afety, Phase 2) at the Paul Scherrer Institut and the large-scale thermal-hydraulic test facility PANDA. This will be accomplished by linking the extensive capabilities of the NHTSL with key aspects of HYMERES-2 and PANDA. Steam condensation in a large pool is an important phenomenon for both current light water reactors and advanced concepts incorporating passive safety approaches. The NHTSL can contribute through advanced instrumentation, testing and applications to PANDA in the areas of condensation and re-evaporation of steam. Experimental studies at NHTSL have been performed focusing on phenomena for both PWRs and BWRs. Projects been carried out in a number of related areas including convective boiling and condensation, flooding with steam and water in a large diameter vertical tube and water inlet sub-cooling effects on flooding, condensation with in environments with non-condensable gases, and evaluation of reflux condensation heat transfer of steam-air mixtures. These activities will provide the framework to extend the database on the performance of safety component operation and solve important issues in BWR systems.

Through the capabilities and research activities of the Nuclear Heat Transfer Systems Laboratory, the collaboration with HYMERES-2 closely coincide with the NEST criteria of (1) carrying out state-of-the-art science and technology in a real-world context, (2) providing hands-on training opportunities for students, (3) participating in and contributing to a multidisciplinary, multinational endeavor, and (4) serving to strengthen our university nuclear program. The participation of NHTSL in HYMERES-2 and NEST will contribute significantly to the education and development of students on key questions of reactor safety and performance.

It is envisioned that students at both the Master's and Doctoral levels will be involved and benefit. To meet this objective, the following support is requested:

- One-month visits to the PANDA facility and participation HYMERES-2 tests. Two visits are anticipated. The requested support for travel and accommodations for each visit would be 1500 € for the flight and 30 days at 100 € for accommodations, for 4500 € for each visit, and 9000 € total for both visits.

- Participation in the HYMERES-2 meetings. It is anticipated that there will be two meetings each year over the three-year duration of HYMERES-2, for a total of six meetings. The requested support for travel and accommodation each meeting is 1500 € for the flight and 3 days

accommodations at 100 € per day, for a total of 1800 € per meeting. The request for six meetings then is 10800 € total to participate in the HYMERES-2 meetings.

A6: Contribution provided by Universidad Politécnica de Madrid, Spain

Universidad Politécnica de Madrid (UPM) is going to participate in the HYMERES 2 project providing analytical support to several experimental tests done in the PANDA facility. The numerical analysis will be performed with the GOTHIC code and with another CFD codes such as ANSYS CFX if needed.

The UPM group in nuclear safety and thermal hydraulics has a wide experience with full containment models and numerical analysis of experimental facilities, see Ref. 1-8. The UPM team will help to define the experimental tests and to analyze the data obtained in the experiments in order to contribute with best guidelines for numerical simulation and code validation.

The economic resources for HYMERES-2 in the UPM allow to have a PhD student full time working during the project and also cover the travel expenses to the meetings. Unfortunately, they don´t cover the student mobility and we consider that is a key factor of success to be in contact with the PSI and KTH for our work at UPM.

Therefore, it is proposed to have an internship at PSI to learn about the experimental facility and to be present at some of the test (with preference of those related with suppression pools and safety components activation) that the UPM will simulate in the project. It will allow to have a better understanding of the physical phenomena and the instrumentation and control of the test facility. The best estimate time for this internship is 3 months.

In a second step, we propose that the PhD student can work at the KTH university in Sweden with the group of Prof. Kudinov, as they are the reference group in suppression pools. It will allow to learn the advanced ways of conducting a numerical analysis for direct contact condensation with the GOTHIC code to simulate with the state-of-the-art knowledge the PANDA suppression pool tests at the UPM. The best estimate time for this internship is also 3 months.

The financial support needed for these two internships is:(i) Internship at the PSI, Duration of the visit: 3 months. Total requested support for travel and accommodation: flight 500 EUR 3*1830 €/month = 5990 EUR.

(ii) Internship at KTH, Duration: 3 months. Total requested support for travel and accommodation: flight 500 EUR 3*1830 €/month = 5990 EUR.

In case it is not possible to get financing for both internships, we will choose one of them.

References

1. **Steam condensation simulation in a scaled IRWST-ADS simulator with GOTHIC 8.1**. Samanta Estévez-Albuja, Gonzalo Jimenez, Suleiman Al Issa, Rafael Macián-Juan, Kevin Fernández-Cosials, César Queral. Nuclear Engineering and Design 334 (2018) 96–109.

2. **Study of hydrogen risk in a PWR-W containment during a SBO scenario; Tau parameter definition and application on venting strategy analysis**. Kevin Fernández-Cosials, Gonzalo Jimenez, Rafael Bocanegra, César Queral. Nuclear Engineering and Design 325 (2017) 164–177
3. **Analysis of the equipment and instrumentation qualification criteria using 3D containment models**. G. Jimenez, K. Fernandez-Cosials, R. Bocanegra, C. Queral. Nuclear Engineering and Design 323 (2017) 28–38.
4. **Hydrogen distribution and Passive Autocatalytic Recombiner (PAR) mitigation in a PWR-KWU containment type**. Emma Lopez-Alonso , Davide Papini, Gonzalo Jimenez. Annals of Nuclear Energy 109 (2017) 600–611.
5. **Analysis of a gas stratification break-up by a vertical jet using the GOTHIC code**. Mikel Kevin Fernández-Cosials, Gonzalo Jimenez, Emma Lopez-Alonso. Nuclear Engineering and Design 297 (2016) 123–135.
6. **Development of a PWR-W GOTHIC 3D model for containment accident analysis**. Rafael Bocanegra, Gonzalo Jimenez, Mikel Kevin Fernández-Cosials. Annals of Nuclear Energy 87 (2016) 547–560.
7. **Proposed methodology for Passive Autocatalytic Recombiner sizing and location for a BWR Mark-III reactor containment building**. César Serrano, Gonzalo Jimenez, M. del Carmen Molina, Emma López-Alonso, Daniel Justo, J. Vicente Zuriaga, Montserrat González. Annals of Nuclear Energy 94 (2016) 589–602.
8. **BWR Mark III containment analyses using a GOTHIC 8.0 3D model**. Gonzalo Jimenez, César Serrano, Emma Lopez-Alonso, Ma del Carmen Molina, Daniel Calvo, Javier García, *César Queral, J. Vicente Zuriaga, Montserrat González. Annals of Nuclear Energy 85 (2015) 687–703.*

A7: Contribution provided by Seoul National University, Korea

In the event of an accident at a nuclear power plant, steam and hydrogen can be released to containment buildings. The steam condensation, thin liquid film formation, and its re-evaporation may occur and they influence the pressure and temperature distributions in various regions of containment [1]. For accurate prediction of these phenomena using a CFD code, application of a liquid film model and its validation are required and In this context, the local liquid film behavior in re-evaporation/condensation environment have been studied through an experiment using optical measurements [2]. Meanwhile, CFD analyses have been conducted at Seoul National University on film-wise condensation in the presence of non-condensable gases and tested condensation models which can consider liquid film behaviors. For these analyses, a commercial CFD code, STAR-CCM+, and an inhouse code developed by KAERI (Korea Atomic Energy Research Institute), CUPID, were used incorporated with liquid film models [3].

In the framework of the HYMERES2 project, SNU provides analytical support for pre- and post-test analyses of the experiments at PSI with CFD codes and CUPID focusing on the liquid film behaviors, such as condensation and re-evaporation. Various types of liquid film modelling approaches shall be tested, such as interface tracking, two-fluid model, and fluid-film model. Comparison of the simulation results with different models can provide insight for efficient and accurate modelling of the liquid film in the containment CFD simulation. Constitutive relations required for the liquid film modelling will be summarized and validation of those models against PSI experiments can contribute to establishment of a constitutive model package for the containment thermal-hydraulics. The models that need to be tested would be interfacial and wall shear stresses, wall and interfacial heat transfer models, etc.

The approximate financial support will be for a PhD student, who will spend an internship at PSI, Duration of the visit: 4 months. Total requested support for travel and accommodation: flight 1’500 EUR + 4*2’000 €/month = 9’500 EUR.

(ii) Two short-term stays for HYMERES-2 workshops: flight costs each 1’500 € + 3 days x 100 €/day = 1’800 €/stay, i.e. 3’600 € in total.

[1] M. Andreani et al.: On the unexpectedly large effect of the re-vaporization of the condensate liquid film in two tests in the PANDA facility revealed by simulation with the GOTHIC code, XCFD4NRS, (2008), 10-12.

[2] M. Guillaume, et al.: Measurement of liquid films thickness in a condensing and re-evaporating environment using attenuation of near infrared light. Nuclear Engineering and Design, 336, (2018), 64-73.

[3] J. H. Lee, G. C. Park and H. K. Cho: Improvement of CUPID code for simulating filmwise steam condensation in the presence of noncondensable gases, Nuclear Engineering and Technology, 47(5), (2015), 567-578.

A8: Contribution provided by IRSN and CNRS-ICARE, FRANCE

During a severe accident (SA) in a nuclear power plant, hydrogen (H2) can be produced from exothermal oxidation of fuel cladding or fuel assembly canisters and other hot metallic components. In case of failure of in-vessel corium retention, a large amount of carbon monoxide (CO) in addition to H2 and other gases may be produced during molten core concrete interaction (MCCI) in the reactor pit. As a consequence, local concentrations of H2 and CO can exceed the flammability limit of the mixture and induce strong dynamic pressure loads which may threaten the containment structures and technical equipment, including safety important systems (SISs). To assess the efficiency of the mitigation systems and strategies, the use of validated tools is requested. To this end, the characterization of phenomena affecting the evolution of gas species distribution (i.e. hydrogen, carbon monoxide transport, mixing, etc.) and their combustion is of primary importance. HYMERES2 project aims to provide well detailed experimental results for hydrogen distribution and the SAMHYCO-NET project aims to address the recombination and combustion of such flammable gas in different configuration (homogenous and stratified) and different scale (small, medium and large).

For the distribution, the recombination and the combustion of hydrogen and carbon monoxide, the radiative heat transfer evaluation stills an open issue. Actually, detailed measurement are still missing to validate and improve the existing models.

IRSN and CNRS are going to participate in the NEST/HYMERES-2 project initiative by

- providing both experimental and analytical support for the development and interpretation of the PANDA tests:
    - CNRS-ICARE will contribute to radiative heat measurement in the PANDA facility,
    - IRSN will contribute to pre and post analysis of the performed tests using both LP and CFD codes,
- establishing a bridge between HYMERES-2 and SAMHYCO-NET communities to share knowledge and needs. The link between the two projects may help the definition of tests to be performed in PANDA for distribution and in ENACCEF-2 for combustion.

In this framework, a postdoctoral researcher shall be supported through the NEST/HYMERES-2 initiative. It is envisaged that the following support shall be needed:

(i) Visits to the PANDA facility and participation in the tests (Number of visits: 2 , Duration of each visit: 1 month). Total requested support for travel and accommodation: 2 x (flight 500 EUR + 30 days x 100 EUR) = 7000 EUR.

(ii) Participation in the HYMERES-2 meetings (Number of meetings: 3 years x 2 per year = 6)- Total requested support for travel and accommodation: 6 meetings x (flight 500 EUR + 3 days x 100 EUR) = 6x800 = 4800 EUR.

A9: Contribution provided by The University of Tokio, Japan

The visualization group at The University of Tokyo (UTVIS) has been conducting experimental and computational research about various thermal-hydraulics phenomena that existed in the Fukushima Daiichi's multiple-unit accident. Particularly, aerosol dynamics, dispersion, and control with water sprays, thermal stratification in the suppression pools have been investigated by incorporating detailed spatiotemporal experimental data obtained with advanced measurement techniques such as PIV [1,2,3, 4,5]. Our laboratory has UTARTS (**U**niversity of **T**okyo **A**erosol **R**emoval **T**est facility with **S**prays) facility, which is a cylindrical containment spray test facility for aerosol research, and two suppression pool experimental setups. Our group has been also developing in-house PIV system and temperature measurement methods incorporating various advanced post-processing techniques to extract the data of the fluid flows in various flow domains [6, 7].

Computational efforts include the CFD simulations by using open-source CFD code OpenFOAM, STARCCM+, RELAP/SCDAP, and validation of the models to resolve local thermal-hydraulics phenomena for understanding the accident progression and exploring the interactions with other subsystems of an integrated plant.

UTVIS group thinks to contribute to the NEST-HYMERES-2 project with the following potential research topics:

1- **Aerosol dispersion and control with water sprays:** Radioactive aerosols pose significant risks to the environment either during nuclear accidents or during the decommissioning activities of nuclear power plants. UTVIS group performs experimental and computational researches related to the effective control of aerosol dispersion during decommissioning activities of nuclear power plants at the UTARTS test facility. Regarding this research topic, NEST fellows can visit UTVIS laboratory for conducting either experimental or computational research for spray and aerosol science.

2- **Integrated tests and computational study of hydrogen transport in multi-compartment systems:** In the Fukushima Daiichi accident, the hydrogen generated in Unit 3 reactor pressure vessel was discharged into the suppression pool together with the steam, from the suppression chamber it flowed into the drywell which was primarily filled with nitrogen gas. From the drywell of Unit3, it flowed into Unit 4 reactor building, which was initially filled with the air, via a common vent line and some portion of it leaked into the reactor building of Unit 3 through deformed flanges. A few important coupled phenomena that existed sequentially during this process are worth to be explored: (A) The investigation of noncondensable gas effects on the steam suppression efficiency and direct contact condensation. (B) Global and local transient behaviour of hydrogen (helium) in an integrated system of connected compartments with the help of detailed helium distribution measurements providing the evolution of local helium concentrations. We expect that both studies can provide unique data set for the validation of CFD, LP codes, and the analysis of the interaction of a local phenomenon (A) with a global phenomenon (B) of hydrogen transport.

Participation of UTVIS laboratory as follows:
a) We can host and support the NEST fellows in our laboratory about the above relevant research topics.

b) Two of our students are also anticipated visit PANDA facility and participate to HYMERS-2 tests for one-month period in PSI..
c) Attending HYMERES-2 meetings, two times a year.

Participation to PANDA tests: Duration of one-month stay at PSI in a year, required financial support is 2000 € (flight) + 30 days * 100 € (accommodation) = 5000 €. For two students; 2 (students) x 2(visits) x 5000€ = 20000 € in total.

Participation in HYMERES-2 meetings: For the meetings of HYMERES-2, required financial support per meeting is 2000 € (flight) + 3 (days) * 100 € (accommodation) = 2300€. For six meetings; 2300€ * 6(meetings) * 1(student) = 13800€ in total.

References:

[1] H. Liang, Q. Zhou, N. Erkan, and S. Suzuki. Improvement of aerosol spray scavenging efficiency with water mist. Journal of Aerosol Science, 105697 (2020).
[2] L. Hui, N. Erkan, V. Solans, and S. Suzuki. Numerical Simulation and Validation of Aerosol Particle Removal by Water Spray Droplets with OpenFOAM During the Fukushima Daiichi Fuel Debris Retrieval. Frontiers in Energy Research 8:102 (2020).
[3] Jo Byeongnam, Nejdet Erkan, Shinji Takahashi, Daehun Song, Wataru Sagawa, and Koji Okamoto. "Thermal stratification in a scaled-down suppression pool of the Fukushima Daiichi nuclear power plants." *Nuclear Engineering and Design* 305 (2016): 39-50.
[4] Song Daehun, Nejdet Erkan, Byeongnam Jo, and Koji Okamoto. "Relationship between thermal stratification and flow patterns in steam-quenching suppression pool." *International Journal of Heat and Fluid Flow* 56 (2015): 209-217.
[5] Song Daehun, Nejdet Erkan, Byeongnam Jo, and Koji Okamoto. "Dimensional analysis of thermal stratification in a suppression pool." *International Journal of Multiphase Flow* 66 (2014): 92-100.
[6] Cai, Jiejin, Byeongnam Jo, Nejdet Erkan, and Koji Okamoto. "Effect of non-condensable gas on thermal stratification and flow patterns in suppression pool." *Nuclear Engineering and Design* 300 (2016): 117-126.
[7] Qian Zhou, Nejdet Erkan and Koji Okamoto, "Ex situ calibration technique for simultaneous velocity and temperature measurements inside water droplets using temperature-sensitive particles." Measurement Science and Tech. 28 (2017):075203 (17pp).

APPENDIX B

FRAMEWORK AGREEMENT

ON THE OECD NUCLEAR ENERGY AGENCY (NEA) JOINT UNDERTAKING ON NUCLEAR EDUCATION SKILLS AND TECHNOLOGY (NEST)

FRAMEWORK AGREEMENT

ON THE OECD NUCLEAR ENERGY AGENCY (NEA) JOINT UNDERTAKING ON NUCLEAR EDUCATION SKILLS AND TECHNOLOGY (NEST)

FRAMEWORK AGREEMENT

On the OECD Nuclear Energy Agency (NEA)
Joint Undertaking on Nuclear Education Skills and Technology (NEST)

Preamble

The signatories of this Framework Agreement on the OECD Nuclear Energy Agency (NEA) Joint Undertaking on Nuclear Education Skills and Technology (NEST), duly designated by their Governments (hereinafter individually referred to as a "**NEST Country**", or collectively as the "**NEST Countries**") and listed in Appendix A (hereinafter individually referred to as a "**Party**", or collectively as the "**Parties**"),

CONSIDERING that the mission of the NEA is to, *inter alia*, assist its member countries in maintaining and further developing, through international co-operation, the scientific, technological and legal bases required for a safe, environmentally sound and economical use of nuclear energy for peaceful purposes;

CONSIDERING that, pursuant to Article 5 of its Statute, the NEA is entrusted with promoting the formation of international joint undertakings for the production and uses of nuclear energy for peaceful purposes, and that this Framework Agreement is concluded under Article 5 of the Statute of the NEA;

DESIRING to co-operate in the development of scientific, technical and any other relevant skills of young generations of scientists and engineers, through state-of-the-art research activities in a multinational and multidisciplinary context which would cover technical issues such as nuclear science, technology and applications, nuclear engineering, radioactive waste management, licensing and regulation of nuclear activities, and non-technical issues such as stakeholder involvement, business and economic factors, nuclear programmes or project management, nuclear law and social science, to meet a broad range of national needs of the NEA member countries in the nuclear field;

WISHING to improve the attractiveness of engagement in the nuclear field for young people;

AGREE to take part in the NEA Joint Undertaking on Nuclear Education Skills and Technology (hereinafter referred to as the "**NEST Framework**") on the terms and conditions described in this agreement (hereinafter referred to as the "**Framework Agreement**").

Article 1

DEFINITIONS

In this Framework Agreement, the following words and expressions have the following meanings:

Act of Adhesion	means the act in the form set forth in Appendix B to be signed by an Applicant.
Applicant	means an organisation designated by the government of a country, whether an NEA member country or not, where it has its headquarters, wishing to adhere to this Framework Agreement.
Framework Agreement	means the terms and conditions of this Framework Agreement on the OECD Nuclear Energy Agency (NEA) Joint Undertaking on Nuclear Education Skills and Technology (NEST).
Leading Organisation	means the leading organisation that shall serve as a NEST Project manager and shall report to the Management Board.
Management Board	means the body having overall responsibility for the management of the NEST Framework, as described in Article 3.
NEA	means the OECD Nuclear Energy Agency.
NEST Activities	means educational, training and/or mentoring activities to broaden the awareness of nuclear science, technology and applications; such activities will be organised for the common benefit of NEST Fellows participating in different NEST Projects or in the same NEST Project.
NEST Budget	means the budget funded by the contributions of the Parties in accordance with this Framework Agreement which shall be used to provide funding to NEST Fellows, NEST Projects and NEST Activities as determined by the Management Board.
NEST Criteria	means the criteria that all NEST Proposals shall have to conform to in order to be eligible by the Management Board as provided in Article 4(b) and (c).
NEST Country	means the country of a government that has designated one Party or several Parties to this Framework Agreement.
NEST Fellow	means a post-graduate, graduate or undergraduate student or a young professional engaged in technical and scientific nuclear related activities that is selected to participate in a NEST Project and NEST Activities.
NEST Framework	means the NEA joint undertaking established by this Framework Agreement.
NEST Participating Organisation	means any university, research organisation, regulatory body, industrial or other organisation, whether governmental or not, that has agreed to participate in a NEST Project and which has its headquarters in a NEST Country.
NEST Project	means a NEST Proposal that is accepted by the Management Board and for which the relevant NEST Participating Organisations have signed an implementing agreement, a NEST Project Agreement.

NEST Project Agreement	means the agreement signed by the NEST Participating Organisations for a NEST Project to implement the NEST Proposal that has been accepted by the Management Board.
NEST Proposals	means all proposals made by a Party or by any other organisation responding to a call for proposal issued by the Management Board.
Party	means a signatory to this Framework Agreement duly designated by a government and listed in Appendix A.
Purpose	means the purpose of the NEST Framework, as defined in Article 2.
Secretariat	means the NEA staff members.

Article 2

PURPOSE

The purpose of the NEST Framework (hereinafter referred to as the "**Purpose**") is to:

1) attract, train and facilitate skills development of post-graduate, graduate, and undergraduate students in fields of interest to the nuclear sector (encompassing both technical fields, such as nuclear science and engineering, radioactive waste management, nuclear safety, nuclear medicine, and non-technical fields in areas such as nuclear related economics and social sciences) and young professionals engaged in both technical and non-technical nuclear-related activities (hereinafter referred to as "**NEST Fellows**"**)** by transmitting practical knowledge and offering hands-on training; and

2) assist the NEST Countries in maintaining and strengthening academic nuclear related education programmes and building both technical and non-technical skills in the field of nuclear science, safe use of nuclear technology and applications (whether in medicine, environment or other) through the establishment of sustainable international exchanges and collaboration activities between universities, and between universities and (i) research organisations, (ii) regulatory bodies, (iii) the industry and (iv) any other organisation, whether governmental or not (hereinafter referred to as the "**NEST Participating Organisations**").

Article 3

MANAGEMENT BOARD

(a) The Parties delegate overall responsibility for the management of the NEST Framework as described in paragraph (c) hereunder to a "**Management Board**" established under this Article.

(b) Where a NEST Country designates one Party to this Framework Agreement, the Party shall be entitled to designate one member of the Management Board.

Where a NEST Country designates more than one Party to this Framework Agreement, such designated Parties shall be represented by a single member at the Management Board, and

they shall be considered as a single party when determining the NEST Budget. The Parties designated by the same NEST Country may, however, participate in NEST Projects and NEST Activities separately. At least one alternate per member of the Management Board shall be designated by the Parties in case the member is not available.

The Parties shall notify the Secretariat in writing the name, title and contact details of their designated and alternate members for the Management Board, and whatever changes thereof.

(c) The Management Board shall:

1) adopt unanimously the NEST programme of work and NEST Budget for the following calendar year;

2) approve unanimously:

i. payments to be made from the NEST Budget; and

ii. the funding allocated from the NEST Budget for each NEST Project or NEST Activity, as provided in Article 4 hereunder and for each NEST Fellow, as provided in Article 5(c) hereunder;

3) select unanimously NEST Projects based on the NEST Criteria and the requirements provided in Article 4(c) hereunder, and NEST Activities which can contribute to the Purpose;

4) consider and approve reports on NEST Projects and NEST Activities implemented in accordance with the NEST programme of work and NEST Budget;

5) determine the evolution of the NEST Framework;

6) establish guidelines and procedures, consistent with the Purpose and this Framework Agreement, as may be required for the sound management of the NEST Framework;

7) consider any Applicant wishing to become a Party to this Framework Agreement in accordance with Article 11;

8) consider all matters brought before it by any Party or the Secretariat; and

9) carry out any other functions conferred upon it by this Framework Agreement, including those pertaining to the NEST Projects detailed in Article 4 hereunder.

(d) Unless otherwise specified in this Framework Agreement, the Management Board shall operate and reach its decisions on a consensus basis (i.e., without taking a vote and if no objection is raised). Each member of the Management Board shall have one vote. Where unanimity is required under this Framework Agreement, the Management Board members have an obligation to cast a vote; absent members shall vote via email sent to the Secretariat before the meeting.

(e) The Management Board shall elect a Chair and a Vice-Chair from amongst its members for a period of two (2) years. The Chair and Vice-Chair may be re-elected only once in their respective positions, unless otherwise unanimously decided by the Management Board. The Management Board can decide to elect a new Chair and Vice Chair as circumstances dictate.

The Chair and the Vice-Chair's term will start on a 1st of January and end on a 31st of December.

(f) The Management Board should meet at least once a year or as called by its Chair. A special meeting shall be called by the Chair after receiving a request from a simple majority of the members.

(g) The Management Board shall operate in accordance with the confidentiality obligations provided in Article 8 hereunder.

Article 4

NEST PROJECTS AND NEST ACTIVITIES

(a) To achieve the Purpose, the NEST Framework shall be implemented through NEST Projects and NEST Activities in accordance with the criteria and procedures detailed in this Article.

(b) NEST Projects shall conform to the following criteria (hereinafter referred to as the "**NEST Criteria**"):

1) be multinational, i.e. including at least three (3) NEST Countries;

2) address concrete and multidisciplinary challenges in the field of nuclear science, technology and applications, including both technical and non-technical aspects;

3) offer hands-on training opportunities in the field of nuclear science, technology and applications to NEST Fellows. The Parties are also encouraged to offer skills development and education programmes; and

4) any other criteria identified by the Management Board.

(c) Procedure to establish a NEST Project:

1) NEST Projects may be initiated either through (i) proposals made by a Party (or multiple Parties), or (ii) the issuance of a call for proposal(s) by the Management Board. All proposals made by a Party or by any other organisation responding to a call for proposal (hereinafter referred to as the "**NEST Proposals**") shall only be considered by the Management Board if they meet the NEST Criteria and shall at least:

i. be consistent with this Framework Agreement.;

ii. identify (i) the leading organisation who shall serve as a NEST Project manager and shall report to the Management Board (hereinafter referred to as the "**Leading Organisation**"), and (ii) all other NEST Participating Organisations, each of which shall have its headquarters established in a NEST Country;

iii. specify the management structure and duration of the NEST Project;

iv. include a programme of work and related budget consistent with the NEST programme of work and the Purpose;

v. include (i) the process and/or criteria to select NEST Fellows (such as their affiliation to a NEST Participating Organisation), (ii) specifications on any necessary restrictions (such as information access restrictions) and (iii) the education and training plan for selected NEST Fellows;

vi. include the collaboration plan between NEST Participating Organisations;

vii. include the reporting responsibilities of the Leading Organisation to the Management Board on (i) the NEST Project programme of work, (ii) the expenditures of the NEST Project and (iii) the final selection of NEST Fellows;

viii. set forth the provisions applicable to the disclosure, protection and ownership of information and intellectual property rights provided to and/or arising from the NEST Project;

ix. specify when and what information relating to the execution of the NEST Project will be made available to the NEA member countries in accordance with Article 5(c)(iv) of the NEA Statute;

x. provide that the NEST Participating Organisations shall ensure the completion of any formalities required for the participation of the NEST Fellows in the NEST Project; and

xi. specify, where an entity from a country that is not from a NEST Country is included as part of a NEST Proposal, the contribution of this entity and associated added value for the NEST Project, as well as the proposed support to the entity.

2) The Management Board shall unanimously select among the NEST Proposal(s) that meet the minimum requirements detailed in Article 4(c)(1) above and the NEST Criteria, and determine the budget to be allocated thereto; and

3) A selected NEST Proposal shall become a NEST Project through the issuance by the Management Board of a notice of acceptance of the NEST Proposal and subsequent signature of the implementing agreement (hereinafter referred to as the "**NEST Project Agreement**") by all the NEST Participating Organisations to that NEST Project. In the event of any inconsistency between this Framework Agreement and a NEST Project Agreement, the Framework Agreement shall prevail. The NEST Project Agreements shall also provide provisions to protect confidential information which shall be at least as restrictive as the ones provided in Article 8 hereunder.

(d) NEST Activities shall contribute to the Purpose through opportunities that broaden the awareness of nuclear science, technology and applications by addressing topics related to nuclear engineering, radioactive waste management, licensing and regulation of nuclear activities and non-technical issues (such as stakeholder involvement issues, business and economic factors, nuclear programmes and projects management, nuclear law and social science) which will be organised for the common benefit of NEST Fellows participating in different NEST Projects or in the same NEST Project.

Article 5

NEST FELLOWS

(a) NEST Fellows shall (i) carry out research tasks within the NEST Project in which they have been selected to participate and (ii) participate in NEST Activities.

(b) NEST Leading Organisations shall report to the Management Board on the NEST Fellows selected for their respective NEST Projects and describe in such report the NEST Fellows' respective assignments and achievements within the NEST Project.

(c) If a NEST Fellow is affiliated with a NEST Participating Organisation participating in the NEST Project for which s/he has been selected, the costs associated with her or his participation in such NEST Project or related NEST Activity (such as travel and associated living expenses, cost of training) may be fully or partly funded by the NEST Budget, as determined by the Management Board based on the NEST Proposal.

NEST Fellows that are not affiliated with a NEST Participating Organisation may participate in NEST Projects and NEST Activities, but shall not benefit from the NEST Budget, unless otherwise unanimously agreed by the Management Board.

Article 6

FINANCE

(a) The NEST programme of work and budget will be prepared in accordance with the Purpose with the support of the Secretariat as described in Article 7(b). As provided in Article 3(b), where a NEST Country designates more than one Party to this Framework Agreement, such designated Parties shall be considered as a single party when determining the NEST Budget. Each Party commits to the NEST Budget the amount of contributions to be determined in the NEST programme of work and NEST Budget adopted by the Management Board in accordance with Article 3(c)(1).

(b) The contributions from the Parties shall be paid in Euros into an account designated by the Secretariat. Payments shall be made according to invoices issued to the Parties or to any entity paying on their behalf by the Secretariat upon the approval of the Management Board. The Secretariat shall manage these contributions and shall, following the approval of the Management Board as required under Article 3(c)(2)(i), reimburse the Secretariat costs, pay invoices for work performed according to the programme of work and provide the NEST Fellows, the NEST Projects and the NEST Activities with the funding agreed by the Management Board as provided in Article 3(c)(2)(ii).

Article 7

OECD NUCLEAR ENERGY AGENCY (NEA)

(a) The Parties take note that, in accordance with the NEA Statute, the NEA encourages the broadest possible participation in the NEST Framework by its member countries, and endeavours to co-ordinate the NEST Framework's activities with its other work in this field. The Secretariat will report on a yearly basis to the Steering Committee for Nuclear Energy on the state of the affairs and the development of the NEST Framework.

(b) The Parties agree that the Secretariat supports the NEST Framework and provides technical secretariat services to the NEST Framework, and more specifically the Management Board. The Secretariat also provides financial management services to the NEST Framework, in accordance with the financial regulations and practises of the OECD, which include preparing and presenting the financial reports on the NEST Budget to the Management Board for approval.

Article 8

CONFIDENTIAL INFORMATION

(a) All information in whatever form or mode of communication, which is disclosed by a Party (the "**disclosing Party**") to any other Party (the "**receiving Party**") in connection with the implementation of the NEST Framework (such as but not limited to information regarding the NEST Proposals, the NEST Projects, the NEST Activities) and which the disclosing Party has explicitly marked as "confidential" at the time of disclosure or, when disclosed orally, has identified as confidential at the time of disclosure and has confirmed the confidential nature of the information in writing within five (5) calendar days from oral disclosure at the latest, is considered as "**Confidential Information**" under this Framework Agreement.

Except to the extent expressly authorised by this Framework Agreement or otherwise agreed in writing by a Party, each Party agrees that it shall keep confidential and shall not publish or otherwise disclose and shall not use for any purpose other than as provided for in this Framework Agreement any Confidential Information disclosed to it, in whatever form or mode of communication, by the disclosing Party, except to the extent that the receiving Party can demonstrate that the Confidential Information:

1) was already known to the receiving Party, other than under an obligation of confidentiality, at the time of disclosure by the other Party;

2) was generally available to the public or part of the public domain at the time of its disclosure to the receiving Party, or became available to the public or part of the public domain thereafter (other than through an act or omission in breach of this Agreement);

3) was disclosed to the receiving Party by a third party who had no confidential obligation;

4) was independently discovered or developed by the receiving Party without the use of Confidential Information belonging to the disclosing Party, as documented by the receiving Party; or

5) was identified, in writing, by the disclosing Party as not Confidential Information, or if the receiving Party received prior written approval from the disclosing Party to disclose the Confidential Information.

The receiving Party shall comply with requests for Confidential Information by government authorities or tribunals having jurisdiction. In such case, the receiving Party shall notify the disclosing Party of any requests or subpoenas requiring the disclosure of Confidential Information in writing immediately upon receipt, and shall consult with the disclosing Party in order to address any attempts to obtain Confidential Information and attempt to find a mutual solution, subject to the requirements of applicable law. .

(b) Any Party wishing to publish any document (such as reports, journal articles, conference papers) concerning the NEST Framework, must submit it for prior approval of the Management Board, which approval process shall be determined by the Management Board. Any publications relating to the NEST Projects or NEST Activities shall be dealt with in the NEST Project Agreements.

(d) Any Party that wishes to involve a third party in matters pertaining to the NEST Framework Agreement must obtain the prior written approval of the Management Board and ensure that the third party enters into a non-disclosure agreement to protect the Confidential Information which shall be at least as restrictive as the one provided in this Article 8.

(e) Where necessary, additional rules and procedures regarding protection, use, and disclosure of Confidential Information shall be adopted by the Management Board acting by unanimity and in conformity with this Framework Agreement.

Article 9

LEGISLATIVE PROVISIONS

(a) Activities under this Framework Agreement shall be subject to the laws and regulations applicable in the State on whose territory such activities are carried out.

(b) Responsibilities and any related costs for work carried out by each Party under this Framework Agreement rest with that Party.

Article 10

SETTLEMENT OF DISPUTES

(a) Attempts should be made to amicably resolve any dispute between the Parties concerning the interpretation or application of this Framework Agreement. Any of the concerned Parties may submit the dispute for mediation before the Management Board which will unanimously adopt a proposed mediation settlement. If no settlement is reached between the concerned Parties, including with the Management Board's mediation, the dispute shall be referred to the NEA Director-General for further mediation.

(b) All disputes arising out of or in connection with the present Framework Agreement shall, upon mutual written agreement of the disputing Parties, be finally settled under the Rules of Arbitration of the International Chamber of Commerce by one arbitrator appointed in

accordance with the said Rules. The arbitral procedures shall take place in Paris (France) and be conducted in the English language. The arbitrators shall decide any such dispute by reference to the terms and conditions of this Framework Agreement and any applicable laws and regulations, and their decision shall be final and binding on the Parties concerned.

(c) Unless otherwise unanimously agreed in writing by the disputing Parties, this Framework Agreement shall be governed by the laws of France.

Article 11

ADHESION AND WITHDRAWAL OF PARTIES

(a) A government, whether from an NEA member country or not, may designate an organisation whose headquarters are based in its country (hereinafter referred to as the "**Applicant**") to become a Party to this Framework Agreement by submitting a written application to the Secretariat and the Management Board. The Management Board may either reject or unanimously accept the application, subject to any additional condition that it might determine.

(b) Where an application is unanimously accepted by the Management Board in accordance with paragraph (a) of this Article:

1) an act of adhesion (the "**Act of Adhesion**") in the form set forth in Appendix B shall be submitted by the Secretariat to the Applicant for signature, to which a copy of this Framework Agreement shall be annexed. The Act of Adhesion shall specify that the Applicant assumes all the rights and obligations of a Party under this Framework Agreement, and meets any condition unanimously determined by the Management Board, if any.

2) The Applicant shall become a Party to this Framework Agreement upon receipt by the Secretariat of the Act of Adhesion duly signed by an authorised representative of the new Party.

3) Following the adhesion of a new Party, Annex A shall be modified by the Secretariat to include the new Party and the amended version shall be sent to all the Parties.

(c) With the prior approval of the Management Board, a Party may be replaced by another organisation if required by the government that had designated the Party to be replaced. The process set forth in paragraphs (a) and (b) of this Article shall apply.

(d) A Party may withdraw from this Framework Agreement by providing twelve-month prior written notice to the other Parties, unless otherwise unanimously agreed by the Management Board. The withdrawal of a Party under this paragraph shall not affect the withdrawing Party's rights and obligations incurred prior to withdrawal, or the rights and obligations (including funding) of the other Parties to this Framework Agreement, unless otherwise unanimously agreed by the Management Board.

(e) If a Party fails to fulfil its obligation(s) under this Framework Agreement, the Chair of the Management Board may decide to send notice to the defaulting Party specifying the nature of the defaulting obligation(s) and specifically invoking this Article. If the defaulting Party fails to remedy the defaulting obligation(s) within ninety (90) days after its receipt of notice

invoking this Article, the defaulting Party shall be considered to have withdrawn from this Framework Agreement.

Article 12

FINAL PROVISIONS

(a) The activities of the Parties under this Framework Agreement shall be subject to the availability of appropriated funds, personnel and other resources. If a Party fails to fulfil its obligation(s) under this Framework Agreement due to unavailability of appropriated funds, personnel and other resources, Article 11(e) shall apply.

(b) This Framework Agreement shall enter into force upon signature by all the Parties listed in Appendix A. It shall remain in force for a period of ten (10) years. The Secretariat will consult the Management Board and the Parties on the future of the NEST Framework two (2) years before the termination of this Framework Agreement.

(c) This Framework Agreement may be amended or terminated at any time by the unanimous written agreement of all the Parties.

(d) The original of this Framework Agreement shall be deposited with the NEA and a certified copy of the Framework Agreement shall be provided to each Party upon its entry into force.

(e) The provisions of Article 8 (Confidential information) and Article 10 (Settlement of disputes) shall survive the termination of this Framework Agreement and shall continue to apply to any withdrawn Party.

(f) Activities undertaken under this Framework Agreement shall be conducted in the English language.

This Framework Agreement may be signed in counterparts, all of which, when taken together, shall constitute the ***Framework Agreement on the OECD Nuclear Energy Agency (NEA) Joint Undertaking on Nuclear Education Skills and Technology (NEST)***.

For **Belgian Nuclear Research Centre (SCK•CEN)**

Name of Signatory: Peter Baeten

Position of Signatory: Deputy Director-General

Date of Signature: 3/1/2019

Signature:

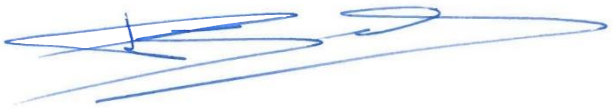

For **Natural Resources Canada (NRCan/RNCan)**

Name of Signatory: Mr. Marco Presutti

Position of Signatory: Director General, Electricity Resources Branch

Date of Signature: DEC 2 1 2018

Signature: 

For **Commissariat à l'énergie atomique et aux énergies alternatives (CEA)**

Name of Signatory: François JACQ

Position of Signatory: Administrateur Général

Date of Signature: 18/01/2019

Signature:

For **Institut de Radioprotection et de Sûreté Nucléaire (IRSN)**

Name of Signatory:

Position of Signatory:

Jean-Christophe NIEL
Director General
IRSN

Date of Signature: 09/01/2019

Signature:

For ~~Global Research for~~ Safety (GRS)
Gesellschaft für Anlagen- und Reaktorsicherheit (GRS) gGmbH

Name of Signatory:	Hans J. Steinhauer	Dr. K. Stummeyer
Position of Signatory:	Managing Director	Head of Project Management Agency
Date of Signature:	14.2.2019	
Signature:		

Name of Signatory:	
Position of Signatory:	
Date of Signature:	
Signature:	

For **Italian National Agency for New Technologies, Energy and Sustainable Economic Development (ENEA)**

Name of Signatory:

DEPARTMENT OF FUSION AND TECHNOLOGY
FOR NUCLEAR SAFETY AND SECURITY

Position of Signatory:

The Director
Dr. Aldo Pizzuto

Date of Signature: 21/XII/2018

Signature:

For **National Institute for Nuclear Physics (INFN)**

Name of Signatory: FERNANDO FERRONI

Position of Signatory: PRESIDENT

Date of Signature: 25 GEN. 2019

Signature:

For **Ispettorato nazionale per la sicurezza nucleare e la radioprotezione (ISIN)**

Name of Signatory: Mauritio PERNICE

Position of Signatory: Director

Date of Signature: 15/01/2019

Signature:

For **Istituto Superiore di Sanità (ISS)**

Name of Signatory: PROF. GUALTIERO RICCIARDI

Position of Signatory: PRESIDENT

Date of Signature: Roma, 21.02.2018

Signature:

ISTITUTO SUPERIORE DI SANITÀ

For **Università degli Studi di Milano**

Name of Signatory: IL RETTORE
Elio Franzini

Position of Signatory:

Date of Signature: 28 DIC. 2018

Signature:

For **Japan Atomic Energy Agency (JAEA)**

Name of Signatory: Kazumasa Hioki

Position of Signatory: Director, Office of Strategy and International Affairs

Date of Signature: 25 December 2018

Signature:

For **Korea Atomic Energy Research Institute (KAERI)**

Name of Signatory: Won-Pil BAEK

Position of Signatory: Executive Vice President

Date of Signature: January 14, 2019

Signature: Wonpil Baek

For **The State Atomic Energy Corporation ROSATOM**

Name of Signatory: Nikolay Spasskiy

Position of Signatory: Deputy Director General

Date of Signature: 15.02.2019

Signature:

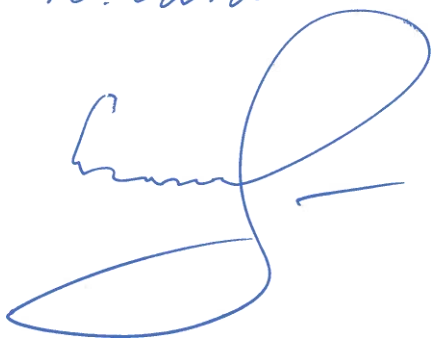

For **Paul Scherrer Institut (PSI)**

Name of Signatory: Andreas Pautz

Position of Signatory: Head of Nuclear Energy and Safety Division

Date of Signature: 17.12.2018

Signature:

Prof. Dr. Andreas Pautz
Head of Nuclear Energy and Safety
Research Division
Paul Scherrer Institut

For **U.S. Department of Energy (DOE)**

Name of Signatory: Edward G. McGinnis

Position of Signatory: Principal Deputy Assistant Secretary

Date of Signature: 12/21/18

Signature: 

Appendix A

LIST OF THE PARTIES

List of the Parties and their representation in the Management Board

The NEST Parties are identified in the table below.

NEST Country	List of the Parties	Representation in the Management Board
BELGIUM	Belgian Nuclear Research Centre (SCK•CEN)	One member
CANADA	Natural Resources Canada (NRCan/RNCan)	One member
FRANCE	- Commissariat à l'énergie atomique et aux énergies alternatives (CEA) - Institut de Radioprotection et de Sûreté Nucléaire (IRSN)	One member
GERMANY	Gesellschaft für Anlagen- und Reaktorsicher (GRS) gGmbH Global Research for Safety (GRS)	One member
ITALY	- Italian National Agency for New Technologies, Energy and Sustainable Economic Development (ENEA) - National Institute for Nuclear Physics (INFN) - Ispettorato nazionale per la sicurezza nucleare e la radioprotezione (ISIN) - Istituto Superiore di Sanità (ISS) - Università degli Studi di Milano	One member
JAPAN	Japan Atomic Energy Agency (JAEA)	One member
KOREA	Korea Atomic Energy Research Institute (KAERI)	One member
RUSSIAN FEDERATION	The State Atomic Energy Corporation ROSATOM	One member
SWITZERLAND	Paul Scherrer Institut (PSI)	One member
UNITED STATES	U.S. Department of Energy (DOE)	One member

Appendix B

ACT OF ADHESION

TO THE FRAMEWORK AGREEMENT ON THE OECD NUCLEAR ENERGY AGENCY (NEA) JOINT UNDERTAKING ON NUCLEAR EDUCATION SKILLS AND TECHNOLOGY (NEST)

The [*insert name of the new Party to the Framework Agreement*] (hereinafter referred to as the "**Signatory**");

CONSIDERING that, in accordance with Article 11(a), the Signatory was designated by [*insert name of the ministry/other governmental institution that designated the Signatory to participate in the NEST Framework as a Party*] in a letter dated [*insert date*] to become a Party to the Framework Agreement on the OECD Nuclear Energy Agency (NEA) Joint Undertaking on Nuclear Education Skills and Technology (NEST) which entered into force on [*insert date*] (hereinafter referred to as the "**NEST Framework Agreement**");

CONSIDERING that, in accordance with Article 11(a) of the NEST Framework Agreement, the Signatory subsequently submitted an application to the Management Board to become a Party to the NEST Framework Agreement, on [*insert date*];

CONSIDERING that the Management Board of the NEST Framework Agreement unanimously accepted the Signatory's application on [*insert date*], in accordance with Article 11(a) of the NEST Framework Agreement; and

CONSIDERING Article 11(b)(1) of the NEST Framework Agreement:

Article 1

The Signatory hereby signs this Act of Adhesion to become a Party to the NEST Framework Agreement and agrees to assume all rights and obligations of a Party under the NEST Framework Agreement. [*Include the additional conditions determined by the Management Board, if any*]

Done this [*insert day*] day of [*insert month and year*]

For the Signatory:

Name:

Title:

Date:

Signature:

The Head of the Office of Legal Counsel of the OECD Nuclear Energy Agency hereby certifies that the present copy conforms to the original text deposited with the Director-General of the OECD Nuclear Energy Agency.

Boulogne-Billancourt, 25 February 2019

HEAD OF THE OFFICE OF LEGAL COUNSEL

Ximena VÁSQUEZ-MAIGNAN

APPENDIX C

ACCEPTANCE LETTER OF THE NEST MANAGEMENT BOARD FOR THE NEST PROJECT PROPOSAL NEST-HYMERES-2

Ref.: NEST/2019-07-24/003

Boulogne Billancourt, 24 July 2019

Andreas Pautz
Paul Scherrer Institut
OHSA/E71
Forschungsstrasse 111
5232 Villigen PSI
Schweiz

Dear Prof. Pautz,

RE: Your NEST project proposal HYdrogen **M**itigation **E**xperiments for **Re**actor **S**afety, Phase 2 **(HYMERES-2)**

At the NEST Management Board meeting of 28 March 2019, your NEST HYMERES-2 proposal was presented.

The NEST Management Board discussed the merits of your proposal and evaluated its adherence to the NEST Criteria as specified in the NEST Framework Agreement.

As Chair of the NEST Management Board, I am pleased to announce that your proposal has been accepted and is thus ready to be launched.

The NEST Management Board decided to allocate 60000 € for 2019 to the NEST HYMERES-2 project to be able to start its activities.

I will now invite you to start the preparations of your NEST Project Agreement, whose template can be found in Annex 1 to this letter.

Furthermore, I would like to remind you that you are requested to submit yearly to the Management Board, a progress report including both the financial and technical reporting. In order to collate the information, I will be grateful if you could report on the status of development of the project and its activities as well as expenditure to the NEST Secretariat by using the excel file "Table NEST activities and budget follow-up" (Annex 2).

Finally, your point of contacts for all future communications related to this project are Markus Beilmann, markus.beilmann@oecd-nea.org, responsible for the NEST HYMERES project and Antonella di Trapani, antonella.ditrapani@oecd-nea.org for the overall NEST Framework coordination.

On behalf of the NEST management Board, I thank you again for your time and effort in preparing the NEST proposal and look forward to hearing about its outcomes and impacts.

Yours sincerely,

Dr Andreas Pautz
Chair of the NEST Management Board

Appendix B: Master Thesis of Ms. Lea Zimmermann: "Experimental Characterization of Flow Velocity Development Downstream of Tube Bends"

Master Thesis
Msc Nuclear Engineering 2019

Experimental Characterization of Flow Velocity Development Downstream of Tube Bends

Lea Zimmermann

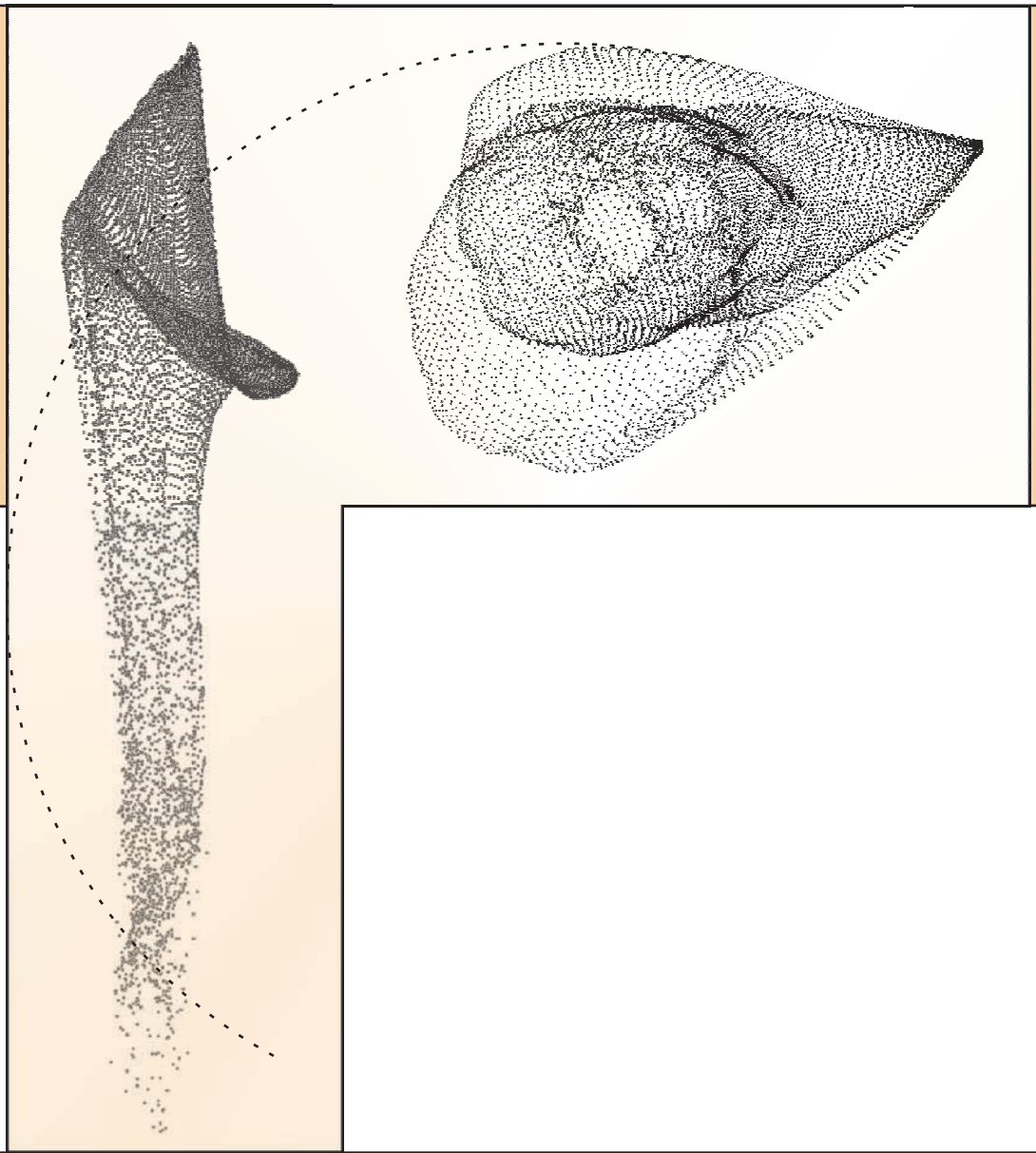

PAUL SCHERRER INSTITUT
PSI

ETH
Eidgenössische Technische Hochschule Zürich
Swiss Federal Institute of Technology Zurich

Cover

Scatter plot of a time average 3D velocity field at the tube exit showing the correlation of the velocity components (Vx versus Vz - left, and Vx versus Vy - right) in pixel units.

Eidgenössische Technische Hochschule Zürich
Swiss Federal Institute of Technology Zurich

Master Thesis - MSc Nuclear Engineering

Experimental Characterization of Flow Velocity Development Downstream of Tube Bends

Lea Zimmermann
leazi@student.ethz.ch
Paul Scherrer Institut
ETH Zurich

August 7, 2019

Supervisor: Dr. Ralf Kapulla

Abstract

Large scale hydraulic experiments with relevance for nuclear safety conducted in the PANDA facility at Paul Scherrer Institut (PSI) require a thorough quantification of initial and boundary conditions when used as an input or benchmark for numerical calculations. Consequently, the velocity field of a steam jet at the tube exit is of some importance when analyzing the ability of a steam jet to break up a helium stratification in an enclosed vessel. To better understand the influence of a bend in the upstream geometry of the supply tube on the flow field, experiments are conducted in a scaled down model (1:5) where detailed measurements of velocity fields are more easily feasible. Those results are compared to velocity measurements conducted for the same Reynolds number at the original tube in a large scale experiment and show a good agreement. This finding supports the future use of scaled components. Additionally, a simplified 90° bend geometry with constant inner diameter followed by straight tubes of various length is considered. For both experiments (scaled tube and simplified tube geometry) a 3D particle image velocimetry (PIV) measurement technique is employed to measure velocity fields in a plane just above the tube exit (6 mm), allowing to measure the velocity components in x, y and z direction. For both geometries the influence of the Reynolds number on the flow field is investigated, revealing no dependence for the scaled tube geometry whereas a Reynolds dependency is seen for the simplified 90° bend up to a certain downstream distance. The distortions of the flow induced by the bend continuously decrease downstream of the bend, however at the last available measurement position (10 diameters downstream) the flow was not yet fully recovered when compared to a fully developed turbulent tube flow.

Acknowledgement

I would like to thank Domenico Paladino, head of the group for experimental thermal-hydraulics at Paul Scherrer Institut (PSI) for offering me the opportunity to conduct my master thesis in his group.

Special thanks belong to my supervisor Ralf Kapulla. With his experience and profound knowledge about particle image velocimetry (PIV) he supported me while performing experiments as well as in the process of data evaluation. I thank him for his time and the many constructive and inspiring discussions we had.

I thank Wilhelm Bissels for his help in setting up the experimental facility and his technical support. Further I thank Sidharth Paranjape, Kevin Manohar, Max Fehlmann and Simon Suter for their support.

Contents

List of Figures

List of Tables

Nomenclature

Symbol	**Meaning**
α	Confidence level
δ	Curvature
μ	Mean value
ν	Kinematic viscosity
σ	Standard deviation
A	Area
D	Inner diameter
f	Frequency
I_p	Inclination parameter
m	Mass
N	Number of samples
p	Pressure
q	Significance level
Q	Flow rate
R	Pipe radius
R_c	Radius of curvature of the bend
t	Time
T	Temperature
U	Bulk velocity
V_x	In-plane velocity in x-direction
V_y	In-plane velocity in y-direction
V_z	Axial velocity in z-direction
w	Axial velocity

Abbreviation	**Meaning**
CCD	Charge-coupled device sensor
CMOS	Complementary metal-oxide semiconductor
De	Dean number
DNS	Direct numerical simulation
LDA	Laser Doppler anemometry
LES	Large eddy simulation
N**	Measurement series for scaled tube
Nd:YAG	Neodymium-doped yttrium aluminum garnet
PANDA	Experimental large scale facility at PSI
PIV	Particle image velocimetry
POD	Proper orthogonal decomposition
PSI	Paul Scherrer Institut
Re	Reynolds number
St	Strouhal number
TKE	Turbulent kinetic energy

1. Introduction

The first section 1.1 gives a brief explanation on why it is of importance to characterize flow velocity profiles downstream of tube bends. In the subsequent section 1.2, findings from selected literature related to curved tubes are summarized.

1.1 Motivation

In case of a severe accident in a nuclear power plant, hydrogen is produced due to zirconium-steam interactions at high temperatures and might accumulate in certain regions of the containment. In case of a hydrogen deflagration, the containment integrity can be threatened [6]. The experimental thermal-hydraulics group at Paul Scherrer Institut (PSI) analyzes the breakup of helium stratifications – the helium represents the hydrogen – in a large vessel by injecting a vertical steam jet (figure 1.1) in order to keep the hydrogen equivalent helium concentration below the deflagration limit. These tests are performed at the experimental facility PANDA at PSI and the results are used as input and benchmark for numerical calculations. Since it is of great importance to accurately define the initial and boundary conditions for numerical calculations, the flow profile at the exit of the steam injection tube must be known, especially because it may be influenced by the bend and the expansion nozzle located at about 10 diamters (D) before the the tube exit (for details of the injection tube see figure 3.1).

To determine the flow profile at the tube exit, particle image velocimetry (PIV) measurements are performed. However, in-situ measurements in the large vessels of PANDA are difficult to conduct due to the limited optical access and are restricted to 2D PIV measurements (only two velocity components of the flow can be measured). Therefore, it was decided to build a small scale experiment with the same tube geometry scaled by 1:5. This approach simplifies measurements considerably as the scaled tube is more accessible. Furthermore, 3D PIV measurements are possible, allowing to recover a full velocity field at the tube exit.

The scaled tube geometry mimicking the original PANDA injection tube is unique and a comparison to data found in literature is not possible. Furthermore, the straight tube after the bend has a fixed length and an investigation of the flow development downstream of the bend is not possible. For these two reasons and to do more fundamental research, the velocity field downstream of a simplified 90° bend with constant diameter and various exit tube lengths is analyzed in a second step. Thus, the present thesis comprises sets of velocity measurements for two tube geometries, i) the scaled tube of the PANDA experiments and ii) a tube with 90° bend and a constant inner diameter.

Figure 1.1: *Drywell of the experimental PANDA facility with the bent steam injection tube inside.*

1.2 Literature Review

Flows in straight tubes are well studied and understood but comparatively little is known about the flow behavior in or past bends. A rather extensive and therefore well cited review on bent tubes of Berger et al. [1] provides a profound theory part, however only covering laminar flow. Therefore, the following summary focuses on experimental as well as numerical studies investigating *turbulent* flow in or past 90° bends. For an extended summary on recent experiments and simulations, please refer to the review of Kalpakli [7] from 2016.

Before moving to rather recent studies, the findings of Dean [8] in 1927 are worth to mention. He conducted analytical studies of laminar flow in bent tubes and mentioned the appearance of counter rotating vortices formed after bends in laminar flows, thereafter named Dean cells.

The transition to turbulence in curved tubes was first investigated by Sreenivasan and Strykowski [9], showing that a turbulent inlet flow in a straight tube can become laminar when entering a coiled tube and returns to its turbulent state in a straight tube downstream of the coil, however remaining laminar until higher Reynolds numbers than upstream of the coil. Bends therefore have a stabilizing effect on the flow. More recently, Kühnen et al. [10] conducted PIV and laser Doppler velocimetry (LDA) experiments in toroidal tubes and Canton et al. [11] studied the flow in a toroidal tube by direct numerical simulation as well as linear stability analysis to investigate the onset of instabilities based on the two parameters Re-number and bend curvature. Linear instabilities are present for all curvatures $\delta = r/R_c \geq 0.002$ (with tube radius r and bend curvature radius R_c), undergoing a Hopf bifurcation at Re $\approx$ 4'000 followed by a periodic regime ($Re = D \cdot U/\nu$, with inner diameter D,

bulk velocity U and kinematic viscosity ν).

Two important experimental studies on turbulent flow in bends are from Enayet et al. [12] and Sudo et al. [4]. Enayet investigated a 90° bend with a curvature of $\delta = 0.18$ by means of LDA. He performed measurements of the axial velocity at the bend inlet (0.58 diameters (D) upstream), at 30°, 60° and 75° degrees bend angles as well as 1D and 6D downstream of the bend for laminar and turbulent flows (Re = 43'000). Static pressure measurements at the bend wall were presented for the turbulent flow, showing positive radial pressure gradients at the outside wall of the bend at the inlet (0°), steady in the midsection (25° to 75°) of the bend and negative towards the bend outlet (from 75° to 1D downstream). At the inside wall of the bend, opposite pressure gradients of doubled value were found. The pressure gradient at the bend entry leads to a shifting of the maximum velocity region towards the inside of the bend and the thickness of the outer wall boundary layer increases with respect to the inner wall. As the pressure gradient starts to change direction towards the tube exit, the maximum velocity is shifted towards the outside of the tube. The effect of secondary flow persists downstream the bend and is still visible at the last measurement position 6D downstream. Later on, Sudo [4] used hot wire anemometry to measure axial and radial velocities at Re = 60'000 for a 90° bend with curvature $\delta = 0.25$ at various locations between 1D upstream and 10D downstream of the bend. Sudo confirmed the findings of Enayet about the maximum axial velocity being located close to the outside wall at the bend exit. He further showed that the axial velocity becomes more uniform with downstream distance, however the secondary flow was not yet fully dissipated after 10D. To see a fully symmetric flow profile - as upstream of the bend - a longer downstream section would be needed. A follow up study of Sudo investigated a U-bend of 180° [13], again showing a maximum axial velocity shifted towards the outside wall at the bend exit. However, 10D downstream (last measurement) of the U-bend the flow distortion had only recovered slightly with the maximum velocity still shifted towards the outside wall.

Al-Rafai et al. [14] measured axial velocities at Re = 34'132 by LDA and compared the experimental results with a numerical calculation of a k-ε turbulence model for two different curvatures, $\delta = 0.07$ and $\delta = 0.14$. It was found that the intensity of the secondary flow is higher for the larger curvature due to increased pressure gradients. The results of the k-ε turbulence model have shown a poor agreement with the experimental data. A summary on turbulence models applied to the flow in curved tubes found in [7] shows that many studies using k-ε models struggled to agree with experimental data. Different turbulence models were compared to the experimental data of Sudo [4] in the study of Kim et al. [5], showing that k-ε models are able to predict the maximum axial velocities at the outside rather well but have difficulties in predicting the flow at the inside. Kim has used the best performing model to compare against his own experimental LDA measurements of a 90° bend ($\delta = 0.17$) at Re = 50'800, Re = 101'600 and Re = 203'200 at downstream distances of 3.5D, 10D and 50D, showing increasingly symmetric velocity profiles with downstream distance for all Re-numbers. Kim claims to see no Re-number dependence

in the structure of the flow past a bend, however this statement was given based on the comparison of axial flow profiles only.

Kalpakli [3] presented a study investigating the swirling of the inlet flow as well as the influence of the Re-number on the flow 0.67D downstream a 90° bend of curvature $\delta = 0.31$ for Re = 14'000, Re = 24'000 and Re = 34'000. He further compared hot-wire measurements to PIV measurements, concluding that hot-wire measurements represent the flow in an acceptable manner, with increasing accuracy at higher swirling of the inlet flow. The swirling flow leads to a diminishing secondary flow in a curved tube, therefore the flow becomes more symmetric. The Re-number study reveals an increase in the normalized velocity for higher Re-numbers at the inside of the bend, whereas almost no influence is seen at the outside of the bend, concluding that the effect of bends is more profound for higher Re-numbers.

An early study of Tunstall and Harvey [15] in 1968 investigated a sharp bend (L-shape) for Re-numbers between Re = 40'000 - 220'000. The axial velocity was measured with a hot wire resulting in a velocity profile at different downstream locations. Visual observations of the air stream by means of injected talc and wool tufts resembled a single swirling vortex, circulating about the axis. Contrary to laminar flow, the flow direction was found to switch between clockwise and anti-clockwise direction in an abrupt manner. A small gold shim flag was installed at 2.2D downstream of the bend to quantify the switching frequency (swirl switching) of the flow direction. The Strouhal number - defined as $St = f \cdot D/U$ with frequency f, inner tube diameter D and bulk velocity U - derived from the flag switching was found to depend on the Re-number (St $\approx$ 0.001 for Re = 100'000 vs. St $\approx$ 0.004 for Re = 220'000). The switching frequency decreased with decreasing Re-number and was not observed for laminar flow. Tunstall and Harvey assumed that the switching was caused by turbulent fluctuations upstream of the bend and the flow separation at the inner bend. Thirty years later, Brücker [16] investigated a 90° bend ($\delta = 0.5$) at Re-numbers of 2'000 and 5'000 by means of PIV technique. The switching of the secondary flow was observed for the higher Re-number measurement where the flow is turbulent but not for the laminar flow at Re = 2'000. The power spectral density of the axial velocity revealed three prominent Strouhal numbers (St = 0.03, 0.12 and 0.2) where the Dean vortices were alternatively shifted towards the upper or lower part of the tube. A single rotating vortex as found by Tunstall and Harvey was not observed. More recently, low order reconstructions based on proper orthogonal decomposition (POD) have been used to analyze turbulent tube flows. Sakakibara et al. [17] used stereo PIV to capture the three dimensional velocity field and applied POD to find the different structures of the flow. Measurements were taken at Re = 120'000, curvature $\delta = 0.75$ and at downstream distances 2D to 15D. The three most energetic modes of the POD were used to reconstruct the flow revealing swirl switching. It was noticed that the different modes evolve with downstream distance and their share of contribution changes. The power spectrum of the POD coefficients show peaks at St = 0.02 - 0.08. Since the study of Sakakibara, multiple studies have used POD to analyze the swirl switching phenomena for experimental studies [18, 19, 20] as well as numerical ones [21, 22]. A recent direct numerical

simulation (DNS) of a 90° tube bend and subsequent POD analysis was performed by Hufnagel et al. [23]. For the modeled bend of curvature $\delta = 0.3$ at a Re-number of Re = 11'700, a switching frequency of St ≈ 0.16 was found while for a lower curvature of $\delta = 0.1$, the Strouhal number was St ≈ 0.045. A wave like structure forming in the bend is claimed to cause the swirl switching. This could possibly be related to a global instability caused by the bend as described by [11, 10]. However, no connection to the upstream straight tube was found, indicating that the swirl switching is caused by the bend itself. Even though the swirl switching of the Dean vortices has attracted some interest in resent studies (see overview in table 1.1) neither an apparent relation to the experimental parameter like bend curvature, the Re-number or the tube diameter was found nor are the findings (numerical value of the St-number) consistent among different authors. This might be i) an indication that this phenomenon is not yet fully understood and ii) it is a hint that additional research into this topic is deliberately required. Since the typical time scale of the swirl switching is beyond the available maximum recording rate (15 Hz and therefore a maximum St-number of 0.12, respectively 0.06 if aliasing is avoided) of the laser used for the present study, our own data do not allow to contribute to this discussion.

Author	Year	Re	curvature δ	z/D	St	frequency $[Hz]$	measurement technique
Tunstall and Harvey [15]	1968	100	1	2.2	0.001	0.2	hot wire, flag
		220	1	2.2	0.004	1.7	hot wire, flag
Brücker [16]	1998	5	0.5	1.5	0.03, 0.12	0.02, 0.09	PIV
Rütten et al. [24]	2001	5, 10	0.17, 0.5	2.5	0.0055, 0.014, 0.2-0.3	-	LES
		27	0.17, 0.5	2.5	0.2-0.3	-	LES
Rütten et al. [25]	2005	5,10	0.17, 0.5	2.5	0.2-0.3	-	LES
		27	0.17, 0.5	2.5	0.01, 0.2-0.3	-	LES
Ebara et al. [26]	2010	200, 400	1	0	0.5	4, 7.5	pressure sensor
Sakakibara et al. [17]	2010	120	0.75	2	0.02-0.07	1-3.4	PIV
Sakakibara et al. [27]	2012	300	-	0, 0.2, 0.4	0.5	60.1	PIV
Hellström et al. [18]	2013	25	0.5	5, 12, 18	0.16, 0.33	2.5, 5.2	PIV
Kalpakli and Örlü [19]	2013	34	0.31	0.67	0.04, 0.12, 0.18	5.7, 17.2, 25.8	PIV
Carlsson et al. [22]	2015	34	0.32, 0.5, 0.7	0.67	0.003-0.01, 0.13	-	LES
		34	1	0.67	0.0003-0.01, 0.13, 0.5-0.6	-	LES
Kalpakli et al. [3]	2015	23	0.39	2	0.1	21.5	PIV
Noorani and Schlatter [21]	2015	11.7	0.1, 0.3	torus	0.087, 0.06, 0.113	-	DNS
Jain [28]	2017	34.8	0.33	0.25	0.07, 0.13, 0.2-0.4	3.9, 7.3, 11.2-22.3	PIV
		34.8	0.33	1	0.03, 0.13	1.6, 6.2	PIV
Hufnagel et al. [23]	2017	11.7	0.3	2	0.03, 0.13, 0.4-0.6	-	DNS, 2D POD
	2017	11.7	0.3	2	0.16, 0.32	-	DNS, 3D POD
Wang et al. [29]	2018	5.3	0.4	1, 2, 3	0.2-0.3, 0.5	-	DNS

Table 1.1: *Summary of experimental and numerical studies investigating the swirl switching behavior, with Re-number (Re), curvature δ, downstream distance after the bend in diameters (z/D), Strouhal number (St) and the frequency in Hz based on own calculation from values extracted from literature. Abbreviations: particle image velocimetry (PIV), laser Doppler velocimetry (LDA), large eddy simulation (LES), direct numerical simulation (DNS) and proper orthogonal decomposition (POD).*

2. Theory of Flow in Curved Tubes

The present chapter aims to give a short summary about the topic of flow in curved bends. First, some basic definitions are introduced. The Reynolds number is defined as

$$Re = \frac{U \cdot D}{\nu}$$

with the bulk velocity U, tube diameter D and kinematic viscosity of the fluid ν. A measure for the strength of the bend is the curvature $\delta = R/R_c$, a ratio between tube radius R and radius of curvature of the bend R_c (measured from origin to centerline, as illustrated in figure 2.1). The Dean number combines Re-number and curvature:

$$De = 2 \cdot \sqrt{\delta} \cdot Re. \tag{2.1}$$

Care must be taken when working with Dean numbers as multiple definitions are used, sometimes even in parallel (e.g. see definition of D, K and κ - all used in [30, 1]).

Fluid flows in curved bends lead to the formation of secondary flows. The present analysis assumes a steady flow with a real viscous fluid in a rigid walled tube. In this case, the centrifugal pressure gradient in the mean flow plays an important role in forming secondary flows [1]. Even though the experiments introduced in the following chapters of this thesis are conducted in the turbulent flow regime, the theory of flow in curved bends is introduced for laminar flow, as this information is more readily available. For a laminar, fully developed flow entering a curved tube

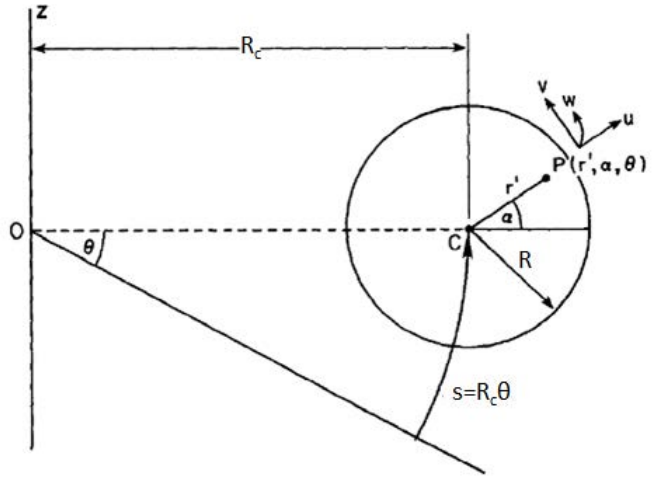

Figure 2.1: *Toroidal Coordinate System. Figure taken from [1].*

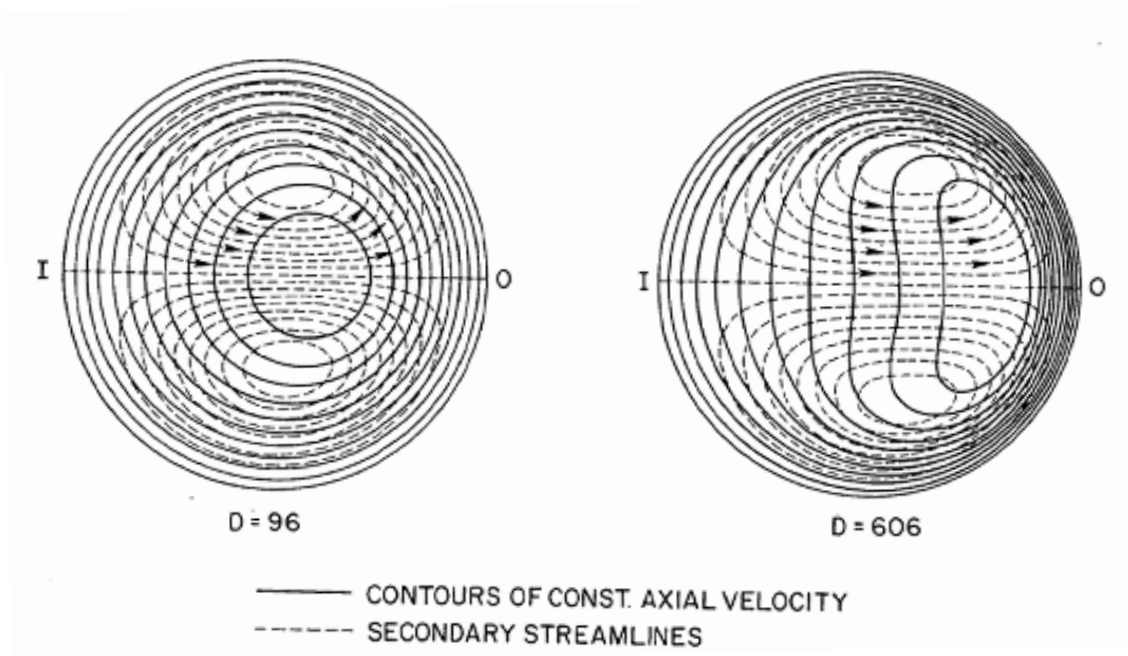

Figure 2.2: *Secondary flow (Dean vortices) streamlines and axial velocity contours with inner bend I and outer bend O at two different Dean numbers, D = 96 and D = 606. The definition of the Dean number D used in [1] compared to the definition of De given in equation 2.1 results in* $D = De/\sqrt{2}$. *Figure taken from [1].*

of radius R and radius of curvature R_c, the secondary motions are investigated in this section. The toroidal coordinate system (r', α, θ) in figure 2.1 with velocity components (u, v, w) is used for the following description.

Portions of fluid of mass m traveling in the middle of the tube (along radius R_c) with a streamwise (axial) velocity w in θ direction experience a centrifugal acceleration w^2/R_c and therefore a lateral force mw^2/R_c. Flow at the inner and outer bend has a lower velocity w due to the no slip condition. Upstream of the bend, the maximum velocity w_{max} occurs in the middle of the tube. Furthermore, the radius of curvature R_c is smallest at the inside of the bend and largest at the outside of the bend. Together, this leads to a maximum of the centrifugal force in the inner half of the tube and a minimum at the outer bend. The resulting lateral pressure gradient enhances a fluid motion from the fast moving central region towards the outside of the bend and a subsequent replacement of the central flow with slow moving fluid from the inside of the bend. This results in a secondary flow in the form of two counter rotating helical vortices which start to form in the bend and persist some distance downstream. These so called Dean vortices are illustrated in figure 2.2. The two vortices are symmetric with respect to the axis $\theta = 0°$. Portions of fluid travelling a curved bend show a helical moving path. The axial velocity profile is no longer parabolic but skewed towards the outside of the bend [31].

The axial wall shear stress on the outside wall is increased by curvature and

decreased on the inside wall. Also, on the outside wall where the shear stress is highest, a boundary layer develops. The secondary flow remains as a two vortex structure at heigher Dean numbers, however the vortex centers move towards the outer bend as does the maximum of the axial velocity.

With increasing Dean number, boundary layers grow. At the outer bend the fluid is entering these boundary layers whereas it is leaving them at the inner bend. In addition, the centrifugal force grows with increasing Dean number and therefore the circumferential velocity increases. Thus, the boundary layer grows near the inner bend and is thinning at the outer bend as more fluid is sucked into the boundary layer at the outside [1]. The formation of the secondary boundary layer leads to a skewing of the Dean vortices. The flow depends more strongly on the Dean number rather than the curvature itself.

Pressure drop measurements along the upstream tube, bend and downstream tube start to differ from a straight tube flow (Poiseuille flow) already a few diameters upstream of the bend [32], indicating that a secondary flow starts to form. The critical Re-number describes the transition from laminar to turbulent flow. Experimental work [10, 9] describe an increase in critical Re-number with increasing curvature at first, but after reaching a maximum (around $\delta \approx 0.04$) the critical Re-number drops with further increase of curvature. For classical tube flow the critical Re-number is $Re_{crit} \approx 2'300$. In tubes, the transition to turbulent happens gradually and turbulent straight tube flow can relaminarize within the bend. A more recent DNS study [11] supports these findings and further performs an instability analysis.

In general it can be said that bends distort the velocity profile and generate secondary flow. At the same time the flow stability is increased. Experiments confirm the transition to turbulent flow rising to Re-numbers up to 5000 [30, 1].

3. Experimental Setup and Parameter Variation

This chapter introduces the experimental setup used to conduct experiments with two different tube geometries. The first geometry is a scaled version of a steam injection tube used in the PANDA facility at PSI, from here on called scaled tube. Details about the scaled tube geometry and the different measurements conducted with it are given in section 3.1. The second geometry consists of a tube with a 90° bend of constant inner diameter of 40 mm and different tubes past the bend to allow for measurements at different downstream distances, as described in section 3.2. As the same air supply loop and PIV setup is used to conduct both measurements, they are introduced in section 3.1 only. Detailed information about the PIV components are given in chapter 4.

3.1 Scaled Tube

The scaled tube geometry is a 1:5 scaling of the steam injection tube used in the drywell of the PANDA facility at PSI. While steam is injected in the PANDA facility, ambient air at 23°C and 0.98bar is used instead for the scaled tube, allowing to simplify the experimental setup considerably. The airflow rate is chosen to reach similar Re-numbers for PANDA and scaled tube. As shown in figure 3.1, the straight tube (piece B) upstream of the $\sim 103°$ bend (piece C) of curvature $\delta = 0.31$ has an inner diameter of 17mm and a length of 357mm (21D). This tube is inclined by 12.9° and connects upstream to a horizontal transition tube (piece A) of 31.2mm inner diameter and 95.6mm length. A flexible hose is connecting the gas supply loop with this transition tube. After the bend, an expansion rises the inner diameter to 40mm (piece D). The exit tube (piece E) therefore has a diameter of 40mm and a length of 400mm (10D). A comparison of media and size between PANDA and scaled tube is given in table 3.1. In order to mimic the double walled tube used for insulation purposes in PANDA, a plastic ring is placed around the tube exit, imitating a wall thickness of 5.5mm. This is done because it is not known if the wall thickness has an effect on the flow entrainment around the tube exit. Therefore, deviations between PANDA and scaled tube are eliminated.

The experimental facility is equipped with a two loop gas supply system to generate the necessary airflow for the experiments (figure 3.2). As the present experiments required only one fluid at ambient conditions, the use of Line #2 was sufficient and the available heaters were not used. The pressurized air supply of PSI was used to generate the airflow and a pressure control valve allowed to adjust the flow rate. Based on flow rate measurements with a coriolis mass flow meter, a controller tuned the pressure control valve to reach the nominal flow rate. Pressure, temperature

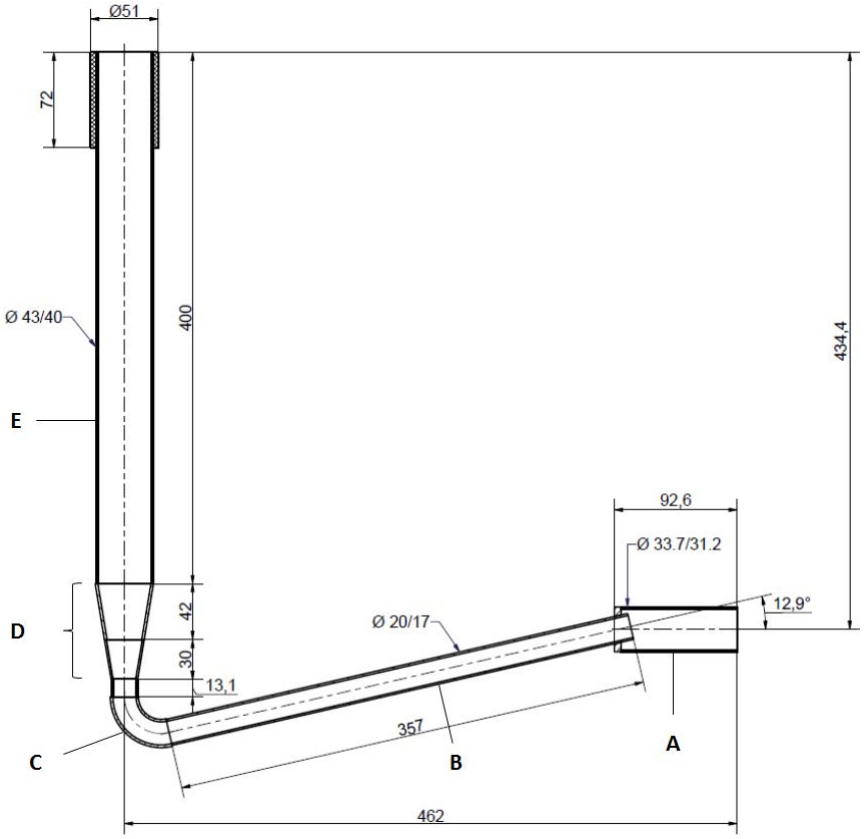

Figure 3.1: *Technical drawing of the scaled tube with dimensions in mm.*

	units	PANDA Tube	Scaled Tube
medium		steam	air
geometric scaling	-	5	1
temperature	$°C$	150	23
pressure	bar	1.3	0.98
diameter	m	0.2	0.04
length straight tube	m	2	0.4
mass flow rate	g/s	30	7.58
volumetric flow rate	m^3/s	0.044	0.007
density	kg/m^3	0.673	1.152
kinematic viscosity	m^2/s	$2.106 \cdot 10^{-5}$	$1.600 \cdot 10^{-5}$
bulk velocity	m/s	1.42	5.24
Re-number	-	$\approx 13'500$	$\approx 13'100$

Table 3.1: *Scaling parameters of the investigated (scaled) tube compared to the original PANDA tube.*

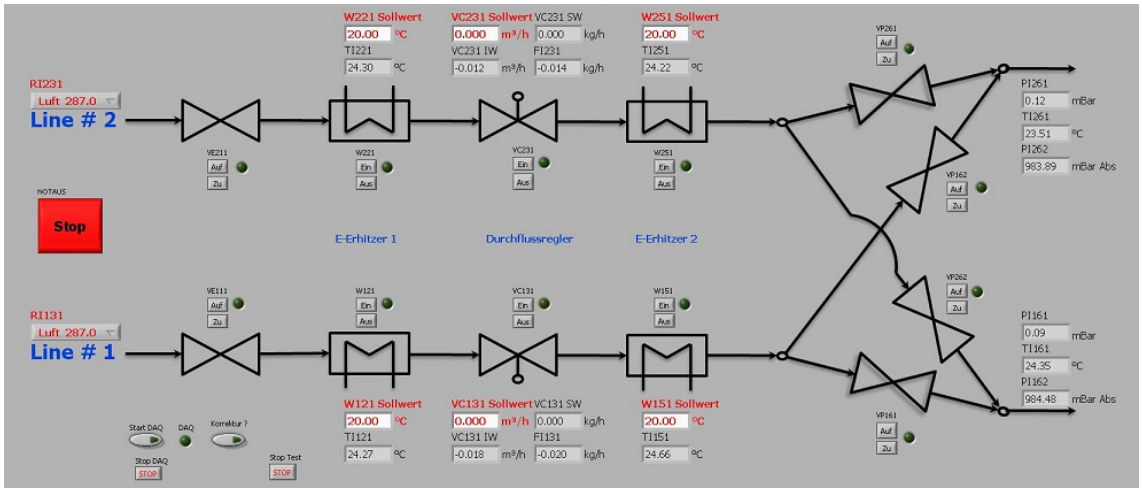

Figure 3.2: *Control scheme of the loop supplying the air flow for the experiments.*

and flow rate were recorded during measurements and analyzed in section 4.2.1. Pressure sensors are piezoresistive measuring cells and the temperature sensors are of the type PT100.

For the PIV measurement, two cameras, a laser with collimating lense, a mirror and a seeder were needed. In order not to be exposed to the stream of seeding particles, the cameras see the tube exit via a mirror. This is seen in a picture of the setup in figure 3.3. The collimating lense produces a horizontal lightsheet. The coordinate system has its origin in the center of the tube, with x- and y-coordinates describing the width and depth respectively and the z-coordinate pointing in downstream direction (axial direction). Because a mirror was used, the images were mirrored with

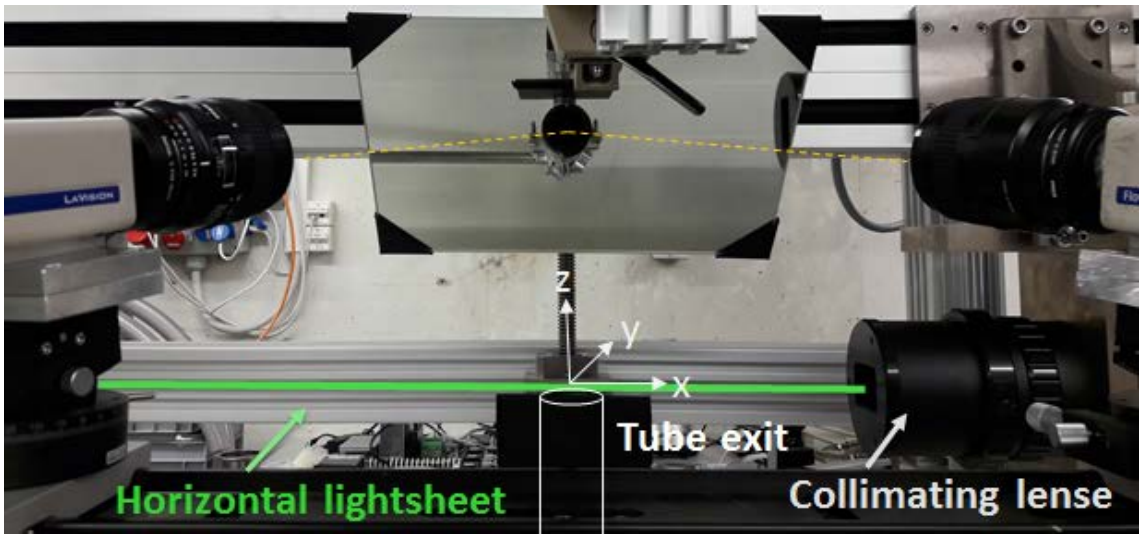

Figure 3.3: *Picture of experimental PIV setup with two cameras imaging the tube exit via a mirror and a collimating lense producing a horizontal light sheet.*

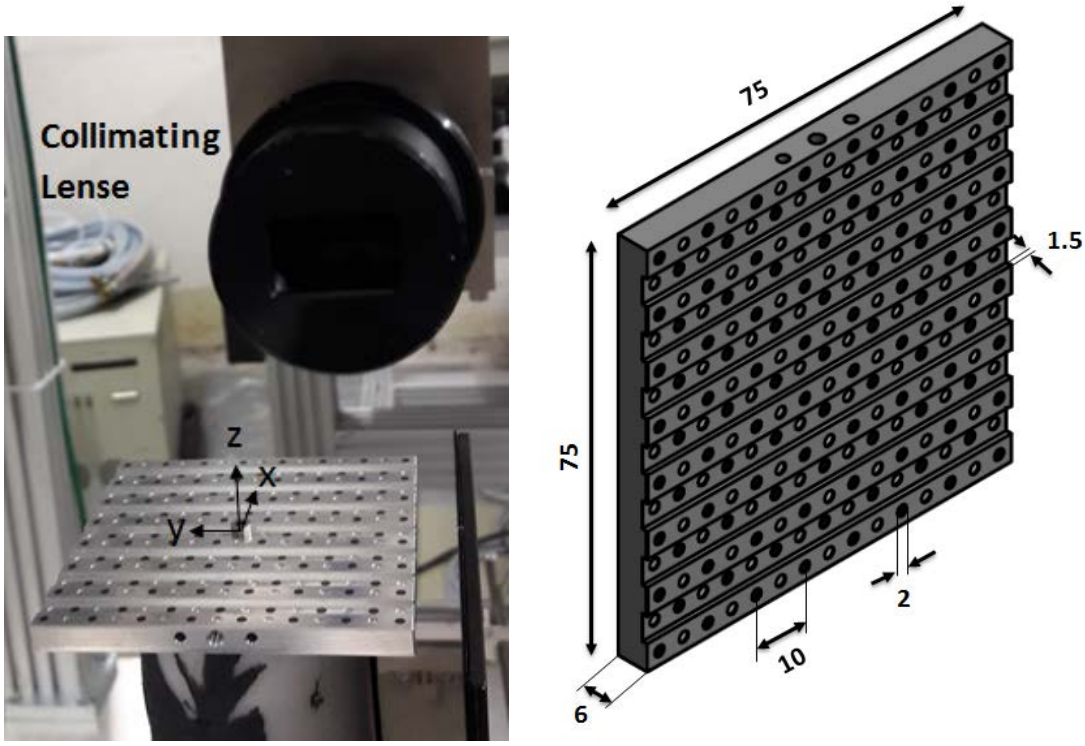

(a) Calibration target placed onto the tube exit with coordinate system

(b) Calibration target with dimensions in mm

Figure 3.4: *Calibration target for 3D PIV measurements.*

respect to the y-axis. This must be corrected either during the calibration or in the post-processing of the raw images. Details about the used equipment are given in section 4.1.1.

When performing 3D PIV measurements, a 3D target is necessary to calibrate the cameras in order to relate the size of one pixel to a length. The calibration target consisted of 15x15 dots with every other row of dots displaced by 1.5mm in z-direction, allowing a calibration of the x, y and z-positions (figure 3.4 b). The 6mm thick target was placed onto the tube exit and the laser sheet was adjusted to touch the upper rim of the target (figure 3.4 a). Therefore, the origin of the coordinate system was located 6mm above the tube exit (in z direction).

The first set of experiments (N04) was a study of the Re-number dependence of the flow with six Re-numbers covering the range from Re = 7'800 to Re = 16'600. A list of the six Re-numbers and the corresponding bulk velocities is given in table 3.2. All of the additional measurements (N05 - N10) conducted for Re = 13'100, tested either the repeatability or the influence of different (eventually) flow modifying components upstream of the 103° bend on the resulting rotational component in the x-y-plane of the jet. Experiment N05 was a repetition of N04 for Re = 13'100. For experiments N06 and N08, honeycombs were placed in the upstream flow of the scaled tube, first before the particle injection only (N06) and then additionally at

Re-number -	Bulk velocity m/s	normalization parameter $V_{z,max}$ m/s
7'800	3.1	3.5
9'700	3.9	4.4
11'700	4.7	5.2
13'100	5.2	5.8
14'600	5.8	6.5
16'600	6.6	7.4

Table 3.2: *Normalization parameters used for scaled tube experiments for the corresponding Reynolds number and bulk velocities.*

the end of the flexible hose, 60mm before the scaled tube (N08). The honeycombs were used to eliminate possible rotational components along the axis of the main flow direction, thus ensuring that all measured rotational components were caused by the specific tube geometry. The locations of the honeycombs are indicated in red in figure 3.5. For both locations, two honeycombs of 50mm length and 3mm cell diameter were placed directly behind each other. The 2m long flexible hose between particle injection and scaled tube was replaced from measurement N07 on. The previously installed hose had a slightly oval cross section whereas the new one had a spiral support structure to ensure a circular cross section. For measurement N09, a new calibration was performed but was otherwise a repetition of N08. For the last measurement (N10), an additional 90° bend of curvature $\delta = 0.4$ was installed approximately 1D upstream of the scaled tube (figure 3.6). This additional bend represented a worst case scenario in terms of possible disturbances introduced to the flow, since in the PANDA facility, many meters of tubes, including multiple bends, lie in between the steam injection tube and the steam generator but the bends are

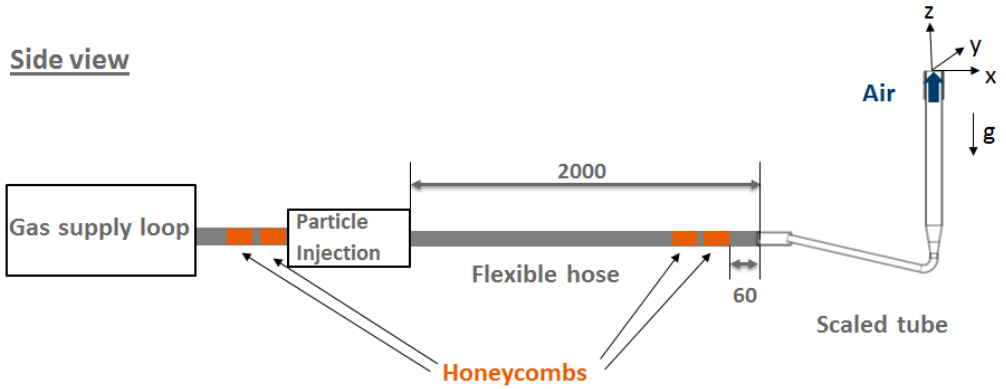

Figure 3.5: *Location of honeycombs before the particle injection (left) and before the scaled tube geometry (right). Dimensions in mm.*

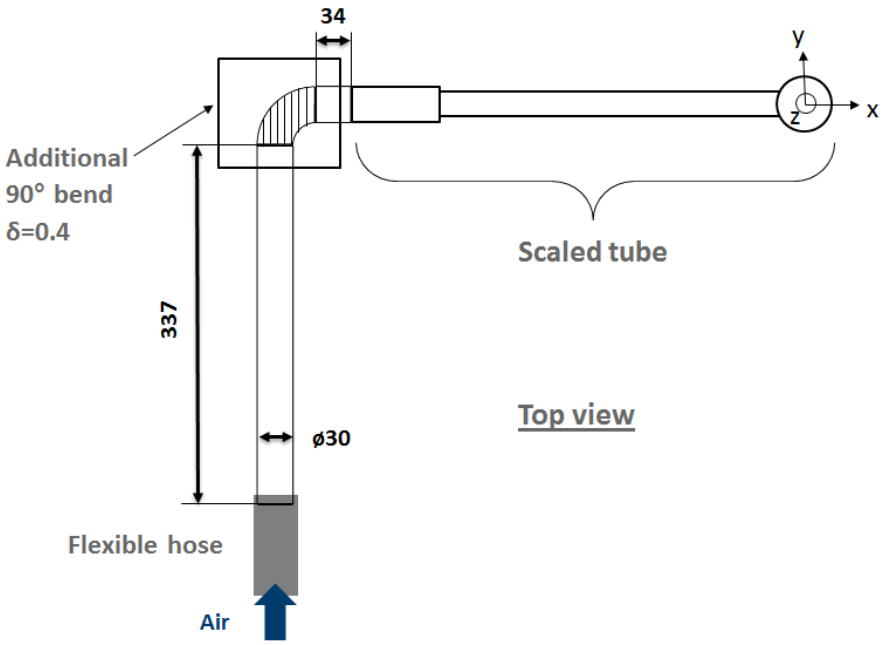

Figure 3.6: *Additional 90° bend placed upstream of the scaled tube for measurement N10. Dimensions in mm.*

located far further upstream. Consequently, whatever distortion was introduced by this additional bend represents a maximized effect compared with the situation in PANDA. If it can be shown that this bend has no significant influence on the flow, this will indicate that it is reasonable to neglect the bends upstream the injection tube in our analysis. All seven measurements (N04-N10) are summarized in table 3.3.

Series	Description
N04	Re number variation (Re = 7'800 to Re = 16'600)
N05	Repetition measurement at Re = 13'100
N06	Honeycombs before particle injection
N07	New flexible hose with circular cross section and smooth inner surface
N08	Additional honeycombs before scaled tube
N09	Repetition of N08 with new calibration
N10	Additional 90° bend upstream of scaled tube

Table 3.3: *Measurement matrix for scaled tube with components modifying the flow conditions upstream as well as a measurement to test for the repeatability (N09).*

3.2 90° Bend

Compared to the scaled tube introduced above, the 90° bend geometry had the same curvature of $\delta = 0.31$ but the inner diameter was a constant value of 40mm upstream of the bend, in the bend and downstream of the bend. Upstream and downstream tubes were plexiglass tubes whereas the bend was 3D printed (figure 3.7). To avoid reflections of the laser light on the plexiglass tube, the inside and outside of the tube exit were sprayed in black.

Five exit tubes of different length between 80mm (2D) and 400mm (10D) were available and can be screwed onto the 90° bend (figure 3.8). The lowest measurement position (no exit tube mounted) was 32mm (0.8D) downstream of the bend. All six measurement positions are listed in table 3.4. The length of the straight upstream

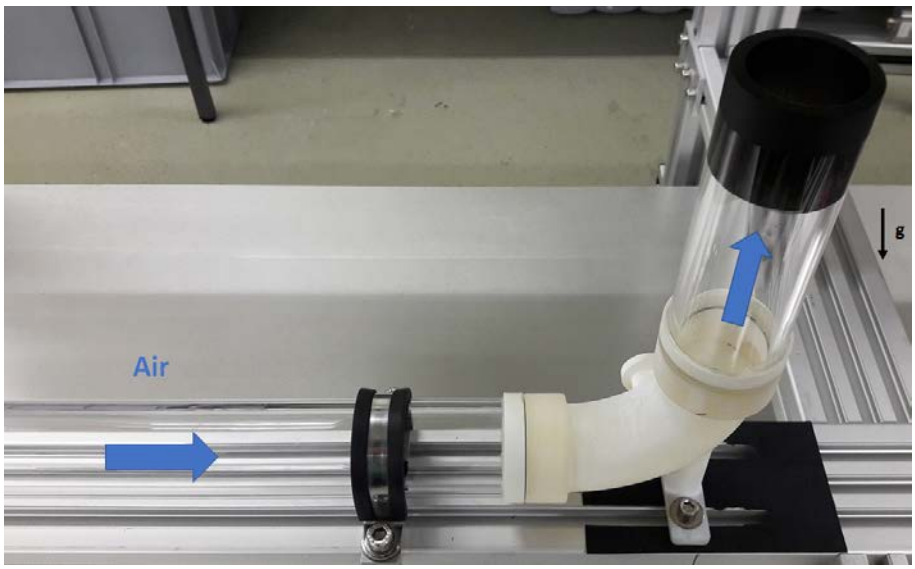

Figure 3.7: *90° bend with inlet tube (upstream) and exit tube of length of 4D (downstream).*

Height $[D]$	Height $[mm]$
0.8	31
2	80
4	160
6	240
8	320
10	400

Table 3.4: *Measurement positions downstream of 90° bend given in diameters D of the tube and in mm.*

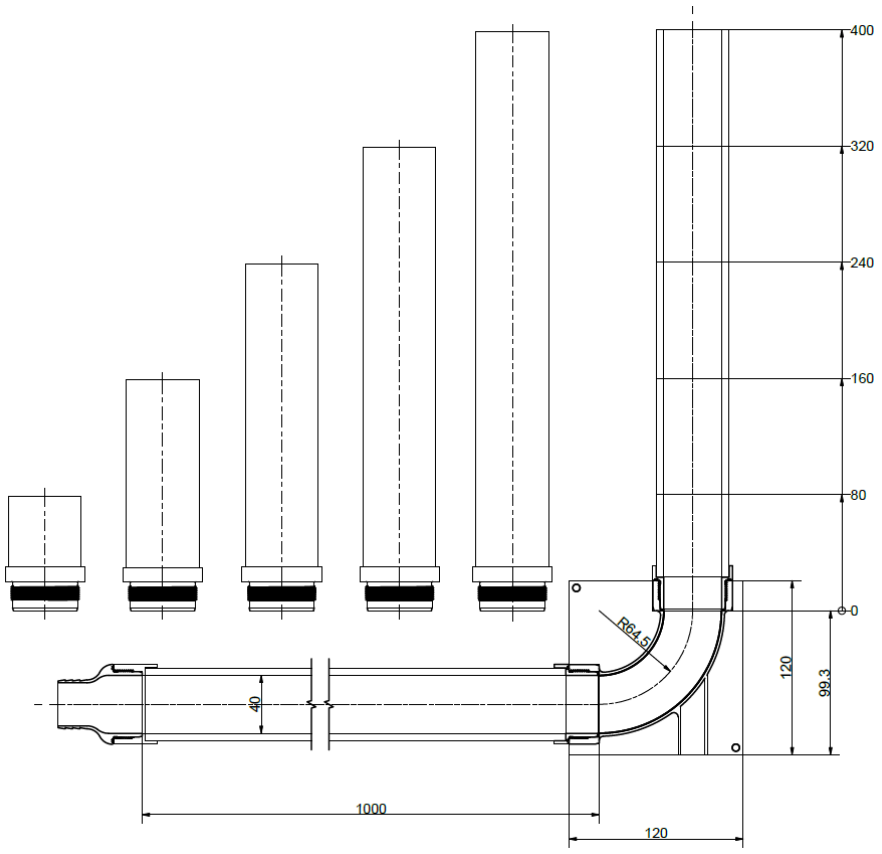

Figure 3.8: *Technical drawing of the 90° bend with its exit tubes of different length. Dimensions in mm.*

Abbreviation	Re-number [-]	Bulk velocity $[m/s]$
Re1	4'900	1.9
Re2	7'800	3.1
Re3	12'600	5.1
Re4	17'500	7.0
Re5	27'200	10.9

Table 3.5: *Re-number abbreviations, their corresponding numerical values and the associated bulk velocities.*

tube was 1000mm (25D), ensuring that the inlet flow was fully developed. At each height, measurements at Re-numbers of Re = 4'900, Re = 7'800, Re = 12'600, Re = 17'500 and Re = 27'200 were conducted. Corresponding bulk velocities are found in table 3.5.

4. Measurement Technique and Analysis

4.1 PIV Theory and Analysis

In the following sections, the reader should get a short overview and introduction into the method of Partice Image Velocimetry (PIV). The topic is examined from a theoretical as well as an applied perspective. Details about the experimental PIV setup used for the following experiments are given. The analysis of the raw images and the necessary post processing steps are described. In a second part, section 4.2, the gas supply loop data conducted during an experiment is evaluated in order to validate the stability of the fluid temperature, pressure and flow rate. Finally, the method of error calculation is introduced.

4.1.1 PIV Theory and Measurements

The flow visualization technique PIV will be introduced briefly in this section. For further information, please refer to [2, 33]. The basic idea is to illuminate tracer particles added to a flow. The illumination takes place twice within a short time frame and the scattered light of the particles is recorded by cameras. Based on the displacement of the particles between the light pulses, it is possible to analyze the fluid flow. The displacement is found with a spatial cross correlation algorithm, based on fast Fourier transform (FFT). A basic 2D PIV setup with laser, tracer particles and imaging optics (camera) is shown in figure 4.1. From this illustration it becomes clear that the flow can be evaluated in the plane of the laser sheet only. When using a single camera to image the tracer particles, it is possible to calculate the velocity of the particles in the plane of the light sheet, meaning in two directions. However, if the tracer particles are imaged simultaneously by two cameras, both imaging the flow from different angles, it is possible to retain the depth information of the particle movement as well. Therefore, all three velocity components can be determined [33]. This method is named stereoscopic PIV or 3D PIV.

For the PIV analysis, the so called image plane is divided into smaller areas, depicted as interrogation windows (figure 4.2). The particle displacement Δx between the first light pulse at time t and the second light pulse at time t' is calculated with a spatial cross-correlation for every interrogation window as an ensemble movement of all particles in this interrogation window. The resulting velocity is $v = \Delta x/\Delta t$, with $\Delta t = t' - t$, the time between two laser pulses. Depending on the flow velocity of the fluid, Δt must be adapted to avoid particles leaving the interrogation window during Δt. In practice, Δt is set in a way to allow the particles in streamwise

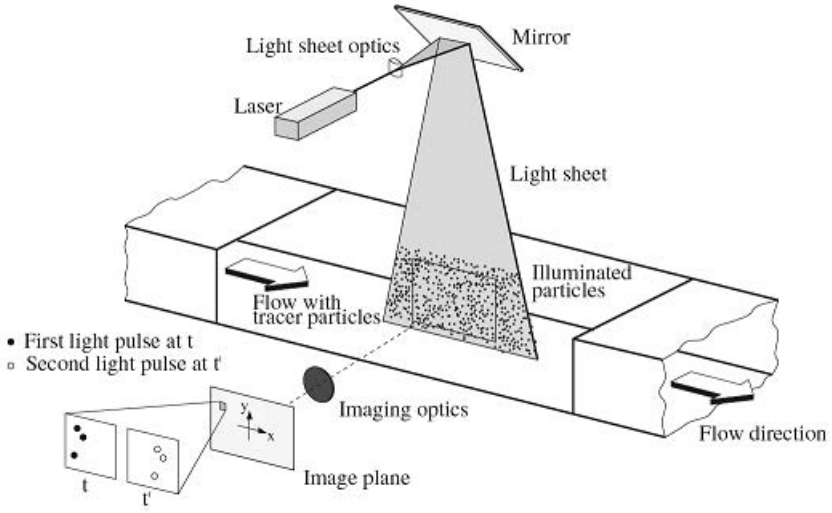

Figure 4.1: *Basic Setup for a PIV measurement, figure taken from [2].*

direction to travel about 10 pixels during this time interval, i.e. approximately one quarter of the size of the first interrogation window.

Before every measurement, a calibration is necessary to relate the size of one pixel to a length and define its spatial orientation. For this purpose, a calibration target is mounted in the desired flow measurement region (figure 3.4).

For the PIV measurements conducted in this project, a stereoscopic (3D) PIV technique was used, allowing to measure all three velocity components. The 0.5mm thick horizontal laser lightsheet was set to (horizontally) cross through the fluid jet exiting a tube. The used laser was a Nd:YAG laser with a wavelength of 532nm, 200mJ power and a maximum sampling frequency of 15Hz. In order to avoid degrading the camera lenses with tracer particles, the flow above the tube exit was imaged via a mirror. Two cameras were installed, both alligned in the same horizontal plane, facing the mirror with a 50° angle inbetween them (figure 3.3 in chapter 3). The used CCD cameras were Kodak MegaPlus ES 1.0 both equipped with Nikon lenses with a focal length of 60mm, aperture 1:2.8D and f-stop set to f/4. The tracer particles were of Polyethylenglycol and had a diameter of 3-6μm. A Laskin nozzle was used to generate the droplets [34]. The droplets were small enough to follow the flow. Drag effects can be neglected. Generally, the particles should be as small as possible to follow the flow most accurately. However, larger particles have the benefit of stronger light scattering. A higher power light source is needed to compensate the weaker scattering of small particles.

With one camera pixel corresponding to $0.074mm$, the effective spatial resolution for the used setup was $0.296 \times 0.296mm^2$. When using a final interrogation window size of 32x32 pixels with 87% overlap, the final effective resolution was 4x4 pixels. The temporal resolution is limited either by the pulsing frequency of the laser or the speed of the capturing rate of the CCD cameras. The alternative use of the more modern complementary metal oxide semiconductors (CMOS) sensors instead of the CCD technology would allow image sampling in the kHz range. In the performed

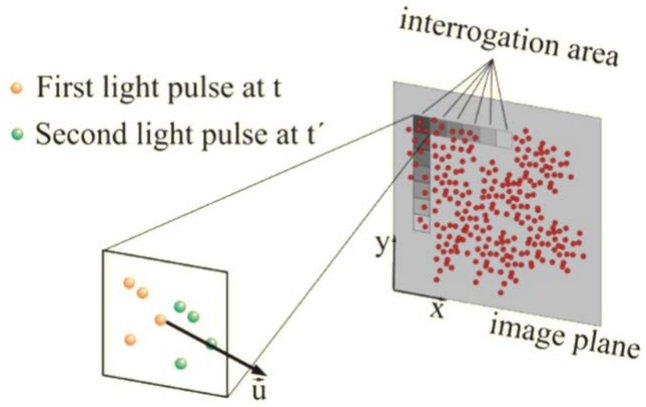

Figure 4.2: *Interrogation area (window)*

experiments, the temporal resolution was limited by the maximum laser pulsing frequency of 15Hz. For all measurements, 1024 images were taken at a sampling frequency of 15Hz.

To conduct the PIV measurements, the commercial software DaVis 8.3 from LaVision was used.

4.1.2 PIV Analysis

Because the exit of the tube, where the PIV measurements were conducted, was not in a small, enclosed container, the surrounding area of the tube exit could not be sufficiently filled with seeding particles. Reasonable velocity measurements were therefore only possible at the tube cross section, where sufficient seeding was present. In order not to evaluate the few velocity measurements in the surrounding of the tube exit, a mask was fitted around the cross section of the tube exit images, enforcing a pixel value of zero everywhere around the tube. In order to place such a mask, the average of all 1024 images was calculated for both sets of images (from the two cameras). Due to the inclined camera positions, a dewarping algorithm was used. A mask was then positioned around the tube exit. The positioning of the mask by eye was verified by comparing the location of the center of the mask (x_m, y_m) with the zero point of the coordinate system. Good alignment was found with a maximal deviation of the mask center of 8 pixels in x direction and 6 pixels in y direction, which corresponds to 0.6 and 0.4mm respectively. Once the mask was set, an inverse dewarping step was applied to the mask.

The instantaneous velocity fields will unavoidably contain spurious velocity vectors, requiring a potent post processing to clear out these outliers. False vectors were identified by comparing every velocity vector with its neighboring vectors. If one vector deviated strongly, either in magnitude or direction, from the surrounding vectors, it was identified as spurious vector. Most outliers were found at the edge of the data field. The presence of spurious vectors is less severe if looking at mean values of the averaged velocity fields but, for example, can greatly distort the calculated standard deviations.

The final output generated by the analysis performed with DaVis contains the average velocity fields in all three directions (V_x, V_y, V_z), the standard deviation of these velocity fields (σ_{Vx}, σ_{Vy}, σ_{Vz}), the turbulent kinetic energy (TKE) and the Reynolds stresses (R_{xy}, R_{xz}, R_{yz}, R_{xx}, R_{yy}, R_{zz}). Furthermore, uncertainty fields for all mentioned quantities are calculated [35].

The complete post processing of the PIV raw data was performed in DaVis 8.3 from LaVision.

4.2 Experimental Parameters

4.2.1 Gas Loop Data Analysis

The experimental facility was equipped with a gas supply system as described in chapter 3 and illustrated in figure 3.2. During the performance of experiments, pressure, temperature and flow rate of the fluid flow were measured to crosscheck with the target values. Temperature and pressure were measured with a PT100 sensor and a piezoresitive measuring cell respectively, at the exit of the flow supply system, before the fluid entered the experimental loop. A coriolis mass flow meter was used to measure the mass flow rate, which was then converted to a flow rate based on the measured temperature and pressure. Temperature T and pressure p influence fluid properties as density and viscosity and therefore the Re-number. A

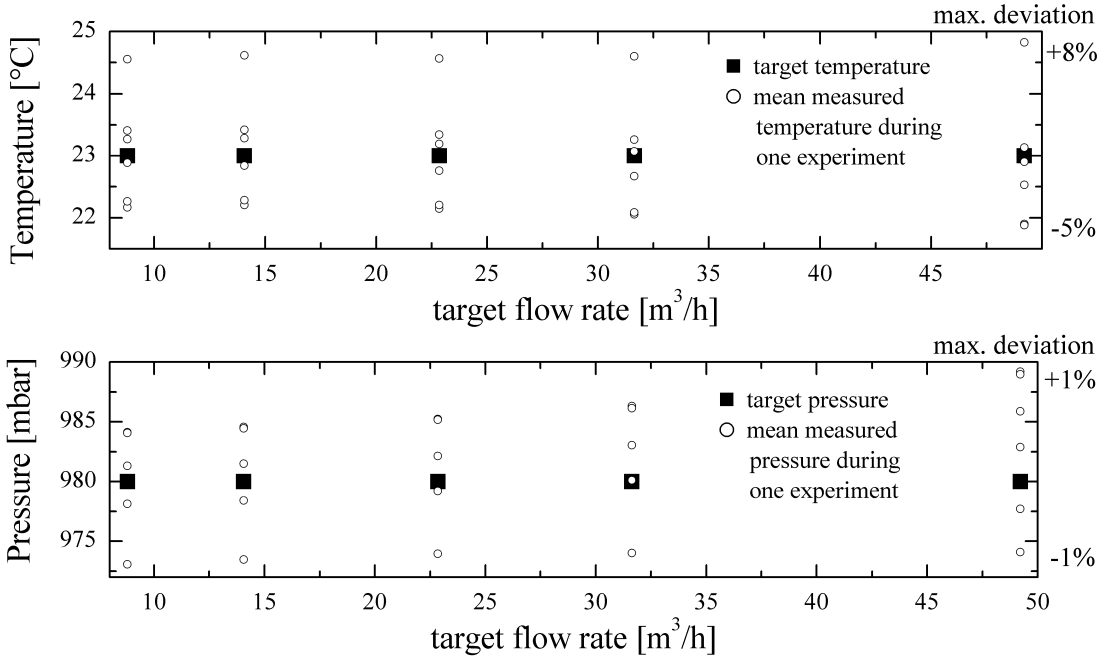

Figure 4.3: *Comparison of measured vs. target temperature and pressure for all measurements of the 90° bend for the 5 flow rates corresponding to the 5 investigated Re-numbers.*

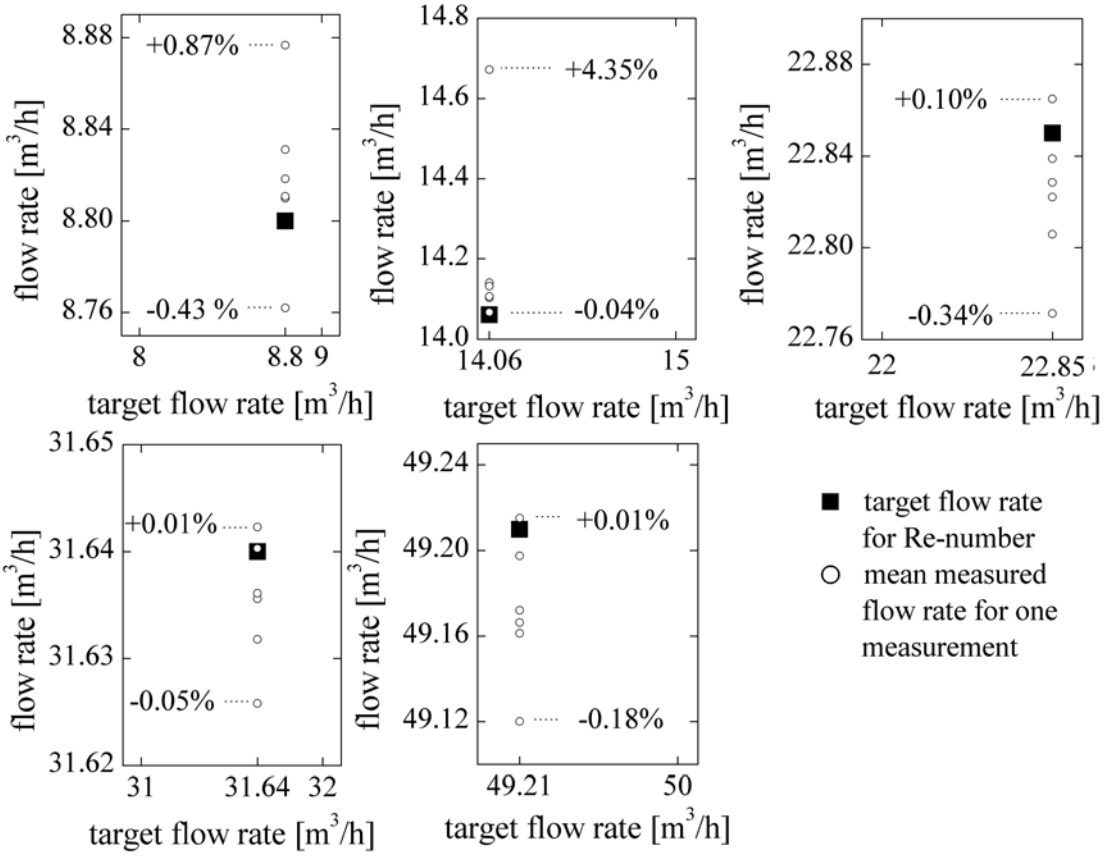

Figure 4.4: *Comparison of measured flow rates vs. target flow rates for all measurements of the 90° bend for the 5 flow rates corresponding to the 5 investigated Re-numbers. Maximum and minimum deviations from the target value are indicated in %.*

target temperature of $T = 23°C$ and a target pressure of $p = 980mbar$ were taken for Re-number calculations. The average temperature and pressure values were plotted against the target flow rate of the measurement in figure 4.3. The temperature deviated less than 8% from the target value whereas pressure deviated no more than 1%. Re-number calculations are influenced by less than 5% by the temperature and pressure variations. Without further noting, all following calculations assume $T = 23°C$ and $p = 980mbar$.

Averaged flow rate measurements for every experiment were compared to the given targeted flow rate. Except for a single measurement at a flow rate of $14.06m^3/h$, measured flow rates deviated less than 1% from the target flow rates (figure 4.4). Given this good agreement, all following calculations assumed target flow rate conditions if not stated otherwise. As measured temperature, pressure and flow rate values agreed well with the results of the 90° bend loop data, a detailed analysis of the gas loop data for the scaled tube measurements was foregone.

4.2.2 Error Calculation

The following error calculation was used when presenting mean values of the scaled tube data in section 3.1. Mean values are calculated in the following way:

$$\mu = \frac{1}{N}\left(\sum_{i=1}^{N} x_i\right) \tag{4.1}$$

and the standard deviation accordingly:

$$\sigma = \sqrt{\frac{1}{N-1}\sum_{i=1}^{N} |x_i - \mu|^2}. \tag{4.2}$$

The mean is estimated with 99% confidence:

$$\left[\mu \pm t_{\alpha,N-1} \cdot \frac{\sigma}{\sqrt{N}}\right] \tag{4.3}$$

with coefficient $t_{\alpha,N-1}$ from the Student's distribution for the degree of freedom $N-1$, confidence level $\alpha = 99\%$ and significance level $q = 1 - \alpha = 1\%$ [36].

5. Results and Discussion

The following chapter presents and analyzes the experimental results found in the course of the present master thesis. Care has been taken to condense the extensive set of data in order to support the main findings and to give the reader an overview of the performed work.

In a first section, the scaled tube experiments are discussed and compared to PANDA in situ measurements. A second section presents the findings of the 90° bend experiments, including a comparison of the results with literature.

5.1 Scaled Tube

The scaled tube results are analyzed in the first part of this section, followed by a comparison of the data with PANDA in-situ measurements in the second part.

5.1.1 Analysis of Scaled Tube Measurements

To start into the discussion about the scaled tube measurements, the three velocity fields V_x, V_y, V_z at the tube exit after the bend are analyzed. These fields represent average velocity values (averaged over 1024 instantaneous velocity fields). The velocity fields are presented with respect to the coordinate system pictured in figure 3.3 (chapter 3) with the origin ($x = y = 0$) located in the axis of the tube (figure 5.1). For a better orientation and for the sake of the discussion of the results, the locations top, bottom inside and outside are introduced in figure 5.1 b). These locations are defined with respect to the top view onto the tube exit. Inside and outside depict the inside and outside of the bend (see also figure 5.1 b). The V_x and V_y velocity components range from -0.3 m/s to +0.3 m/s. The maxima are located at the bottom right for V_x (figure 5.1 a) and at the outside for V_y (figure 5.1 b). The velocity minima for V_x and V_y are found at the top right and bottom inside, respectively. While the minimum of V_x is located along the top circumference, the minimum for V_y stretches towards the middle with a triangular shape. When looking at the in-plane vector field of V_x and V_y in figure 5.1 c), a weak counterclockwise rotation of the entire jet is seen as expected based on the direction of the in-plane velocities indicated by black arows in figure 5.1 b) and c). However, this rotation of the flow must be put into perspective to the velocity magnitudes of V_z. The in-plane velocities V_x and V_y have a magnitude $< 4\%$ of the streamwise velocity V_z. This statement holds true for all Re-numbers considered here. Given this information, the observed rotational component of the flow is very weak. Based on this observation, the following analysis mostly focuses on the streamwise velocity component V_z. This main flow component reaches velocities up to 6 m/s for Re = 13'100. The

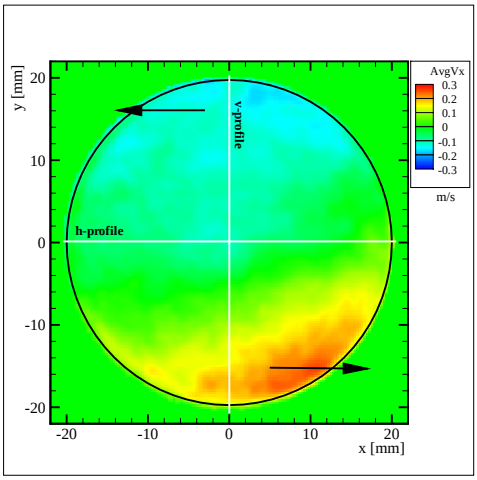

(a) Velocity field of V_x

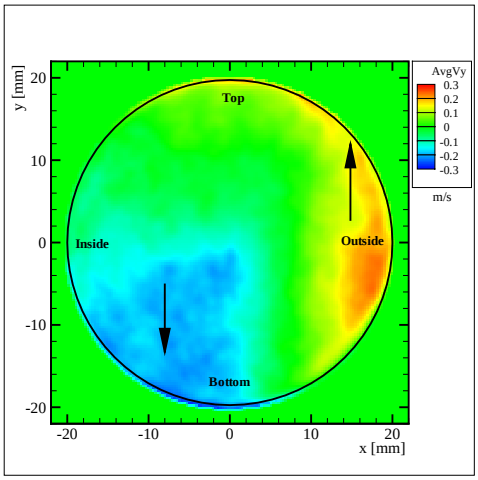

(b) Velocity field of V_y

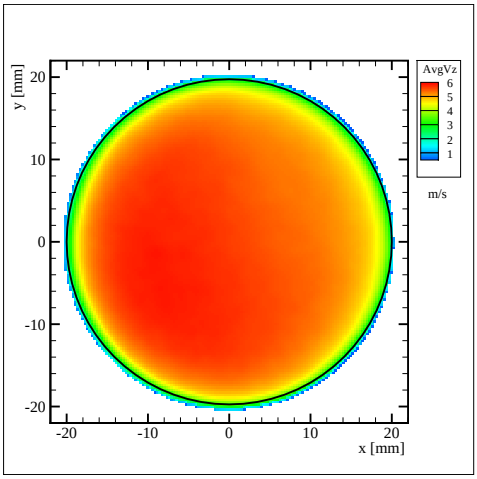

(c) Velocity field of V_z

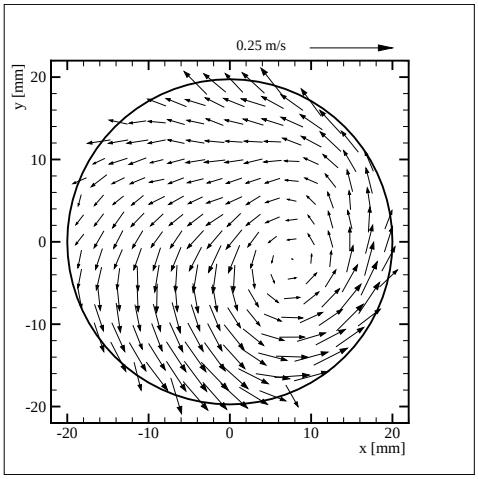

(d) In-plane vector field of V_x and V_y

Figure 5.1: *Averaged velocity fields and streamlines for the three velocity components V_x, V_y, and V_z for the scaled tube measurement N04 conducted for Re = 13'100.*

velocity maximum is located towards the inside and strong velocity gradients are seen towards the border of the jet in figure 5.1 c).

As plots of full velocity fields are difficult to compare, most of the following graphs depict horizontal or vertical cross sections of the full velocity field. Horizontal profiles were extracted at $y = 0$ and vertical profiles at $x = 0$ (see figure 5.1 a). A first set of measurements was dedicated to investigate the Re-number dependence of the flow profiles at the scaled tube exit. Six Re-numbers between $Re = 7'800$ and $Re = 16'600$ were analyzed. For this purpose, horizontal profiles of the normalized velocity of V_z are shown in figure 5.2, top. The x-axis indicates the position along the cross section normalized with the tube radius R. The axial velocity is normalized with the maximal axial velocity in the horizontal cross section $V_{z,max}$, thus resulting

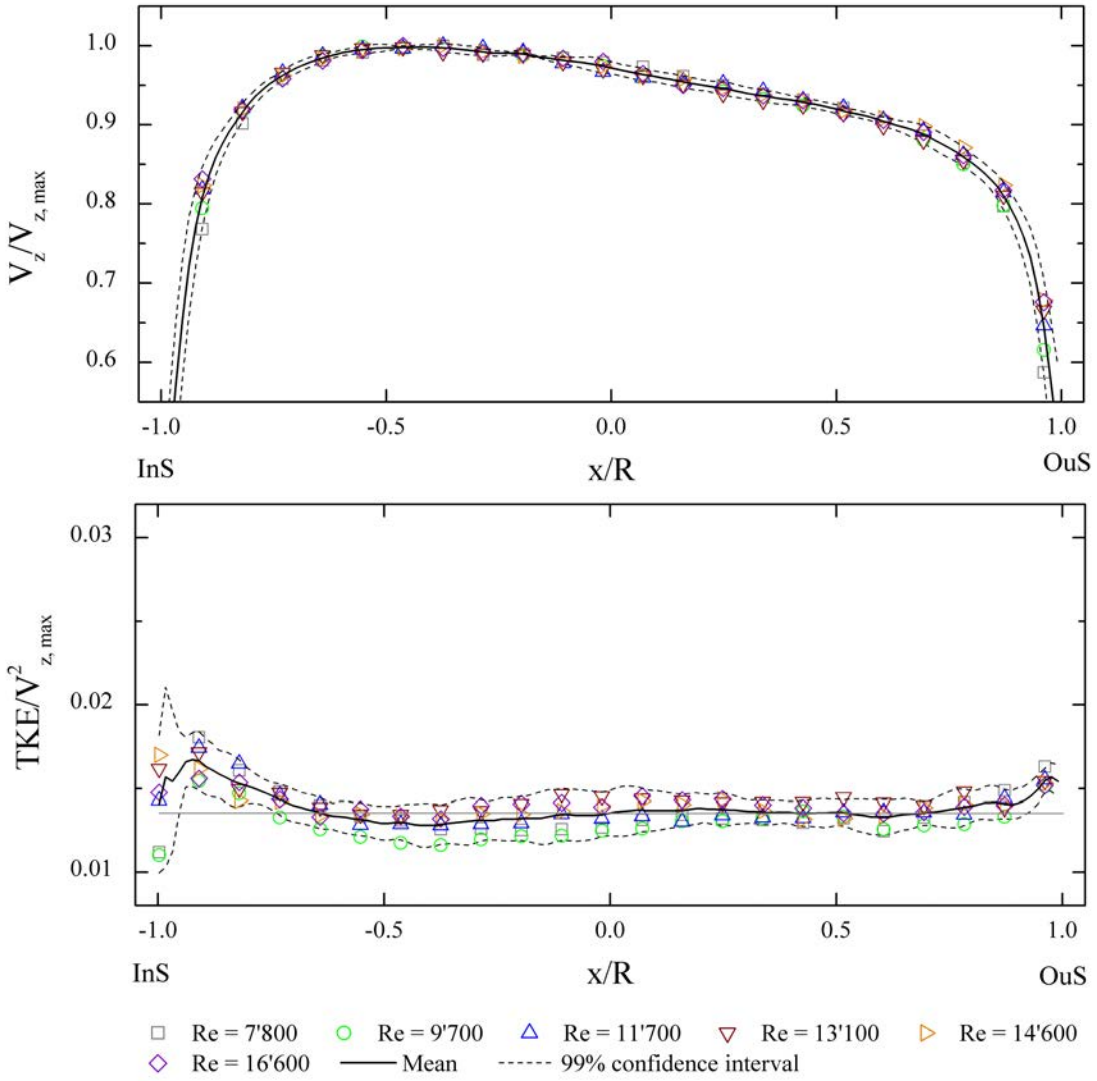

Figure 5.2: *Horizontal profiles of the normalized axial velocity $V_z/V_{z,max}$ (top) and the normalized $TKE/V^2_{z,max}$ (bottom) with the Re-number as parameter. Results from measurement series N04. Every sixth measurement point is plotted.*

in a maximum normalized velocity of $V_z/V_{z,max} = 1$ at $x/R \approx -0.5$. Even though a small inclination of the velocity is visible – with the higher velocity at the 'inner' side – almost no dependence on the Re-number is visible, i.e. the inclination is independent of the Re-number. Only towards the boundary of the jet, where large velocity gradients are present, some deviations between the measurements are visible. However, they are still within the indicated 99% confidence interval. The error margins were calculated according to equation 4.3. The normalized turbulent kinetic energy (TKE) in the bottom of figure 5.2 is in the order of 0.014 $TKE/V^2_{z,max}$, indicated by a grey horizontal line. Generally, TKE variations between the different Re-numbers are weak and within the 99% confidence interval for the core region

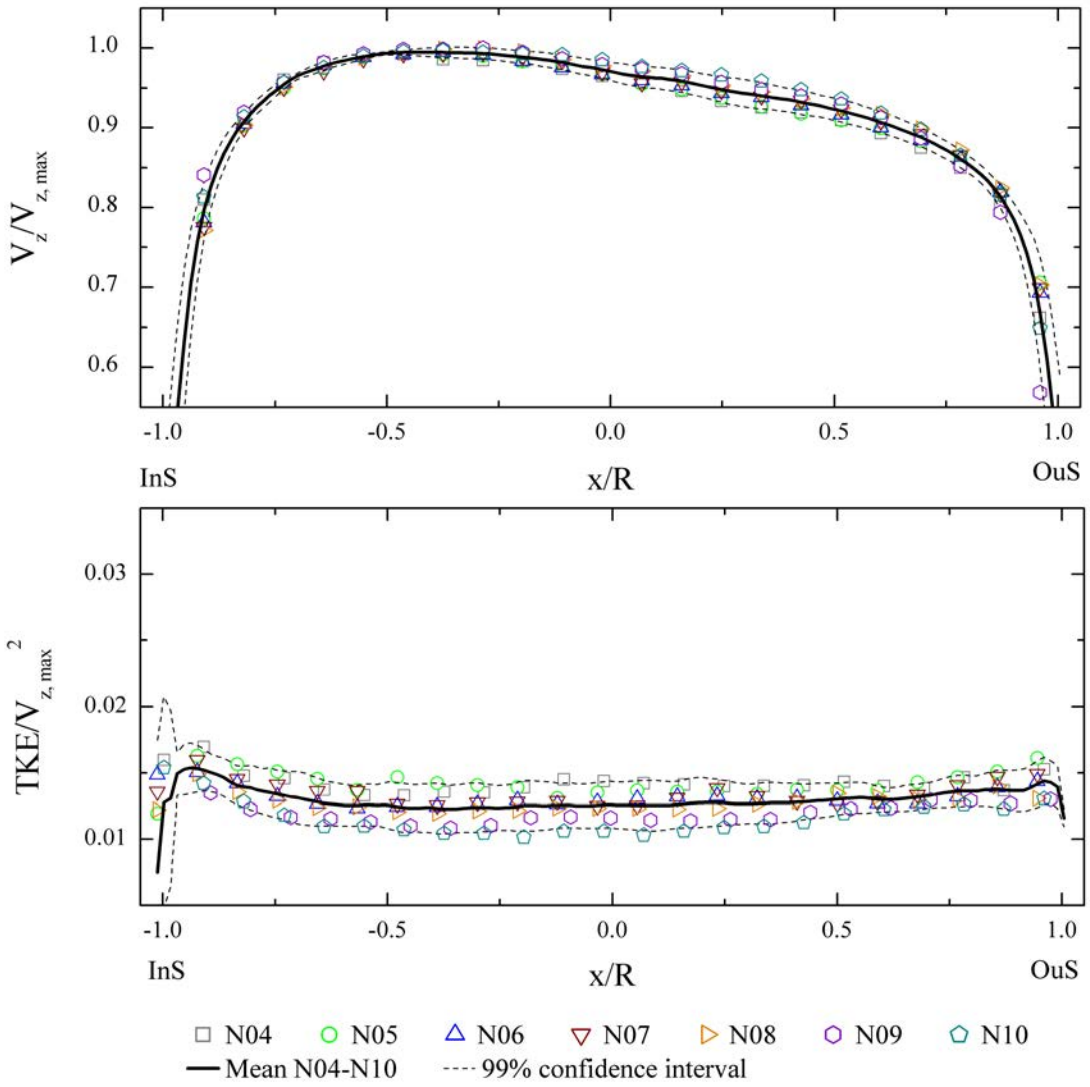

Figure 5.3: *Horizontal profiles of the normalized axial velocity $V_z/V_{z,max}$ (top) and the normalized $TKE/V_{z,max}^2$ (bottom) for different measurements N04-N10 at Re = 13'100, see also table 3.3.*

$-0.8 < x/R < 0.8$. The TKE only increases after $x/R < -0.8$ where velocity gradients are large. Overall, it can be summarized that the Re-number has a very weak influence on the flow for the range of Re-numbers considered here (7'800 to 16'600). Based on this finding, Re-number inaccuracies due to small temperature, pressure or flow rate deviations from the nominal value as discussed in section 4.2.1 have no noticeable effect on the flow characteristics.

Even though the slight rotation of the jet flow is reasonably weak (figures 5.1 a, b and c), it must be analyzed whether it was an effect caused by the scaled tube geometry or if it was introduced upstream of the scaled tube already. For this purpose, multiple measurements with adaptions upstream of the flow were conducted to eliminate a possible rotation of the inlet flow. The measurement series were

numbered starting with N04 (only the recordings at Re = 13'100 was used from this series) until N10 (table 3.3 in chapter 3). Further information about the individual measurements are given in section 3.1. All measurements were conducted at the same Re-number Re = 13'100. As for the Re-number variation, horizontal profiles of the normalized axial velocity, as well as the normalized TKE are analyzed to compare the different measurement series (figure 5.3). The indicated mean is the mean of all measurements (N04 through N10) and the indicated error is for $\alpha = 99\%$. Small variations of the streamwise velocities are noticeable but are still within the error bounds (figure 5.3, top). The deviations are too small to see a systematic dependence on the measurement series. Again, larger deviations are only found close to the boundary between the jet and the quiescent ambient, i.e. for $x/R < -0.8$ and $x/R > 0.8$.

For the TKE, only the measurement N10 is in parts slightly below the error bounds. However, here a trend of decreasing TKE with the addition of the honeycombs is seen (N06 vs. N05 and N08 vs. N07). A first drop in TKE is noticed when honeycombs are placed before the particle injection (N06). With the new flexible hose, the TKE increases slightly. This was not expected, since the old hose was slightly elliptic. The additional honeycombs just before the scaled tube (N08) only show a marginal decrease in TKE. Some decrease in TKE is seen for the repetition measurement of N08 (N09). This decrease is in the same order as the decrease induced by the first honeycombs before the particle injection. Based on this, it is questionable to argue that the previous trend of decreasing TKE is actually linked to the presence of flow straighteners.

As already mentioned, the only measurement which falls in parts slightly below the error bounds is N10 with an additional 90° bend upstream of the scaled tube. At a fist glance it looks as if the additional bend would lower the TKE, however this is only the case in the middle of the cross section. At the boundaries the TKE is higher compared with measurement N09 and the variation in TKE along the cross section has increased, indicating a weak destabilisation effect of the flow due to the additional bend. The rotational component of the flow keeps its counter clockwise orrientation for N04 through N09. However, for the additonal 90° bend in N10, the rotation changes to a clockwise orientation (not shown). In-plane velocity magnitudes stay comparable.

All mentioned phenomena happen on a very small scale and overall it must be concluded that the influence of the honeycombs and the new hose are close to not detectable. Even an additonal 90° bend upstream of the flow (to maximize a possible distortion) has only a minor influence on the flow. Because the in-plane rotational flow is very weak, the change in rotation direction for the additional 90° bend has little influence on the axial flow. Therefore, it is reasonable to investigate the scaled tube with a straight inlet tube, even though in the PANDA facility it is preceded by multiple bends far further upstream.

Besides analyzing the gas loop data (section 4.2.1), the accuracy of the flow rate compared to the nominal flow rate can be evaluated by integrating the axial velocity V_z along the tube cross section to compute the flow rate Q as

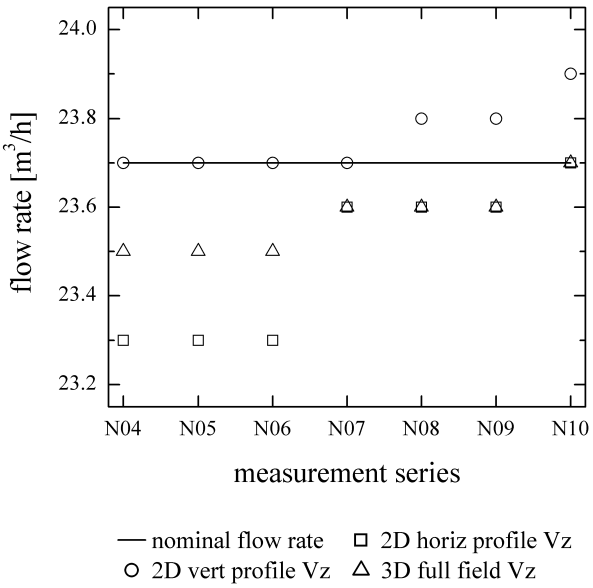

Figure 5.4: *Comparison of calculated flow as obtained through integration of horizontal (i), vertical (ii) and entire flow field (iii) with nominal flow rate (for V_z).*

$$Q = V_z \cdot A = V_z \cdot \pi \cdot R^2 = \int_{-R}^{R} V_z \cdot \pi \cdot r dr \tag{5.1}$$

with tube radius $R = 20mm$ and cross section A. Calculations are performed based on three different approaches. The first two take the horizontal (i) or vertical (ii) velocity profiles and solve the integral in equation 5.1. These two approaches are called "2D horizontal profile" and "2D vertical profile" respectively.

By using the entire profile as shown in figure 5.2, top for the integration, the 2D methods even out flow asymmetries as they basically rotate the horizontal or vertical profile to get full velocity fields. This is equivalent with integrating the left and the right half of the profile separately and calculating the average of both results. A third method (iii), using the full velocity field simply multiplys every velocity value $V_{z,i}$ with the size of the corresponding integration window $A_i = 0.296mm \cdot 0.296mm$, which corresponds to the spatial resolution of the velocity field. This last method is called "3D full field". The flow rates are calculated for all measurements N04 through N10 and are compared to the nominal flow rate of $23.7m^3/h$ (figure 5.4). The maximum deviation of the integrated flow rate to the nominal flow rate is 2% over all calculation techniques. A good agreement between integrated and nominal flow rate is found. Compared to the "3D full field" integration technique, the "2D profiles" show good results as well, indicating that the horizontal and vertical velocity profiles allow a good representation of the full axial velocity field.

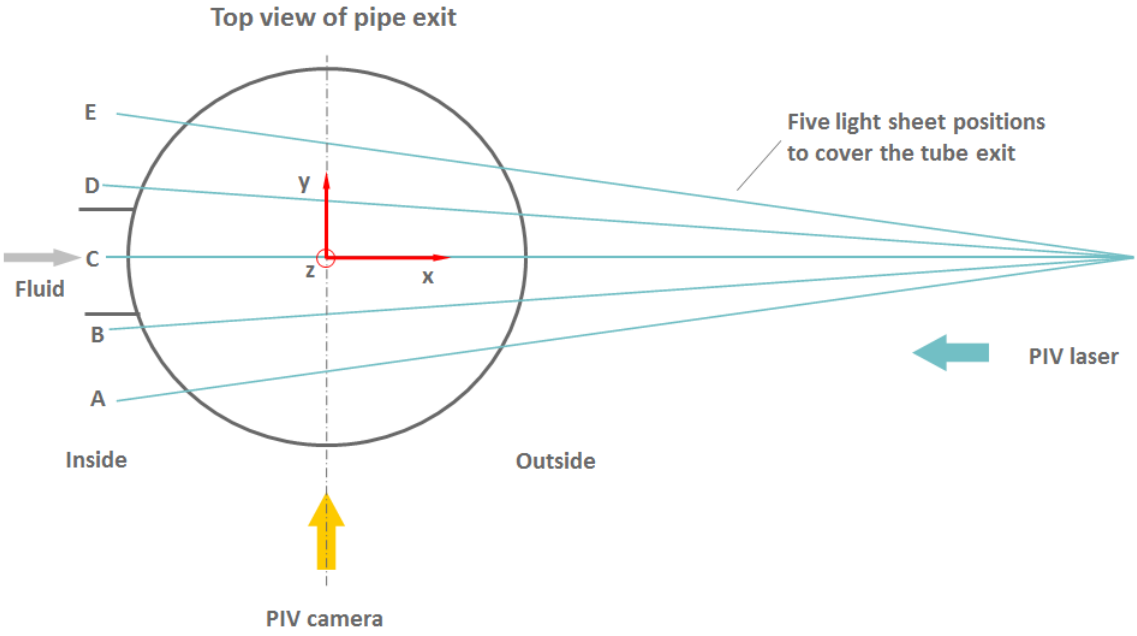

Figure 5.5: *Schematic of the five vertical light sheet positions for the PANDA in situ measurements.*

The integrated flow rates increase slightly during the measurements N04 to N10 for all calculation methods. Even though chances are very low ($1/2^6$) that this increase is not significant, no physical explanation can be given for this increase.

5.1.2 Comparison between PANDA in situ and Scaled Tube

Results from the scaled tube measurements were compared with PANDA in situ measurements to justify and verify the use of scaled tube results for the PANDA facility. The two measurement sets (PANDA in situ and scaled tube) were conducted at (almost) the same Re-numbers of Re = 13'100 for the scaled tube and Re = 13'500 for PANDA measurements. Based on the Re-number variation study presented in the previous section, this slight discrepancy in Re-numbers is assumed to have almost no influence on the flow and is neglected.

Because of the limited optical access, only 2D PIV measurements were possible in the PANDA facility. The lightsheet in PANDA was placed vertically above the tube exit. Therefore, only a cross section of the velocity field could be measured and the measureable velocity components reduced to V_x and V_z. In order to still get some information about the spatial characteristics of the velocity field across the tube exit, measurements were performed at five cross sectionss as shown in figure 5.5. Because the laser was fixed at one location and could only be rotated (but not vertically moved), the five light sheet positions was not parallel but all originate from the same point. The middle light sheet at position C has a horizontal orientation (with respect to the terminology introduced in figure 5.1 a) and can be directly compared with the corresponding results from the scaled tube measurements. Details of the

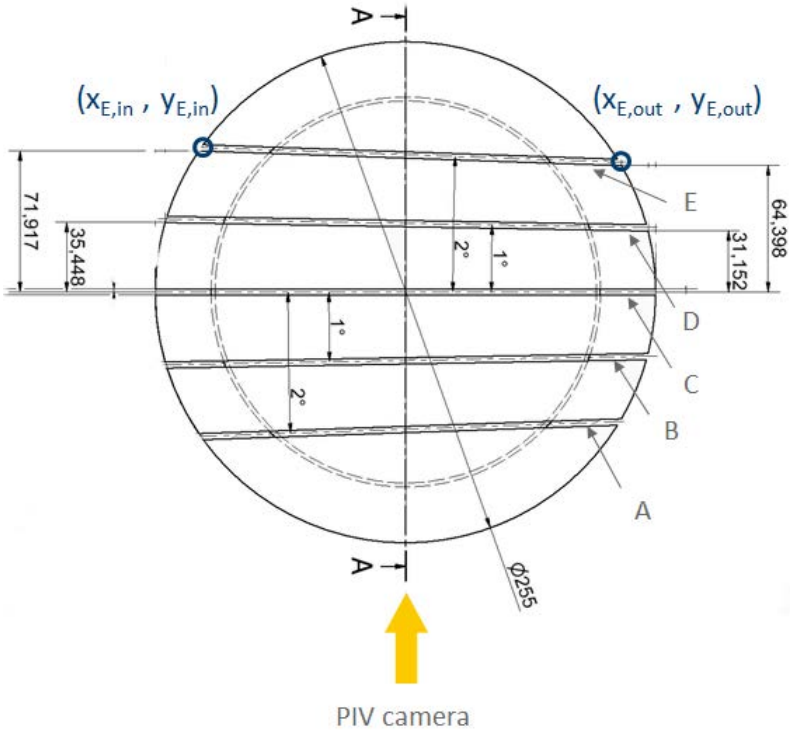

Figure 5.6: *Technical drawing of the vertical light sheet positions A through E for PANDA in situ measurements.*

light sheet positions can be found in figure 5.6. The positions B and D are inclined by 1° and at position A and E by 2°, respectively. Lightsheets A - E cross the y-axis at $x = 0$ at the following normalized y-positions: $y_A/R = -0.68$, $y_B/R = -0.33$, $y_C/R = 0$, $y_D/R = 0.33$ and $y_E/R = 0.68$.

In order to make the scaled tube measurements comparable, five cross sections at the corresponding positions A - E (figure 5.6) must be extracted (same y_i/R values as for PANDA). The extraction of these cross sections is not straight forward, and will be explained in the following. Lets define the coordinates $(x_{E,out}, y_{E,out})$ as the point where the uppermost light sheet (position E) is crossing the tube at the outside and $(x_{E,in}, y_{E,in})$ for the crossing at the inside. For the scaled tube it follows a distance of $y_{E,in} - y_{E,out} = 1.5mm$ which corresponds to five measurement points (spatial resolution of the velocity field is $\Delta x = \Delta y = 0.296mm$). Based on these dimensions we test in the following three different methods to extract the velocity data from the scaled tube experiments to match the results with the PANDA in situ measurements. First, the inclination is neglected and data along horizontal lines are extracted ('straight'). To improve the procedure, an inclined line is selected according to measurement planes A through E and velocities are taken from the nearest available location with respect to these lines ('inclined'). As an alternative, the data can be interpolated between the two closest y-positions ('interpolated').

All three methods were tested for the measurement series N04 at Re = 13'100 at position D (figure 5.7). The label 'straight' represents the first method, 'inclined'

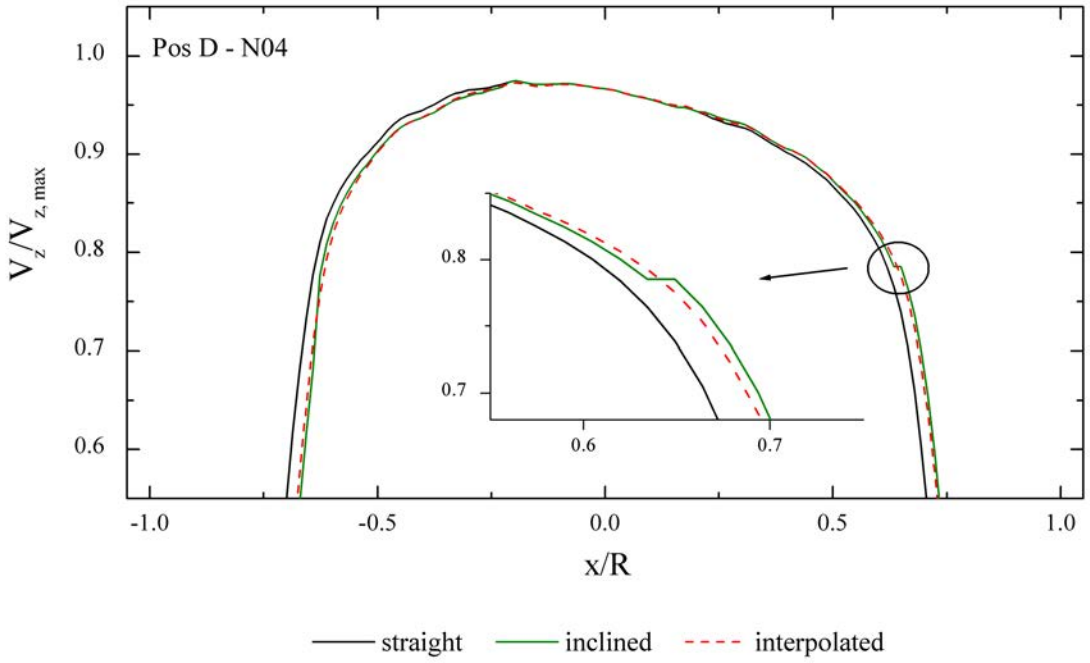

Figure 5.7: *Comparison of three different extraction techniques from the scaled tube measurements for position D to match the PANDA in situ measurement planes.*

the second and 'interpolated' the third method. Extracting straight profiles is not an option as they deviate too much from the other two profiles. Even though the interpolation method is considered the most accurate, the improvement of the interpolation method compared to the inclined cross section is small, if one neglects the (additional) elimination of the small steps visible for the 'inclided' method. These steps result from the 'nearest location' condition the velocity vectors are selected from with respect to the 'true' position represented by line D, i.e. the nearest vectors are selected from different rows of the velocity field grid with spacing $\Delta x = \Delta y = 0.296mm$ as indicated in the enlargement of the black circle in figure 5.7. Furthermore, it must be kept in mind that the interpolation is not perfect either and has a certain error as well. It was therefore decided that the 'inclined' extraction method is sufficient. This decision is further supported by the fact that the accuracy of the light sheet positioning for the PANDA in situ measurement is $\pm 3mm$ which corresponds to an accuracy of $\pm 0.6mm$ for the scaled tube (scaling of 1:5).

The horizontal velocity profiles of the axial velocity measured in PANDA were compared to the scaled tube results (the average from series N04 to N10 as presented in figure 5.3 for position C) at all five positions A through E (figure 5.8). All velocities are normalized with their respective maximum axial velocity taken from profile C for a given Re-number (see table 3.2 and A.1). The represented scaled tube data is the mean velocity of measurements N04-N10 with dotted lines corresponding to the upper and lower margins of the 99% confidence interval.

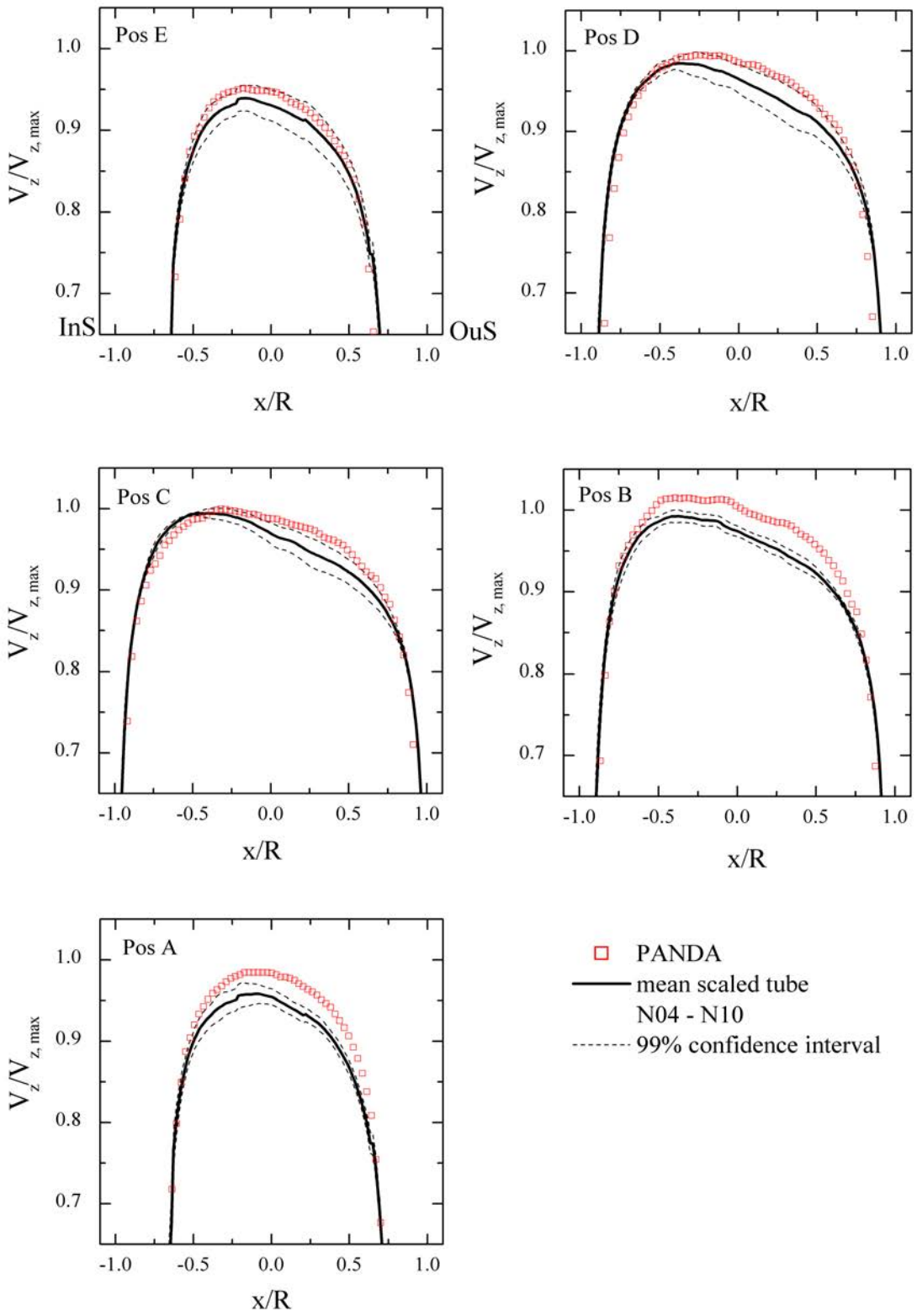

Figure 5.8: *Comparison of horizontal normalized $V_z/V_{z,max}$ profiles for position A to E as measured with the scaled tube (ST) and for PANDA in situ.*

Errors for the PANDA measurements are too small to be displayed. In the core region of the flow, velocity values from the PANDA measurements are at the upper limit of the 99% confidence interval of the scaled tube measurements for positions E and D, slightly above for position C and deviate most for positions B and A. Overall, the values from PANDA are consistently a bit higher in the core of the jet flow, especially for position B and A. The only exception is the inside region ($x/R < -0.4$) of profile C. However, the agreement is still fairly well and sufficient for comparison purposes. Towards the boundary region of the jet, deviations are stronger which is expected due to the stronger velocity gradients. Especially position C reveals that the velocity profile in PANDA is flatter compared with the scaled tube results. For the scaled tube, the maximum velocity is at the inside of the bend and the profile decreases towards the outside. Even though equally visible, this behavior is less distinct for the PANDA profile. Overall, the agreement is good and supports the future usage of the (or a) scaled tube to characterize the tube exit velocity conditions in the PANDA facility.

A comparison of the in plane normalized velocity component $V_x/V_{z,max}$ between the scaled tube and the PANDA results for position B is shown in figure 5.9. As for V_z, the velocity component V_x is normalized with $V_{z,max}$ of profile C. The horizontal velocity profile V_x of the PANDA measurement shows a reverse inclination compared with the scaled tube. Measurements beyond $x/R = \pm 1$ are available because contrary to the scaled tube measurements in PANDA the drywell is filled with seeding particles, allowing to measure velocities not only in the jet but in the surrounding region as well. Additionally, the PANDA measurements are (i) not everywhere within the error bounds of the mean scaled tube velocity and (ii) deviate in the inside ($x/R < -0.3$) and outside part ($x/R > 0.3$) beyond the error margins. However, one needs to keep in mind that the V_x velocity component is considerably

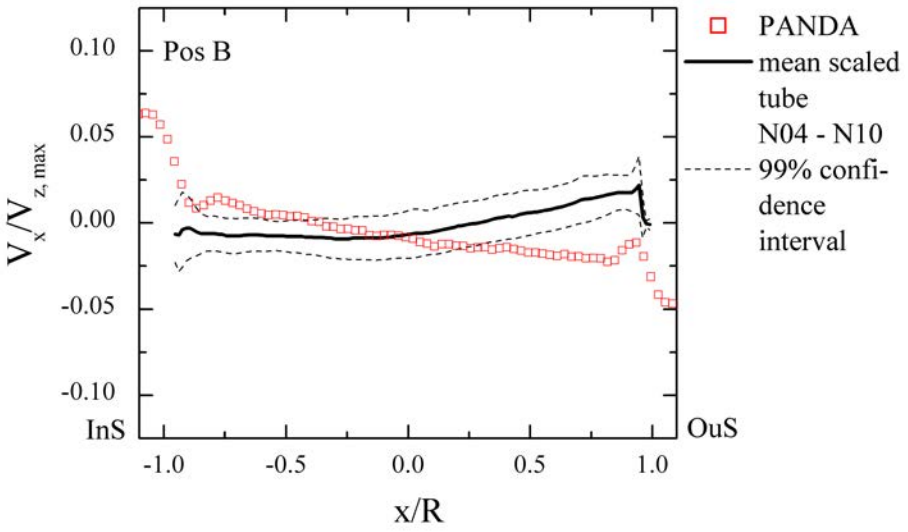

Figure 5.9: *Comparison of horizontal $V_x/V_{z,max}$ profiles for position B of scaled tube and PANDA in situ measurements.*

smaller compared with the axial velocity and therefore has only a minor influence onto the overall similarity of the two flows. The scale difference ($\approx 100:1$) between the axial (V_z) and the in-plane velocity magnitude (V_x and V_y) has consequences for the PIV recording accuracy for the scaled tube measurements.

A rule-of-thumb requires that the Δt between the two laser pulses is adjusted such that particles in main flow direction travel by approximately 8 pixels (1/4 of the length of an interrogation window). With a horizontal light-sheet (scaled tube set-up) perpendicular to the main flow direction of the jet (worst case and usually not recommended), this rule-of-thumb is violated. The small light sheet thickness does not allow for a particle to travel 8 pixels. For the scaled tube (Re = 13'100) a typical (mean) particle displacement amounts to 4 pixels (which corresponds to $\approx 6m/s$). The dynamic range of a PIV system is also in the order of 100:1, i.e. for the recording of the (instantaneous) in-plane velocities one touches the resolution limit (0.04 pixel which corresponds to $\approx 0.06m/s$) of the PIV system. Velocity values for V_x and $V_y$are in the range of ± 0.3 m/s . Therefore, the instantaneous values of V_x and V_y are close to the lower limit of resolution. Because averaged velocity fields are analyzed, the data is still resilient, as averaging over a large set of data (N = 1024) filters out noise and makes the data more robust.

Horizontal normalized TKE profiles for both PANDA and scaled tube measurements show a very flat profile in the middle region of the tube, with $TKE/V_{z,max}^2 \approx 0.015$, indicating little variations in turbulence (figure 5.10). For the scaled tube, an increase of the error margins of the mean TKE profiles at the boundary of the jet is present, as the upper and lower error bounds start to grow. This is seen e.g. in profile C at $x/R \approx -1$. In the core region, TKE of PANDA and scaled tube are similar. For profiles B, C and D the TKE of the PANDA data in the core of the flow are within the error bounds spanned by the scaled tube results. The two outermost profiles A and E reveal a slightly higher TKE in the core of the flow for the PANDA measurements. The main difference is found in the TKE-spikes visible for the PANDA results at the inside and the outside boundary of the jet for all positions A to E. A corresponding behavior is not visible for the scaled tube results. This difference might be explained as follows.During an experiment in PANDA, a hot steam jet leaves the tube (150°C) and enters into a colder surrounding (108°C). Even though the tube itself is insulated by a double walled tube with a vacuum (≈ 0.1bar) to minimize heat transfer (conduction) between the inner and outer tube, the outer tube temperature will increase in the course of the experiment due to radiative heat transfer. Thus, the gas temperature in the vicinity of the outer tube surface will increase accordingly and ultimately form a rising natural circulation pattern which interferes with the outer parts of the jet flow at the tube exit. The convectional flow at the tube exit disturbs the otherwise regular flow pattern of the jet and is believed to be the cause for the spikes in TKE at the jet boundary. Similar spikes at the jet boundary are seen in the horizontal cross sections of the standard deviations σ_{Vx} and σ_{Vz} (not shown). In the middle region of the jet, standard deviations of the velocities for PANDA measurements agree very well with the scaled tube data.

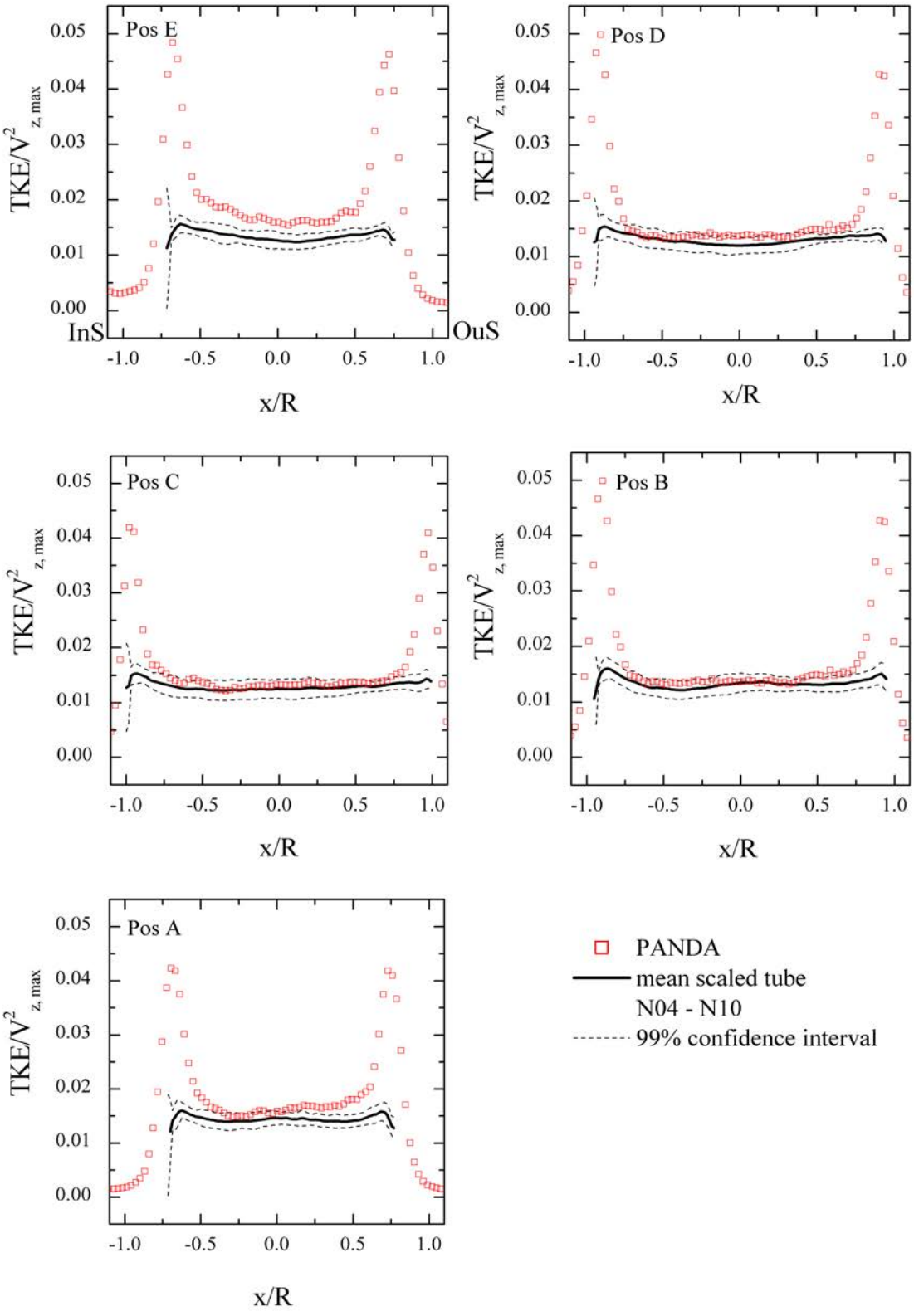

Figure 5.10: *Comparison of horizontal normalized $TKE/V^2_{z,max}$ profiles for positions A - E measured for the scaled tube and in PANDA.*

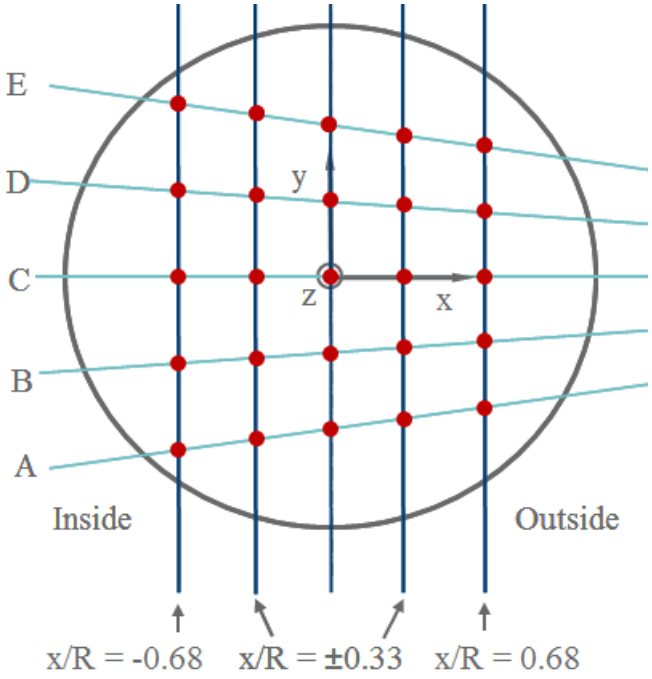

Figure 5.11: *Horizontal cross sections (light blue lines) and vertical cross sections (dark blue lines) with the data points used for the vertical comparison of PANDA data (red circles)*

Up to now, only horizontal profiles obtained from the scaled tube and the PANDA data were compared. To make an attempt to compare vertical profiles, the following procedure was applied. From the 3D velocity field of the scaled tube, vertical (and parallel) flow profiles are extracted. Vertical cross sections are placed at $x/R = 0$, $x/R = \pm 0.33$ and $x/R = \pm 0.68$ (dark blue lines in figure 5.11). For the PANDA data, only the five (horizontal) cross sections at position A to E are available. To obtain some sort of vertical data, five data points can be extracted from every horizontal cross section (PANDA data) at the location where they intersect with the vertical cross sections (scaled tube data). These points are highlighted in red in figure 5.11. The five data points are then compared to the vertical cross sections of the scaled tube. As an example, the plot of the axial velocity V_z at position $x/R = 0$ is shown in figure 5.12. As for the horizontal profiles, the agreement between the measurements is well enough. This is true for all evaluated parameters V_z, V_x, σ_{Vz}, σ_{Vx} and TKE (not shown). Again, for the parameters of standard deviation and TKE, the outermost data points for the PANDA measurements are very high. This might be due to the appearance of a convectional flow explained in the paragraph above. Overall, a sufficient agreement between PANDA measurements and scaled tube are achieved.

In the horizontal cross section plots of $V_z/V_{z,max}$ (figure 5.3) it was noticed that the PANDA profiles seem a bit less inclined compared to the scaled tube results. To quantify this observation, the normalized inclination parameter $\mathrm{I}_p = \Delta V/V_{z,max}$ is introduced which characterizes the steepness of the inclination. To calculate I_p,

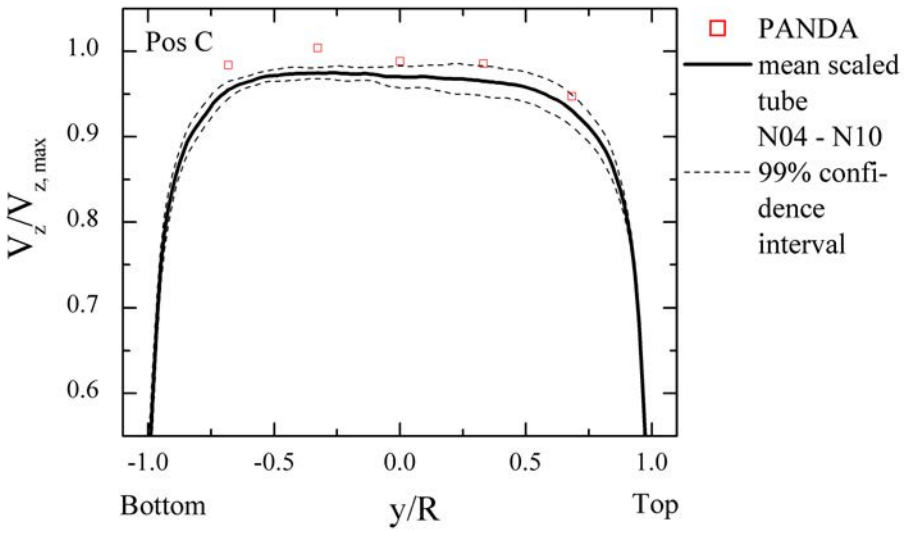

Figure 5.12: *Comparison of the normalized vertical $V_z/V_{z,max}$ profiles of scaled tube and PANDA in situ measurements.*

the difference ($\Delta V/V_{z,max}$) between the normalized axial velocity values at positions $x/R = 0.33$ $\left(V_a = V_z/V_{z,max}|_{x/R=0.33}\right)$ and $x/R = -0.33$ $\left(V_b = V_z/V_{z,max}|_{x/R=-0.33}\right)$ are determined and it follows for the calculation of the inclination parameter $I_p = V_b - V_a$ (figure 5.13). For vertical profiles, the normalized velocity values are extracted at $y/R = 0.33$ and $y/R = -0.33$, respectively. The values for $\Delta V/V_{z,max}$ are given in percent (%) with respect to the maximum $V_{z,max}$ resulting from the C profile. For the scaled tube results, a mean value is calculated based on the I_p for

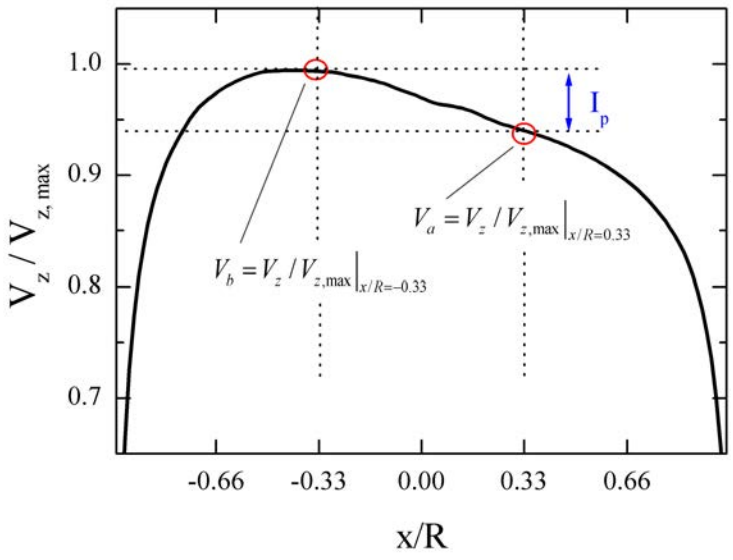

Figure 5.13: *Definition of the inclination parameter I_p for the normalized horizontal profile of the axial velocity$V_z/V_{z,max}$.*

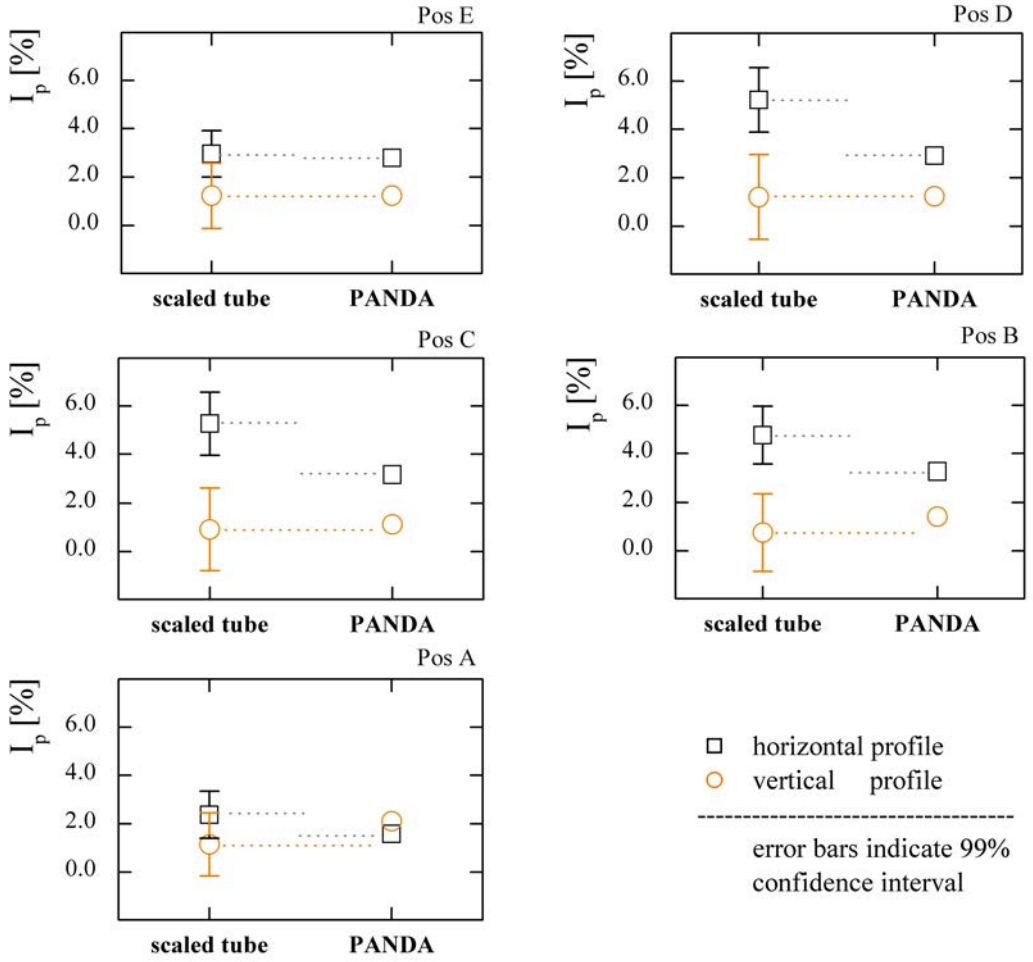

Figure 5.14: *Comparison of the steepness parameter I_p calculated for horizontal and vertical normalized axial $V_z/V_{z,max}$ profiles. The results for the scaled tube represent the average obtained for the measurements N04-N10 whereas the PANDA data represent a single measurement.*

series N04 to N10 and the calculated 99% confidence interval. The results of this calculation and the comparison with the corresponding PANDA data are presented in figure 5.14. Looking at the I_p data for the horizontal profiles, all profiles – scaled tube as well as PANDA– show a positive I_p, indicating a decrease of velocity towards the outside. The decrease in horizontal direction is consistently higher for the scaled tube compared to PANDA. The difference becomes more pronounced for the middle profiles B, C and D. For the scaled tube, I_p values range from 2% to 6%. whereas one finds for PANDA a range between 1% and 4%.

The vertical profiles show a smaller incline in the range of 0.5% to 2%. The differences between scaled tube and PANDA with respect to the inclination parameter are small and more constant over the vertical profiles as indicated by the orange dotted lines in figures 5.14. This indicates that the full velocity field is more sym-

metrical in vertical direction and the main (but still small) asymmetry introduced by the bend geometry is found in horizontal direction.

Overall, the agreement between the flow measured in situ in the PANDA facility and the flow measured for the scaled tube approach is sufficient. This leads to the conclusion that future flow investigations can be analyzed with a scaled tube only. The advantage for scaled tube measurements are a much better accessibility, faster and more flexible setup and adjustments as well as the availability of 3D PIV allowing to measure all three velocity components of the flow field.

5.2 90° Bend

The analysis of the 90° bend is split into three parts. The first section analyzes profiles of axial velocity and TKE, including a selection of full velocity profiles. Thereafter, the repeatability of the measurements is investigated. The section is concluded by a comparison of the analyzed data with literature.

5.2.1 Analysis of 90° Bend Measurements

After the scaled tube analysis in section 5.1, a second, more standard 90° bend geometry with a constant inner diameter was investigated. The new experimental setup allowed to vary between six exit tube lengths after the bend, covering the range from 0.8D to 10D with D = 40mm depicting the inner diameter of the tube. For every exit height, measurements were conducted for five Re-numbers. Therefore, a total of 30 measurements were performed. As an example and overview for the downstream development of the flow, the axial velocity fields at Re = 17'500 are shown in figure 5.15. Throughout the following analysis, the values for the Re-numbers are abbreviated as shown in table 3.5 in chapter 3. However, it must be noted, that the lowest investigated Re-number of 4'900 should be treated as a special case, because the flow may not yet be fully turbulent as a bend tends to increase the transition to turbulence to higher Re-numbers (see discussion of the corresponding literature in chapter 2).

Velocity fields for the axial velocity component V_z measured 6 mm above the tube exit for tube length of 0.8D and 10D past the 90° bend are shown in figure 5.16 a) and b) for a Re-number of 12'600. The color scale covers a velocity range up to 6m/s (red). The velocity field just after the bend (0.8D downstream) shows a sickle shaped maximum at the outside ($x > 0$) and is symmetric with respect to the horizontal axis $y = 0$. Very similar axial velocity fields are found in [20, 19]. 10D after the bend, the maximum velocity has decreased while its area has increased(figure 5.16 b), indicating that the velocity field is more homogeneous compared with the flow shortly past the bend (0.8D). For the gradual homogenization of the axial flow field, see figure 5.15.

Nonetheless, a somewhat higher velocity is still present at $x \approx 13$ mm compared with $x \approx -13$ mm. Looking at the in-plane velocities V_x and V_y presented in a

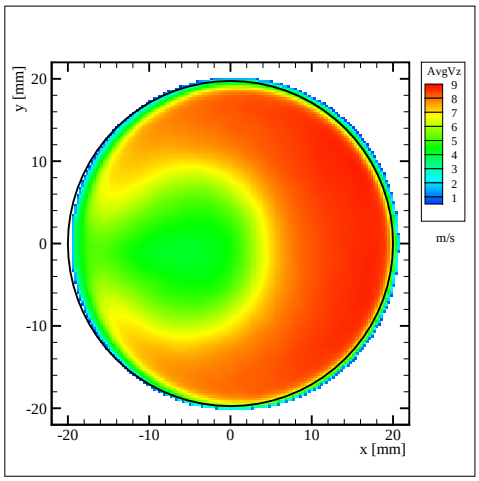

(a) Velocity field V_z at 0.8D

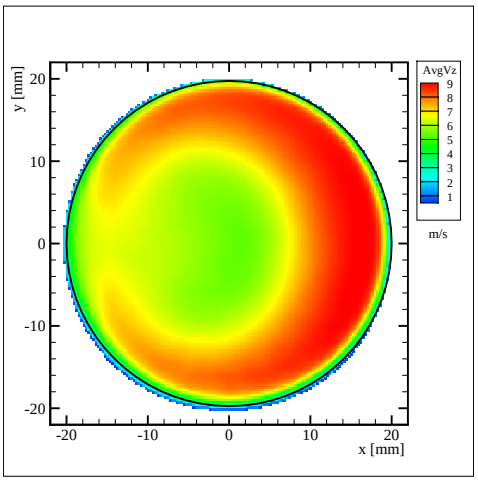

(b) Velocity field V_z at 2D

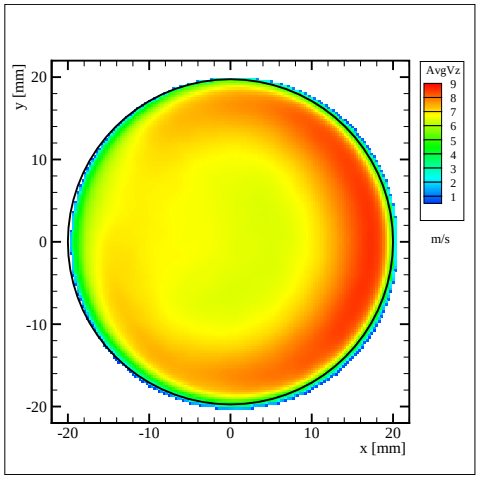

(c) Velocity field V_z at 4D (N02)

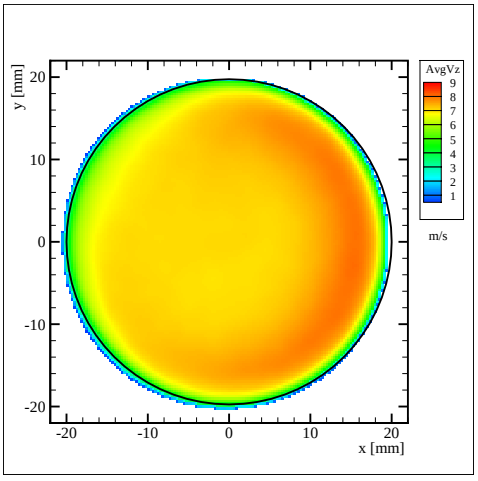

(d) Velocity field V_z at 6D

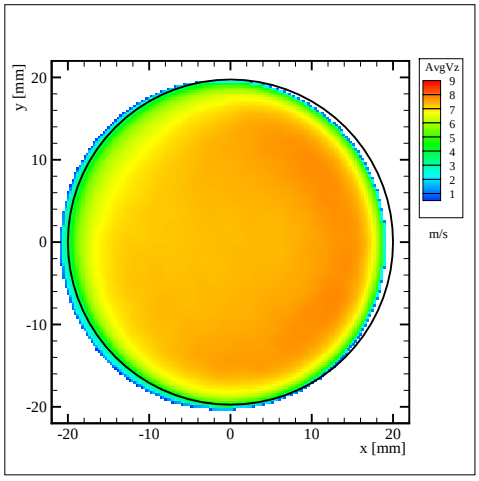

(e) Velocity field V_z at 8D

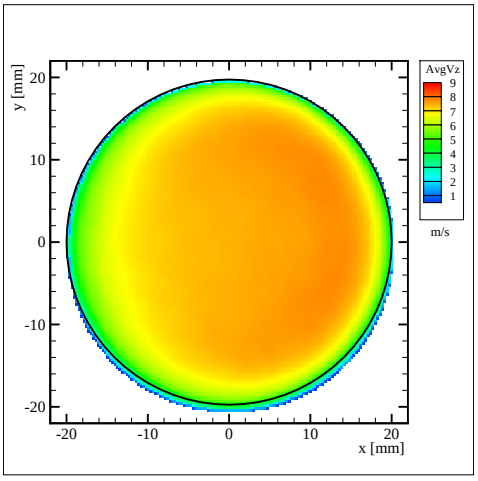

(f) Velocity field V_z at 10D

Figure 5.15: *Axial velocity profiles V_z for the 90° bend at Re = 17'500 at all measured heights (0.8D to 10D). The color scale ranges from 1 m/s (blue) to 9 m/s (red).*

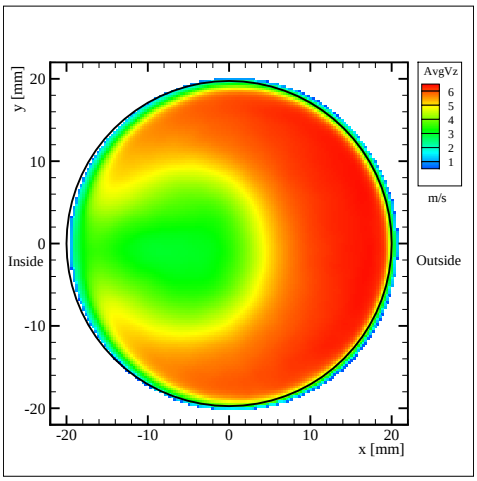

(a) Velocity field V_z at 0.8D

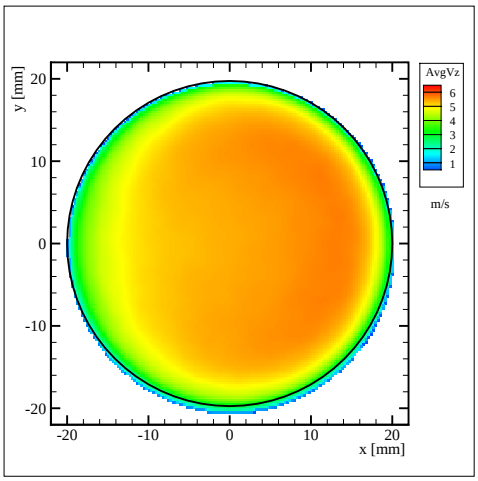

(b) Velocity field V_z at 10D

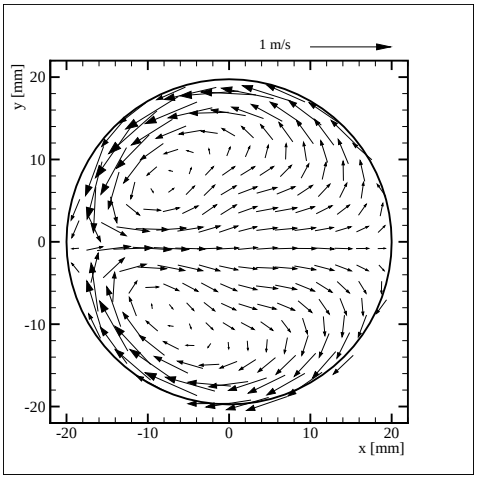

(c) In-plane vector field at 0.8D (V_x,V_y)

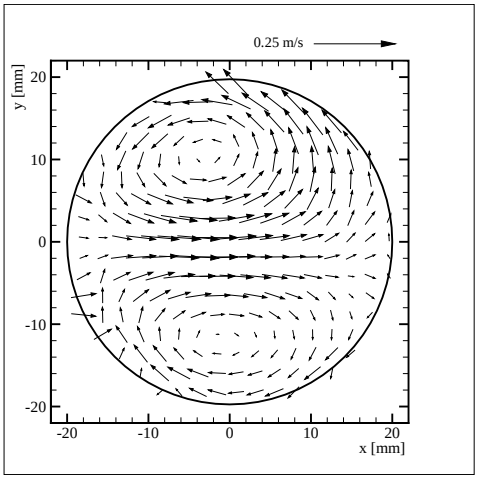

(d) In-plane vector field at 10D (V_x,V_y)

Figure 5.16: *Axial velocity profiles V_z and in-plane vector fields for the 90° bend at Re3 = 12'600 at height 0.8D and 10D.*

vector field in figure 5.16 c) and d), the typical Dean vortices introduced in chapter 2 are seen. The magnitude of the in-plane velocities decreases from 0.8D to 10D, indicated by the magnitude of the reference vectors in figures 5.16 c) and d). While the magnitude of the in-plane velocities at 0.8D reach up to 25% of V_z, they decrease to values smaller than 5% at 10D. Additionally one can see a shift of the Dean vortex center towards the middle ($x \approx 0$) at a distance of 10D past the bend.

For the following discussion, plots of horizontal velocity profiles extracted at $y = 0$ from the velocity fields are shown, since profiles are more easily to compare and to highlight resemblances or differences. To enter the discussion, the velocity profiles of the normalized axial velocity are analyzed with respect to their Re-number dependence. For this purpose, the different Re-number measurements are compared for six downstream distances in figure 5.17. All velocity values are normalized with

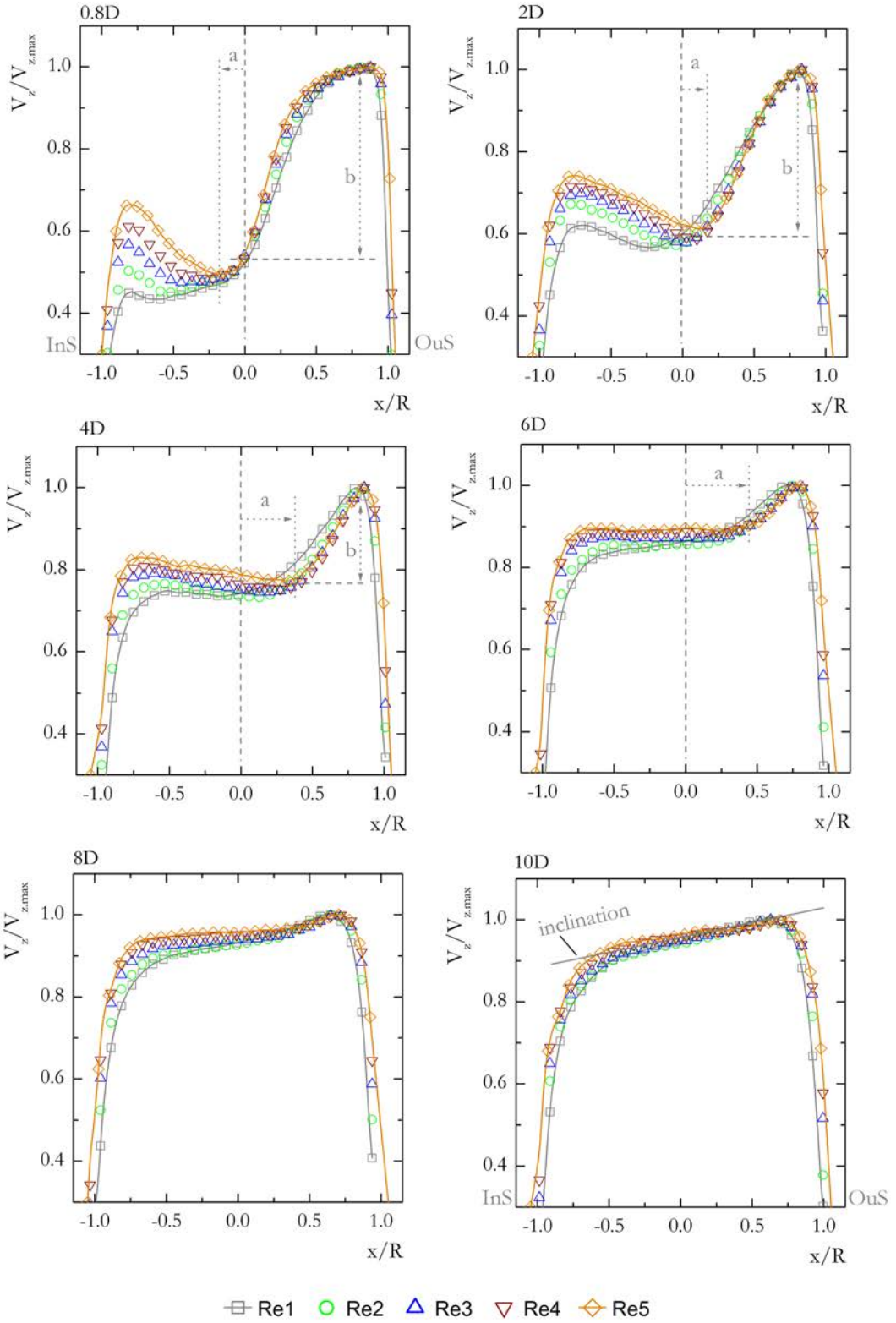

Figure 5.17: *Horizontal profiles of the normalized axial velocity V_z extracted at $y = 0$ for different downstream distances (0.8D to 10D) past the 90° bend with the Re-number as parameter (for Re values see table 3.5).*

the maximum streamwise velocity of the horizontal profile at the given height and Re-number. Normalization values are provided in Appendix A, table A.2.

Just after the 90°-bend (0.8D), two distinct regions can be identified. The axial velocity profile shows on one hand a strong Re-number dependence for $x/R < -0.2$ at 0.8D as depicted by the distance 'a' from the tube axis (figure 5.17) with a considerable spread resulting systematically in higher velocities for higher Re-numbers. On the other hand – for $x/R > -0.2$ – the Re-number dependence is weaker, i.e. the flow field is composed of two areas. One area in which the self-similar presentation fails ($x/R < -0.2$) and one ($x/R > -0.2$) where it holds true for the entire Re-number range considered here. Following the flow in downstream distance, the amplitude-spread of the Re-dependence at the inside becomes smaller and almost vanishes for position 10D. At the same time, the horizontal extent increases as depicted by the location of the distances marked with 'a' in figure 5.17. The undulation of the velocity magnitude as depicted by the amplitude mark 'b' decreases with downstream distance and all the velocity profiles flatten out and converge to a similar shape – still gently inclined – as seen in the velocity profile presented for 10D. Therefore, whatever the initial Re-number is, the flow field shows self-similar characteristics along the entire cross section after 10D. The visible inclination at 10D shows that the memory of the flow – the disturbance introduced by the 90° bend – is still not completely lost. Results from the literature show [5] that the development of a fully symmetric turbulent velocity profile characteristic for tube flow requires additional 30D to 40D downstream distances. Interestingly, the inclination shown in figure 5.17 for 10D is exactly opposite to the inclination observed for the scaled tube results (figure 5.2 (top) and 5.3 (top)).

To cross check the Re-number dependency with results found in literature, axial velocity measurements from Kalpakli et al. [3] are compared to our own data. Kalpakli performed PIV measurements 0.67D downstream a 90° bend with a curvature of $\delta = 0.31$ at Re = 14'000, Re = 24'000 and Re = 34'000 (summarized in table 5.1). His data is compared to our own measurements at 0.8D, $\delta = 0.31$ and at similar Re-numbers in figure 5.18. Both data sets show a Re-dependency for $x/R < -0.2$ whereas the Re-dependence vanishes for $x/R > -0.2$. For $x/R < -0.2$, higher Re-numbers result in higher normalized velocities, indicating that bend effects become stronger with increasing Re-numbers which is in line with our own results. Besides the similar Re-dependency, our own horizontal flow profiles show a similar shape compared with the data of Kalpakli even though our data are slightly lower in the Re-number independent part and a bit higher in the Re-number dependent part. At the outside, $x/R > 0.8$ the two data sets show almost identical normalized velocities.

Profiles of the normalized TKE for the scaled tube at downstream distances of 0.8D, 2D, 6D and 10D for all five Re-numbers are shown in figure 5.19. The values are normalized with the square of the maximum streamwise velocity $V_{z,max}$ and range between 0.005 and 0.04. After the bend at 0.8D, the TKE profiles show a strong variation, with maximum values at the inside ($x/R \approx -0.8$) and minimum values around $x/R \approx 0.4$. Overall, the profile decreases in between these extrema but one

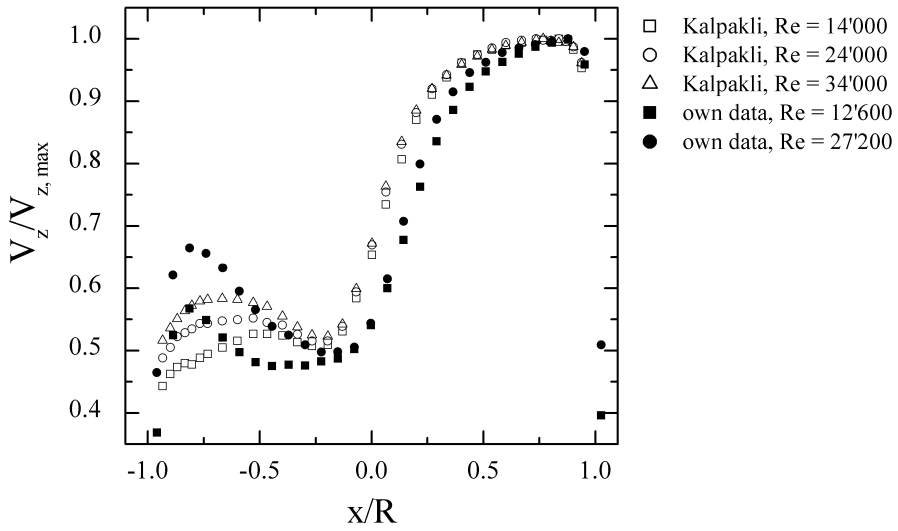

Figure 5.18: *Comparison of 90° the bend measurements with results of Kalpakli et al. [3].*

Author	Re-number	curvature δ	z/D
Kalpakli et al.	14'000	0.31	0.67
	24'000		
	34'000		
own data	12'600	0.31	0.8
	27'200		

Table 5.1: *Experimental conditions for the publication of Kalpakli et al. [3] and own data presented in figure 5.18, with downstream distance z/D in [D].*

sharp increase around $x/R \approx 0.1$ is seen, where a weak Re-number dependency can be seen. The sharp increase is higher and wider for lower Re-numbers. Overall, the Re-number independence is much stronger for the TKE profiles compared with the axial velocities shown in figure 5.17. Already at a downstream distance of 2D, the peak values have decreased and the Re-variation is smaller. Reaching a height of 6D, the profile has become very flat, no more Re-dependence is visible and further changes with increasing height are marginal (e.g. to 10D).

Horizontal profiles of the in-plane velocities V_x shown in figure A.1 (in the Appendix A) and V_y in figure A.2 as well as the standard deviations (figure A.3) of the velocities all share the trend of flatter, more equalized profiles at increasing distance after the bend. The Re-number dependency of the standard deviations is weak 0.8D downstream of the bend and decreases further with distance. The two in-plane velocities reveal much stronger Re-dependencies than the standard deviations, which continuously decrease with downstream distance. For vertical cross sections,

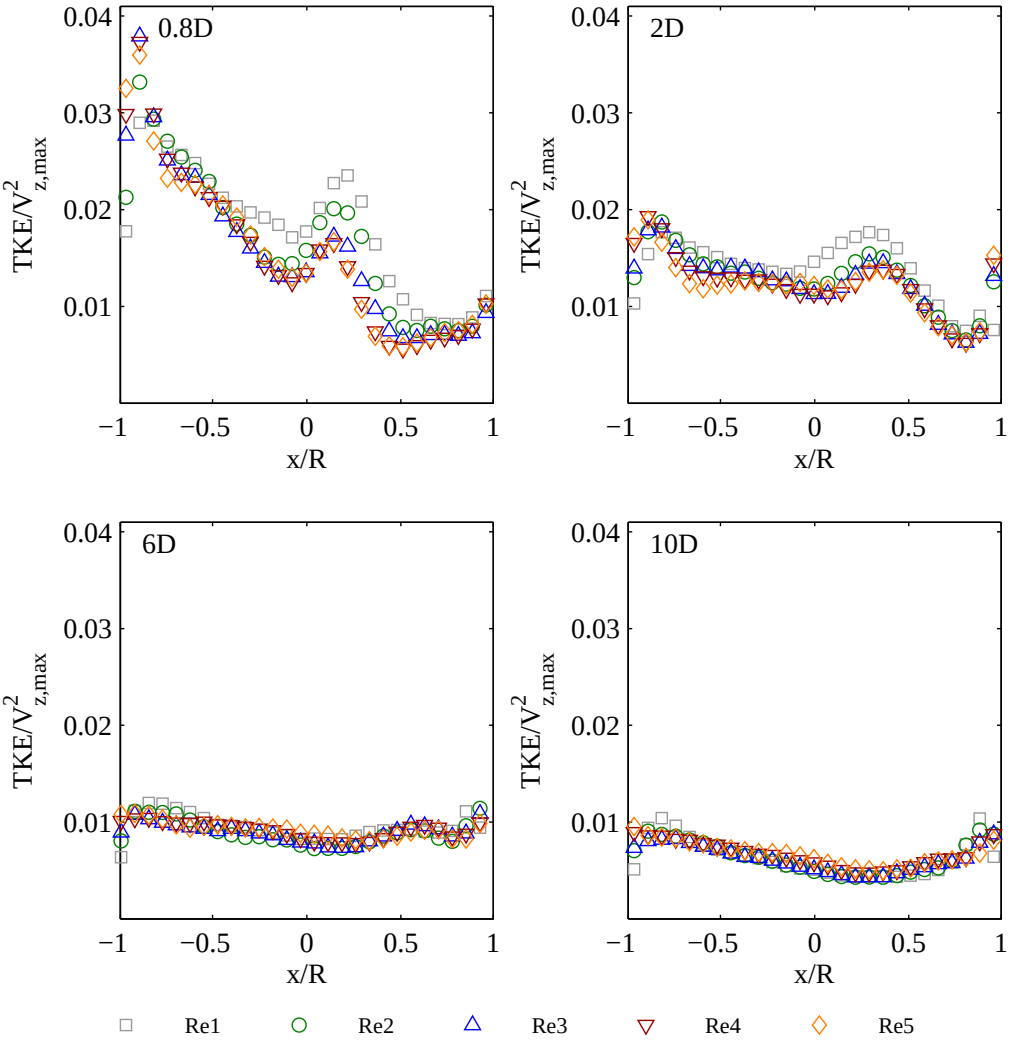

Figure 5.19: *Horizontal profiles of the normalized TKE at heights of 0.8D, 2D, 6D and 10D, each for Re1 to Re5.*

a flattening of the profiles with downstream distance is noticed for all quantities V_x, V_y, V_z and TKE (see vertical profile of V_z in figure A.4 and TKE in figure A.5 shown in the Appendix A). As for the horizontal cross sections, the most significant changes in the profiles evolve close after the bend until 6D downstream. The vertical axial velocity profiles show only a very weak Re-number dependency in the core of the flow for downstream distances between 2D and 8D whereas the TKE shows a larger Re-variation which decreases with downstream distance and is almost no more noticeable after 10D.

So far, only the Re-number was taken as parameter for the discussion. However, it might be instructive to compare velocity profiles at different downstream distances but with the Re-number held constant. This type of comparison is shown for the

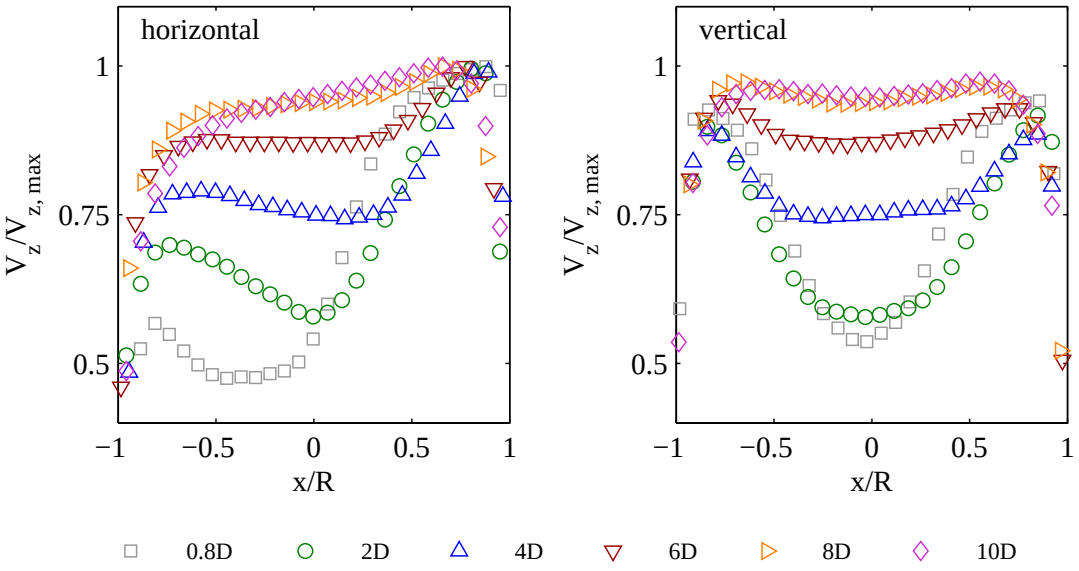

Figure 5.20: *Horizontal (left) and vertical (right) profiles of the normalized axial velocity $V_z/V_{z,max}$ at Re3 = 12'600 with downstream distance as parameter.*

normalized axial velocity for Re = 12'600 in figure 5.20 in terms of horizontal (left) and vertical (right) velocity profiles. The development of the horizontal V_z profiles have already been discussed in the context of figure 5.17, but with the Re-number as parameter. Following the velocity profiles with downstream distance (figure 5.20 left), it becomes apparent that the major changes in terms of the momentum Re-distribution evolve along a distance from 0.8D to 4D whereas one finds only marginal changes from 8D to 10D, i.e. the re-distribution process considerably slows down such that it takes another 30D to 40D to end with a fully developed turbulent tube flow, as stated above. Just after the bend (0.8D), the vertical profile (figure 5.20 right) has the shape of a letter M – the signature of a top-bottom symmetry of the flow – with maxima at $x/R = \pm 0.8$ and a minimum value at $x = 0$. The minimum becomes less deep for increasing downstream distances until only a slight dip is left at 10D. Horizontal and vertical profiles show the same behavior with increasing downstream distance. Both transition from a highly undulated flow to an almost flat velocity profile, showing that the flow gradually recovers downstream of the bend.

Since considering only vertical and horizontal velocity profiles, they are not representative for the total velocity field. In order to show that a horizontal velocity profile can represent the general trend of the velocity field, the standard deviations of the velocity profiles and fields are calculated and compared.

For this comparison, only the core regions of the velocity fields and horizontal profiles are compared, because the strong velocity gradients in the boundary regions

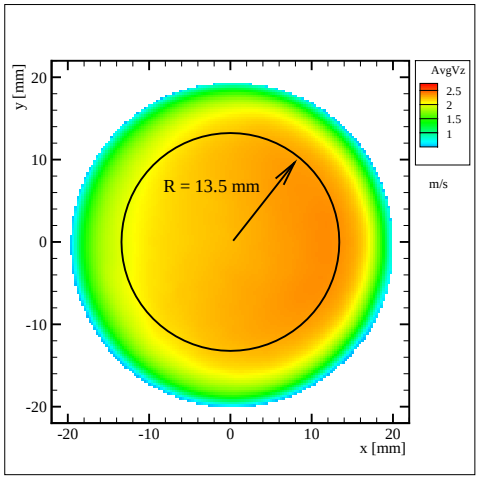

Figure 5.21: *Axial velocity field V_z at distance 10D downstream for Re1 = 4'900 with the black circle indicating the mask used for the calculation of the standard deviation.*

of the flow would otherwise dominate the comparisons. Therefore, a circular mask of radius $R \approx 13.5mm$ is placed onto the flow fields, considering only velocities inside this mask and neglecting the outer region. The size of the mask is such that even the largest boundary layer, found at the lowest Re-number and maximum downstream distance of 10D (shown in figure 5.21), is excluded from the comparison. This results in a velocity field of N = 6361 velocities and a horizontal profile of N = 91 velocities. The standard deviations are calculated for the normalized axial velocities $V_z/V_{z,max}$ for the horizontal profiles and the velocity fields for every measurement to quantify the deviation from the mean velocity. This comparison is based on the assumption that the normalized velocity profiles at a given downstream distance are similar, which is shown for 2D in figure 5.22. The results of the standard deviations presented in figure 5.23 a,b) show a decreasing standard deviation with downstream distance, indicating that the velocities deviate less from the mean value and the flow therefore becomes more equalized with downstream distance. The standard deviations of the velocity profiles and the velocity fields show the same trend but the values of the velocity field are about 20% lower, which can be assigned to the fact that the velocity fields e.g. in figure 5.15 have the largest velocity gradient in the horizontal cross section. The main changes in standard deviation occur until a distance of 4D, thereafter the values are almost constant. The slightly higher standard deviation at 10D compared to at 8D might be connected with the growing boundary layer and/or the rotation of the symmetry line in the velocity field from 8D to 10D (see figure 5.15 e,f). The standard deviation decreases with increasing Re-numbers, indicating that the flow is more homogeneous at higher Re-numbers.

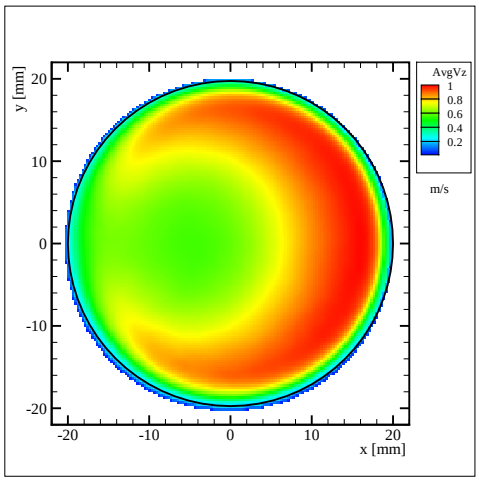

(a) Normalized velocity field $V_z/V_{z,max}$ at Re1

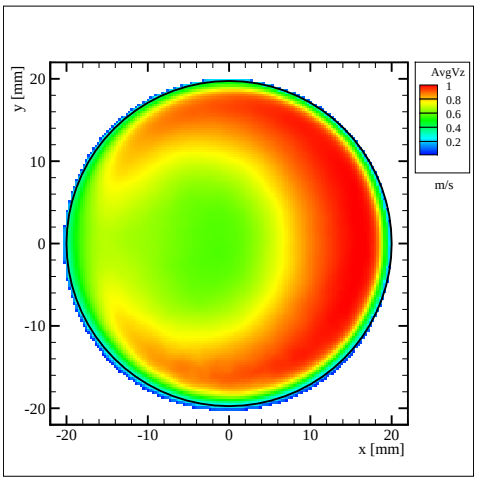

(b) Normalized velocity field $V_z/V_{z,max}$ at Re2

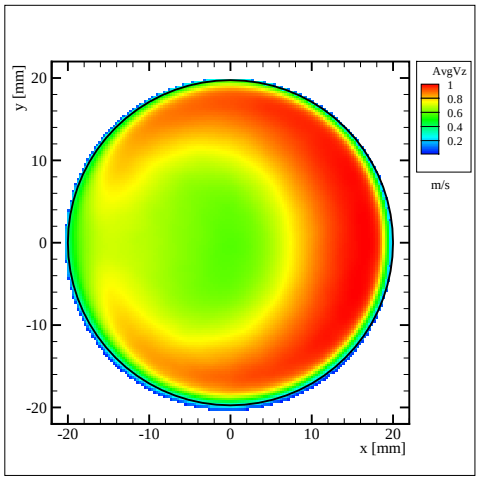

(c) Normalized velocity field $V_z/V_{z,max}$ at Re3

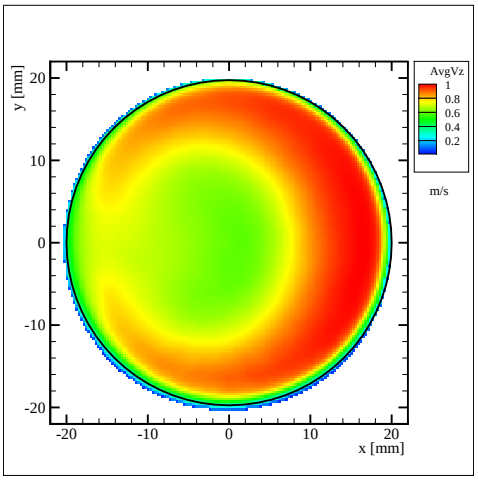

(d) Normalized velocity field $V_z/V_{z,max}$ at Re4

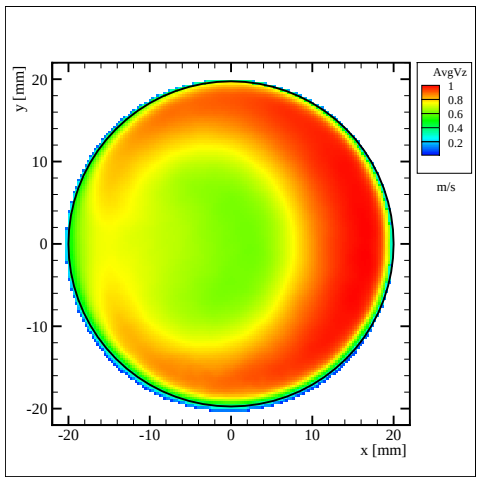

(e) Normalized velocity field $V_z/V_{z,max}$ at Re5

Figure 5.22: *Normalized axial velocity profiles $V_z/V_{z,max}$ for the 90° bend at a downstream distance of 2D for all measured Re-numbers Re1 to Re5.*

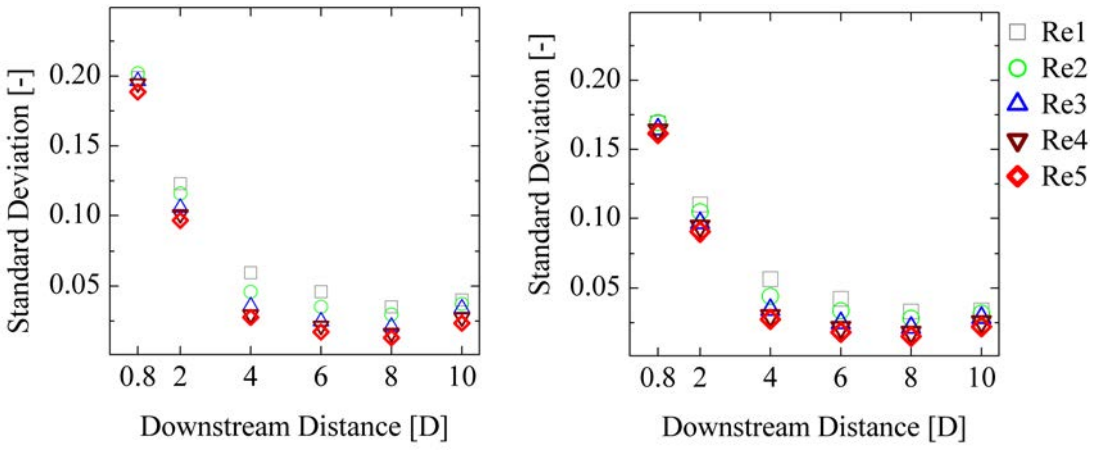

(a) Standard deviation of normalized V_z for the horizontal profiles

(b) Standard deviation of normalized V_z for the velocity fields

Figure 5.23: *Normalized standard deviation of $V_z/V_{z,max}$ for all measurements at different downstream distances and Re-numbers for the horizontal profiles and the full velocity fields.*

5.2.2 Repeatability

A new calibration should be performed whenever a series of measurements is conducted at a new height, as this requires some changes on the setup. However, for the measurements at 2D a new calibration was not performed due to some technical issues and the calibration for 10D was used instead. In order to show that this measurement is still valid and to test at the same time for the repeatability of the results, the measurement at 4D was once performed with the calibration of 10D (S01) and once with a new calibration (S02). From these two measurements, the velocities V_z and V_y as well as the standard deviations of V_z and V_y are compared at Re = 4'900 and Re = 27'200 in figure 5.24. All values are given with physical units [m/s]. Overall, the two measurements S01 and S02 show an excellent agreement. Some minor deviations are seen for the velocity in y-direction at Re = 27'200 but the magnitude of V_y is much smaller compared to V_z, therefore it has little influence on the overall flow field. Based on these results, it can be confirmed i) that using the calibration from a previous run is a valid approach and ii) that the repeatability is given. In all previous graphs, the measurement S02 is shown at height 4D.

5.2.3 Comparison with Literature

In the following section, experimental data from the literature is compared with the data set presented in section 5.2 for horizontal axial velocity profiles of 90° bends. To make the different data sets comparable, all data are normalized in the same manner - by the maximum axial velocity of the horizontal profile. The flow development with increasing exit tube length is compared in figure 5.25. For a better

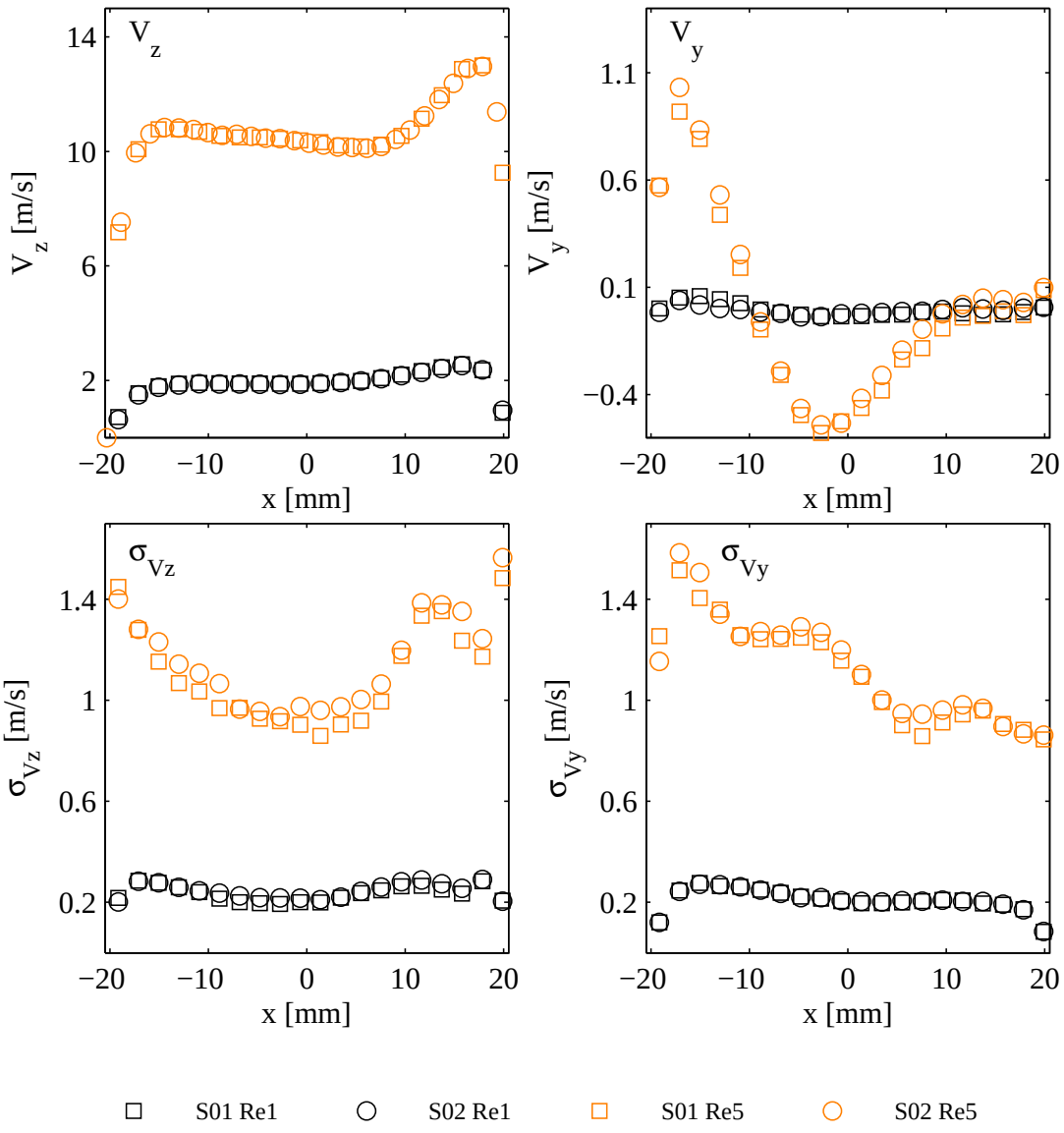

Figure 5.24: *Measurements at downstream distance 4D with the calibration of the 10D measurement (S01) and comparison with a separate run with a new calibration (S02) for Re1 = 4'900 and Re5 = 27'200. Velocities V_z , V_y (top) and the corresponding standard deviations σ_{Vz}, σ_{Vy} (bottom) are shown in [m/s].*

overview, the comparison is spread over four graphs, where each graph compares one or two downstream distances. The top left graph shows velocity profiles measured approximately at a downstream distance of 1D past the bend, the top right graph compares 2D and approximately 4D data, the bottom left graph compares profiles at 5D and 6D and the bottom right graph shows velocity profiles for 10D and,

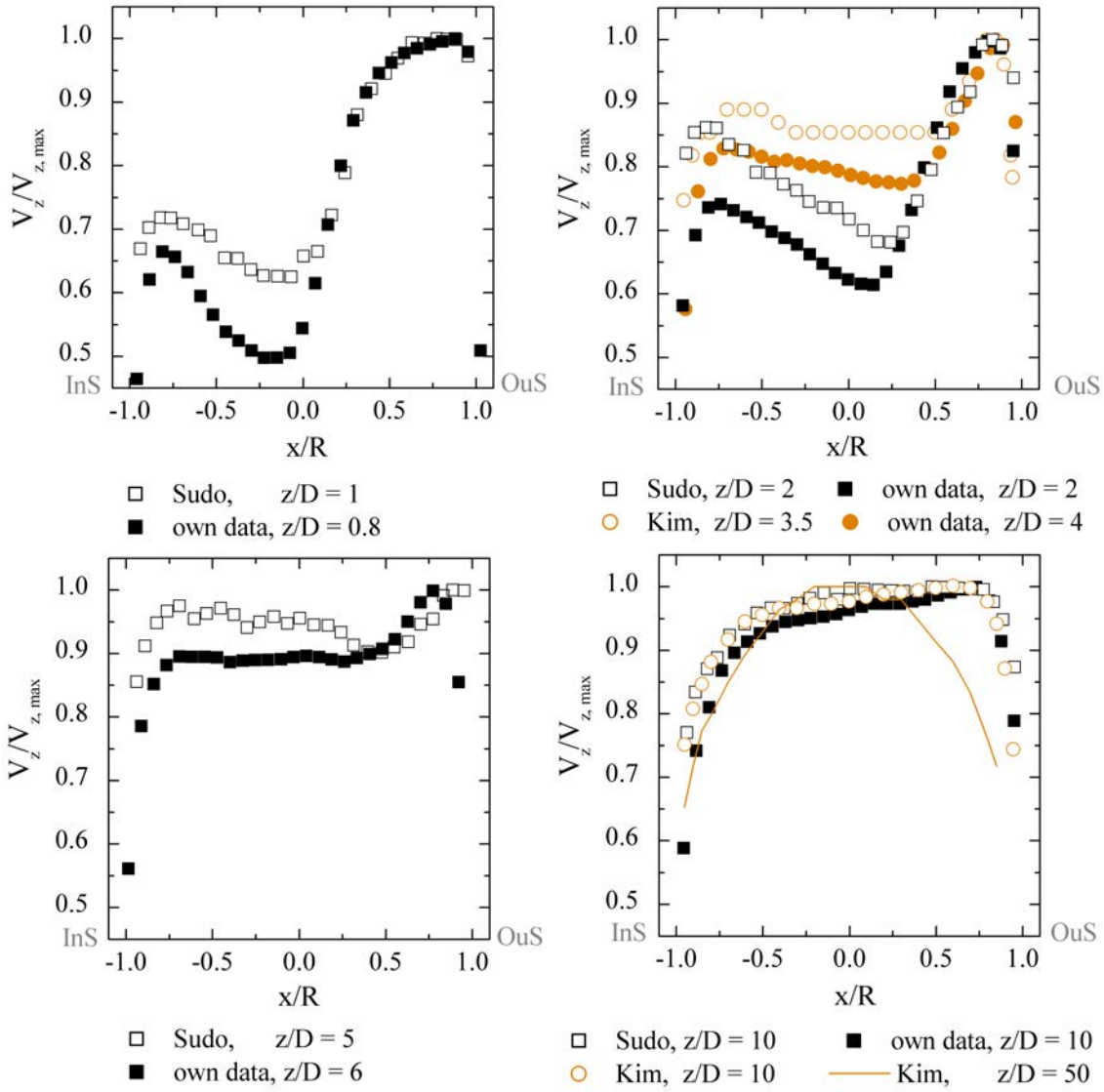

Figure 5.25: *Comparison of own 90° bend data at different downstream distances with data from Sudo et al. [4] and Kim et al. [5].*

additionally, 50D . One data set is taken from Sudo et al. [4] who has performed measurements with a hot wire anemometer downstream a 90° bend of curvature $\delta = 0.25$ at distances between 0D and 10D and a Re-number of Re = 60'000 (fluid is air). Further, the LDA measurements of Kim et al. [5] for $\delta = 0.17$, Re = 50'800 and downstream distances of 3.5D, 10D and 50D are used for comparison. Measurements labeled with "own data" indicate the measurements conducted for this thesis. The experimental parameters are summarized in table 5.2. When the different measurement sets are compared for the same (or very similar) downstream distances, our own data shows consistently lower values for the Re-number dependent part located at the inside (InS) of the cross section. This Re-dependent part is indicated in figure 5.17 with distance 'a'. In our Re-number study we found that the

Author	Re-number	curvature δ	z/D
Sudo et al.	60'000	0.25	0, 0.5, 1, 1.5, 2, 3, 5, 7, 10
Kim et al.	50'800	0.17	3.5, 10, 50
own data	27'200	0.31	0.8, 2, 4, 6, 10

Table 5.2: *Experimental conditions for data taken from Sudo et al. [4], Kim et al. [5] and own data presented in figure 5.25.*

amplitude in the Re-dependent part of the flow grows with increasing Re-number. As the measurements of Sudo and Kim are conducted at Re = 60'000 and Re = 50'800 whereas the own data is measured at Re = 27'200, it is reasonable to assume that our own data shows lower values in the Re-dependent part of the cross section. On the other hand, in the Re-number independent part, the profiles are very similar and collapse onto each other. One can further see that 10D downstream of the bend the shape of the three data sets become very similar, with the data from Sudo (highest Re-number) showing the highest velocities (bottom right graph in figure 5.25), i.e. whatever differences are found among different experimental setups with respect to the shape of the velocity profiles close to the bend (≈1D), these differences seem to converge to a universal profile already after 10D. The solid line in this graph shows a measurement of Kim [5] 50D downstream the tube bend. Its shape indicates that a fully recovered flow has been reached. Taking this as a reference, the flow after 10D, even though having flattened out, has not yet fully recovered.

Even though not all experiments investigated the same curvature (Kim $\delta = 0.17$, Sudo $\delta = 0.25$ and own data $\delta = 0.31$) and not the same Re-number, the comparison to literature presented in figures 5.25 and 5.18 (presented in section 5.2) show good agreement with the measurements performed for this thesis - given the trend of Re-number dependency based on figure 5.17 is taken into account. Therefore, it can be concluded that the found results are trustworthy.

6. Conclusion and Outlook

In this thesis, 3D PIV measurements at the tube exit downstream of two different tube geometries were performed to investigate and quantify the influence of bends on the downstream flow field development.

The first tube geometry was a 1:5 scaling of the steam injection tube used in the large scale experimental facility PANDA at PSI. Horizontal profiles of normalized axial velocity and turbulent kinetic energy are analyzed for numerous Re-numbers (Re = 7'800 to Re = 16'600), revealing no Re-number dependence of the flow at 10 diameters downstream of the bend. Because a very weak rotational in-plane velocity component was noticed, honeycombs were placed at two locations upstream of the flow, however having no noticeable effect on the resulting velocity fields. Even adding an additional 90° bend – to maximize the distortion – upstream of the bend under investigation had only marginal effects. To test the applicability of the scaled tube results for the large scale steam injection tube in PANDA, they were compared against in situ flow measurements at the exit of the original PANDA tube. Due to technical limitations, only 2D PIV measurements were feasible in PANDA, allowing to measure only the two velocity components located in a vertical plane above the tube exit. Hence, the in situ measurements performed at five positions were compared to the five corresponding cross sections of the scaled tube measurement, revealing a good agreement. Therefore, it is valid for future investigations to only analyze the scaled tube, which allows to profit from the advantages of the 3D PIV measurements as well as the easier accessibility.

The second geometry was a simplified 90° bend with constant diameter and variable exit tube lengths. A setup frequently found in the literature. For this tube geometry a considerable Re-number dependency was seen at the inner side of the flow (with respect to the bend) while on the outer side of the flow the scaled axial velocities collapse onto each other, i.e. they show self-similar behavior. With increasing downstream distance, the velocity profiles flatten progressively and the Re-number dependency vanishes until it is no longer present after 10 diameters, but a weak inclination is still present. The standard deviation of the velocity profiles and velocity fields are analyzed, confirming that most changes in the flow happen close after the bend, where most turbulence is present and the flow then gradually transitions towards a common - still weakly inclined - flow field after 10D, in line with findings from the literature. A comparison of our data to literature supports our findings and confirms that our results are trustworthy.

As a next possible step, it would be important to investigate the flow entrainment at the tube exit, as it is not yet known if it is influenced by the wall thickness of the tube. These experiments could be performed with the available scaled tube geometry. As the PANDA in situ measurements were conducted at Re = 13'500 and Re = 40'000, it could be interesting to also perform scaled tube measurements

at Re = 40'000 to extend the comparison between the two measurements.

To extend the fundamental research, i) honeycombs could be placed in the 90° bend, trying to suppress distortions before they are formed and therefore limiting the influence of bends on downstream flow and ii) a set of additional experiments with different bend curvature parameters might be helpful to shed light on to the influence of this parameter on the developing flow field.

References

[1] SA Berger, L Talbot, and LS Yao. Flow in curved pipes. *Annual review of fluid mechanics*, 15(1):461–512, 1983.

[2] M Raffel, C E Willert, S T Wereley, and J Kompenhans. *Particle image velocimetry: a practical guide*. Springer, second edition edition, 2007.

[3] A Kalpakli Vester, S Sattarzadeh, and R Örlü. Combined hot-wire and PIV measurements of a swirling turbulent flow at the exit of a 90° pipe bend. *Journal of Visualization*, 19(2):261–273, 2016.

[4] K Sudo, M Sumida, and H Hibara. Experimental investigation on turbulent flow in a circular-sectioned 90-degree bend. *Experiments in Fluids*, 25(1):42–49, 1998.

[5] J Kim, M Yadav, and S Kim. Characteristics of secondary flow induced by 90-degree elbow in turbulent pipe flow. *Engineering Applications of Computational Fluid Mechanics*, 8(2):229–239, 2014.

[6] R Gharari, H Kazeminejad, N Mataji Kojouri, and A Hedayat. A review on hydrogen generation, explosion, and mitigation during severe accidents in light water nuclear reactors. *International Journal of Hydrogen Energy*, 43(4):1939–1965, 2018.

[7] A Kalpakli Vester, R Örlü, and P H Alfredsson. Turbulent flows in curved pipes: recent advances in experiments and simulations. *Applied Mechanics Reviews*, 68(5):050802, 2016.

[8] W R Dean. Xvi. note on the motion of fluid in a curved pipe. *The London, Edinburgh, and Dublin Philosophical Magazine and Journal of Science*, 4(20):208–223, 1927.

[9] KR Sreenivasan and PJ Strykowski. Stabilization effects in flow through helically coiled pipes. *Experiments in Fluids*, 1(1):31–36, 1983.

[10] J Kühnen, M Holzner, B Hof, and HC Kuhlmann. Experimental investigation of transitional flow in a toroidal pipe. *Journal of Fluid Mechanics*, 738:463–491, 2014.

[11] J Canton, P Schlatter, and R Örlü. Modal instability of the flow in a toroidal pipe. *Journal of Fluid Mechanics*, 792:894–909, 2016.

[12] MM Enayet, MM Gibson, AMKP Taylor, and M Yianneskis. Laser-doppler measurements of laminar and turbulent flow in a pipe bend. *International Journal of Heat and Fluid Flow*, 3(4):213–219, 1982.

[13] K Sudo, M Sumida, and H Hibara. Experimental investigation on turbulent flow through a circular-sectioned 180 bend. *Experiments in Fluids*, 28(1):51–57, 2000.

[14] WN Al-Rafai, YD Tridimas, and NH Woolley. A study of turbulent flows in pipe bends. *Proceedings of the Institution of Mechanical Engineers, Part C: Mechanical Engineering Science*, 204(6):399–408, 1990.

[15] MJ Tunstall and JK Harvey. On the effect of a sharp bend in a fully developed turbulent pipe-flow. *Journal of Fluid Mechanics*, 34(3):595–608, 1968.

[16] Ch Brücker. A time-recording DPIV-study of the swirl switching effect in a 90° bend flow. In *Proceedings of the Eight International Symposium on Flow Visualization, Sorrento, Italy*, 1998.

[17] J Sakakibara, R Sonobe, H Goto, H Tezuka, H Tada, and K Tezuka. Stereo-PIV study of turbulent flow downstream of a bend in a round pipe. In *14th International Symposium on Flow Visualization, EXCO, Daegu, South Korea, June*, pages 21–24, 2010.

[18] L Hellström, M Zlatinov, G Cao, and A Smits. Turbulent pipe flow downstream of a 90° bend. *Journal of Fluid Mechanics*, 735, 2013.

[19] A Kalpakli Vester and R Örlü. Turbulent pipe flow downstream a 90° pipe bend with and without superimposed swirl. *International Journal of Heat and Fluid Flow*, 41:103–111, 2013.

[20] A Kalpakli Vester, R Örlü, and P H Alfredsson. Pod analysis of the turbulent flow downstream a mild and sharp bend. *Experiments in Fluids*, 56(3):57, 2015.

[21] A Noorani and P Schlatter. Swirl-switching phenomenon in turbulent flow through toroidal pipes. *International Journal of Heat and Fluid Flow*, 61:108–116, 2016.

[22] C Carlsson, E Alenius, and L Fuchs. Swirl switching in turbulent flow through 90° pipe bends. *Physics of Fluids*, 27(8):085112, 2015.

[23] L Hufnagel, J Canton, R Örlü, O Marin, E Merzari, and P Schlatter. The three-dimensional structure of swirl-switching in bent pipe flow. *Journal of Fluid Mechanics*, 835:86–101, 2018.

[24] F Rütten, M Meinke, and W Schröder. Large-eddy simulations of 90°-pipe bend flows. *Journal of turbulence*, 2:003, 2001.

[25] F Rütten, W Schröder, and M Meinke. Large-eddy simulation of low frequency oscillations of the dean vortices in turbulent pipe bend flows. *Physics of Fluids*, 17(3):035107, 2005.

[26] S Ebara, Y Aoya, T Sato, H Hashizume, Y Kazuhisa, K Aizawa, and H Yamano. Pressure fluctuation characteristics of complex turbulent flow in a single elbow with small curvature radius for a sodium-cooled fast reactor. *Journal of Fluids Engineering*, 132(11):111102, 2010.

[27] J Sakakibara and N Machida. Measurement of turbulent flow upstream and downstream of a circular pipe bend. *Physics of fluids*, 24(4):041702, 2012.

[28] A Jain. Experimental investigation of turbulent flow in a pipe bend using particle image velocimetry. Master's thesis, McMaster University, 2017.

[29] Z Wang, R Örlü, P Schlatter, and Y M Chung. Direct numerical simulation of a turbulent 90° bend pipe flow. *International Journal of Heat and Fluid Flow*, 73:199–208, 2018.

[30] P.K. Kundu and I.M. Cohen. *Fluid Mechanics*. Elsevier Science, 2010.

[31] S Vashisth, V Kumar, and K Nigam. A review on the potential applications of curved geometries in process industry. *Industrial & Engineering Chemistry Research*, 47(10):3291–3337, 2008.

[32] H Ito. Pressure losses in smooth pipe bends. *Journal of Basic Engineering*, 82(1):131–140, 1960.

[33] Ronald J. A and Jerry W. *Particle Image Velocimetry*. Cambridge University Press, 2011.

[34] H-E Albrecht, Nils Damaschke, Michael Borys, and Cameron Tropea. *Laser Doppler and phase Doppler measurement techniques*. Springer Science & Business Media, 2003.

[35] A Sciacchitano and B Wieneke. PIV uncertainty propagation. *Measurement Science and Technology*, 27(8):084006, 2016.

[36] S G Rabinovich. *Measurement errors: theory and practice*. AIP American Institute of Physics, 1995.

A. Appendix

Re-number -	normalization parameter $V_{z,max}$ $[m/s]$
13'500	1.64

Table A.1: *Normalization parameters used for the PANDA experiment.*

		normalization parameter $V_{z,max}$					
Re-number	Bulk velocity $[m/s]$	0.8D	2D	4D	6D	8D	10D
		$[m/s]$					
4'900	1.9	2.6	2.7	2.5	2.4	2.4	2.4
7'800	3.1	4.0	4.3	4.0	3.7	3.6	3.6
12'600	5.1	6.4	6.6	6.3	5.9	5.7	5.7
17'500	7.0	8.7	9.1	8.6	8.0	7.7	7.7
27'200	10.9	13.3	14.0	13.1	12.4	11.9	12.0

Table A.2: *Normalization parameters used for the 90° bend experiments for the corresponding Reynolds numbers and exit heights.*

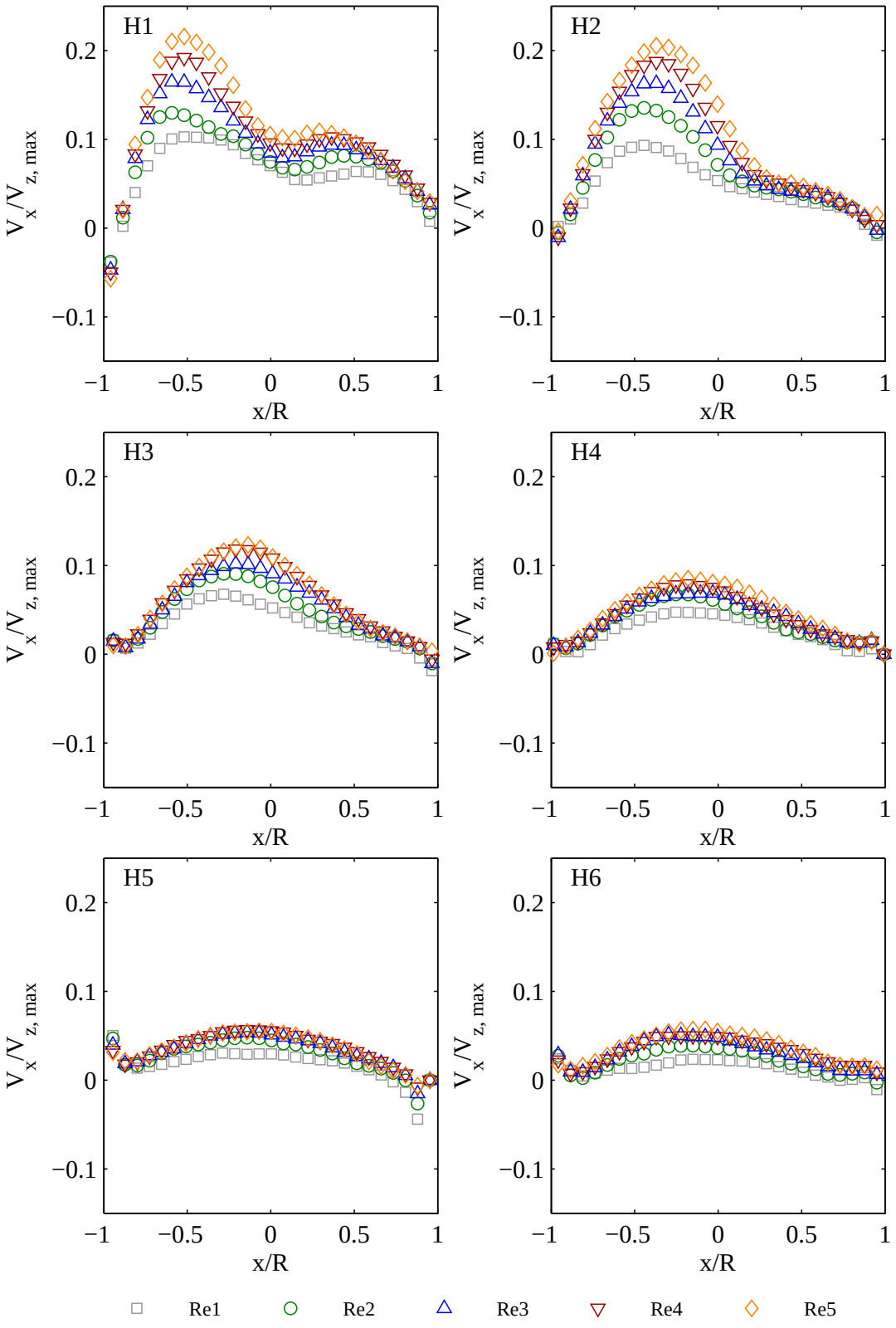

Figure A.1: *Horizontal profiles for the normalized axial velocity V_x extracted at y = 0 for different downstream distances (0.8D to 10D) past the 90° bend with Re-number as parameter.*

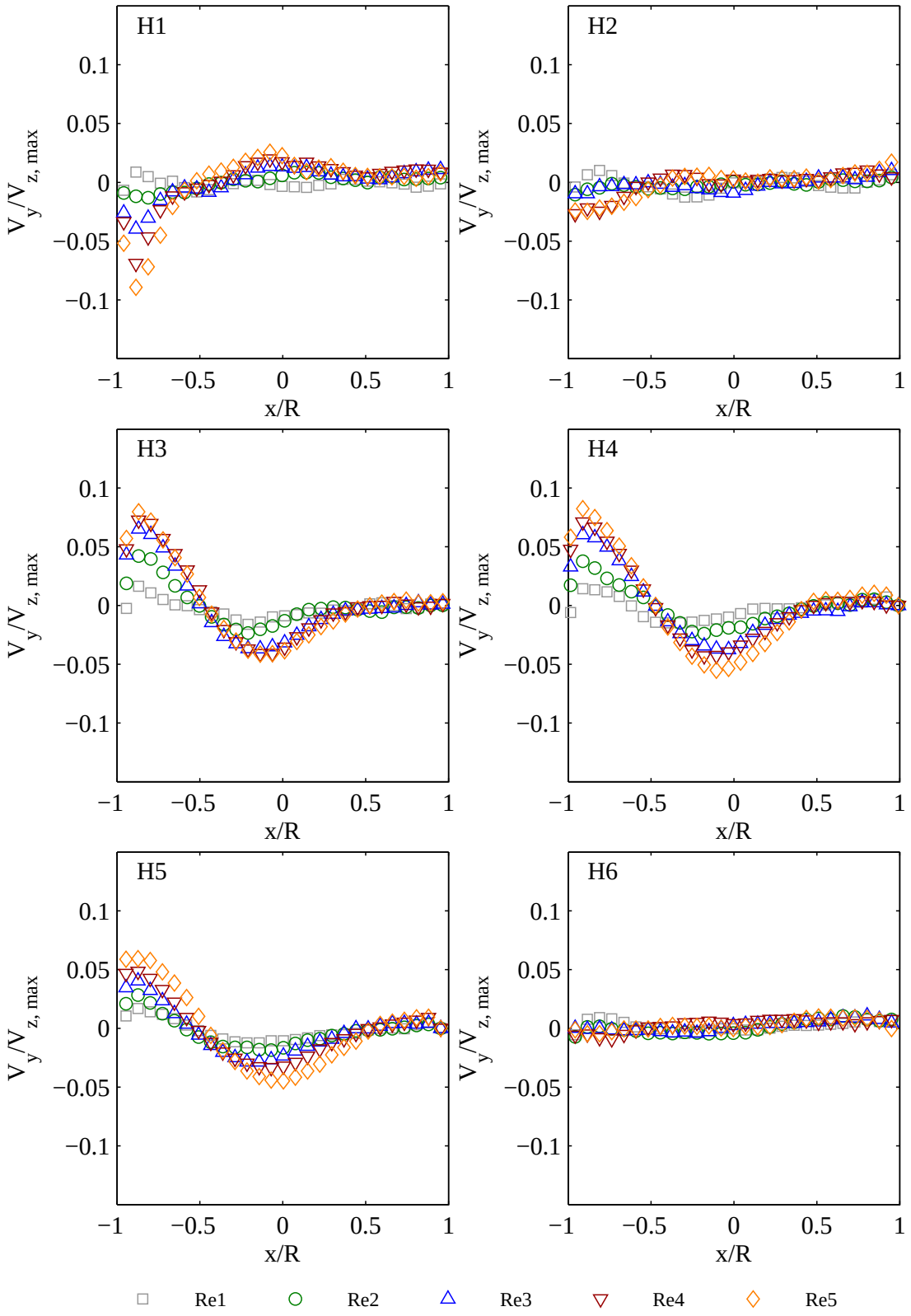

Figure A.2: *Horizontal profiles for the normalized axial velocity V_y extracted at y = 0 for different downstream distances (0.8D to 10D) past the 90° bend with Re-number as parameter.*

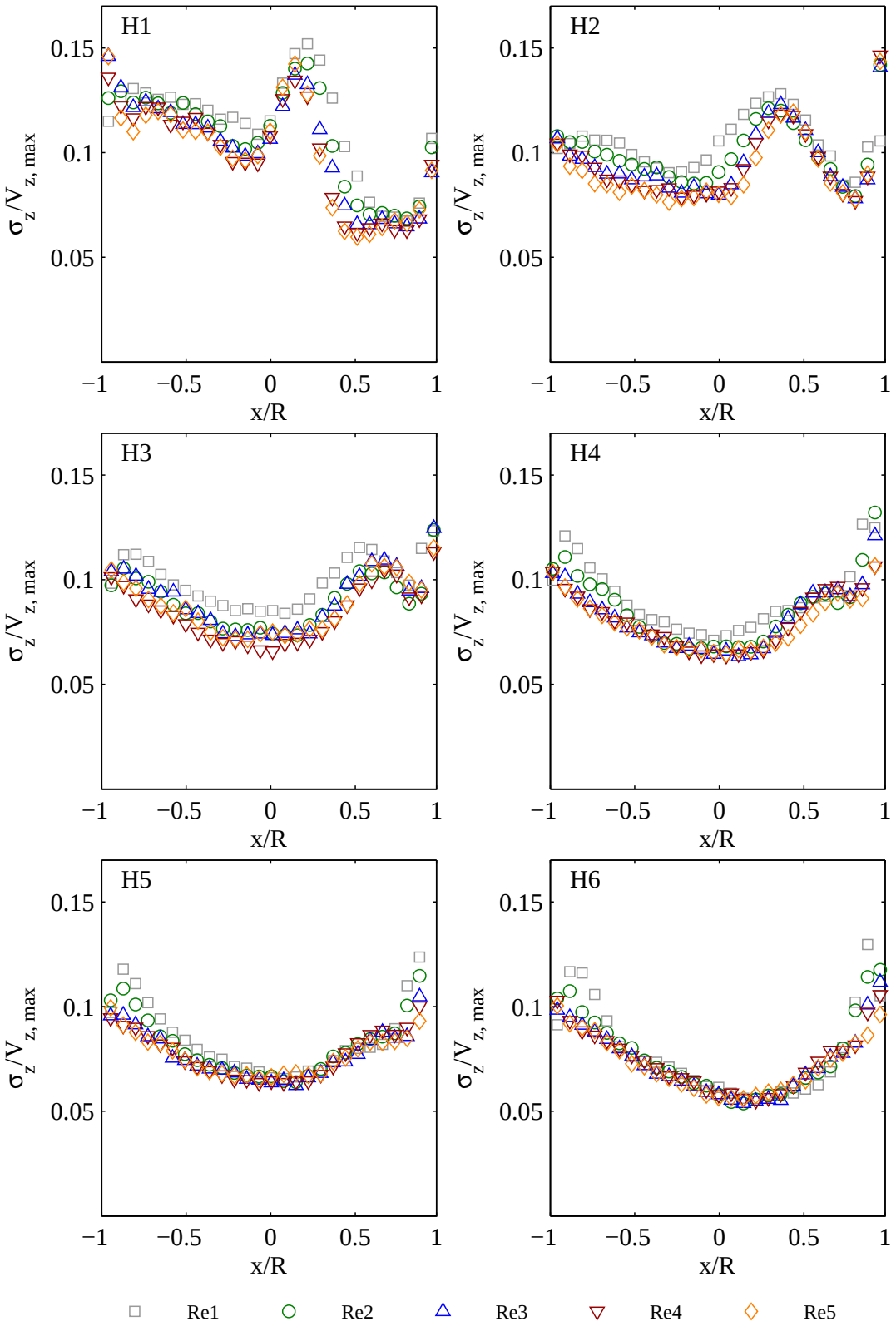

Figure A.3: *Horizontal profiles for the normalized standard deviation of V_z extracted at $y = 0$ for different downstream distances (0.8D to 10D) past the 90° bend with Re-number as parameter.*

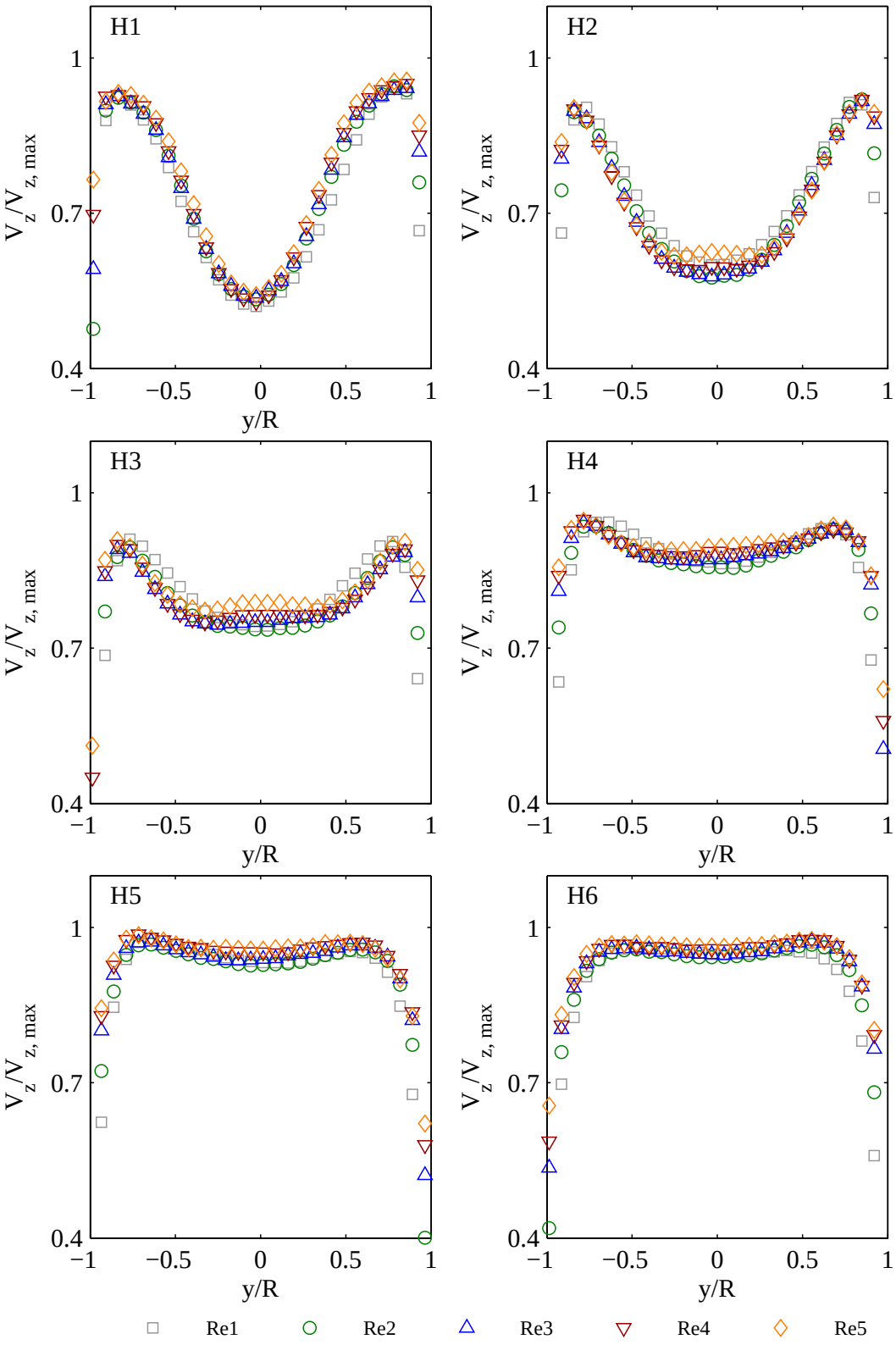

Figure A.4: *Vertical profiles for the normalized axial velocity V_z extracted at $x = 0$ for different downstream distances (0.8D to 10D) past the 90° bend with Re-number as parameter.*

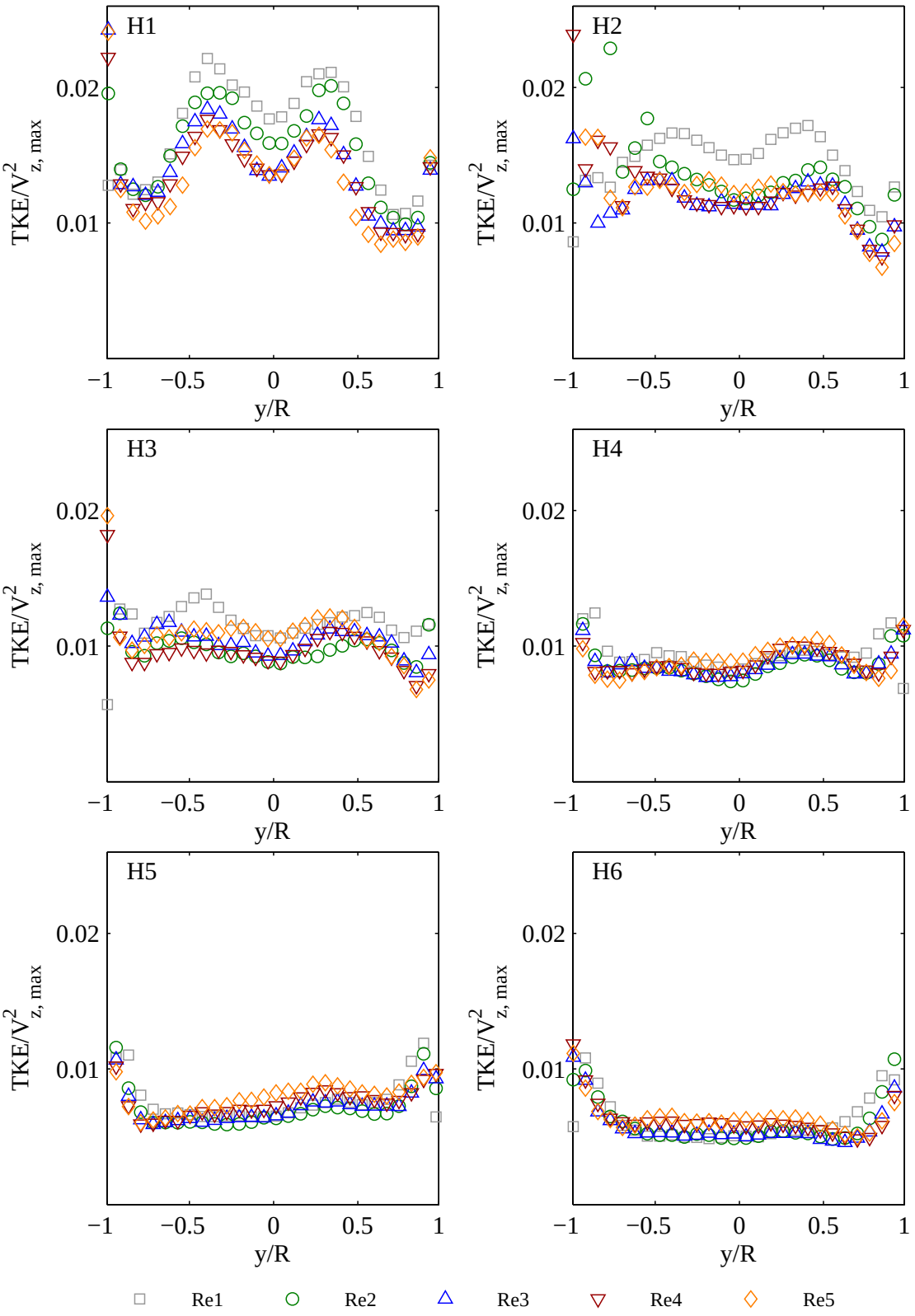

Figure A.5: *Vertical profiles for the normalized TKE extracted at $x = 0$ for different downstream distances (0.8D to 10D) past the 90° bend with Re-number as parameter.*

Appendix C: Publication "Self-similarity for statistical properties in low-order representations of a large-scale turbulent round jet based on the proper orthogonal decomposition" by R. Kapulla, K. Manohar et al.

Experimental Thermal and Fluid Science 123 (2021) 110320

Contents lists available at ScienceDirect

Experimental Thermal and Fluid Science

journal homepage: www.elsevier.com/locate/etfs

Self-similarity for statistical properties in low-order representations of a large-scale turbulent round jet based on the proper orthogonal decomposition

R. Kapulla [a,*,1], K.H. Manohar [b,1], S. Paranjape [a], D. Paladino [a]

[a] Paul Scherrer Institute, 5232 Villigen, Switzerland
[b] University of Calgary, 2500 University Drive NW, Calgary, Alberta T2N 1N4, Canada

ARTICLE INFO

Keywords:
Proper Orthogonal Decomposition (POD)
Self-similarity
Low-order representation (LOR)
Turbulent round jet
Large scale experiment
Particle Image Velocimetry (PIV)

ABSTRACT

This study is an experimental investigation into the self-similarity behavior of first and second order statistical quantities derived from a jet flow based on a) the original data and b) its low-order representations derived from the Proper Orthogonal Decomposition (POD) and c) a comparison of both. The flow under investigation is an air-helium turbulent round jet with Re ≈ 15 400 emerging from a tube into an ambient containing identical gas mass fraction and temperature as the jet at a constant pressure. Instantaneous two-dimensional velocity field measurements were obtained for downstream distances of 5.5*d* to 17.4*d* in the plane of the axis of the jet, via Particle Image Velocimetry. The snapshot POD algorithm was then applied to this data set to generate low-order representations with rank approximations 1, 5, 10 and 50. These then serve as the basis to derive the respective (rank truncated) statistical properties. All properties are non-dimensionalized with a self-similar framework as obtained from the original jet data. It is found that the statistical properties obtained from the low-order representations a) resemble in shape the asymptotic outline of the original jet and b) that the maximum values (for a given low-order representation) exhibit asymptotic states with increasing downstream distances. This is a strong indication that i) self-similar behavior is equally found in the low-order representations and that ii) this finding is mainly controlled by the large-scale vortices. The sole exception is the axial velocity root-mean-square values, where a distinct dip in the center line of the flow is found. This dip is successively filled up by smaller-scale turbulence for higher order truncations. Additionally, a new criterion – based on the maximum cross-correlation obtained through successive time traces of the temporal POD modes – is suggested to distinguish physically relevant modes from the POD basis in a more quantitative and explicit manner compared to traditional energy-based criteria.

1. Introduction

The identification and interpretation of vortical structures in highly turbulent flows and their significance for the underlying flow physics has been a field of research since the 1960s. Now commonly accepted, the re-discovery of well-organized vortices was so surprising to some researchers at that time that they '*…attempted to eliminate them, looking for possible resonances, splitter plate vibrations, etc., but none were found.*' [1]. Since then – after this paradigm shift [2] – the internal organization, formation, development, stability, interaction, and importance of these vortical structures have been the subject of extensive experiments and numerical simulations [3–8].

Even though experimental results or numerical simulations typically have high dimensionality (degrees of freedom), they can often be well-characterized by (low-dimensional) dominating coherent structures. For instance, these structures can be found in the vortex street behind a circular cylinder [6], in shear layers [1] or in the wake flow past an array of wind turbines [9]. The latter reference provides an pragmatical approach in how low-order representations of the turbulent flow might contribute to practical answers of interest. In contrast to the increasing availability of highly resolved data obtained from experiments and numerical simulations, there is a correspondingly significant need to describe high-dimensional fluid systems in a more elementary fashion. This would in turn contribute to a better understanding of the large-scale dynamics of coherent structures [10], control [11,12], estimation [13],

* Corresponding author.
E-mail address: ralf.kapulla@psi.ch (R. Kapulla).
[1] These authors have contributed equally to this work.

https://doi.org/10.1016/j.expthermflusci.2020.110320
Received 31 July 2020; Received in revised form 27 November 2020; Accepted 6 December 2020
Available online 8 January 2021

Nomenclature

Abbreviations

2D	two-dimensional
Re	Reynolds number
CCD	charge coupled device
FOV	field of view
HW	hot wire
LDA	laser Doppler anemometry
LOR	low order representation
mn	mode number
PIV	particle image velocimetry
POD	proper orthogonal decomposition
RMS	root mean square
ROM	reduced order model

Symbols

$\mathbf{A}$	matrix with dimensions $\mathbf{A} \in \mathbb{R}^{NxN}$ whose columns contain the orthonormal eigenvectors of $\mathbf{C}$
$\mathbf{C}$	autocovariance matrix with dimensions $\mathbf{C} \in \mathbb{R}^{NxN}$
$\mathbf{T}$	matrix with dimensions $\mathbf{T} \in \mathbb{R}^{NxN}$ containg the temporal modes
$\mathbf{U}$	matrix with dimension $\mathbf{U} \in \mathbb{R}^{MxN}$ containing all the velocity components for all the snapshots
$\overline{V}, \overline{U}$	time-averged transversal and axial velocity components
D	vessel diameter in mm
d	tube inner diameter in mm
f	frequency
M/2	number of velocity vectors in one instantaneous 2D PIV recording
N	number of snapshots/PIV recordings
p, q	horizontal and vertical dimensions of an instantaneous velocity field, $p \cdot q = M/2$
q_U, q_V	factors quantifying the statistical independence of the PIV recordings in transversal an axial direction
$R_{u'u'}, R_{v'v'}$	Reynolds (normal) stresses
$R_{u'v'}$	Reynolds (shear) stresses
r	rank truncation
$t_{i,u}, t_{i,v}$	integral time scales for velocity components U, V
T	temperature
t	time
u', v'	mean-free transversal and axial velocity fluctuations
U, V	transversal and axial velocities of the jet
V_0	velocity at the tube exit
$V_g, V_p, r_{0.5}, x_c$	fit parameters to define the self-similarity framework
x^*, y^*, z^*	coordinate system located at the bottom of the PANDA vessel
y/d	non-dimensional downstream distance with $y^* = 4000\text{mm} = y/d = 0$ at the tube exit
k	turbulent kinetic energy $k_{mc,r}, k_r$ energy contained in the spatial domain of the rank *r* truncated data for matrix **U** assembled either from the mean-contained (*mc*) or the mean-free velocity components, respectively $k_{mc,sum}, k_{sum}$ entire energy contained in the spatial domain of the data either for matrix **U** assembled from mean- contained (*mc*) or the mean-free velocity components, respectively

Subscripts/Superscripts

mc	mean-contained
rms	root mean square
T	transposed of a matrix
*	depicting re-ordered matrices, example $\mathbf{A}^*$

Greek symbols

β	spreading rate of the jet
$\in$	uncertainty/errors of the PIV measuremets
η	non-dimensional axial velocity
λ_e	eigenvalues of matrix **C**
$\mathbf{\Lambda}$	diagonal matrix with dimensions $\mathbf{\Lambda} \in \mathbb{R}^{NxN}$ whose diagonal entries are the eigenvalues λ_e
$\mathbf{\Phi}$	matrix with dimensions $\mathbf{\Phi} \in \mathbb{R}^{MxN}$ containg the spatial modes/basis functions
μ	time averaged mean
$\rho_{T_{mn}, T_{mn+1}}$	cross-correlation function for successive temporal modes *mn* and *mn* + 1
σ	standard deviation/confidence limit
ξ	non-dimensional transversal distance
$max(\rho_{T_{mn}, T_{mn+1}})$	maximum of the cross-correlation function for successive temporal modes *mn* and *mn* + 1

prediction [14] or closure modeling [15] in a wealth of applications. Thus, there is a necessity for reduced-order models (ROMs) [16]. ROMs effectively filter out the small-scale turbulent structures which do not contribute much to the convergence towards a valid representation of the essential flow physics according to [9,17].

The conceptually equivalent approach in obtaining ROMs is valid, since the large-scale dynamics in high-dimensional fluid systems typically evolve on a low-dimensional (coherent) subspace. An orthogonal-based representation of this subspace can be obtained via the POD as described by [18]. As opposed to the original formulation of the classical POD method [19], the method of snapshots introduced in [20] has proved to be an effective and computationally-forgiving alternative algorithm to calculate the POD modes for a given data set – provided that the number of spatial data in a snapshot (the number of vectors within the measurement domain) exceeds the total number of snapshots. It is commonly accepted that truncating the POD series to the first few dominant POD modes reconstructs the ensemble to capture a certain amount of turbulent kinetic energy while highlighting the large-scale dynamics of the flow [17,9]. This argument is solely based on an energy concept – and therfore a mean quantity – these modes represent, while neglecting the equally valid perspective of the 'coherence' of the modes; which is much more difficult to quantify. In essence, there is no commonly accepted consensus on what numerical value or strict criterion is attributed to the phrase 'first few' modes. This leads to our suggestion to derive a quantitative criterion by using the maximum cross-correlation coefficient calculated from successive time traces of the underlying temporal POD modes as outlined in Section 4.2.2.

Since jets belong to the so-called 'building-block' flows they have been extensively studied in the past. For axisymmetric jets, refer to [21–25]. Consequently, substantial research has been conducted on the application of POD to jet flow. The first implementation was done by [26] and for the near field past the tube exit see [27]; 28,29,27 on a highly buoyant jets; [30] on a confined co-flowing jet; [31–33] on planar jets; [34–37] for axisymmetric jets and for jets in cross flow [38]. All these works have detected large-scale vortical structures [32] in the most energetic modes. An additional – and complementing – classical subject for jet flows is self-similarity or self-preservation [23,39,40]. The work of [41] confirms the theoretical prediction of [42] that a family of local states in jets and plumes exist for which partial self-similarity is attained – but more importantly, that global self-preservation for the entire state space is reached through a universal route. This suggests that the large-scale structures play an important role in the self-preservation of jet flows. Additionally, it was shown by [32] that the POD modes of a planar jet preserve self-similarity. In the analysis of their experimental

campaign, the authors demonstrated that the large-scale dynamics ('large-scale' referring to spatial scales comparable to the jet width) described by the first few modes are self-preserving with increasing downstream distance.

The reduced representation of flows through low-order representations (LORs) are an increasingly popular subject in the context of turbulence control [12] to avoid or minimize unwanted turbulence-induced side effects such as jet noise [43], noise from '*airframes, fans, and jet exhausts*' [44] or inefficiencies in combustion processes [45]. This is because low-dimensional data could highlight certain flow features that are otherwise masked (and therefore not accessible) by the complexity of the (fully turbulent) flow. It has to be emphasized that the POD method is data-driven. That is, the calculated spatial and temporal modes (or basis functions and their corresponding time-varying coefficients, respectively) used to describe the functional space in which the flow ensemble resides in (see Section 3) are fully determined from the data [46]. Consequently, a trade-off is to be expected between the convenience offered by the nature of generating data-driven basis functions and the concept of generalizing these basis functions to describe the underlying physical system. This tension will not be resolved in the present considerations.

In the present paper, LORs of the jet are used instead of ROMs to study self-similarity in the low-order dynamics governed by the dominant POD modes. The asymptotic behavior of the statistics of the LORs in a self-similar context would give an idea as to what the corresponding behavior in the ROMs would look like. This can then provide modelers with certainty to construct POD-based ROMs while having confidence that they preserve self-similarity states within the considered flows. Hence, POD-based experimentally obtained LORs are used here as a more direct way to study self-preservation of the ROMs. To the best knowledge of the authors in this paper, no work has been done on the preservation of self-similarity in LORs of a turbulent round jet.

The subject of the present paper is the detailed analysis of the jet velocity fields (experimental data-set: H2P1_16_S03 taken from the HYMERES-2 project [48,49]) to investigate: a) the extent up to which LORs also exhibit self-similar behavior and b) the ability of the LORs to represent the underlying turbulence magnitudes and shape compared to the original signals. All of these results will be compared with the classical jet results taken from [22]. The focus will be on the first and second order velocity moments derived from the original two dimensional (2D) PIV recordings: axial (time-averaged) mean velocities $\overline{V}$, the respective root-mean-squared (RMS) signals u' and v', the turbulent kinetic energy k and the Reynolds shear stress $R_{u'v'}$; and these will be compared with the different rank approximations obtained using the first 1, 5, 10 and 50 modes – which represent the LORs under consideration.

The experimental method, the measurement technique and the boundary conditions of the experiment are described in Section 2. An algorithmically oriented outline of the snapshot POD as presented in [50] used in this work is briefly explained in Section 3. The relevant results will be extensively discussed in terms of the statistical distributions and in the context of self-similarity in Section 4. We end the paper – as usual – with conclusions and the necessary future work in Section 5.

2. Experimental methods

The experiments were conducted at constant ambient pressure (0.996 bar). To maintain this pressure during the experiment, a funnel was mounted as close as possible to the axis of the experimental setup at the bottom of the vessel and the funnel was connected to a vent line, thus minimizing possible distortions introduced by the outflow of the exhaust gas to compensate for the jet inflow, Fig. 1.

A commercial Particle Image Velocimetry (PIV) system from LaVision was used for the base recording of in-axis 2D jet velocity measurements in the PANDA vessel [47]. The PIV system consisted of a Quantel Twins B double-pulse laser with maximum output energy of 380 mJ and a two double frame CCD cameras of type (LaVison) Imager Pro X, which are identical to the PCO.1600 cameras having a resolution of 1600×1200 pixels. After calibration of the images, a spatial resolution of 0.6×0.6 mm^2/*pixel* was achieved. For the calculation of the velocity fields, a final interrogation window size of 32×32 pixels with 75% overlap was used. This corresponded to an effective spatial resolution of 4.8×4.8 mm^2. The base analysis of the recorded particle images towards velocity fields was done with the commercial software DaVis 8.4 from LaVison.

The two available PIV cameras were mounted in front of the upper vessel window on a translation stage consisting of two goniometers and a rotation table. By vertically inclining the upper camera it was possible to record two different field-of-views (FOVs) in total (Pos_A and Pos_B), see Fig. 1. Since Pos_A and Pos_B were recorded simultaneously, the resulting velocity fields were stitched together and treated as one recording. Di-Ethyl-Hexyl-Sebacat (DEHS) droplets dispersed by a spraying nozzle were used as seeding particles by injecting them into the air-helium stream, which was in turn directed into the vessel through the injection tube. The PIV system setup for the in-vessel measurements provided 2D velocity fields with an acquisition rate of $f = 5$ Hz. For the calculation of statistical quantities, $N = 1024$ PIV image pairs were averaged, resulting in a total averaging time of 204.8s. The optical recording system consisted of two CCD cameras each equipped with Nikon lenses (AF Nikkor, focal length $f_v = 28$ mm; the aperture set to $f_{\#} = 2,8$ each) which were operated in the diffraction limit; that is, the particle image sizes on the CCD chip become independent of the physical particle size, resulting in particle image sizes larger than 3 pixels on average. According to the recommendations given in [51], this is sufficient to minimize or eliminate peak-locking, which would introduce a bias in the velocity calculations towards (pixel shift based) integer values. The corresponding calculation of the frequency response of the particles used – not discussed in detail here – can be found in [52].

To calculate decent first and second order statistical quantities such as the mean axial velocity $\overline{V}$ or the corresponding velocity fluctuations v', a prerequisite is that the samples are statistically independent [53]. A common interpretation of statistical independence is: Record the next sample when the 'memory of the flow' is lost. A usual quantitative test on the statistical independence is obtained through an integration of the auto-correlation function of the respective signal, which results in an integral time scale t_i. Statistical independence requires that the time between successive samples are at least $2t_i$ apart which corresponds to a sampling frequency of $f \geqslant 1/(2t_i)$. The actual sampling frequency of $f = 5$ Hz for the present experiments was chosen such that this criteria is met (on average) for both velocity components U and V in the core of the jet. To test the required condition, the $2T_i$ criteria was calculated for each vector point for the velocity components U and V separately on the basis of an auto-correlation function. The resulting values were converted into dimensionless numbers – q_U and q_V – depicting on average – the required step size with respect to the original series of snapshots $1, 2, 3, 4, 5 \ldots, N$ for a given location in the PIV plane for which one would find the next statistically independent sample, i.e. $q_u = 2t_{i,u} \cdot f$ and $q_v = 2t_{i,v} \cdot f$. The result of this calculation is presented in Fig. 2 for the velocity components U and V in addition to with an approximate outline of the expanding jet. The graphs read as follows: For $q_U \approx q_V \approx 1$, all samples of the series of snapshots $1, 2, 3, \ldots, N$ are statistically independent, i.e. the measurements in the core of the jet – as intended – meet this criterion. For $q_U \approx q_V \approx 2$ only samples $1, 3, 5, \ldots, N-1$ of the original series are independent. And this – through the effective number of (independent) samples – is considered in the respective statistical calculation according to [54] within the data presented in this article. The relaxed criterion of statistical independence ($q_U \approx q_V \approx 2$) is typically met in the outer parts of the jet (labeled as 'transitional') where the velocities are lower. There are even regions where $q_U \approx q_V \approx 10$ (or even higher). These regions are in the far field where the jet meets the stagnant

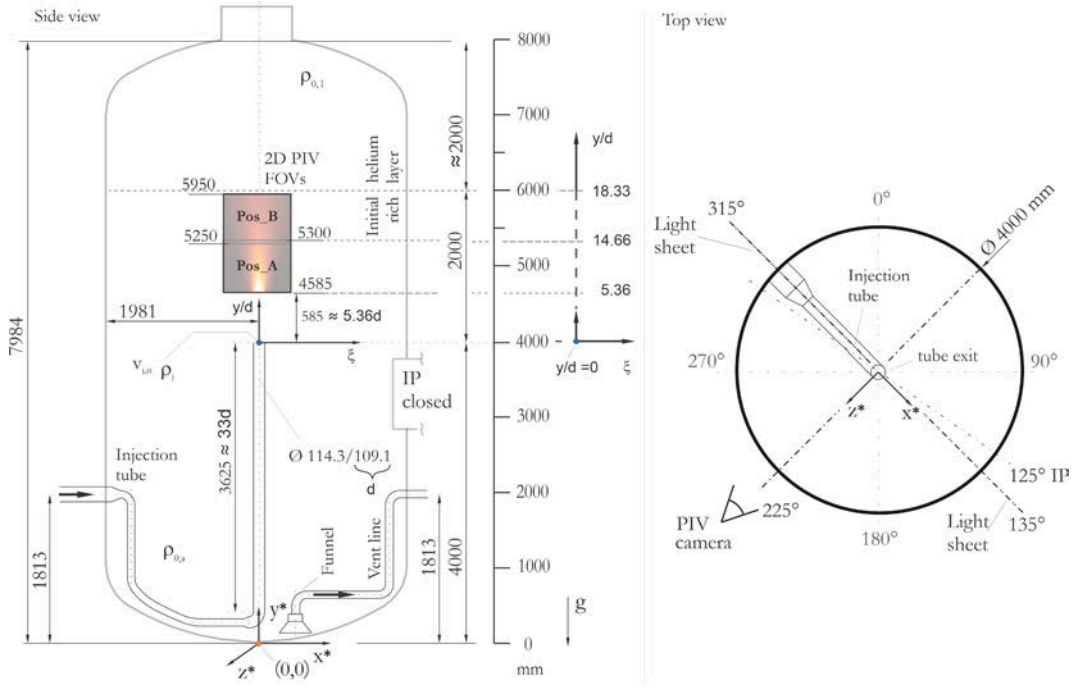

Fig. 1. Schematic of side (left) and top view (right) of the PANDA experimental facility [47] setup used for the experimental results under consideration along with the main dimensions. Numbers '1234' in mm – dimensions with respect to the global coordinate system (x^*, y^*, z^*) of the PANDA facility located at the bottom of the vessel. Non-dimensional numbers '1234' $(\xi, y/d)$ with respect to the coordinates downstream of the tube exit with $y^* = 4000$ mm $= y/d = 0$ to present the jet results.

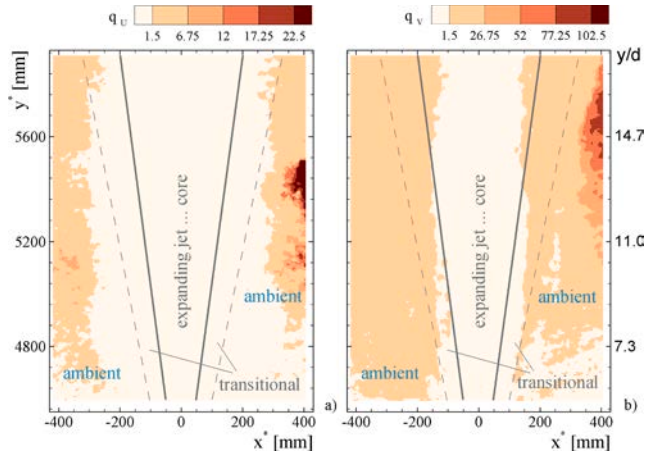

Fig. 2. Dimensionless numbers for the transversal U and axial V velocity – q_U a) and q_V b) – depicting (on average) the required step-width with respect to the (original) series of snapshots $1, 2, 3, 4, 5 \ldots, N$ for a given location in the PIV plane to quantify the next statistically independent sample. For $q_U \approx q_V \approx 1$ all samples of the series of snapshots $1, 2, 3, \ldots, N$ are statistically independent, i.e. the core of the jet meets this criterion completely for U and to a certain extent also for V..

ambient where the flow memory spans longer durations. Thus, they can be neglected. Since we do not have time-resolved measurements, we instead focused on verifying statistical independence in the obtained samples. Consequently velocity spectra are not subject of the present considerations.

Errors in the entire axial velocity field are presented in Section 4. A gas mixture composed of 24.7g/s air and 0.3g/s helium at ambient temperature was injected to the tube. This corresponds to Re ≈ 15 400 when using the tube inner diameter of d = 109.1 mm and the respective kinematic viscosity using the REFPROP program from the National Institute of Standards and Technology (NIST) [55]. The jet emerged from a tube with a length of 33d at ambient temperature ($T = 29.7°C$) into a surrounding with identical air-to-helium composition and temperature. Thus, there were no buoyancy effects. The main coordinate system to describe the vessel dimension is located at the bottom of the vessel (x^*, y^*, z^*) and the tube exit is located at $y^* = 4000$ mm with respect to this global coordinate system. Jet properties are subsequently described with respect to the non-dimensionalized coordinate system located at the tube orifice $(\xi, y/d)$, Fig. 1. The two components of the velocity vector are depicted using the Reynolds decomposition – the spanwise component through $U = \overline{U} + u'$ and the axial component through $V = \overline{V} + v'$.

2.1. Convergence of statistics

To test for the convergence for most of the statistical properties as derived from a relatively small sample of N = 1024 statistically independent sampled snapshots, we provide two types of graphs. Convergence plots of the mean axial $(\overline{V})$ and transverse $(\overline{U})$ velocities, as well as the corresponding normal Reynolds stresses $R_{u'u'}$ and $R_{v'v'}$ extracted at $\xi = 0, y/d = 16.3$ as a function of sample size N, Fig. 4. For further assessment we add the complementing profiles of the Reynolds stresses $R_{u'u'}$, $R_{v'v'}$ and $R_{u'v'}$ extracted at $y/d = 16.3$ for sample sizes of N = 200, 400, 600, 800 and 1000, see Fig. 3. We additionally provide error margins of the measurements on a 3σ level for the converged set of N = 1000 samples.

We find that the data-scatter at a selected point of the respective quantities relaxes and converges considerably past $N > 500$, Fig. 4. Even though noting the difference for the asymptotic value of $R_{u'u'}$ between our measurements and the chosen reference [22], we find a close match past $N > 500$ for the pre-converged measurements and $R_{v'v'}$ as presented in [22], Fig. 4. A similar behavior past $N > 500$ can be derived from the measured profiles of the Reynolds stresses $R_{u'u'}$, $R_{v'v'}$ and $R_{u'v'}$ at $y/d = 16.3$ Fig. 3. It is also shown that the reference measurements provided by [22] for $R_{u'u'}$ (—) and $R_{w'w'}$ (—) – the latter quantity that we could not measure – confirms the assumption of an axis-symmetry of the relevant statistical properties within the jet relevant for our considerations.

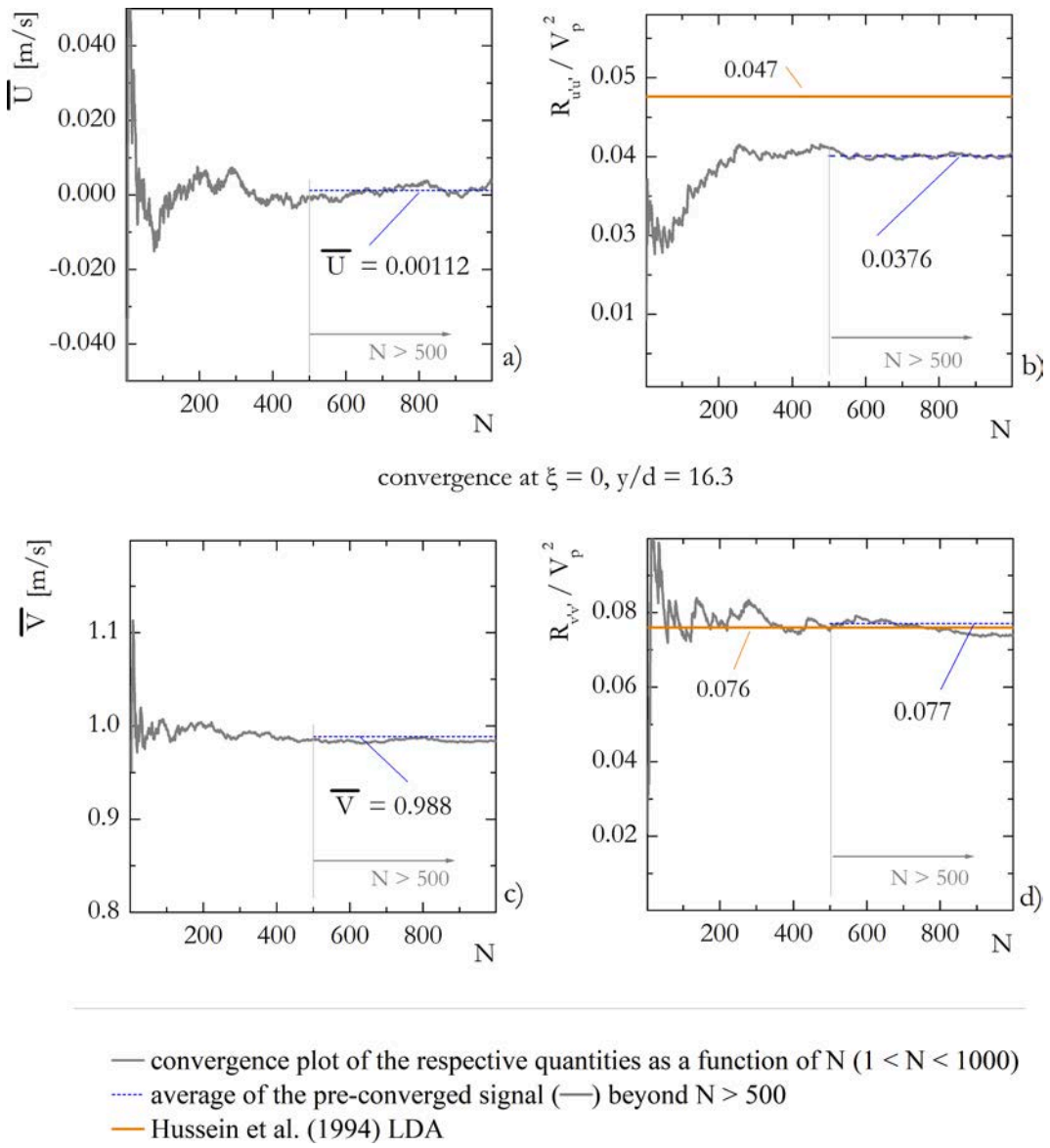

Fig. 3. Horizontal profiles of the normalized Reynolds stresses $R_{u'u'}$, $R_{v'v'}$ and $R_{u'v'}$ for sample sizes of N = 200, 400, 600, 800, 1000 extracted at downstream distance y/d = 16.3. The error margins on a 3σ level are presented for the converged sample sizes of N = 1000. Our results are compared with data taken from [22].

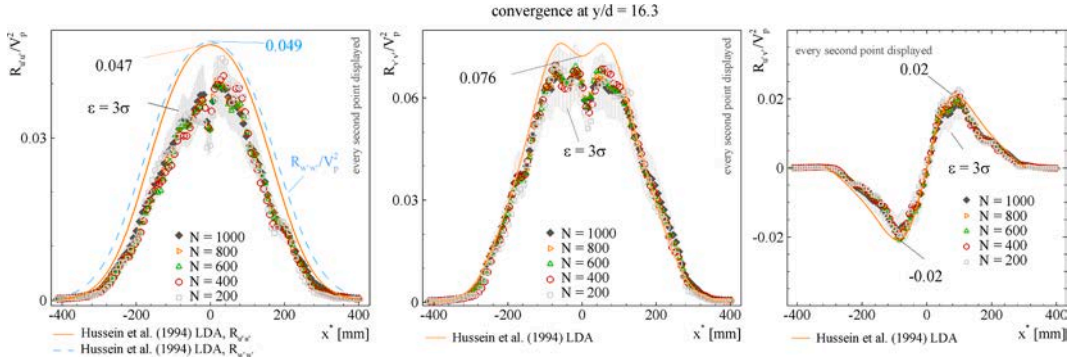

Fig. 4. Convergence plots of first and second order velocity moments extracted at location $\xi = 0, y/d = 16.3$ as a function of sample size N. Our results are compared with data taken from [22]. The pre-converged mean beyond N > 500 is indicated.

3. Snapshot Proper Orthogonal Decomposition algorithm

The Proper Orthogonal Decomposition (POD) decomposes a flow data set into modes that are ranked based on their energy contribution to the system dynamics [18]. The snapshot POD algorithm introduced by [20], is applied to the PIV data-set of 2D velocity fields measured in this

study. The algorithm used is taken from [50] and is extended to matrix space for the case of 2D data, and was implemented in an in-house Matlab code.

A collection of N instantaneous velocity snapshots, each containing p·q = M/2 velocity vectors are sampled at equi-temporal intervals, Fig. 5. Each snapshot is defined as a 2D velocity field $\vec{U} = (U, V)$ with the two mean-free velocity components u' and v' according to the Reynolds decomposition. Note that the following analysis can be extended to include 3D velocity fields without loss of generality. With these vector components u' and v' at each vector location, an ensemble matrix $\mathbf{U} \in \mathbb{R}^{M\times N}$ can be constructed, Eq. (1). Here, $\mathbf{U} \in \mathbb{R}^{M\times N}$ is the matrix space of real numbers of dimension M × N. The M = 2·p·q vector components of each snapshot are arranged into single-column vectors that are assembled into matrix **U**. The same velocity arrangement can also be used for *mean-contained* velocity components *U* and *V*. In this case the first spatial POD mode – labeled conventionally as the 'zero mode' – approximately represents the mean field.

$$\mathbf{U}\left(t\right) = \begin{bmatrix} u'_{1,1}(t_1) & u'_{1,1}(t_2) & \dots & u'_{1,1}(t_N) \\ u'_{2,1}(t_1) & \ddots & \dots & u'_{2,1}(t_N) \\ \vdots & \vdots & \ddots & \vdots \\ u'_{p,q}(t_1) & u'_{p,q}(t_2) & \dots & u'_{p,q}(t_N) \\ v'_{1,1}(t_1) & v'_{1,1}(t_2) & \dots & v'_{1,1}(t_N) \\ v'_{2,1}(t_1) & \ddots & \dots & v'_{2,1}(t_N) \\ \vdots & \vdots & \ddots & \vdots \\ v'_{p,q}(t_1) & v'_{p,q}(t_2) & \dots & v'_{p,q}(t_N) \end{bmatrix} \tag{1}$$

The POD algorithm divides the spatio-temporal ensemble of velocities **U** into space-dependent orthonormal POD modes $\mathbf{\Phi} \in \mathbb{R}^{M\times N}$ (spatial modes, also referred to as the basis functions) and time-dependent orthogonal modes $\mathbf{T} \in \mathbb{R}^{N\times N}$ (referred to as temporal modes), respectively, through the following relationship [50]:

$$\mathbf{U} = \mathbf{\Phi}\mathbf{T}^{T} \tag{2}$$

with the superscript 'T' referring to the transpose of a matrix.

The following snapshot POD algorithm is employed to obtain the spatial and temporal modes:

1. Compute the autocovariance matrix $\mathbf{C} \in \mathbb{R}^{N\times N}$ as follows:

$$\mathbf{C} = \frac{1}{N}\mathbf{U}^{T}\mathbf{U} \tag{3}$$

2. Calculate the eigendecomposition of **C**:

$$\mathbf{C} = \mathbf{A}\mathbf{\Lambda}\mathbf{A}^{T} \tag{4}$$

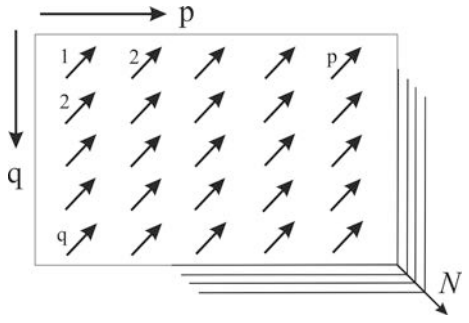

Fig. 5. Collection of N snapshots of 2D velocity fields each with dimension M, i.e. p·q = M/2→2·p·q = M with M depicting the total number of vector components.

where $\mathbf{A} \in \mathbb{R}^{N\times N}$ is an orthogonal matrix whose columns contain the orthonormal eigenvectors of **C**; and $\mathbf{\Lambda} \in \mathbb{R}^{N\times N}$ is a diagonal matrix whose diagonal entries are the eigenvalues λ_e of **C** with 1⩽e⩽N.

3. Sort the columns of **A** and **Λ** so that they are arranged in descending order with respect to the eigenvalues in **Λ** to obtain the reordered matrices $\mathbf{A}^*$ and $\mathbf{\Lambda}^*$ such that $\mathbf{\Lambda}^* = \mathrm{diag}(\lambda_1, \lambda_2, \dots, \lambda_N)$ where $\lambda_1 > \lambda_2 > \dots > \lambda_N$.
4. Scale the eigenvectors in $\mathbf{A}^*$ and project them onto the ensemble **U** to obtain the spatial POD modes as follows:

$$\mathbf{\Phi} = \frac{1}{\sqrt{N}}\mathbf{U}\mathbf{A}^{*}(\mathbf{\Lambda}^{*})^{-0.5} \tag{5}$$

5. Project the spatial modes in **Φ** onto the ensemble **U** to obtain the time-dependent temporal POD modes:

$$\mathbf{T} = \mathbf{U}^{T}\mathbf{\Phi} \tag{6}$$

The total energy $k_{mc,sum}$ contained in the 2D spatial domain assembled from the mean-contained (*mc*) velocity components is a function of the eigenvalues in $\mathbf{\Lambda}^*$ as follows:

$$k_{mc,sum} = \mathrm{tr}\left(\frac{1}{2}\mathbf{\Lambda}^{*}\right) = \frac{1}{2}\sum_{e=1}^{N}\lambda_e \tag{7}$$

with '*tr*' depicting the trace operator of a matrix. If the velocity fields used for the construction of **U** are mean-free, then the total energy translates into the turbulent energy $k_{mc,sum} = k_{sum}$.

LORs are obtained by truncating the POD series at a certain mode number r. In this paper, the resultant reduced-order reconstruction of the *i*'th snapshot is called a rank r approximation of the original instantaneous velocity field $\vec{U}_i$. The mathematical relationship that represents the reconstruction of the instantaneous velocity field *i* of the measured ensemble with a rank *r* approximation can be expressed as:

$$\mathbf{U}_{i,r} = \sum_{e=1}^{r}\mathbf{\Phi}_e\mathbf{T}_{ie} \tag{8}$$

with the index 'e' in $\mathbf{\Phi}_e$ depicting the e'th column of **Φ** and index 'ie' in $\mathbf{T}_{ie}$ representing the row-column relationship in **T**.

Finally, the total energy $k_{mc,r}$ (for mean-free velocities, the energy k_r) contained in a rank r reconstructed ensemble of N snapshots is given by:

$$k_{mc,r} = \frac{1}{2}\sum_{e=1}^{r}\lambda_e \tag{9}$$

4. Results and discussion

The time-averaged axial velocity field (N = 1024 samples) in the range of $-400 < x^* < 400$ mm in the horizontal (span wise) direction and $4600 < y^* < 5900$ mm in the vertical (axial) direction is presented in Fig. 6 together with the corresponding uncertainty field. For each statistical quantity, error propagation was used to calculate the corresponding uncertainty with a confidence limit of 3σ (99.1 %) by using the so-called effective number of samples, see Fig. 2. For example, the calculated uncertainty ϵ for the mean axial velocity $\overline{V}$reads as $\overline{V} \pm \epsilon$, which yields $\overline{V} = 1.46 \pm 0.024$ m/s at location $(x^*, y^* = 0, 5200)$. Since the details of the error calculation are beyond the scope of this article, the interested reader is referred to [54].

With the tube exit located at an elevation of $y^* = 4000$ mm (Fig. 1), we cover the non-dimensional downstream distances from 5.5d to 17.4d for the jet past the tube exit. An overview of the different phenomena and the physics in turbulent jets can be found in [56] and a more recent

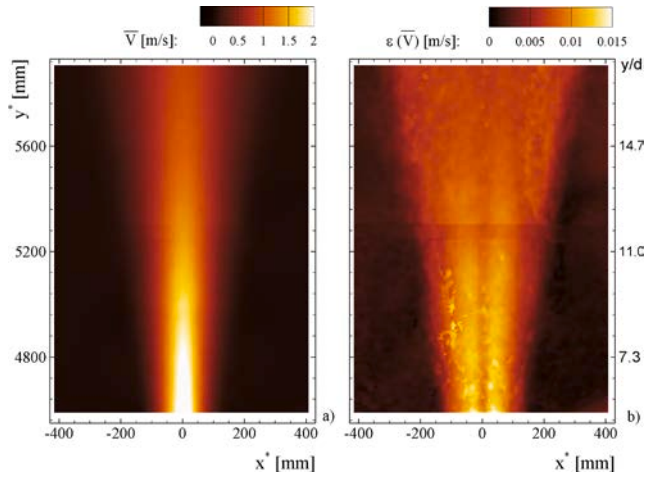

Fig. 6. Time-averaged axial velocity field $\overline{V}$ for experimental series H2P1_16_S03 a) with respect to the coordinate system x^*, y^* and b) the corresponding error ϵ on a significance level of 3σ (99.1%). The error calculation is based on [54].

review of experimental data is provided in [40].

4.1. Self-similarity

In order to discuss preservation of self-similarity in the LORs, self-similarity it must first be examined and derived for the original velocity fields.

4.1.1. Mean axial velocity

The self-similarity concept for the jet requires that physical quantities when appropriately normalized with a local characteristic transverse length scale – the half-width radius of the jet, $r_{0.5}$ – and a local characteristic velocity scale – the peak value V_p – collapse onto each other. The axial velocity profiles as well as other first and second order velocity moments show shape invariance with respect to downstream distance. For more details of self-similarity in the context of jet flows, refer to [39,40]. A more general discussion of the underlying dimensional analysis for physical processes can be found in [57]. It is agreed upon that the axial velocities can be well-approximated by a Gaussian function. Additionally we account for a non-zero offset V_g of the axial velocities and a deflection x_c of the jet out of the injection tube axis (see Fig. 7). This results in the following fit function to the experimental data:

$$\overline{V} = \overline{V}_g + \overline{V}_p \cdot \exp\left\{ -\ln\left(2\right)\left(\frac{x^* - x_c}{r_{0.5}}\right)^2 \right\} \tag{10}$$

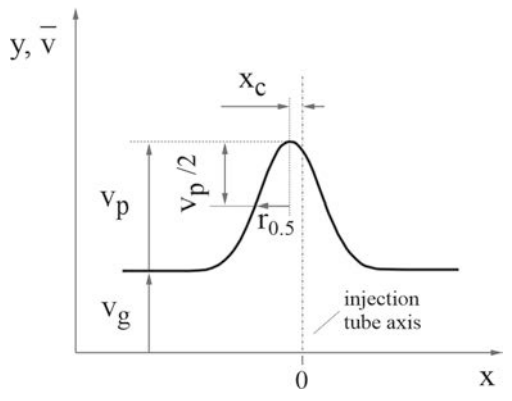

Fig. 7. Parameters for the fit function according Eq. (10).

or in non-dimensional form:

$$\eta = \exp\{ -\ln(2)\cdot\xi^2 \} \tag{11}$$

with the non-dimensionalized axial velocity $\eta = (V - V_g)/V_p$ and the non-dimensionalized transversal coordinate $\xi = (x^* - x_c)/r_{0.5}$ representing the new framework for the self-similarity presentation of the measurements. Extracting horizontal profiles of the axial velocity V from Fig. 6 at different downstream distances y/d results in the non-dimensional representation of the axial velocities according Eq. (11) as shown in Fig. 8.

Almost right from the beginning of our data ($y/d = 5.8$), i.e. just after the potential core of the jet, which is expected to persist up to $y/d \approx 5$ [39], the data points collapse identically onto the Gaussian function depicted in green, thus confirming the self-similarity assumption for the jet. The only minor deviation from the Gaussian fit is found around the jet center ($\xi = 0$). To better describe this decay, additional profiles are extracted from Fig. 6 and the non-dimensional velocity decay in the center of the jet ($\xi = 0$) is presented as a function of downstream distance y/d in Fig. 8 (b). It is shown that the axial velocity approaches the asymptotic value with increasing y/d. To test for the consistency with the literature we provide the results of the measurements from [22] which were recorded much further downstream ($10 \leqslant y/d \leq 100$) compared with our results in Fig. 8 (c). It is found that i) the hot wire (HW) data from [22] almost identically fall onto the Gaussian, ii) our data extracted at $y/d = 16.33$ – except for the jet core – fall onto the Gaussian and ii) there are some deviations between the HW- and the laser Doppler Anemometry (LDA) data. The discussion of the latter is beyond the scope of this article. The development of the four fit parameters $V_g, V_p, r_{0.5}$ and x_c according eq. (10) with non-dimensional downstream distance y/d is presented in Fig. 9. The behavior of the baseline offset $V_g = 0.031 \pm 0.01$ [m/s] and the center-line offset $x_c = -0.73 \pm 1.7$ [mm] as seen in Fig. 9 (a) and (d), respectively, depict a variation with downstream distance that is at least two orders of magnitude lower than that of the velocity amplitude V_p and the jet width $r_{0.5}$. Even though $V_g > 0$ signifies a weak re-circulation surrounding the jet, it is plausible to deem this variation negligible so that the similarity variables η and ξ can be reduced to the common definitions used in literature [58]. It is noteworthy to mention that both the axial velocity V_p in the center and the half-width radius $r_{0.5}$ exhibit a transitional region from the potential core ($y/d \approx 5$) to $y/d \approx 10$. This is observed by two factors – the slightly different slope for the growth of the jet (characterized by $r_{0.5}$) beyond $y/d > 10$, and in a change in the decay characteristic for V_p (see Fig. 9 b). Based on these observations, we consider our own experimental results for the axial mean velocity self-similar past $y/d > 10$.

The variation of the jet width $r_{0.5}$ with downstream distance shown in Fig. 9 c) provides insight into the jet spreading rate β as defined in [58]. Our value of $\beta = 0.090$ falls in between what is provided through the literature, e.g. 0.086 by [23], 0.094 by [22] based on LDA measurements, 0.096 in [21] and 0.102 in [22] based on HW measurements. This seems to indicate that the confinement of the PANDA vessel [47] – confinement ratio D : d of 36.53, which is much lower than those of the facilities used by [22] – 192 and ≈ 697, respectively – plays no prominent role. Although all the above mentioned experiments were conducted at different Reynolds numbers, there is no evidence to suggest that the Reynolds number affects the mean velocity profiles or the jet spreading rate [58]; in contrast to the tube exit conditions [59]. In the present study, the normalized axial velocity in the center V_p/V_0 with V_0 representing the velocity at the tube exit was found to decay with downstream distance at a rate of 6.204, which fits well with the literature value of 6 [39] obtained from theoretical considerations and experimental results of [60]. The velocity at the tube exit V_0 was measured by means of PIV for the present set of experimental conditions. The results are not presented for brevity. When scaled logarithmically on both axes, the normalized axial velocity in the center V_p/V_0 decays in

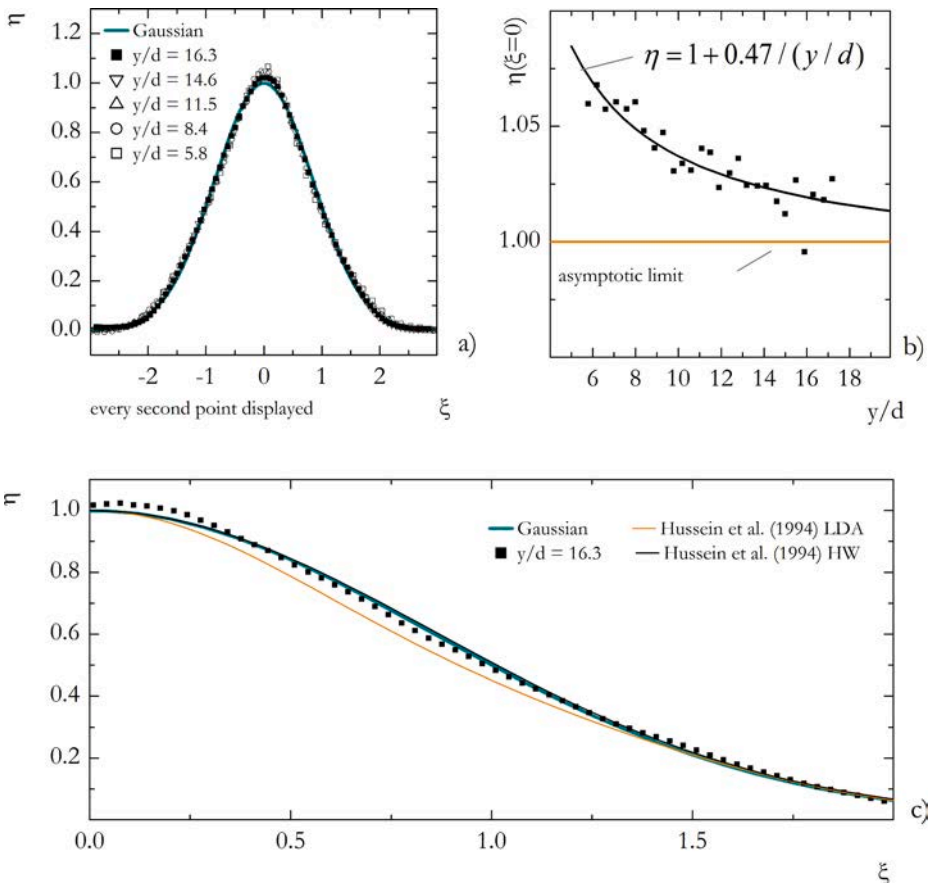

Fig. 8. Axial velocity profiles extracted from Fig. 6 at different downstream distances y/d (a). Downstream decay of the non-dimensional axial velocity η in the jet axis ($\xi = 0$) towards the asymptotic value of $\eta = 1$ (b). Comparison of the present results (■) extracted at $y/d = 16.3$ with the Gaussian and experimental data from [22] obtained through laser Doppler Anemometry (LDA) and hot-wire (HW) measurements (c).

proportion to $(y/d)^{-1}$ in the $y/d > 10$ regime. This was also observed by [39].

Different velocity moments can reach the state of self-similarity at different downstream distances. However, there is no consensus on the definition of these distances, see the discussion of this topic in [40] and the alternate approaches relating the route towards self-similarity to the coherence of the flow at the tube exit as initially outlined in [61] and as applied in the concept of '*number of eddies overturned in time*' in [59]. As an example, the normalized profiles of the axial RMS-values are presented for different downstream distances in Fig. 10 (left). For a measure of reference, the corresponding LDA and HW data of [22] are also plotted alongside. It is found that the development towards self-similarity of the axial RMS-values is much slower compared to the mean axial velocities, Fig. 10 (right). However, there is good agreement with the axial RMS-values obtained by [22] and the values at $y/d = 16.3$ of the present study. On the other hand, the development towards self-similarity is even slower for the radial RMS-values u'. Nevertheless, there is still reasonable agreement at further downstream locations. Consequently, the signals obtained at $y/d = 16.3$ are used for further analysis of the first and second order velocity moments.

4.2. Results of the POD analysis

4.2.1. Mode energy

The snapshot POD as outlined in Section 3 was applied to the entire PIV ensemble (N = 1024) of mean-free velocities pertaining to the H2P1_16_S03 test, i.e. the axial mean velocities (Fig. 6) as well as the radial mean velocities (not shown) were subtracted from all the instantaneous velocity fields before applying the algorithm to obtain the energy distributions among the spatial modes. Eqs. (9) and (9) are applied to study the distribution of these energies and their accumulation with increasing rank order reconstructions, see Fig. 11. The first mode carries the highest proportion of energy compared with the other modes (~3% of the total system energy k_{sum}).

In total, the energies distribute across nearly three orders of magnitude from mode 1 to mode 1024. For the mode energies, we observe a distinct slope change around mode ≈ 10, i.e. we find modal energies within the same order of magnitude for $mn \lesssim 10$ whereas the energies for $mn \gtrsim 15$ decay more rapidly. The former region is attributed to the importance these modes have for the reconstruction. This and the extent of this region is further expanded on in the next Section 4.2.2. Without claiming generality and independence of the underlying flow type, we observe that the energy across modes 15 to 200 scale inversely proportional with the mode number for our data. The cumulative distribution reads as follows: reconstruction of the instantaneous – mean free – velocity fields in terms of a lower dimensional representation contains on average 2.9% of k_r for a rank 1, 12.9% of k_r for a rank 5, 22.1% of k_r for rank 10 and 50% of k_r for rank 50, respectively. Note that a full reconstruction of the instantaneous velocity field would require a rank 1024 reconstruction. An example for the reconstruction of an instantaneous velocity field with different rank approximations is discussed in the Section 4.2.3.

4.2.2. A small step beyond usual POD mode selection criteria

We briefly present some characteristics of the spatial and temporal POD modes to make a link to corresponding observations in the literature while attempting to highlighting a possible blind spot related to the sole focus of the first few – the most energy containing – POD modes as

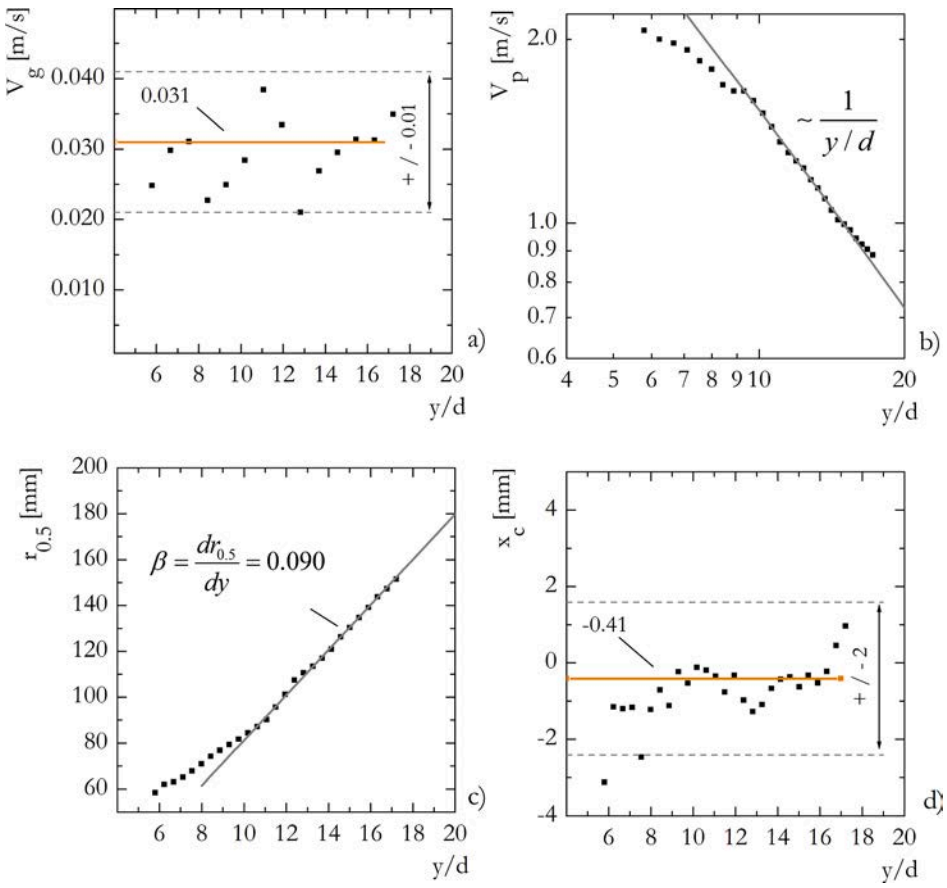

Fig. 9. Development of the four fit parameters $V_g, V_p, r_{0.5}$ and x_c according Eq. (10) with non-dimensional downstream distance y/d .

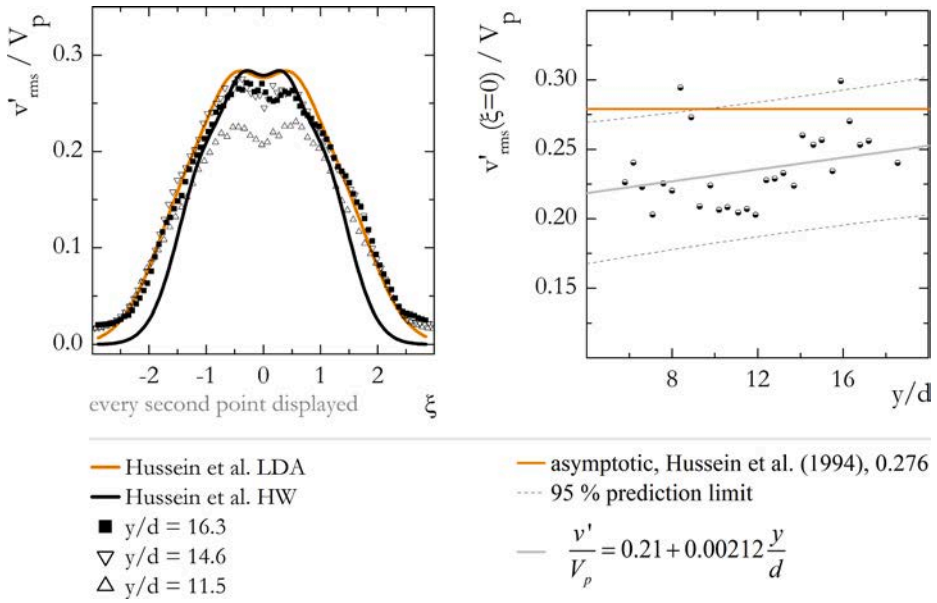

Fig. 10. Normalized axial velocity RMS-values v'_{rms}/V_p with different downstream distances y/d as parameter (left). Comparison of the present results with data from [22]. Downstream increase of the velocity RMS-value in the jet axis ($\xi = 0$) towards the asymptotic value of 0.28 (right).

found in [62,63].

Although not directly apparent from the energies (Fig. 11), the spatial structures of the first two spatial modes, Φ_1 and Φ_2, are almost identical showing the presence of 3 successive vortical structures downstream of $y/d \approx 8$ which are centered around $\xi \approx 0$, except that they experience an average spatial phase shift with $y/d \approx 1.15$ – or multiples of it, Fig. 12 top. This is remarkable since this relation is usually solely attributed to so called (spatial) mode pairs [7,64], i.e. successive spatial modes having almost the same energy as well as distinct phase relationships between their temporal modes (and

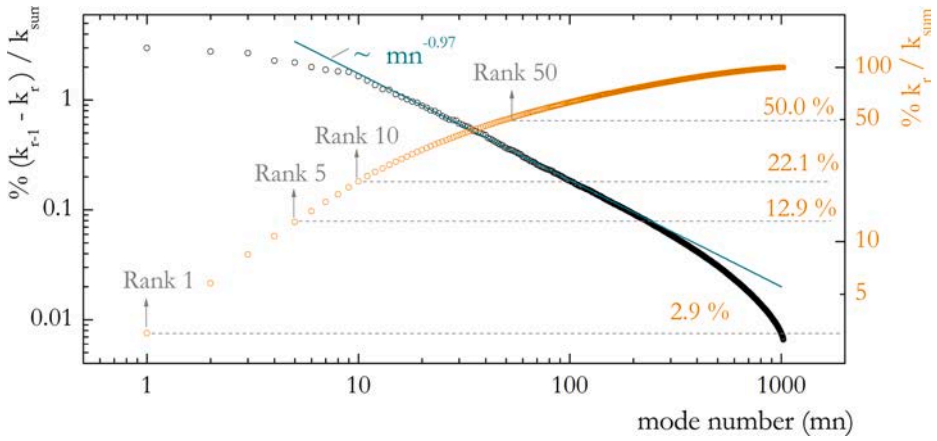

Fig. 11. Distribution of the energy represented by the eigenvalues, λ_e, according Eq. (9) across the different POD modes 1 to 1024 (left axis) and cumulative energy k_r (right axis), according (Eq. (7) presented in %. Ranks 1, 5, 10 and 50 and their associated cumulative k_r-values are indicated. All axes are log-scaled.

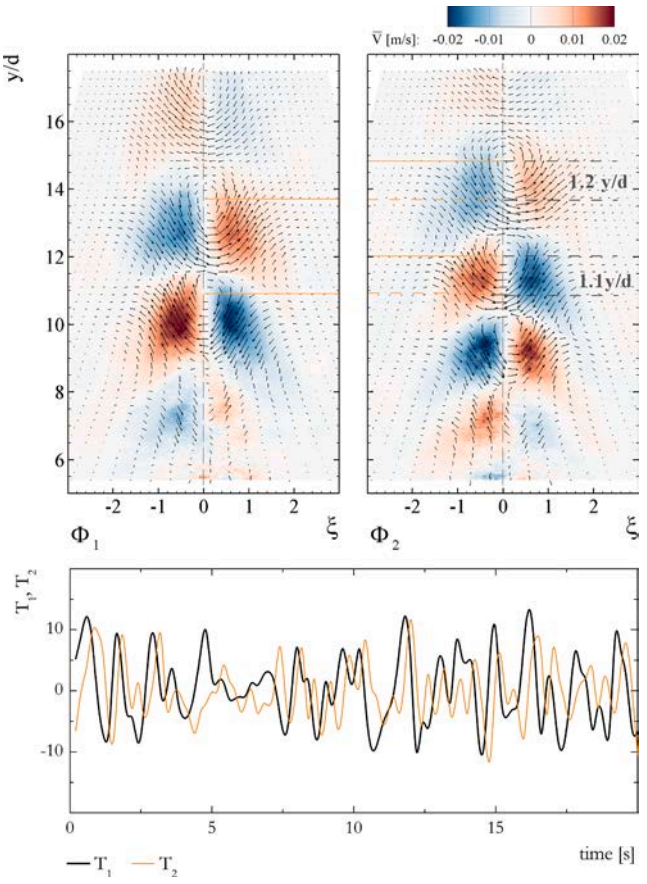

Fig. 12. Average velocities $\overline{V}$ as depicted by the first two spatial POD modes, Φ_1 and Φ_2, presented in non-dimensional coordinates ξ and y/d (top) and the corresponding temporal modes, T_1 and T_2 (bottom) with a B-spline applied to smooth out noise.

fulfilling – eventually – additional criteria [7]) which does not manifest in the present experiments (Fig. 11). The distinct (and more defined) phase relation between the spatial modes is also revealed by the corresponding temporal modes, T_1 and T_2, Fig. 12 bottom which are shown for the first 20 s. After applying a spline function to smooth out the noisy signals, it becomes apparent that the temporal modes – most prominently visible for most (but not all) of the peaks – are shifted in time by one time step t = 0.2 s which corresponds directly to the underlying sampling frequency of $f = 5$ Hz. The above mentioned spatial phase relationship of the vortices must amount to $y/d \approx 2{\cdot}1.15 = 2.3$ since a vortex travels (on average) with a velocity of 1.3 m/s (Fig. 9, $y/d \approx 10$); this corresponds to a distance of 260 mm or $y/d = 2.4$ between successive snapshots.*Cum grano salis,* this corresponds to the observations made in [30] for an experiment conducted at a much higher sampling frequency of 1.5 kHz.

To shed further light on the impact of successive temporal (and therefore also the corresponding spatial) POD modes and their importance for the (rank truncated) calculation of the flow representation, we have calculated the normalized cross-correlation coefficients between successive temporal modes. This idea is based on the observation of so called POD mode pairs, i.e. modes '*that contain different phases for the same or similar spatial structures*' as outlined for example in [64] where a mild turbulent jet in a laminar cross flow is treated. This phase shift is also reflected in the corresponding temporal modes as depicted in [64]. Since it is not expected to find such a 'clean' signal for fully turbulent flows, we have generalized (and relaxed) this concept towards a cross-correlation criterion which quantifies the similarity of successive temporal modes T_{mn} and T_{mn+1}, which is even capable of detecting intermittency. The cross-correlation is calculated according:

$$\rho_{T_{mn},T_{mn+1}}\big|_{max} = \frac{1}{N-1}\sum_{i=1}^{N}\left(\frac{T_{mn,i}-\mu_{mn}}{\sigma_{mn}}\right)\left(\frac{T_{mn+1,i}-\mu_{mn+1}}{\sigma_{mn+1}}\right) \tag{12}$$

where μ_{mn} and σ_{mn} are the mean and standard deviation of the temporal mode mn, respectively; and μ_{mn+1} and σ_{mn+1} are those of the temporal mode mn + 1, see [53] and Fig. 13. Applying Eq. (12) to successive temporal modes, the cross-correlation analysis indicates that the maximum correlations consistently occur at lag = 1 time step; similar to what was found in Fig. 12 for modes 1 and 2.

Furthermore, the upmost importance of the – low order – temporal modes along with the associated spatial modes to represent the underlying large-scale flow dynamics is confirmed by the accordingly higher values of $\max(\rho_{T_{mn},T_{mn+1}})$ between successive time traces for T_{mn} with $1 \leqslant mn \leq 5$. The attribution towards the importance of these first spatial modes within the literature [18,35–37] is proven by the strong correlation decay within this range represented by the approximation shown with a curve fit (—). Conversely, there is considerable contribution towards the flow physics represented by temporal modes T_{mn} with $6 \leqslant mn \leq 21$, see the corresponding discussion in Hamilton et al. [9,17]. While these modes may represent a lower amount of turbulent energy, they should not be neglected since the corresponding successive temporal mode correlations are consistently above a pure noise level of 0.15. It should be noted that even though not necessarily representative for all flows, it is remarkable that i) we find a strong correlation of 0.5 between temporal modes T_{20} and T_{21} which ii) is associated with a

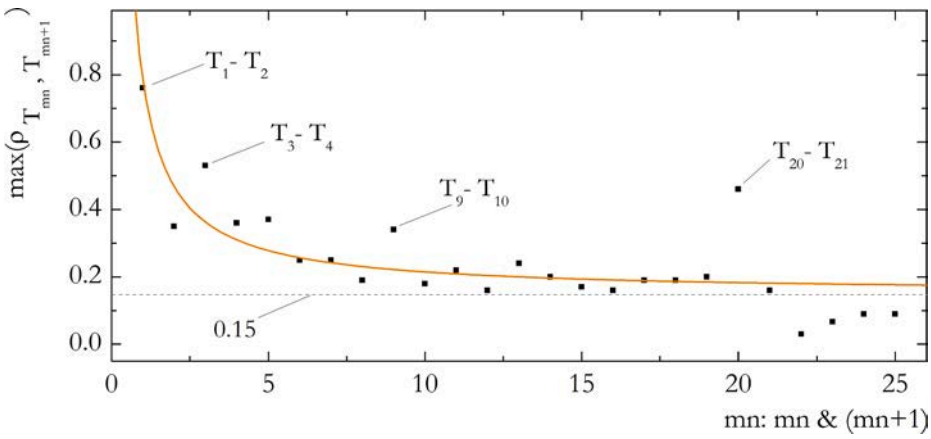

Fig. 13. Normalized maximum cross correlation coefficients $\max(\rho_{T_{mn},T_{mn+1}})$ according Eq. (12) calculated for time traces of successive temporal modes T_{mn}&T_{mn+1} from the POD calculation as a function of the respective mode number mn.

corresponding coherence for the spatial modes, see Fig. 14; while modes beyond 5 are usually neglected in the context of POD based approximations [30,64,62,63]. For Φ_{20} and Φ_{21} we find the same spatial phase relation of $y/d \approx 1.15$ for vortices located past $y/d \approx 10$ as was observed for modes 1 and 2 in Fig. 12. In contrast to Φ_1 and Φ_2 (Fig. 12) the vortices in Fig. 14 experience a left and right offset of $\xi \approx \pm 0.5$ with respect to the center line. The corresponding temporal modes T_{20} and T_{21} are shown in Fig. 14 bottom along with T_{21} lag-shifted. Additionally, it is interesting to note that we observe different phases for the time traces of the temporal modes T_{20} and T_{21}. That is, we find phases with a stronger correlation and phases with a weaker correlation (Fig. 14 bottom) which results on average in a cross correlation of 0.5 – calculated for the entire signals, Fig. 13. These distinct differing time-period-dependent phases are in contrast to successive temporal modes where the cross correlation is consistently constant – irrespective of the time period selected as found in Fig. 12 (bottom). Even though leaving this topic finally as a subject for a more detailed analysis which has to be applied for different flows and without trying to be exhaustive, we briefly note that the former observation is what is typically depicted by the wording 'intermittency'. For example, this intermittency is frequently found for turbulent round jets released through a circular orifice in the region where the tails of the axial velocities meet the stagnant surrounding [65,66]. A theoretical framework for these intermittent transitional phenomena can be found in [67] and an more extended view towards the intermittent transition in the outer parts of a jet flow towards turbulence through Hopf-Bifurcations in [68].

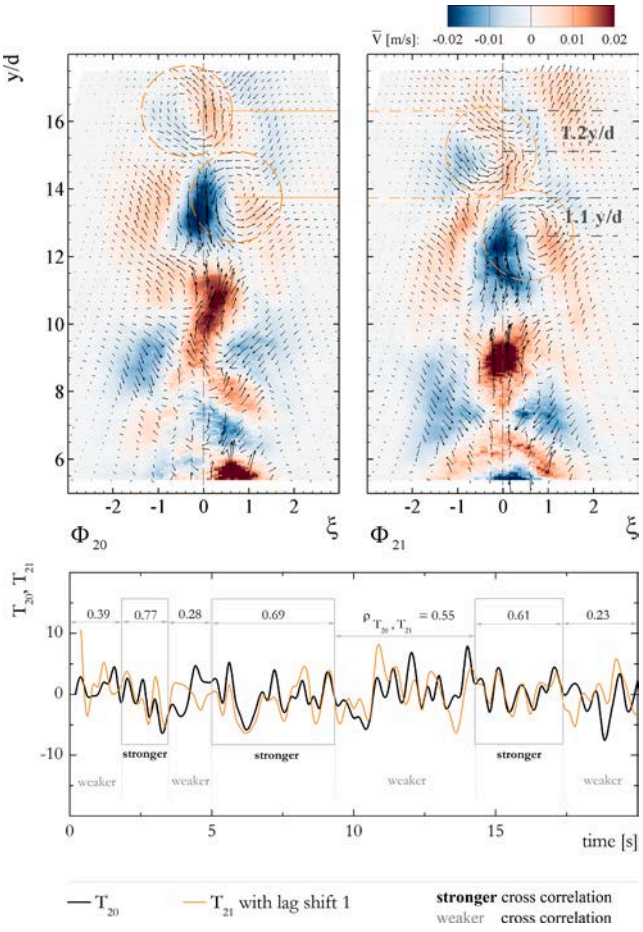

Fig. 14. Average velocity $\overline{V}$ as represented by the spatial POD modes, Φ_{20} and Φ_{21}, presented in non-dimensional coordinates ξ and y/d (top) and the corresponding temporal modes, T_{20} and T_{21} (bottom) with a B-spline applied to smooth out noise. Temporal mode T_{21} is presented with a lag shift of 1 with respect to temporal mode T_{20}. Additionally, the normalized cross-correlation coefficients $\rho_{T_{20},T_{21}}$ between T_{20} and T_{21} are indicated for selected time periods to quantify phases with higher and lower cross-correlation strengths.

The suggested criterion based on the maximized cross-correlation between successive temporal modes of a POD calculation help to identify dynamically relevant modes in a more quantitative way considering temporal and corresponding spatial coherence. Specifically, this approach paves the path to move away from the traditionally strict energy-based criterion provided by the POD to determine dominant modes, and attempts to further constrain the criterion to include – space and time correlated – phase information between successive modes. If this perspective is adopted, it might help to provide a sound criteria for the required rank approximation to represent the flow physics for subsequent – simplified – modeling approaches as found for example in [9] while highlighting the transition and intermittency towards non-coherent contributions to the flow physics past a certain POD mode. Within this context it is noted that this method preserves the energy-based ranking system that the POD provides while directly exploiting phase relationships that may exist between successive modes through insight gained from cross-correlations. This is a more explicit method compared to the eigenvalue-(energy-) based observations found in literature [30,64].

4.2.3. *Velocity field reconstructions*

The reconstruction according to Eq. (8) with the *mean-contained* data was used to calculate LORs with rank 1, 5, 10 and 50 approximations for all $N = 1024$ instantaneous velocity fields of the underlying original measurement series. An example of the reconstruction for $i = 15$ of a

single instantaneous velocity field is presented in Fig. 15. Following the discussion of the distribution of the energy k_r among the ranks (Fig. 11), the LOR approximations up to rank 5 show energetic flow features with large-scale structures without any details, i.e. a slightly meandering, expanding jet flow. This behavior is exactly what was intended by applying the POD to construct a LOR: highlighting large-scale dominant flow structures that might be otherwise covered by small scale turbulent 'noise'. Increasing the rank number successively adds more small-scale details to the flow up to the level of the full reconstruction (N = 1024), which is identical to the corresponding original measurement. Note that i) the meandering (space) or flapping (time) of the jet is visible for ranks up to 10 but it is hardly detectable in the original flow pattern and ii) that the full reconstruction of the instantaneous velocity field (rank = 1024, original) even shows the small areas in the center of the jet with missing velocity content (black spots – some of which are marked with A in Fig. 15) resulting from the post-processing to remove spurious vectors [51]. The latter observation is notable since all the underlying POD modes used for the reconstruction present a continuous full field without blank spots.

4.3. Preservation of self-similarity in the LORs

4.3.1. First order velocity moments

In this section, self-similarity in LORs from POD-rank truncations the first 1, 5, 10 and 50 modes are addressed for the first order velocity moments. For each rank approximation, we calculate the common respective statistical values (average axial mean velocity and RMS-value) through time averaging across all 1024 snapshots as if these approximations would be the primary measurements. The discussion will consider profiles extracted from these LORs as well as downstream traces of these quantities in the jet axis. For the discussion, one has to distinguish two key questions: 1.) How well do the statistical quantities derived from a LOR represent the original data? 2.) Is self-similarity preserved in the LORs?

The mean axial velocities of the original and ranks $1, 5, 10$ and 50 signals from the – mean contained (mc) – snapshots extracted at $y/d = 16.3$ are presented in Fig. 16 a. The results collapse almost perfectly onto each other and only the enlarged inset shows the small differences among the rank approximations. The average standard deviation of the rank approximations and the original signal is 0.0352. This value is small enough to conclude that the rank approximations preserve similarity (and are essentially identical) in the resultant mean velocities (rank 0) of the jet down to numerical noise irrespective of the rank truncation.

We draw four interesting observations with the axial RMS velocity v' distributions (Fig. 16 b). Firstly, all five rank approximations have a similar M-type shape – which is not observed for the transverse velocity RMS values, Fig. 16 c). Secondly, a left–right asymmetry that is present in the magnitude of the side peaks (marks A and C) for low-rank approximations (rank 5 and 10) vanishes for the higher rank approximation (rank 50). Thirdly, this (weak) M-shape is also present in the results from [22] based on experiments conducted farther downstream ($10 \leqslant y/d \leq 100$) compared with the present results. Lastly, the RMS-content increase on average with increasing rank order even though there are some local fluctuations for lower order ranks. This is because the POD acts as a spatio-temporal filter to remove low-energetic turbulent fluctuations manifesting as small-scale flow structures that do not contribute to the large-scale dynamics (see also Figs. 15 and 11).

In contrast to the transverse velocity RMS-values, there is a pronounced RMS-dip in the center line of the axial velocity signals of ranks 5 and 10, Fig. 16 b), mark B. This RMS-dip then relaxes with increasing rank order, eventually becoming difficult to notice in the original signal. The accentuation of the RMS-deficit in the LORs – particularly in ranks 5 and 10 – and the flattening of the profile with increasing rank are noteworthy. The dip in axial RMS velocities corresponds to a reduction in the degree of turbulence, which translates into the removal of – small-scale – fluctuations. Referring back again to Fig. 16 b), a more pronounced dip in the center-line in ranks 5 and 10 implies the removal of low-energetic small scale structures in the core of the jet. Conversely, the flattening of this dip with increasing rank order means that there exists in the original jet highly turbulent low-energy containing flow structures that are filtered out in low-order truncations of the POD; and the introduction of more small-scale turbulence in the jet core with increasing rank adds energy, resulting in this dip to become less pronounced. From another perspective, it can be argued that the M-shape is mainly contained in and caused by intermediate modes in the range of approximately 5 to 10 (and eventually a bit above 10) because the respective LORs have the most pronounced modulation between the side peaks and the RMS-dip in the center, Fig. 16 b). This finding is consistent with results of the POD analysis of a turbulent wake flow past a wind turbine array presented in [17,9] with just using a few POD modes representing the essence of the turbulence of the flow.

To further highlight the development of the axial velocity RMS-deficit with downstream distance y/d, the results from the rank 5 and rank 50 approximations are presented in Fig. 18. The purpose of these graphs is not to identify a single profile but to demonstrate that the convergence towards an asymptotic value can be: a) highly dependent on radial position and, b) different for each rank approximation. For example, the rank 5 center line immediately reaches its asymptotic value at $y/d = 5.7$ (Fig. 18 a, mark B) - much quicker than the higher order ranks of $10, 50$ and the original.

On the other hand, we find a considerable variation at positions marked A and C. Additionally, it is interesting to note that the pronounced deficit in the center-line of the rank 5 RMS-values persists for nearly all downstream distances. To better quantify the downstream development of the two peaks (A and C) and the RMS-deficit (B), the

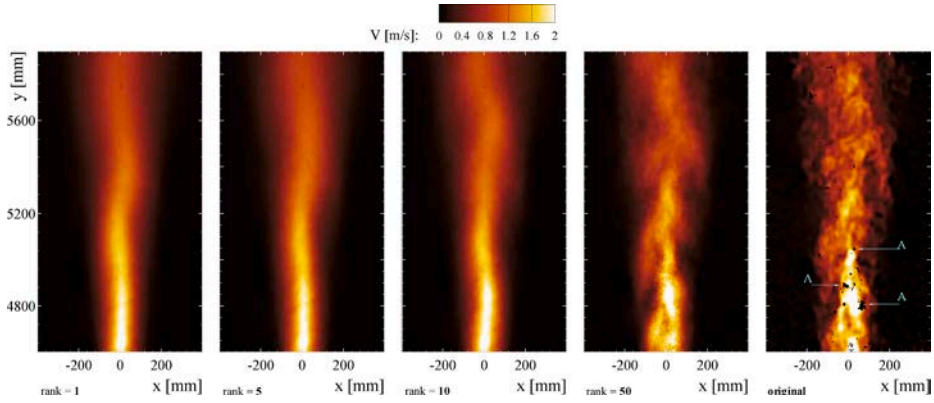

Fig. 15. Reconstructions of an instantaneous velocity field using the first 1, 5, 10, 50, and finally 1024 (original field) POD modes for the velocity field i = 15, respectively. The color coding represents the axial velocity V. The results are shown from left to right with increasing ranks to construct the LORs.

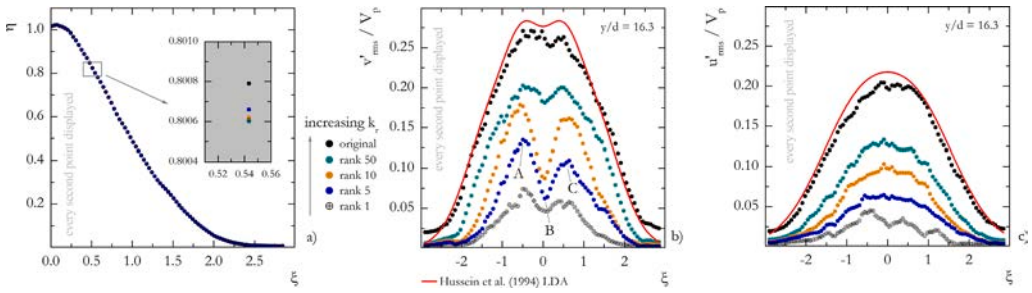

Fig. 16. Comparison of the mean axial velocity distribution among the LORs at $y/d = 16.3$. Inset: Enlarged view of the negligible difference in mean axial velocities between the ranks (a). Comparison of normalized axial (b) and transverse (c) RMS velocity distributions with LORs at y/d = 16.3. Additionally, our own results are compared with data taken from [22] which are considered as asymptotic values.

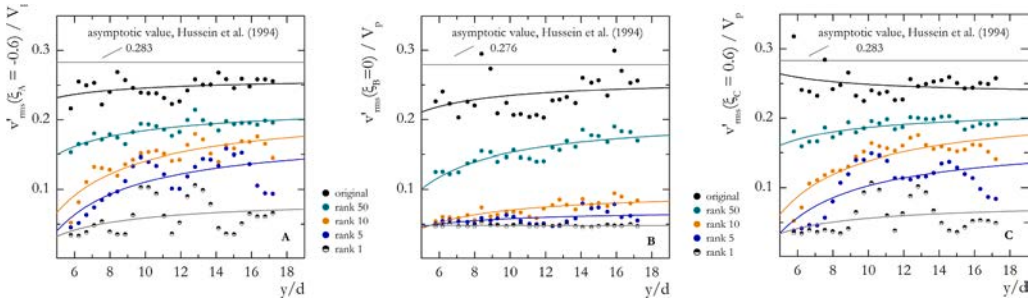

Fig. 17. Comparison of left peak development (A), the RMS-dip development (B) and the right peak development (C) in the axial RMS velocity distributions of the LORs as a function of the downstream distance with the original value as well as the asymptotic values according [22] as reference.

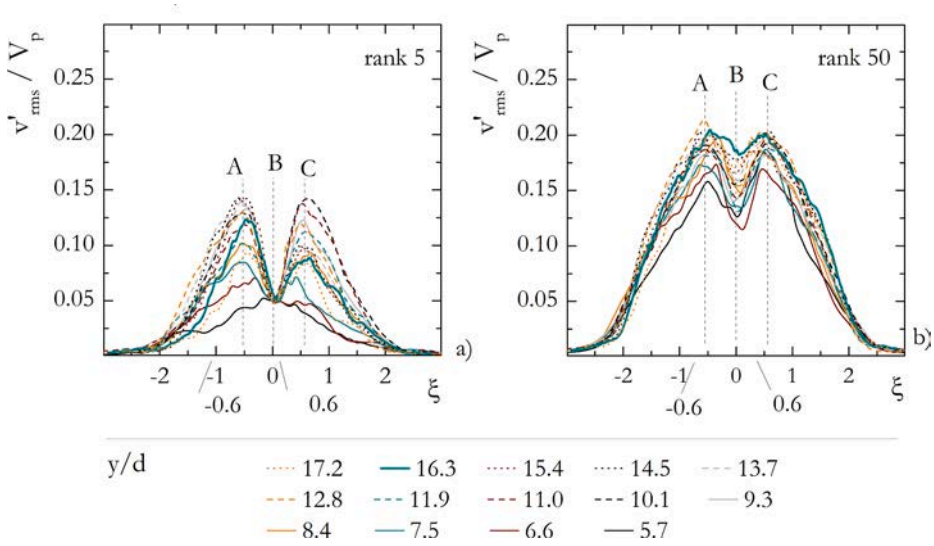

Fig. 18. Rank 5 (a) and rank 50 (b) based approximations of the normalized axial RMS velocity distributions v'_{rms} with the non-dimensional downstream distance y/d as parameter.

respective signals were extracted for all ranks considered (see Fig. 17).

We find negligible variation in the rank 1 and rank 5 axial RMS curves velocities along the center line, whereas the left and right side peaks initially grow and appear to stabilize further downstream (see Fig. 17). The rank 10 center line signal (B) slightly increases, whereas the characteristics of the rank 50 signal (B) correspond to the original one. That is, both tend to approach an asymptotic value even though: a) the asymptotic value is different and, b) a converged value is not yet attained for the downstream distances considered here. For the left peak signals (A), all curves gradually rise at the beginning before they stabilize (see Fig. 17 A). The rank 1 signal converges quicker than the other four signals. The right peak signals show similar behavior, with the rank 1 velocities stabilizing before the other signals, Fig. 17 c. Overall, we found strong indications that even the first order velocity moments of LORs derived from jet flow, exhibit a transition to asymptotic values considering that these absolute values are lower compared with the original data.

4.3.2. *Second order velocity moments*

We restrict the discussion for the second order velocity moments to the Reynolds shear stress $R_{u'v'}$ and the turbulent kinetic energy k. The Reynolds normal stresses and the discussion of the results are (in principle) accessible through the axial and transverse velocity RMS values, see Fig. 16. Since the third velocity component W is not available

through the 2D PIV approach, k is calculated according to:

$$k = \frac{1}{2}\{2u'^2_{rms} + v'^2_{rms}\} \quad (13)$$

This is because it is more reasonable to assume that $w'^2_{rms} = u'^2_{rms}$ for an axisymmetric jet flow as opposed to the generic approach $w'^2_{rms} = \frac{1}{2}(u'^2_{rms} + v'^2_{rms})$. This is confirmed by the results found in [22]. The results on the distribution of $R_{u'v'}$ and k among the LORs at $y/d = 16.3$ are presented in Fig. 19. For the Reynolds shear stress $R_{u'v'}$ we find a remarkable shape invariance, i.e. beginning with the lowest rank approximation of 1, the characteristic shape signature is already present and only differentiates slightly with increasing ranks. This is in contrast to the findings for the axial velocity RMS-values (Fig. 16 b) where we noted a distinct velocity dip in the jet axis ($\xi = 0$), which is gradually filled up with increasing rank approximations, but is never fully filled. This remaining small dip persists much further downstream as shown with the reference data from [22] .

This leads to the conclusion that the shape of $R_{u'v'}$ is mainly controlled by the large-scale structures that dominate the low-rank approximations. Note that this holds true up to the full reconstruction which corresponds to the original signal. That is, the characteristic shape is introduced from the inclusion of the very first POD mode where the first mode represent the largest and most energetically dominant flow structures (Fig. 19 a). The addition of modes (energy) accentuates the magnitude of the side peaks in the $R_{u'v'}$ signals while preserving their shape. This suggests that (i) it is the energetically dominant large-scale structures that drive the shear stress of the flow and (ii) further addition of energy (and smaller scale turbulence) does not contribute to the overall shape but only to local accentuation of the side peaks. This finding is in distinct contrast to the discussion of the axial RMS velocity distributions (Fig. 18) where we found that smaller scale turbulence considerably alters the velocity deficit in the center line. Finally, the original data (•) are in excellent agreement with the reference data from [22] indicating readily attained self-similar behavior for $R_{u'v'}$ for $y/d = 16.3$ past the tube exit. Since the main characteristics of the axial velocity RMS values are incorporated, to a certain extent, in *k* through the application of Eq. (13) it is not surprising to find a corresponding distinct *k* deficit in the jet axis for intermediate rank approximations (5 and 10) as well (Fig. 19 b). But in contrast to the axial velocity RMS distribution, this deficit is already almost filled up in the rank 50 approximation which shows – except for the magnitude – the characteristic shape of either our original data or the reference curve from [22]. That is, smaller scale turbulence – present in higher rank approximations – alters the shape for the k distributions in the core of the jet considerably up to an extent that the velocity deficit is hardly visible. For the peak value of k we miss approximately 13% compared with the reference which is another indication that the self-similar region is not yet fully attained. An observation which is supported by Fig. 21 which presents the corresponding values for k at location $\xi_B = 0$ as a function of downstream distance. Similar to v' (Fig. 17) all the rank approximations for k experience a transition towards an asymptotic value with downstream distance. This is a strong indication that the route to self similarity is mainly dominated by large-scale vortices and to a lesser extent by smaller scale turbulence.

5. Conclusions

Jet experiments were conducted in the large-scale PANDA facility at the Paul Scherrer Institute, Switzerland. The velocity fields of an air-helium jet with Re ≈ 15400 were studied with 2D PIV in the axis of the jet covering downstream distances from 5.5d to 17.4d, with d = 109.1 mm being the inner diameter of the jet emerging tube. The focus of the investigation was self-similarity behavior of first and second order statistical quantities of the velocity field based on a) the original data and b) using low-order representations (LORs) derived from a Proper Orthogonal Decomposition (POD) of the original ensemble. We attempted to answer two central questions: 1) To what extent do the LORs preserve self-similarity? 2) Can the LORs reconstruct the underlying turbulence that is controlled by the flow structures?

It is consistently found that all statistical properties obtained through the LORs a) mimic in shape the asymptotic outline of the original data even for low order truncations and b) that the maximum values (for a given LOR) approach asymptotic states with downstream distances. This is a strong indication that i) self similar behavior is equally found in the LORs and ii) that the self-similarity is mainly embedded in and controlled by the large-scale vortices. The sole exception is the axial velocity RMS values where we found a distinct dip in the jet center line

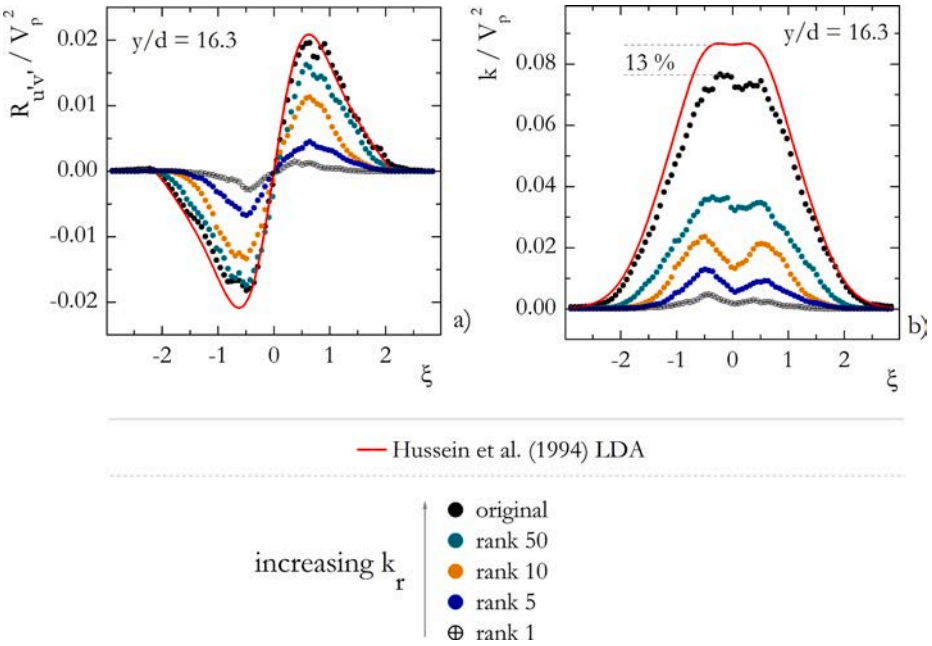

Fig. 19. Comparison of non-dimensional Reynolds shear stresses $R_{u'v'}$ (a) and turbulent kinetic energy k (b) for different LORs at $y/d = 16.3$. The present results are compared with data taken from [22].

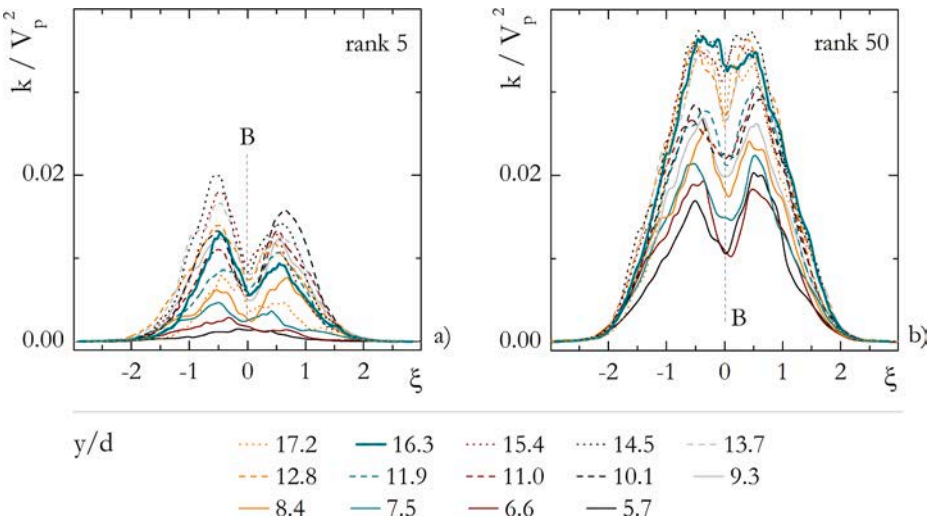

Fig. 20. Rank 5 (a) and rank 50 (b) based approximations of the turbulent kinetic energy k distributions with the non-dimensional downstream distance y/d as parameter.

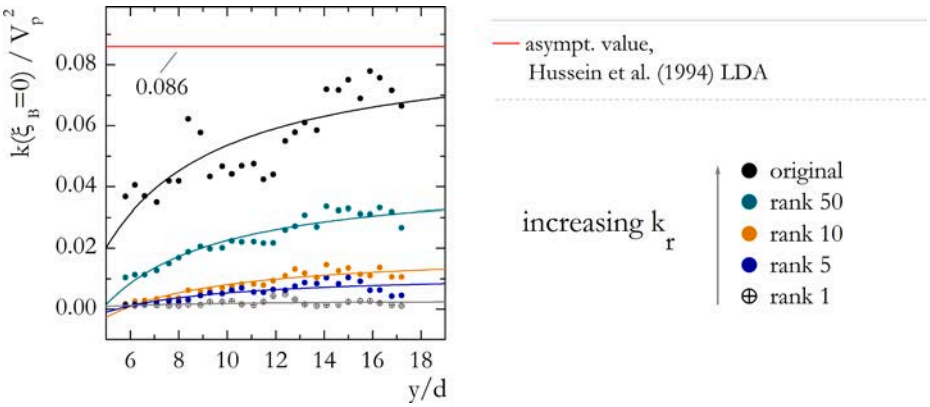

Fig. 21. Comparison of turbulent kinetic energy k extracted at $\xi = 0$ (see Fig. 20) of the LORs as a function of the downstream distance y/d with the original value as well as the asymptotic values according to [22] as reference.

of the flow for lower-order truncations. This dip is successively filled up by smaller-scaled turbulence higher order LORs that are typically not considered for the essential flow processes. With the introduction of a suggested new criterion – based on the maximum cross-correlation obtained through successive time traces of the temporal modes – we attempt to better identify physically relevant POD modes in a more quantitative and more explicit manner compared to energy-based criteria which focus on the 'first few' energy containing modes typically found in literature.

CRediT authorship contribution statement

R. Kapulla: Conceptualization, Data curation, Formal analysis, Investigation, Methodology, Project administration, Resources, Software, Supervision, Validation, Visualization, Writing - original draft, Writing - review & editing. **K.H. Manohar:** Conceptualization, Data curation, Formal analysis, Investigation, Methodology, Project administration, Resources, Software, Supervision, Validation, Visualization, Writing - original draft, Writing - review & editing. **S. Paranjape:** Investigation, Formal analysis, Writing - review & editing. **D. Paladino:** Conceptualization, Writing - review & editing, Supervision, Project administration, Funding acquisition.

Declaration of Competing Interest

The authors declared that there is no conflict of interest.

Acknowledgments

The authors would like to thank Max Fehlmann and Simon Suter for their engaged support in conducting the experiments. Without their profound knowledge of the PANDA facility and their ability to find practical technical solutions for even the wildest scientific ideas it would not have been possible to obtain the results documented in this article. We would also like to take the opportunity to thank Dr. Christopher Boyd from U.S.NRC who initiated these experiments. Dr. Ulrich Doll has reviewed the manuscript several times and provided valuable comments to improve the content. The authors also would like to thank the members of the Management Board and the Program Review Group of the OECD/NEA HYMERES-2 project for their help in defining the test program and evaluating the results.

References

[1] G.L. Brown, A. Roshko, On density effects and large structure in turbulent mixing layers, J. Fluid Mech. 64 (1974) 775–816.
[2] T.S. Kuhn, Structure of Scientific Revolutions, University of Chicago Press, 1996.
[3] B.J. Cantwell, Organized motion in turbulent flow, Annu. Rev. Fluid Mech. 13 (1981) 457–515.

[4] H. Fiedler, Coherent structures in turbulent flows, Prog. Aerosp. Sci. 25 (1988) 231–269.
[5] A.K.M.F. Hussain, Coherent structures and turbulence, J. Fluid Mech. 173 (1986) 303–352.
[6] C.H.K. Williamson, Vortex dynamics in the cylinder wake, Annu. Rev. Fluid Mech. 28 (1996) 477–539.
[7] G. Riches, R. Martinuzzi, C. Morton, Proper orthogonal decomposition analysis of a circular cylinder undergoing vortex-induced vibrations, Phys. Fluids 30 (2018) 105103.
[8] S.K. Robinson, Coherent motions in the turbulent boundary layer, Annu. Rev. Fluid Mech. 23 (1991) 601–639.
[9] N. Hamilton, M. Tutkun, R.B. Cal, Low-order representations of the canonical wind turbine array boundary layer via double proper orthogonal decomposition, Phys. Fluids 28 (2016) 025103.
[10] N. Aubry, P. Holmes, J.L. Lumley, E. Stone, The dynamics of coherent structures in the wall region of a turbulent boundary layer, J. Fluid Mech. 192 (1988) 115–173.
[11] J. Kim, T.R. Bewley, A linear systems approach to flow control, Annu. Rev. Fluid Mech. 39 (2007) 383–417.
[12] S.L. Brunton, B.R. Noack, Closed-loop turbulence control: Progress and challenges, Appl. Mech. Rev. 67 (2015).
[13] J.P. Bonnet, D.R. Cole, J. Delville, M.N. Glauser, L.S. Ukeiley, Stochastic estimation and proper orthogonal techniques for identifying structure decomposition, Exp. Fluids 17 (1994) 314.
[14] N. Akkari, R. Mercier, V. Moureau, Geometrical reduced order modeling (rom) by proper orthogonal decomposition (pod) for the incompressible navier-stokes equations, AIAA Aerospace Sci. Meeting (2018).
[15] J.T.C. Liu, Coherent structures in transitional and turbulent free shear flows, Ann. Rev. Fluid Mech. 21 (1989) 285–315.
[16] P. Benner, S. Gugercin, K. Willcox, A survey of projection-based model reduction methods for parametric dynamical systems, Soc. Ind. Appl. Mathe. Publ. 57 (2015) 483–531.
[17] N. Ali, N. Hamilton, D. DeLucia, R. Bayoán Cal, Assessing spacing impact on coherent features in a wind turbine array boundary layer, Wind Energy, Science 3 (2018) 43–56.
[18] G. Berkooz, P. Holmes, J.L. Lumley, The proper orthogonal decomposition in the analysis of turbulent flows, Annu. Rev. Fluid Mech. 25 (1993) 539–575.
[19] J.L. Lumley, The structure of inhomogeneous turbulent flow, in: Atmospheric Turbulence and Radio Propagation, 1967.
[20] L. Sirovich, Turbulence and the dynamics of coherent structures. Part I, Quat. Appl. Mathe. (1987) 561–571.
[21] N.R. Panchapakesan, J.L. Lumley, Turbulence measurements in axisymmetric jets of air and helium. Part 1. Air Jet, J. Fluid Mech. 246 (1993) 197–223.
[22] H.-J. Hussein, S.-P. Capp, W.-K. George, Velocity measurements in a high-Reynolds-number, momentum-conserving, axisymmetric, turbulent jet, J. Fluid Mech. (1994) 31–75.
[23] I. Wygnanski A N, D.H. Fiedler, Some measurements in the self-preserving jet, J. Fluid Mech 3 (1969) 677–612.
[24] D. Ewing, B. Frohnapfel, W.K. George, J.M. Pedersen, J. Westerweel, Two-point similarity in the round jet, J. Fluid Mech. 577 (2007) 309–330.
[25] C.G. Ball, H. Fellouah, A. Pollard, The flow field in turbulent round free jets, Prog. Aerosp. Sci. 50 (2012) 1–26.
[26] M.N. Glauser, W.K. George, Orthogonal decomposition of the axisymmetric jet mixing layer including azimuthal dependence, in: G. Comte-Bellot, J. Mathieu (Eds.), Advances in Turbulence, Springer Berlin Heidelberg, Berlin, Heidelberg, 1987, pp. 357–366.
[27] B. Viggiano, T. Dib, N. Ali, L.G. Mastin, R.B. Cal, S.A. Solovitz, Turbulence, entrainment and low-order description of a transitional variable-density jet, J. Fluid Mech. 836 (2018) 1009–1049.
[28] R. Watanabe, T. Gono, T. Yamagata, N. Fujisawa, Three-dimensional flow structure in highly buoyant jet by scanning stereo PIV combined with POD analysis, Int. J. Heat Fluid Flow 52 (2015) 98–110.
[29] J.J. Charonko, K. Prestridge, Variable-density mixing in turbulent jets with coflow, J. Fluid Mech. 825 (2017) 887–921, https://doi.org/10.1017/jfm.2017.379.
[30] O. Semeraro, G. Bellani, F. Lundell, Analysis of time-resolved PIV measurements of a confined turbulent jet using POD and Koopman modes, Exp. Fluids 53 (2012) 1203–1220.
[31] Y.M. Shim, R.N. Sharma, P.J. Richards, Proper orthogonal decomposition analysis of the flow field in a plane jet, Exp. Thermal Fluid Sci. 51 (2013) 37–55.
[32] S.V. Gordeyev, F.O. Thomas, Coherent structure in the turbulent planar jet. Part 1. Extraction of proper orthogonal decomposition Eigenmodes and their self-similarity, J. Fluid Mech. 414 (2000) 145–194.
[33] S.V. Gordeyev, F.O. Thomas, Coherent structure in the turbulent planar jet. Part 2. Structural topology via POD eigenmode projection, J. Fluid Mech. 460 (2002) 349–380.
[34] J.H. Citriniti, W.K. George, Reconstruction of the global velocity field in the axisymmetric mixing layer utilizing the proper orthogonal decomposition, J. Fluid Mech. 418 (2000) 137–166.
[35] S. Gamard, D. Jung, W.K. George, Downstream evolution of the most energetic modes in a turbulent axisymmetric jet at high Reynolds number. Part 2. The far-field region, J. Fluid Mech. 514 (2004) 205–230.
[36] M.O. Iqbal, F.O. Thomas, Coherent structure in a turbulent jet via a vector implementation of the proper orthogonal decomposition, J. Fluid Mech. 571 (2007) 281–326.
[37] A.M. Shinneeb, R. Balachandar, J.D. Bugg, Analysis of coherent structures in the far-field region of an axisymmetric free jet identified using particle image velocimetry and proper orthogonal decomposition, J. Fluids Eng., Trans. ASME 130 (2008) 0112021–0112029.
[38] G.A. Freedland, G. Eliason, S. Solovitz, R. Cal, The role of turbulent inflow on the development of a round jet in cross-flow, Int. J. Heat Fluid Flow 84 (2020) 108592.
[39] J. Lee, V. Chu, Turbulent Jets and Plumes - A Lagrangian Approach, Kluwer Academic Publisher, 2003.
[40] G. Lipari, P.K. Stansby, Review of experimental data on incompressible turbulent round jets, Flow, Turbulence Combust. 87 (2011) 79–114.
[41] G. Carazzo, E. Kaminski, S. Tait, The route to self-similarity in turbulent jets and plumes, J. Fluid Mech. 547 (2006) 137–148.
[42] William K. George, The Self-Preservation of turbulent flows and its relation to the initial conditions and coherent structures, Adv. Turbulence (1989) 39–73.
[43] P. Jordan, T. Colonius, Wave packets and turbulent jet noise, Annu. Rev. Fluid Mech. 45 (2013) 173–195.
[44] M. Ihme, Combustion and engine-core noise, Annu. Rev. Fluid Mech. 49 (2017) 277–310.
[45] A.P. Dowling, A.S. Morgans, Feedback control of combustion oscillations, Annu. Rev. Fluid Mech. 37 (2005) 151–182.
[46] S.L. Brunton, J.N. Kutz, Data-driven Science and Engineering - Machine Learning, Dynamical Systems and Control, Cambridge University Press, 2019.
[47] D. Paladino, J. Dreier, PANDA: a multipurpose integral test facility for LWR safety investigations, Sci. Technol. Nucl. Install. 2012 (2012) 239319.
[48] D. Paladino, R. Zboray, M. Andreani, J. Dreier, Flow transport and mixing induced by horizontal jets impinging on a vertical wall of the multi-compartment panda facility, Nucl. Eng. Des. 240 (2010) 2054–2065.
[49] R. Zboray, D. Paladino, Experiments on basic thermalhydraulic phenomena relevant for lwr containments: Gas mixing and transport induced by buoyant jets in a multi-compartment geometry, Nucl. Eng. Des. 240 (2010) 3158–3169.
[50] C. Tropea, A.L. Yarin, J.F. Foss, Handbook of Experimental Fluid Mechanics, Springer, 2007.
[51] M. Raffel, C. Willert, S. Wereley, J. Kompenhans, Particle Image Velocimetry, A Pratical Guide, Springer, Berlin, 2007.
[52] R. Kapulla, G. Mignot, S. Paranjape, L. Ryan, D. Paladino, Large scale gas stratification erosion by a vertical helium-air jet, Sci. Technol. Nucl. Install. (2014).
[53] J. Bendat, A. Piersol, Analysis and Measurement Procedures, A Wiley-Interscience Publication, New York, Chichester, Brisbane, Toronto, Singapore, 1986.
[54] A. Sciacchitano, B. Wieneke, PIV uncertainty propagation, Meas. Sci. Technol. 084006 (2016).
[55] E. Lemmon, M. Huber, M. McLinden, NIST standard reference database 23: Reference fluid thermodynamic and transport properties-refprop, version 9.1, NIST (2013).
[56] C.-J. Chen, W. Rodi, Vertical turbulent buoyant jets: A review of experimental data, Technical Report, NASA, 1980.
[57] L. Yarin, The PI-Theorem - Applications to Fluid Mechanics and Heat and Mass Transfer, Springer, 2012.
[58] S.B. Pope, Turbulent Flows, Camebridge University Press, 2000.
[59] M. Breda, O.R.H. Buxton, Influence of coherent structures on the evolution of an axisymmetric turbulent jet, Phys. Fluids 30 (2018) 035109.
[60] M.L. Albertson, Y.B. Dai, R.A. Jensen, H. Rouse, Diffusion of submerged jets, Trans. Am. Soc. Civil Eng. 115 (1950) 639–664.
[61] W.K. George, The self-preservation of turbulent flows and its relation to initial conditions and coherent structures, in: W.K. George, R. Arndt (Eds.), Advances in Tubulence, Hemisphere, 1989, pp. 39–72.
[62] L. Hufnagel, J. Canton, R. Örlü, O. Marin, E. Merzari, P. Schlatter, The three-dimensional structure of swirl-switching in bent pipe flow, J. Fluid Mech. 835 (2018) 86–101.
[63] A. Kalpakli, R. Örlü, Turbulent pipe flow downstream a 90° pipe bend with and without superimposed swirl, Int. J. Heat Fluid Flow 41 (2013) 103–111. ETMM9.
[64] Z. Wu, D. Laurence, S. Utyuzhnikov, I. Afgan, Proper orthogonal decomposition and dynamic mode decomposition of jet in channel crossflow, Nucl. Eng. Des. 344 (2019) 54–68.
[65] K.R. Dinesh, A. Savill, K. Jenkins, M. Kirkpatrick, LES of intermittency in a turbulent round jet with different inlet conditions, Comput. Fluids 39 (2010) 1685–1695.
[66] R. Camussi, G. Gui, Orthonormal wavelet decomposition of turbulent flows: Intermittency and coherent structures, J. Fluid Mech. 348 (1997) 177–199.
[67] Y. Pomeau, P. Manneville, Intermittent transition to turbulence in dissipative dynamical systems, Commun. Math. Phys. 74 (1980) 189–197.
[68] D. Ruelle, F. Takens, On the nature of turbulence, Comm. Math. Phys. 20 (1971) 167–192.